Coden: JPLPAY
Volume 9, Part A-2, No. 5, May 1971

Journal of Polymer Science

Part A-2: Polymer Physics

Contents

Published by INTERSCIENCE PUBLISHERS a division of John Wiley & Sons, Inc.

Journal of Polymer Science **Part A-2: Polymer Physics**

The Journal of Polymer Science is published in four sections as follows: Part A-1, Polymer Chemistry, monthly; Part A-2, Polymer Physics, monthly; Part B, Polymer Letters, monthly; Part C, Polymer Symposia, irregular.

Published monthly by Interscience Publishers, a Division of John Wiley & Sons, Inc., covering one volume annually. Publication Office at 20th and Northampton Sts., Easton, Pa. 18042. Executive, Editorial, and Circulation Offices at 605 Third Avenue, New York, N.Y. 10016. Second-class postage paid at Easton, Pa. Subscription price, $325.00 per volume (including Parts A-1, B, and C). Foreign postage $15.00 per volume (including Parts A-1, B, and C).

JOURNAL OF POLYMER SCIENCE: PART A-2 VOL. 9, 769–777 (1971)

Investigation of Cooperative Kinetics in Reactions of Functional Groups on Polymer Chains

B. N. GOLDSTEIN, A. N. GORYUNOV, YU. YA. GOTLIB, A. M. ELYASHEVICH, T. P. ZUBOVA, A. I. KOLTZOV, V. D. NEMIROVSKII, and S. S. SKOROKHODOV
Institute of Macromolecular Compounds, Leningrad, U.S.S.R.

Synopsis

The kinetics of aminolysis of 1,2;3,4-*meso*-erythritol dicarbonate and 1,2;3,4;5,6-mannitol, sorbitol, and dulcitol tricarbonates by *n*-butylamine in dimethylformamide solution was investigated. The dicarbonate and tricarbonates are considered respectively as models of dyads and triads in the poly(vinylene carbonate) chain. The theoretical kinetic curves for the dimer and the trimers were calculated by solution of kinetic equations and close agreement with experiment was obtained. A version of the Monte-Carlo method was developed to provide a model for the reaction process by a computer calculation including the neighboring group effect in enhancing reactivity. The theoretical curve for a trimer coincides with the experimental one. These results confirm the accelerating influence of the unreacted neighboring groups. For the polymeric chain the experimental and calculated curves deviate for conversions beyond 10%. This indicates an additional polymer effect, which is as yet unexplained.

A kinetic study of the aminolysis of polyvinyleneccarbonate (PVCa) by *n*-butylamine (BA) in dimethylformamide (DMF) solution at 50°C has been carried out recently by two of us.[1,2] The rate constant of the aminolysis reaction on the polymer chain was shown to be two or three orders of magnitude higher than that for ethylene carbonate. Ethylene carbonate is considered to be a model compound for the monomer unit of PVCa. This acceleration of the reaction was explained as a result of the influence of adjacent unreacted units.[2]

The present study was carried out to confirm the hypothesis of the mutual influence of the neighboring units and to obtain more detailed information on the kinetics of the reaction in DMF. For this purpose some model compounds were synthesized by known methods. The compounds are vinylene carbonate dimer, 1,2;3,4-*meso*-erythritol dicarbonate (EDC)[3] and stereoisomeric trimers, 1,2;3,4;5,6-mannitol tricarbonate (MTC), sorbitol tricarbonate (STC), and dulcitol tricarbonate (DTC).[4]

Taking into account steric peculiarities of the hexitols used and suggesting that in the synthesis of tricarbonates the stereoconfiguration is retained, we can assume that the tricarbonates synthesized are models of isotactic, heterotactic and syndiotactic triads of poly(vinylene carbonate), respec-

tively. The steric arrangement of ethylene carbonate rings in tricarbonate molecules was not determined experimentally; therefore we make this assumption tentatively.

The experimental technique has been described elsewhere.[2] PVCa synthesized by free-radical polymerization with molecular weight 150,000 (sedimentation method) was used.

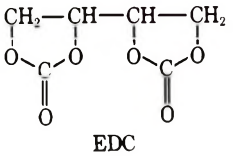

EDC

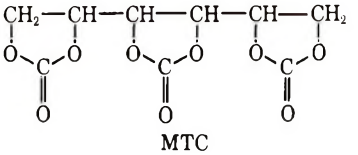

MTC

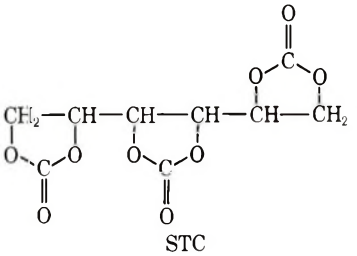

STC

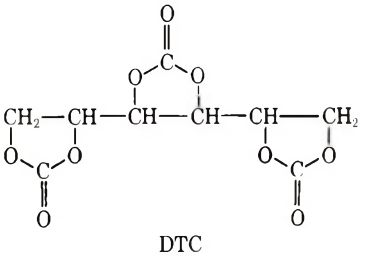

DTC

Consideration of the simplest theoretical kinetic models for a dimer and a trimer according to the hypothesis of the accelerating influence of adjacent unreacted units yields the following results. The scheme of kinetic models taking into account the sequence of the reaction stages for aminolysis of the first, second, and third units is shown in Figure 1. For simplicity the two side units of the trimer (and both units of the dimer) are assumed to be unreactive at their outer —O—C=O group. This assumption is based on
|
O

the extremely low aminolysis rate of ethylene carbonate.[1] In the present investigation this assumption was confirmed by PMR spectral data for the aminolysis products of ECD and MTC. It was shown that the aminolysis products obtained are the derivatives of the corresponding polyols with carbamate groups only at the 1,4 and 1,3 (or 4) and 6 positions, respectively.

The experimental data for aminolysis of the dimer in DMF up to a conversion of 47% follow second-order kinetics with respect to the reagent BA

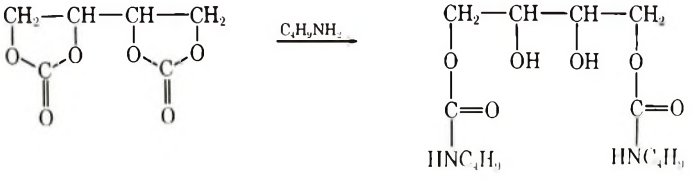

with the single rate constant $K_1^{(D)}$ for the attack on the inner side of the first cyclic unit. The equation for the case studied $C_0 = 2\ [\mathrm{EDC}]_0$ is

$$dC/dt = -2K_1^{(D)}C^2[C - (C_0/2)] \qquad (1)$$

where $C = [\mathrm{BA}]$.

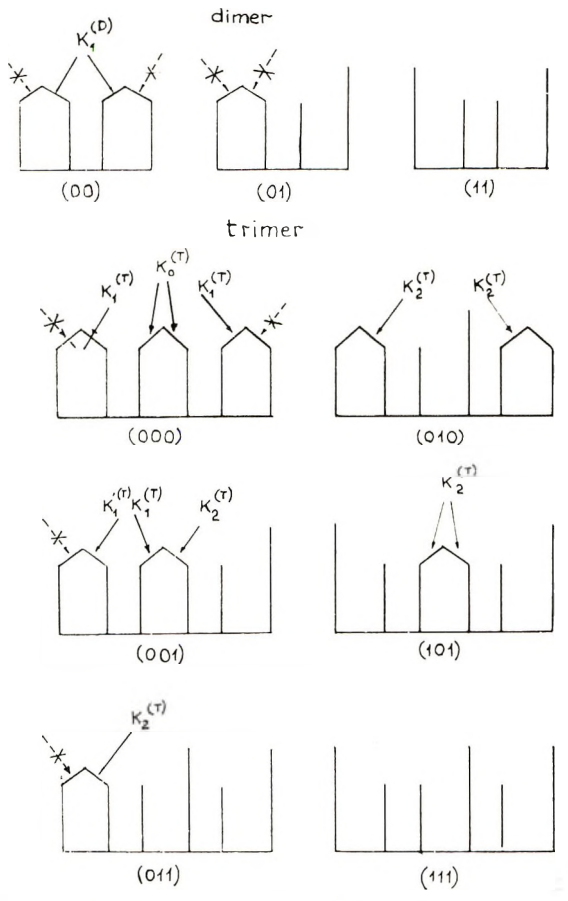

Fig. 1. Schematic representation of kinetic models for aminolysis of dimer and trimer

The value of $K_1^{(D)}$ proved to be a 0.004 l.^{2}/mole^2-sec.

The rate constant $K_2^{(D)}$ for the attack on the unit adjacent to the reacted one is at least two or three orders of magnitude lower. The rate constant $K_2^{(D)}$ was not taken into account because of its very low value.

The kinetic equations for a trimer in the form

$$\begin{aligned}
d[000]/dt &= -(2K_1^{(T)} + K_0^{(T)})[000]C^2 \\
d[010]/dt &= (K_0^{(T)}[000] - 2K_2^{(T)}[010])C^2 \\
d[001]/dt &= (2K_1^{(T)}[000] - (2K_1^{(T)} + K_2^{(T)})[001])C^2 \\
d[101]/dt &= K_1^{(T)}[001] - 2K_2^{(T)}[101])C^2 \\
d[011]/dt &= \{(K_1^{(T)} + K_2^{(T)})[001] + K_2^{(T)}[010] - K_2^{(T)}[011]\}C^2
\end{aligned} \tag{2}$$

were solved by means of the Razdan digital computer by the Runge-Gutta method.

The trimer concentrations at the corresponding stages of the reaction are denoted by [000], [010], etc. A zero indicates an unreacted unit of the model compound and unity indicates a reacted unit.

The initial concentrations were $C_0 = [BA]_0 = 0.20$ mole/l., [DTC] = 0.15 mole/l. (the same concentrations were used for STC and MTC).

In addition to the assumption of the extremely low reaction rate in the outer part of the side units let us assume $K_1^{(T)} = K_1'^{(T)}$. This means that only the influence of the adjacent units is taken into account. There are no direct experimental data on the interrelations of the adjacent ethylene carbonate cyclic units. Therefore it is reasonable to assume two most probable mechanisms for the accelerating influence: the shift of the electron density along the bonds (inductive effect) and the field effect (steric influence). Both effects strongly decrease with increasing distance. Hence we neglect the influence of remote units.

The solutions of the eqs. (2) give families of curves corresponding to different ratios between the constants $K_0^{(T)}$; $K_1^{(T)}$, $K_1'^{(T)}$ and $K_2^{(T)}$. The best agreement with experimental data was obtained for the following set of values of the kinetic constants.

For MTC: $K_0^{(T)} = 0.1$ l.²/mole-sec

$$K_1^{(T)} = K_1'^{(T)} = 0.01 \text{ l.}^2/\text{mole}^2\text{-sec}$$

$$K_2^{(T)} = 0.0005 \text{ l.}^2/\text{mole}^2\text{-sec}$$

For STC:

$$K_0^{(T)} = 0.027 \text{ l.}^2/\text{mole}^2\text{-sec}$$

$$K_1^{(T)} = K_1'^{(T)} = 0.005 \text{ l.}^2/\text{mole}^2\text{-sec}$$

$$K_2^{(T)} = 0.0005 \text{ l.}^2/\text{mole}^2\text{-sec}$$

For DTC:

$$K_0^{(T)} = 0.018 \text{ l.}^2/\text{mole}^2\text{-sec}$$

$$K_1^{(T)} = K_1'^{(T)} = 0.005 \text{ l.}^2/\text{mole}^2\text{-sec}$$

$$K_2^{(T)} = 0.0007 \text{ l.}^2/\text{mole}^2\text{-sec}$$

The experimental data for DTC and the family of calculated curves for the best value of K_0/K_1 and for different ratios K_0/K_2 are shown in Figure 2.

A comparison of the $K_0^{(T)}$ values shows that they depend on the conformation of the stereoisomeric trimers in the following order: isotactic > heterotactic > syndiotactic. However, to make a final decision about the steric factor one must have direct experimental data on the conformation of each cyclic unit of trimers. For instance, no data are available on the strain of the ethylene carbonate rings in dimers and trimers. Nevertheless it is known that the strained *trans*-ethylene carbonate rings in the corresponding carbohydrate derivatives exhibit an increased reactivity towards nucleophilic reagents.[5] Consequently, one can suggest that the reactivity of the unit of PVCa or of the model compounds can be affected not only by inductive and field effects, but also by other factors.

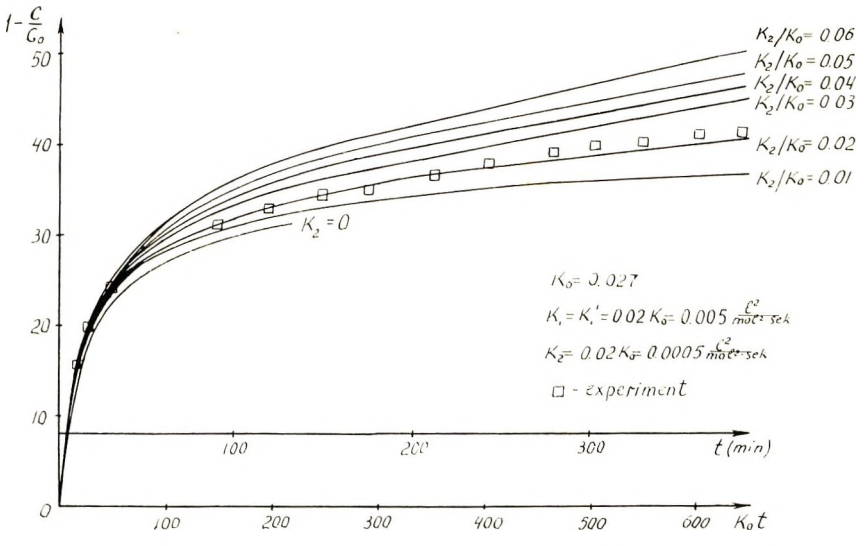

Fig. 2. Computer curves for different ratios K_2/K_0 for trimer and the experimental data for DTC.

Analytical methods giving complicated expressions have been used earlier for solving the problem of the cooperative effects in reactions on macromolecular chains.[6–10] In contrast to this approach, a version of the Monte-Carlo method of providing a model for the reaction process by a computer was developed (see Appendix). The overall reaction in a polymer chain is regarded as a random sequence of reactions on individual units of the chain. The rate constant is assumed to be dependent on the number of adjacent units which have reacted. The scheme of the kinetic models for different stages of the reaction on a triad of monomeric units is shown in Figure 3. A special scheme was developed for fitting the experimental kinetic relations for finite concentrations of the reagent BA on the reduced curve (the reaction order may be determined according to the same scheme). This curve corresponds to infinitely high concentration of the reagent (or to infinitely low concentration of the polymer) or to the case when the reagent concentration is maintained constant.

On the basis of the method proposed, the computer experiment for the case of the trimer was carried out. The same ratios of the rate constants and the same initial reagent concentrations were used as in the analytical calculations discussed above. We have thus obtained a family of theoretical curves corresponding both to the experimental and to the theoretical curves. The latter were derived from analytical solution of kinetic equations. This close agreement between the theoretical and experimental curves for the trimer permits us to calculate the more complicated case of the polymer chain. The computation was carried out by using the kinetic model derived from the trimer model. The resulting curves, given in Figure 4, coincide with curves obtained analytically by Arends.[7] The reaction proved

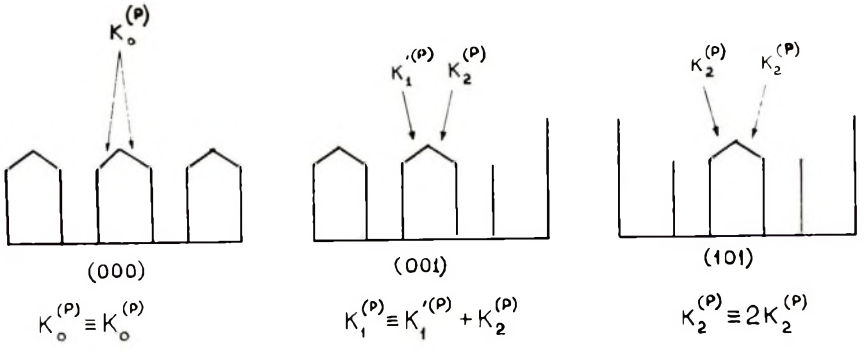

Fig. 3. Schematic representation for aminolysis of polymer.

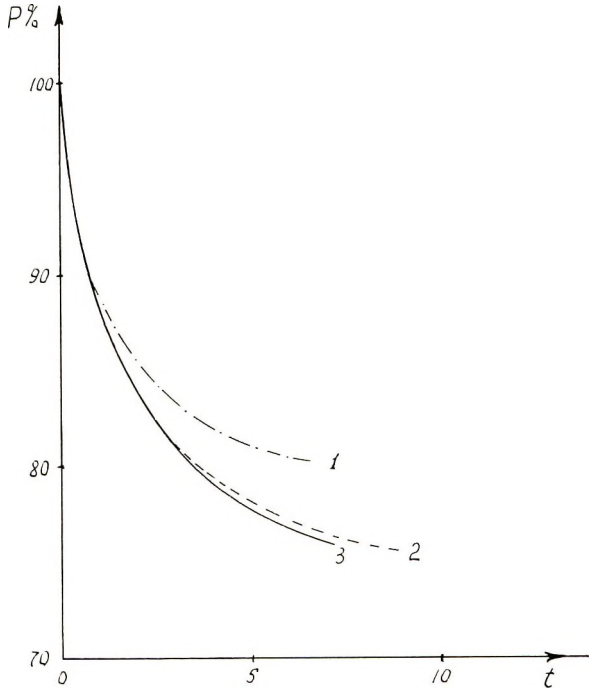

Fig. 4. Kinetic curves for aminolysis of polymer $[polymer]_0 = 0.1586$ base mole/l. $[BA]_0 = 0.0508$ mole/l: (1) chemical experiment; (2) computer experiment with $K'_0 = 0.027$ l.2/mole²-sec; $K_1 = K_2 = 0$; (3) for $K_1 = 0.005$ l.2/mole²-sec; $K_2 = 0.0005$ l.2/mole²-sec.

to be second-order with respect to the reagent. This result is in good agreement with the experimental data for the reaction of the trimer. In contrast to the method of Arends, our method does not involve limitations on the values of the rate constants and of their dependence on reagent concentration. The computer curves were obtained for the range of the initial experimental conditions used and for the ratios between the rate constants at different stages of the reaction evaluated from the model dimer and trimer

kinetics. The theoretical curves deviate from the experimental ones beyond a conversion of 10% (Fig. 4). It is impossible to obtain curves similar to the experimental ones at any ratio of the rate constants for the separate stages of the reaction.

Our analysis of the kinetic features of the reactions for polymer chains and for the model dimer and trimer, confirms the hypothesis of the significant influence of the adjacent units. Unreacted adjacent units increase the reactivity of a reacting unit in comparison with single units. During the reaction the number of unreacted adjacent units decreases and the overall reaction rate drops correspondingly.

Furthermore, for the polymer there is observed an additional effect. It noticeably decreases the reaction rate when the conversion is 10% or higher. The nature of this influence is unknown and needs further investigation. It may be connected with a change in macromolecular conformation during the reaction.

APPENDIX

Monte Carlo Calculations of the Kinetics of Reactions on Polymer Chains

A polymer chain consisting of N monomeric units, each bearing one functional group able to undergo a chemical reaction, is modeled by a linear sequence of elements. Each element can exist in two states 0 (an unreacted unit), and 1 (a reacted unit). Thus each state of the whole polymer chain corresponds to a definite arrangement of numbers 0 and 1.

The reaction on the polymer chain involves the reactions of separate units, i.e., it consists of the transitions $0 \rightarrow 1$ for each unit. The computation made with a BESM-4 computer (2×10^4 operations per second) is based on the following assumptions: (1) the reaction act for each unit proceeds practically instantaneously (the time interval between consecutive acts is much greater than the time required for the act itself); (2) the reaction on each unit is a simple stochastic process, i.e., at any moment the probability of the transition $0 \rightarrow 1$ for a given element is dependent only on the states of adjacent units and on the reagent concentration in solution.

Let us consider a certain state of the chain at a time t, corresponding to a definite sequence of zeros and ones and to a definite value of the reagent concentration [C]. The probability that during a time interval Δt no reaction acts occur and that at the time $t + \Delta t$ a reaction has taken place on the ith unit is expressed by

$$W_i(\Delta t) = W_i^{+}(\Delta t) \prod_{\substack{j=1 \\ j \neq i}}^{N} W_j^{-}(\Delta t) \tag{1}$$

Here, $W_j^{-}(\Delta t)$, the probability that no reaction occurs during the time interval Δt on unit j, is given by

$$W_j^{-}(\Delta t) = e^{-\alpha_j \Delta t} \tag{2}$$

where

$$\alpha_j = K_j[C]^K \tag{3}$$

and K_j is the reaction rate constant for the individual unit with the surroundings specified, and K is the reaction order with respect to the reagent BA.

The probability $W_i^+(\Delta t)$ that the reaction will occur at the time $t + \Delta t$ on unit i of the chain, is given by

$$W_i^+(\Delta t) = \alpha_i e^{-\alpha_i \Delta t} \tag{4}$$

It is evident that the probability of occurrence of reaction on any chain unit at the time $t + \Delta t$ is given by the expression

$$W(\Delta t) = \sum_{i=1}^{N} W_i(\Delta t) = \alpha e^{-\alpha \Delta t} \tag{5}$$

where

$$\alpha = \Sigma \alpha_i$$

Every situation arising during the reaction process, and corresponding to a definite set of zeros and ones, is analyzed as follows. The values of α_i for each element and then the value of α are calculated. Then random numbers ξ_1, ξ_2 uniformly distributed over the interval 0,1 are taken, and the reaction act is supposed to occur at the time $t + \Delta t$ on the ith unit, where Δt and i are determined by equations:

$$\Delta t = -\ln \xi_1/\alpha$$

and

$$\frac{1}{\alpha} \sum_{j=1}^{i-1} \alpha_j \leqslant \xi_2 < \frac{1}{\alpha} \sum_{j=1}^{i} \alpha_j \tag{6}$$

A new situation arising as a result of the transition $0 \rightarrow 1$ on the ith element is analyzed by a similar method. Beginning the computation from the completely unreacted chain (all the elements are in the 0 state) one arrives at the completely reacted chain (all the elements are in the 1 state). In such a manner a kinetic curve for one polymeric chain is obtained. If the number of elements in the chain is great enough, this curve must coincide with the curve, which would be observed in experiments, if processes with the same values of kinetic constants for the assumed stages of reaction occurred on the macromolecule chain in solution. The present results are obtained for a chain consisting of 2000 elements.

It is convenient to carry out the computations specifying that the reagent concentration in solution during the reaction does not vary. Therefore a procedure was developed for fitting the experimental curves obtained for finite initial reagent concentration $[C]_0$ to the case [C] = constant. This procedure consists in dividing the total reaction time into time intervals Δt_i during which the conversion changes from p_i to $(p_i + \Delta p)$. The Δp value

is chosen so low, that the reagent concentration during these time intervals can be considered constant.

Thus, if the reaction order with respect to the reagent is K and the initial polymer concentration is $[C_p]_0$ and if during the reaction one mole of the reagent per unit reacted is consumed a change of conversion from p_i to $(p_i + \Delta p)$ in the case $[C] = [BA] =$ constant will occur in the time interval

$$\Delta t(C) = \Delta t_i \{[C_0] - p_i[C_p]\}^K / [C]^K \tag{7}$$

Thus the change of the time scale according to eq. (7) gives a new kinetic curve corresponding to the case when a constant reagent concentration [C] is maintained in solution.

It is evident that, if the reaction order is estimated correctly, the experimental curves obtained at different initial reagent concentrations must give, after recalculation, coinciding curves. If the order is unknown, but is kept constant, it is possible to estimate it by comparing Δt values obtained for the conversion differences caused by different initial concentrations $[C_0]_1$ and $[C_0]_2$. This order is given by the expression:

$$K = - \frac{\ln (\Delta t_1 / \Delta t_2)}{\ln \{([C_0]_2 - p[C_p])/([C_0]_1 - p[C_p])\}} \tag{8}$$

It should be noted that the procedure leads to good results only if the experimental kinetic data are sufficiently accurate.

We thank Miss Z. A. Udalova for synthetic preparations.

References

1. V. D. Nemirovskiĭ and S. S. Skorokhodov, in *Macromolecular Chemistry, Prague, 1965* (*J. Polym. Sci. C*, **16**) O. Wichterle and B. Sedlaček, Eds., Interscience, New York 1967, p. 147.
2. V. D. Nemirovskii and S. S. Skorokhodov, *Vysokomol. Soedin.*, **9**, 2142 (1967).
3. H. R. Meyer, *Helv. Chim. Acta*, **49**, 1935 (1966).
4. L. Hough, J. E. Priddle, and R. S. Theobald, *J. Chem. Soc.*, **1962**, 1934.
5. W. N. Doane, N. S. Shasha, E. I. Stout, C. R. Russell, and C. E. Rist, *Carbohydrate Res.*, **11**, 321 (1969).
6. J. B. Keller, *J. Chem. Phys.*, **37**, 2854 (1962); *ibid.*, **38**, 325 (1963).
7. C. B. Arends, *J. Chem. Phys.*, **38**, 322 (1963).
8. T. Alfrey and W. G. Lloyd, *J. Chem. Phys.*, **38**, 318 (1963).
9. L. Lazare, *J. Chem. Phys.*, **39**, 727 (1963).
10. A. D. Litmanovich, *Dokl. Akad. Nauk SSSR*, **165**, 353 (1965).

Received July 27, 1970
Revised October 5, 1970

JOURNAL OF POLYMER SCIENCE: PART A-2 VOL. 9, 779–799 (1971)

Fractionation during Crystallization

D. M. SADLER,* *H. H. Wills Physics Laboratory, University of Bristol, Royal Fort, Bristol BS8 1TL, Great Britain*

Synopsis

Extensive gel-permeation chromatography (GPC) results are presented which reveal in much more detail than hitherto the effects of fractionation during the crystallization of polyethylene from solution. It is suggested how these results may be used to assess the affects of fractionation on the production of single crystals. In addition the results are compared with the fractionation which would be expected assuming the crystals to be in equilibrium with the solution. It was found that the results can be explained very well on this basis. A discussion of this rather unexpected result is included.

INTRODUCTION

Fractionation of polymers during crystallization according to molecular weight can be an important factor controlling the growth and structure of semicrystalline polymers, both as a possible source of spherulitic growth,[1] as accompanying the formation of extended chain crystals,[2–5] and as a possible cause of isothermal thickening of lamellar crystals during their growth.[6,7]

Fractionation by crystallization from solution has been studied primarily as a preparative technique. It has been applied to several polymers including polyethylene[8–12] and polypropylene;[12,13] fractionation by branch content is most important in low-density polyethylene,[8] but fractionation by molecular weight can be obtained with high-density polyethylene.[9–12] Pennings has found that fractionation can be improved for high molecular weights if the polymer is stirred during crystallization.[12]

Many experiments using a variety of techniques have been applied to polyethylene crystallized from xylene, yet the reports mentioned above contain little data referring to fractionation in unstirred solutions, and even these data are restricted to average molecular weight values. The present work presents results of gel-permeation chromatography (GPC) on polyethylene fractionated at commonly employed temperatures of crystallization and gives an assessment of the distribution as well as average values of molecular weight. It is hoped that these results will be of assistance when molecular weight effects on other experiments are considered (see below), but also that they will serve as an experimental basis for some understanding of the fractionation process itself as applied to a well-defined system.

* Present address: Centre de Génétique Moléculaire, 91-Gif-sur-Yvette, France.

Data on stirred solutions are of less use from a theoretical view, since less well defined crystal morphologies are involved.[14]

Characterization of molecular weight is becoming of increasing importance in the study of polymer crystals from solution. One source of molecular weight effects is the inhomogeneous distribution of molecular weights in a preparation, as a result of fractionation during crystallization. For example, a significant proportion of polymer may be still in solution after crystallization.[10,11] Depending on whether the resulting suspension is filtered at the crystallization temperature, or later after cooling, the crystals in the dried state will either contain a lower proportion of low molecular weights than the original polymer or will contain a distinct phase of low molecular weight crystal. In either case the assessment by GPC of the effect of fractionation on the molecular weight distributions (MWD) will be of interest in the consideration of effects related to molecular weight.

As regards the relevance of these results to the process of fractionation, an analysis is included here assuming an equilibrium analogous to that obtained in liquid–liquid systems. Such an approach has been applied to (monodisperse) crystalline paraffins[15] and to (polydisperse) polymers in the liquid–liquid system.[16] The calculation here follows that of Kawai;[17,18] modifications of this approach are discussed in the text.

EXPERIMENTAL

Marlex 6009 was dissolved at about 4% (and occasionally at 0.4%) concentration in xylene, and crystallized by slow cooling. The suspensions were slowly heated to about 103.5°C (101°C in the case of the lesser concentration). This solution was then poured into xylene at the crystallization temperature so as to achieve two liters of solution crystallizing at 0.75% (or 0.1%). The crystallization vessel was enclosed in a constant-temperature bath; a coil which circulated liquid from the bath around the interior of the vessel helped to ensure that the equilibrium internal temperature was the same as that of the bath. The heat contained in the hot solution poured in could not be dissipated very quickly however, so that crystals grown at the lower temperatures probably started to grow in the period of cooling.

Crystallization was allowed for about 48 hr, except in the case of crystallization at 92.8°C which was continued for 150 hr. To study the effects of crystallization the suspension was now filtered within the vessel; a syphon arrangement ensured that the suspension could not reach the filter until desired. For dissolution studies crystallization was allowed to proceed as described above, after which the temperature of the bath was cooled to near room temperature. It was then heated to the original temperature again; after another period of 48 hr at this temperature filtration was effected.

The filtrate was allowed to crystallize at room temperature; the polymer was separated in general by filtering the crystals which then grew. The GPC apparatus was used with upper porosity ratings of the sets of columns as follows: (a) 15000, 3000, 700, and 350 Å; (b) 15000, 800, 350, and 350 Å; (c) 1.5×10^5, 15000, 800, and 350 Å.

RESULTS

The crystals formed a sludge of small (a few microns in diameter) basically monolayer units.[19] The fractions of the polymer still in solution at four temperatures of crystallization were approximately as follows: 0.0032

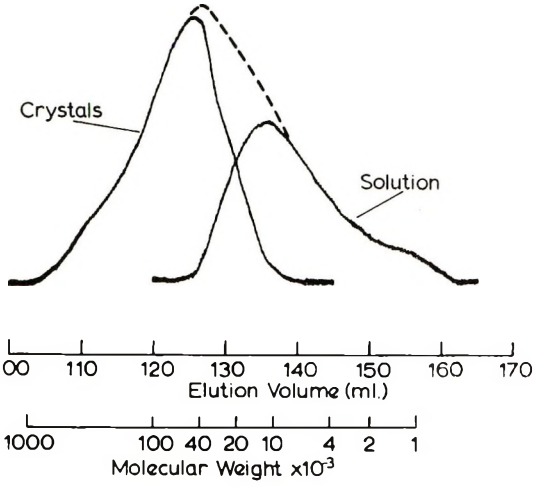

Fig. 1. Chromatograms corresponding to the crystalline and solution phases after crystallization of Marlex 6009 at 0.75% concentration in xylene at 92.8°C for 5 days. The ordinate refers to increments of refractive index, expressed in arbitrary units.

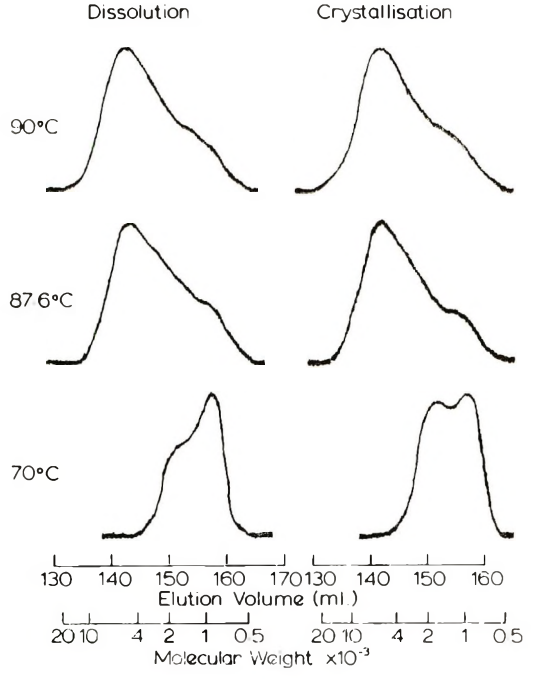

Fig. 2. Chromatograms of polymer separated from solution phase obtained by filtering suspensions, at three temperatures, after two days crystallization, and after two days dissolution. The ordinate shows relative increments in refractive index.

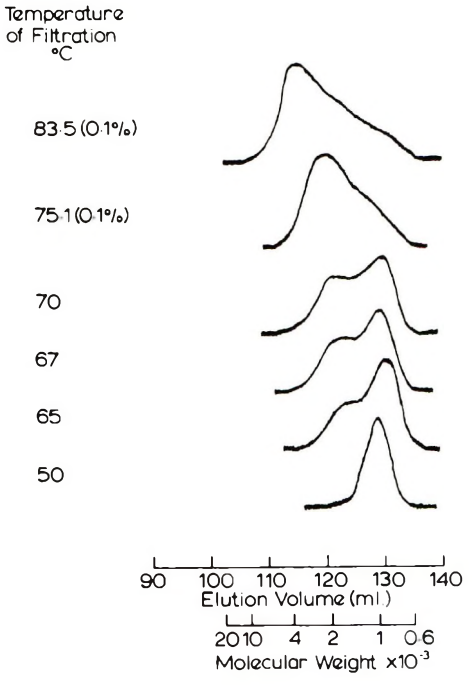

Fig. 3. Chromatograms of solution phase corresponding to different temperatures of filtration after crystallization. Shown are the two results corresponding to an initial concentration of polymer of 0.1% in xylene (all other chromatograms refer to 0.75%). The ordinate shows relative increments in refractive index.

at 50°C, 0.012 at 72.6°C, 0.1 at 87.6°C, and 0.23 at 92.8°C. In Figure 1 are shown chromatograms of polymer in the crystal and solution phases, after crystallization of the whole polymer at 92.8°C. This shows that the MWD has been bisected by the filtration. Figure 2 compares chromatograms of polymer in the solution phase after crystallization and after dissolution. It can be seen that filtering after dissolution results in distributions which are little different from those which result from filtration after crystallization at these temperatures. Figure 3 shows chromatograms corresponding to filtrates prepared at lower temperatures of crystallization. (Included in Figure 3 are two samples produced with an initial polymer concentration of 0.1%.) An unexpected feature of the solution phase chromatograms is the rather sharp peak at a molecular weight of 920. The infrared spectrum of filtrate material produced at 70°C showed no evidence of oxidation, and the absorption given by the terminal double bond on the polyethylene was still present. To investigate any fractionation effects which occur when the filtrate crystallizes at room temperature, the polymer was in one case separated by evaporation under vacuum. Figure 4 shows the resultant chromatogram; also shown are chromatograms for the crystal and solution phases separated by filtration at room temperature. A low molecular weight "tail" has been removed by filtration, but the peak is still

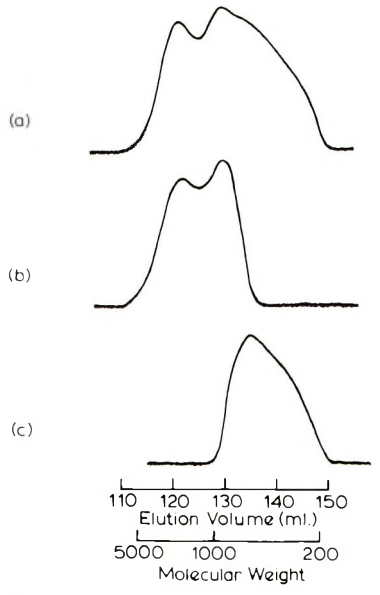

Fig. 4. Chromatograms illustrating the effect of filtration at room temperature upon a sample prepared by filtration at 70°C: (*a*) whole fraction obtained from filtrate by evaporation of solvent; (*b*) fraction separated from solvent by filtering after crystallization at room temperature; (*c*) material still in solution at room temperature, isolated by evaporation of solvent. The ordinate shows relative increments in refractive index.

evident and must therefore have been present in the original Marlex distribution. It forms only 0.3% of the whole polymer and hence could easily have remained undetected hitherto.*

COMPUTATIONS FROM CHROMATOGRAMS

Number- and weight-average molecular weights were calculated and are compiled in Table I. In two cases, duplicate values are shown corresponding to chromatograms obtained using different sets of GPC columns. The chromatograms were analyzed further on the basis that the MWD can be written as:

$$F(P) = f(P)f_P$$

where $F(P)$ is the resultant distribution of material in the separate phase in terms of degree of polymerization P, $f(P)$ is the distribution of the unfractionated polymer, and f_P is a function which described the separation process. The effect of instrumental broadening was assessed by using a resolution calibration obtained with paraffin and polystyrene samples.[23] If a hypothetical Gaussian chromatogram of about the same width as the experimental ones is considered, the broadening resulting from the in-

* The fractions produced in this way can be of direct use for other studies.[20,21] Such fractions are of particular value, since if care is taken to ensure the efficiency of the filtration, high molecular weight tails can be extremely small.[22]

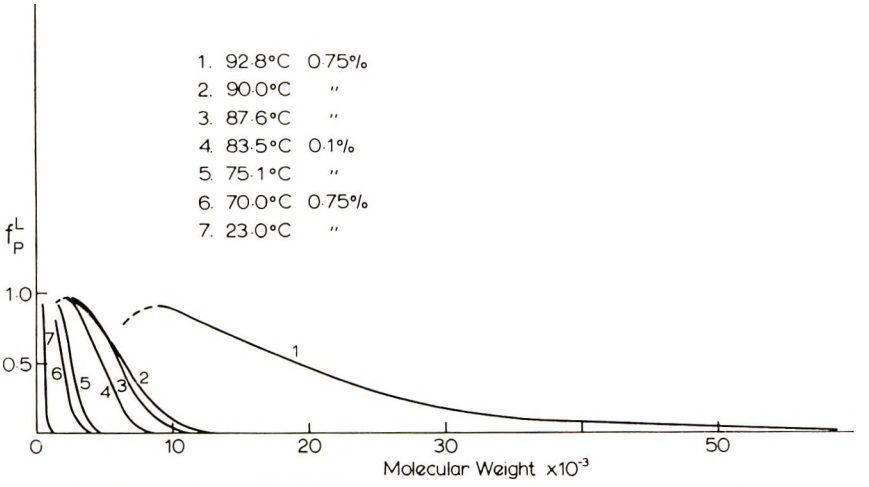

Fig. 5. Separation functions f_P^L describing the fractionation with respect to molecular weight calculated from the chromatograms in the preceding diagrams.

strument will overestimate the width of the true distribution by about 15%.

Ignoring instrumental broadening,

$$f_P = F(P)/f(P)$$
$$= h_1(P)/h_0(P)$$

where $h_1(P)$ is the chromatogram deflection of the solution (or solid) phase and $h_0(P)$ is that of the unfractionated polymer. In Figure 5, $f_P{}^L$ (f_P for the liquid phase) is plotted against molecular weight at various temperatures.

TABLE I
Average Molecular Weights of Polymers in Filtrate

	Crystallized		Extracted		Figure illustrating chromatogram
T, °C	$\bar{M}_w$	$\bar{M}_n$	$\bar{M}_w$	$\bar{M}_n$	
92.8	11000	5030			1
90	4300	2400	3830	2460	2
			3320	2310	
87.6	4280	2600	3680	2440	2
			3370	2370	
83.5	2580	1960			3
75.1	2050	1670			3
72.6	1900	1530			
70	1430	1220	1490	1140	2, 3
67	1400	1240			3
65	1208	1062			3
50	1050	1030			3
23	460	420			4(C)

Presenting the results in the form shown in Figure 5 does not imply that f_P^L is necessarily a function which is independent of the MWD. An experiment is reported elsewhere[21] which bears on the possible dependence of f_P^L upon the initial MWD. Sample 40 of the previous paper[21] (shown in Figure 2 of this communication as being prepared by dissolution at 87.6°C) was crystallized and then filtered at 70°C. A GPC analysis of the crystal phase was then made (Fig. 7 of ref. 21). Analysis of this trace as compared with that of the initial fraction suggests that in this experiment f_P^L is rather smaller than for the case when f_P^L is measured from material fractionated from the whole polymer. In other words, for the lower initial molecular weight material fractionated, a higher proportion of a given molecular weight crystallizes. It is likely therefore that f_P^L does depend on the initial MWD, although unfortunately the data are not sufficient to justify a detailed discussion of this point.

LIQUID–CRYSTAL PHASE SEPARATION

The measurements described here illustrate clearly that different molecular weight species segregate between the liquid and crystal phases. The issue arises of whether this separation can be described as being largely due to kinetic or thermodynamic factors. The approach adopted here is to enquire how good an approximation is the assumption that only thermodynamic considerations need be invoked. In support of this is the observation that the same separation is achieved whether the final state is approached from a less crystalline state (when crystallizing), or from a more crystalline state (dissolution). The dissolution experiment comprises an initial crystallization period, followed by slow cooling, then slow heating, and then a further period at the initial crystallization temperature. The experiment therefore requies that all crystals forming on cooling dissolve again after the temperature has been raised to the initial crystallization temperature. If the fractionation is to be explained mainly on the basis of kinetic factors, these crystals would probably remain undissolved on heating.

One factor which might seem to preclude a purely thermodynamic approach is that once a crystal portion has been enclosed behind a growing face, one would not expect molecules from that portion to be able to dissolve again. A modification of the thermodynamic treatment which allows for this is described in what follows.

There are still uncertainties in the calculation even after allowing for the neglect of kinetic factors. One of the most important is the form of the entropy of mixing for the mixing of polymer chains of different species. The degree to which different chains can mix is dependent on which model is assumed for the structure of the solution and crystal: in the present case two plausible assumptions are made, and the resulting differences are discussed.

LIQUID–CRYSTAL PHASE EQUILIBRIA

This analysis follows in outline that of Kawai.[17,18] For crystals and solution in equilibrium, we have

$$\mu_P{}^{\mathrm{L}} - \mu_P{}^{\mathrm{o}} = \mu_P{}^{\mathrm{S}} - \mu_P{}^{\mathrm{o}} \tag{1}$$

where $\mu_P{}^{\mathrm{L}}$ and $\mu_P{}^{\mathrm{S}}$ are the chemical potentials of the species with degree of polymerization P in the solution and crystal respectively; these states include many other species. Here, $\mu_P{}^{\mathrm{o}}$ refers to a hypothetical liquid polymer containing only species P. The left-hand side of eq. (1) can be evaluated following Flory:[24]

$$\mu_P{}^{\mathrm{L}} - \mu_P{}^{\mathrm{o}} = RT\{\ln v_P{}^{\mathrm{L}} - (x - 1) + V_{\mathrm{L}}x[1 - (1/\bar{x}_n)] + \chi_1 x(1 - V_{\mathrm{L}})^2\} \tag{2}$$

where $v_P{}^{\mathrm{L}}$ is the volume fraction of species P in solution, R and T have their usual meaning, and x is defined by

$$x = P/x_1$$

x_1 being the ratio of the molar volume of the solvent to the volume of the polymer repeat unit, V_{L} is the total volume fraction of polymer in solution, $\bar{x}_n$ is the number-average value of x, and χ_1 is a parameter which describes the energy of interaction of adjacent solvent molecules and polymer repeat units.[24]

Equation (2) contains terms which allow for the entropy of mixing which results when the species P is mixed in solution with other species in the polydisperse material. The right-hand side of equation (1) can be rewritten as:

$$\mu_P{}^{\mathrm{S}} - \mu_P{}^{\mathrm{o}} = (\mu_P{}^{\mathrm{S}} - \mu'_P{}^{\mathrm{S}}) - (\mu'_P{}^{\mathrm{S}} - \mu_P{}^{\mathrm{o}}) \tag{3}$$

where $\mu'_P{}^{\mathrm{S}}$ refers to the monodisperse crystalline state. The term $(\mu_P{}^{\mathrm{S}} - \mu'_P{}^{\mathrm{S}})$ depends on the degree of mixing of different species in the crystals. For a crystal phase which can readjust to give the most likely distributions of species, there are two extreme cases. It is conceivable that the mixing between species is comparable with that in the solution; the calculation of Kawai effectively makes this assumption (see below). It is also possible that all folds are adjacently reentrant, so that the mixing is that which follows from rearranging a one-dimensional array of separate molecules. On this assumption the number of ways of arranging the molecules is given by

$$\Omega = n!/\prod_i (n_i!)$$

where n is the total number of molecules and n_i is the number with degree of polymerization i. On applying Stirling's formula, the entropy of mixing S in the crystal is given by

$$S = -R\sum_i n_i \ln \left[n_i \Big/ \left(\sum_i n_i \right) \right]$$

whence

$$\mu_P^S - \mu'_P{}^S = RT \frac{\partial}{\partial n_P} \sum_i \{ n_i \ln \left[n_i \Big/ \left(\sum_i n_i \right) \right] \}$$

$$\mu_P^S - \mu'_P{}^S = RT \frac{\partial}{\partial n_P} \{ \sum_{i \neq p} \left[n_i \left(\ln n_i - \ln \sum_i n_i \right) \right] \}$$

$$+ RT \frac{\partial}{\partial n_P} \left[n_P \left(\ln n_P - \ln \sum_i n_i \right) \right]$$

$$\mu_P^S - \mu'_P{}^S = RT \ln (n_P/n)$$

$$\mu_P^S - \mu'_P{}^S = RT \ln (v_P^S \bar{P}_n/P) \tag{4}$$

where v_P^S is the volume fraction of species P in the crystal, and $\bar{P}_n$ is the number average value of P.

For a crystal of monodisperse polymer,

$$\mu'_P{}^S - \mu_P{}^o = \frac{\partial}{\partial n_P} [n_P(P\Delta G_u + 2\Delta G_e)] \tag{5}$$

where $\Delta G_u = \Delta G_u(T,T_x)$ is the free energy difference per mole of repeat units between the monodisperse liquid and crystal (T_x is the crystallization temperature) and $\Delta G_e(T,T_x)$ is the modification of this value which results from the presence of molecular ends. Equation (5) assumes that ΔG_e is proportional to the number of ends. This separation of a term describing the thermodynamic effect of chain ends is plausible in view of the way in which the melting points of paraffins can be described.[25,26] In the case of paraffins modifications of this dependence have been proposed,[26,27] but nevertheless eq. (5) is likely to be a useful first approximation.

Combining eqs. (1)–(5), we obtain:

$$RT\{\ln v_P^L - (x-1) + V_L x[1 - (1/\bar{x}_n)] + \chi_1 x(1 - V_L)^2\}$$

$$= \ln (v_P^S \bar{P}_n/P) + P\Delta G_u + 2\Delta G_e \tag{6a}$$

Terms in V_L can be ignored for low concentrations of polymer in solution.[18] Putting $x = P/x_1$, we can rewrite eq. (6a) as:

$$RT \ln v_P^L - \ln (v_P^S \bar{P}_n/P) = 2\Delta G_e - RT + P\{\Delta G_u$$

$$+ (RT/x_1)(1 - \chi_1)\} \tag{6b}$$

and solve to obtain

$$v_P^L/v_P^S = (B/P) \exp\{-\sigma P\} \tag{7}$$

where

$$B = \bar{P}_n \exp\{2\Delta G_e/(RT) - 1\} \tag{8}$$

and

$$\sigma = -\Delta G_u/(RT) - (1/x_1)(1 - \chi_1) \tag{9}$$

Equation (7) is similar to eq. (19) of Kawai,[18] except for the term $1/P$. This arises from the entropy of mixing [eq. (4)]. Kawai concluded that the entropy of mixing in the crystal was negligible; in this case one would expect in eq. (3) that $\mu_P{}^S - \mu'_P{}^S = 0$. Equation (7) would then contain no dependence on $v_P{}^S$, so that $v_P{}^L$, the concentration in the solution, would be independent of the concentration in the solid. In fact eq. (10) of Kawai does introduce a mixing term; this then introduces a dependence upon $v_P{}^S$, and thereby a result the same as for the liquid–liquid system is obtained [eq. (19) of Kawai].

The fraction $f_P{}^L$ of polymer of species P in the liquid phase is given by:

$$f_P{}^L = V'v_P{}^L/(V'v_P{}^L + V''v_P{}^S) \tag{10}$$

where V' and V'' are the volumes of liquid and solid phases, respectively, containing species P. If the assumption is made that V'' is the total crystal volume, the assumption is again made that the crystalline phase is homogeneous. Combining eq. (10) with eq. (7) yields

$$f_P{}^L = 1/(1 + KP \exp\{\sigma P\}) \tag{11}$$

where

$$K = V''/(V'B) \tag{12}$$

This compares with the eq. (22) of Kawai, which is of the form

$$f_P{}^L = 1/(1 + R_1 \exp\{\sigma P\}) \tag{13}$$

where R_1 is a constant.

This is of the form calculated for the liquid–liquid system.[16,24]

Equations (11) and (13) refer to crystals which can readjust themselves (while remaining lamellar) so as to achieve the most likely mixing of different species. An alternative is to assume that only the crystal edges can readjust. One can then apply eqs. (11) or (13) to a system which consists of the solution plus a narrow band of crystal. It is then necessary to assume that eq. (11) or (13) can be applied even when the crystal edge is still growing, i.e., when it is certainly not in complete equilibrium. This may in fact be justified, since in an analogous case of two species of paraffin molecules, calculations have been made which suggest that even when there is a net flux of molecules on to the crystal, the composition of the crystal will still approximate to the composition at equilibrium (Figs. 3 and 4 of Lauritzen et al.[28]).

Equation (11) or (13) can then be applied to successive layers of the crystal, each of which in turn reaches equilibrium with the solution. The distribution which is now partitioned between the liquid and solid phase is not the initial distribution of the polymer, but is determined by the solution phase corresponding to the previous layer-plus-solution system. Equations (11) and (13) then become, when crystallization is complete, respectively:

$$f_P{}^L = [1 + K(N)Pe^{\sigma P}]^{-N} \tag{14}$$

and

$$f_P{}^{\mathrm{L}} = [1 + K(N)Pe^{\sigma P}]^{-N} \tag{15}$$

where N is the number of layers. The parameters K and R_1 are now defined differently, in that V'' is now only the volume of one layer, which in turn is dependent on N, and $\bar{P}_n$ will vary continuously during crystallization, so that K depends not on one single value of $\bar{P}_n$, but on a particular average of the values of $\bar{P}_n$ appropriate for the solution phase at various stages of growth.

COMPARISON WITH EXPERIMENT

Analytical Form of $f_P{}^{\mathrm{L}}$

Equations (11) and (13) can be rewritten in linear form; eq. (11) becomes

$$\ln\{1/(P)[1/(f_P{}^{\mathrm{L}}) - 1]\} = \sigma P + \ln K \tag{16}$$

and eq. (13) becomes:

$$\ln[1/(f_P{}^{\mathrm{L}}) - 1] = \sigma P + \ln R_1 \tag{17}$$

Figure 6 shows an example of the experimental data plotted in these forms. An approximately linear set of points is given in most cases. Equation (17) [corresponding to eq. (13)] gives in general a slightly kinked line as illustrated in Figure 6. Equation (16) [corresponding to eq. (11)] shows no such systematic kink. Equations (11) and (13) were fitted to the data by constructing straight lines as in Figure 6.

Equations (11), (13), (14), and (15) were fitted to the data by using a least-squares-fit computer program. The standard deviations s of the experimental data compared with the computed $f_P{}^{\mathrm{L}}$ are included in Table II. These also suggest that eq. (11) is rather better than eq. (13) for describing the results; they also show that eqs. (14) and (15) are much worse. Figure 7 illustrates an example of experimental and the corresponding computed $f_P{}^{\mathrm{L}}$.

The conclusions are general to most of the sets of data for different T_x; however for $T_x = 50°\mathrm{C}$ the experimental results are of rather poor quality, and for $T_x = 23°\mathrm{C}$ none of the equations were capable of fitting the results well.

Measurement of Parameters and Comparison with Predicted Values

The parameters σ, R_1, K, and N can be measured from the curve-fitting procedures just described.

In eqs. (12) and (13), N is not an independent variable, since it is inversely proportional to the volume V'' of the layers for which the parameters R_1 and K are relevant. For convenience N was taken as a large number (1000). If, in fact, N is larger, the binomial theorem ensures that re-

TABLE II

Parameters Calculated by Fitting the Results to Equations Derived on the Basis of Equilibrium between Crystal and Solution

T_x, °C	Initial polymer concn (2 per ml of solvent)	State[a]	By eq. (11)					By eq. (13)			By eq. (14)			By eq. (15)		
			Computer method			Graphical method										
			$\sigma \times 10^3$	$K \times 10^3$	s	$\sigma \times 10^3$	$K \times 10^3$	$\sigma \times 10^3$	$R_1 \times 10^3$	s	$\sigma \times 10^3$	$NK \times 10^3$	s	$\sigma \times 10^3$	$NR_1 \times 10^5$	s
23	0.0075	X	148	0.0097	0.07	202	8.10^{-5}	165	0.2	0.076	100	0.53	0.14	116	1.2	0.14
50	0.0075	X	83	0.0047	0.051	87	0.004	95.6	0.18	0.049	44.8	0.12	0.045	54.3	4.4	0.047
67	0.0075	X	26.2	0.22	0.022	27	0.18	33	11	0.018	14	0.67	0.023	21	33	0.034
70	0.0075	X	24	0.25	0.0115	23	0.32	29.6	16	0.016	11	0.98	0.039	16.5	62	0.05
72.6	0.0075	X	18.3	0.17	0.026	18.2	0.15	23.2	11	0.024	10	0.42	0.049	15	28	0.065
75.1	0.0001	X	25.6	0.046	0.019	27	0.028	30.2	2.6	0.026	14.3	0.16	0.076	18.8	12	0.087
83.5	0.0001	X	13.8	0.027	0.022	13	0.028	16.7	3.2	0.02	8.25	0.093	0.051	11.3	10	0.06
87.6	0.0075	X	7.04	0.055	0.019	7.3	0.042	8.9	10	0.021	3.87	0.16	0.045	5.78	28	0.058
87.6	0.0075	D	11.1	0.021	0.027	8.6	0.012	13.1	3.3	0.018	5.26	0.11	0.069	7.5	16	0.09
87.6	0.0075	D	8.51	0.079	0.022	8	0.042	10.9	12	0.025	5.2	0.18	0.042	7.58	26	0.05
90	0.0075	X	5.13	0.13	0.027	5.68	0.18	6.9	23	0.037	2.75	0.25	0.063	4.63	42	0.088
90	0.0075	D	6.32	0.1	0.016	7.3	0.042	8.16	17	0.03	3.25	0.23	0.067	5.14	38	0.09
92.8	0.0075	X	1.23	0.12		1.14	0.17	1.76	73		0.6	0.18		1.11	110	

[a] X denotes crystallized; D denotes dissolved.

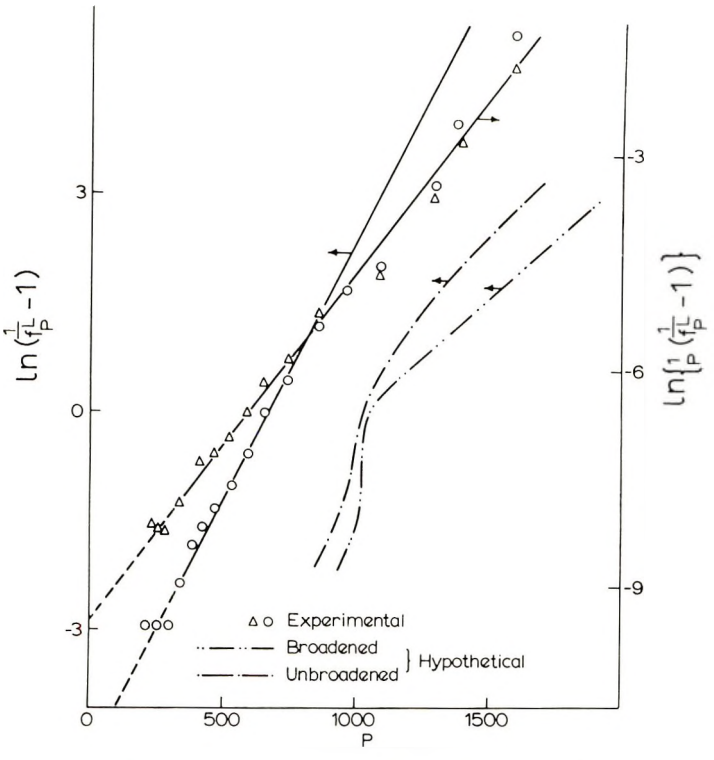

Fig. 6. Example of a plot of functions of f_P^L against degree of polymerization P, designed to check two of the predicted forms for the separation function [eq. (11), right-hand ordinate; eq. (13), left-hand ordinate]. Also shown are curves resulting from a similar analysis of hypothetical Gaussian separation function f_P^L (see the discussion). These latter differ to a degree estimated from the effect instrumental broadening should have.[23]

sulting values of $f_P{}^L$ are the same, as long as the product NV'' remains constant. Table II shows values of σ, R_1, K, NR_1, and NK appropriate to the four equations considered. Clearly, if the fit is not good, the values of these parameters are uncertain: an extreme case is when $T_x = 23°C$, where two different ways of fitting the same equation give very different values for the parameters σ and K.

Estimation of σ. For all the predicted forms for $f_P{}^L$, σ is given in terms of the supercooling as expressed in eq. (9), and ΔG_u refers to crystals with no free energy contribution from ends, but with a lamellar form. In this way, we have

$$\sigma = (-\Delta G_u{}^\circ/RT) - (2m\Delta G_s/l) - [(1/x_1)(1 - \chi_1)] \qquad (18)$$

where $\Delta G_u{}^\circ$ is the free energy of a large perfect crystal, $\Delta G_s = \Delta G_s(T,T_x)$ is the surface free energy, m is the volume of a mole of crystalline polymer, and l is the lamellar thickness. The last term in this equation, $[(1/x_1)(1 - \chi_1)]$, can be evaluated from dissolution points.[18,29] The free energy

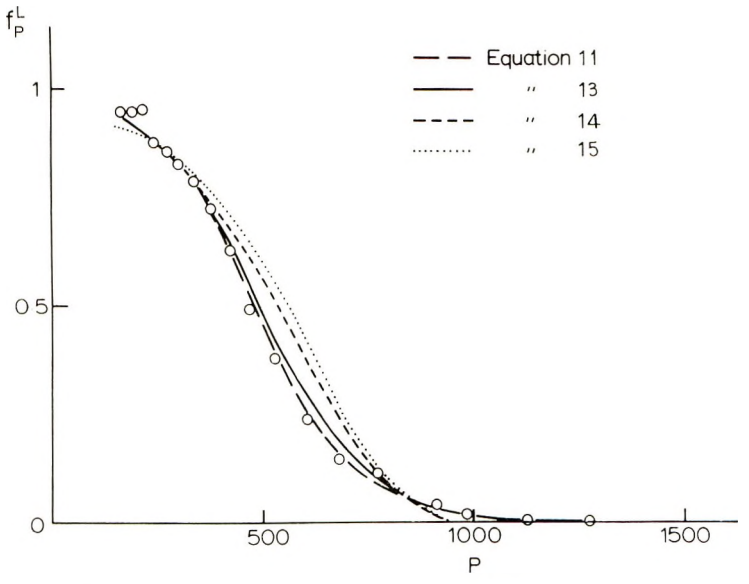

Fig. 7. Detailed illustration of a typical measured f_P^L, together with four analytical f_P^L derived by computer fitting of the data. The sample measured in this example was filtered at 90°C after dissolution. N was taken as 1000 (this is not critical: see text).

ΔG_u° is given by[18,25,26]

$$\Delta G_u^\circ = -\Delta H_u[1 - (T/T_m^\circ)] \tag{19}$$

where ΔH_u and T_m° are the enthalpy and melting point of the "perfect" crystal.

A difficulty in comparing eq. (18) with experiment is the large uncertainty in ΔG_s. For this reason the comparison is made in the following way. Figures 8*a* and 8*b* show the values of σ obtained from fitting eq. (11) with experiment. Also shown in Figure 8*b* is

$$(\sigma + 2m\Delta G_s/l) = -\Delta G_u^\circ/RT - (1/x_1)(1 - \chi_1)$$

as given by eqs. (18) and (19), for $\Delta H_u = 1000$ cal/mole $= 3.18 \times 10^{10}$ erg/mole;[25] $T_m^\circ = 418$°K;[27] $(1/x_1)(1 - \chi_1) = 8.05 \times 10^{-2}$.[29] It can be seen that both this function and the experimental values of σ are linear with $1/T_x$. The large difference between the two sets of results in Figure 8*b* can be equated with the surface term $2m\Delta G_s/l$. Figure 9 shows values of ΔG_s calculated from this difference; l values were taken from low-angle x-ray measurements. Several determinations were made on crystals grown in the present experiments: for $T_x = 20$°C, $l = 90$°A; for $T_x = 50$°C, $l = 90$ Å; for $T_x = 70$°C, $l = 105$ Å; for $T_x = 90$°C, $l = 165$ Å. Values for l at other T_x were interpolated. The lower curve in Figure 9 shows ΔG_s calculated on the assumption of other values for the parameters ΔH_u, T_m°, and $(1/x_1)(1 - \chi_1)$, the ones quoted by Kawai,[18] i.e., 918 cal/mole, 414.3°K, and 9.03×10^{-2}, respectively.

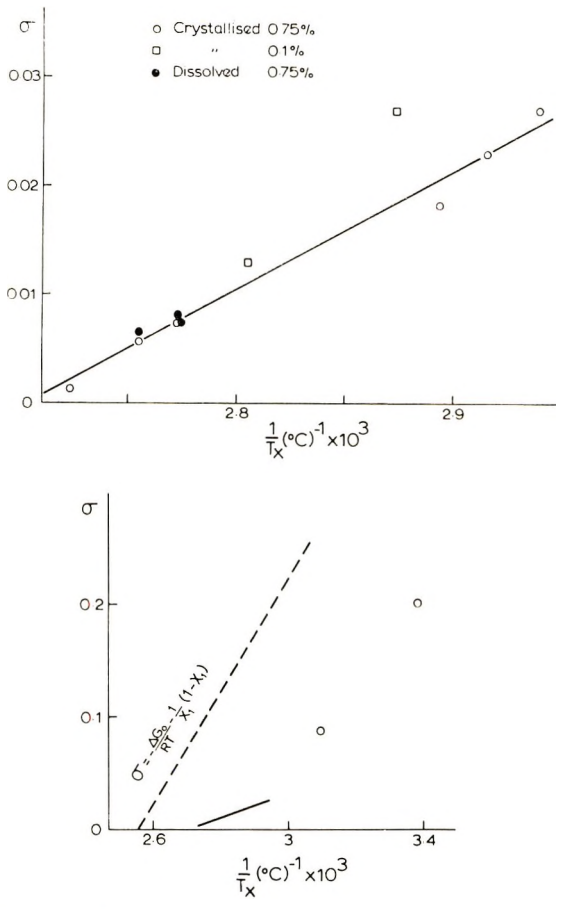

Fig. 8. Experimental values of σ calculated from graphical comparisons of eq. 11 with the data (see also Table II) shown as a function of $1/T_x$: (*a*) individual values of σ for T_x between 92.8°C and 67°C; (*b*) values of σ in (*a*) are shown as a solid line; in addition are shown rather less certain values of σ for T_x = 50°C and 23°C. The broken line shows the predicted values of σ minus the surface-free-energy term [see eqs. (18) and (19)].

Figure 9 now serves as a test of eq. (9) for calculating the quantity σ. It can be seen that the values of ΔG_s which have to be taken to make eq. (11) fit the results are reasonable; also shown in Figure 9 are values of surface free energy calculated from a kinetic theory of folding,[30] which have been shown to be consistent with thermal measurements on single crystals. None of the results for σ shown in Table II would give completely unreasonable values of ΔG_s, though those given by fitting eqs. (14) and (15) would be rather high.

Estimation of the Pre-exponential Terms. Values of K, R_1, NK, and NR_1 shown in Table II vary widely; in general, however, they are of the order of 10^{-4}, 10^{-2}, 10^{-4}, and 10^{-2}, respectively. From eqs. (8) and (12), we obtain

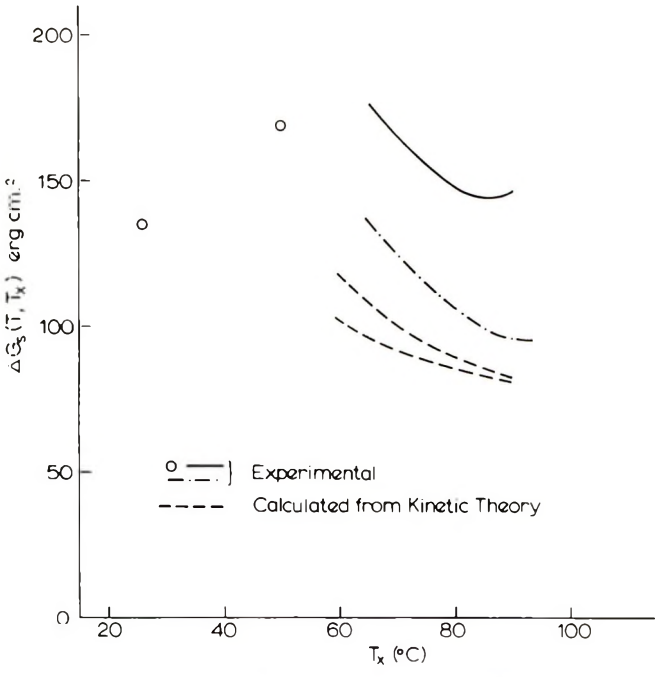

Fig. 9. Values of the free energy attributable to the surfaces of the lamellae, calculated from the difference between measured values of σ and those calculated with no account taken of the surface contribution (Fig. 8*b*). These experimental curves are plotted by using two sets of input data; the upper one (solid line) with ΔH_u° according to Broadhurst,[25,26] and $(1/x_1)(1 - \chi_1)$ according to Mandelkern et al.,[29] the lower one by using the data assumed by Kawai.[18] Also shown are independently estimated values of the surface energy, according to Hoffman et al.[30] The two curves refer to alternative values of ϕ, a parameter which defines the proportion of free energy excess in the forward and backward nucleation processes.

$$K = (V''/V'P_n) \exp\{1 - 2\Delta G_e/RT\} \tag{20}$$

For the higher initial concentration used, V''/V' is slightly less than 0.0075 (most of the polymer has crystallized). For Marlex 6009, the polymer employed, $\bar{P}_n$ is about 600. In this way, from eq. (20), $2\Delta G_e/RT$ is about -1. This is physically unreasonable, since chain-folded crystals of low molecular weights melt at a lower temperature than those of higher molecular weights. Thus, ΔG_e should be positive.

If the results of Kawai[18] are written in the same notation as above, we have

$$R_1 = (V''/V') \exp\{1 - 2\Delta G_e/RT\} \tag{21}$$

In this case $2\Delta G_e/RT$ is calculated to be about $+1$.

In summary: assuming eq. (11), $2\Delta G_e/RT$ is small and negative; assuming eq. (13), it is small and positive. Results are similar in the case of eqs. (14) and (15).

The parameter ΔG_e is a measure of the effect of molecular weight on the

stability of molecules in lamellar crystals with respect to the solution. In principle, this quantity can be assessed independently from melting or dissolution points, but such a determination is rather uncertain.[31] Nevertheless we should ask whether the results given above for ΔG_e are unreasonable. A simple, if rather crude, test is to compare the melting points of paraffins with lamellar crystals of approximately the same thickness containing high molecular weight polyethylene. Paraffin C_{100} crystals melt at about 110°C;[32] polyethylene crystals of thickness 105 Å or more melt at about 120°C. Since perfect high molecular weight crystals should melt at about 145°C, it can be seen that the depression of the melting point of these systems is similar. This suggests that ΔG_e is small compared with the total free energy defect. For paraffins the total free energy defect per mole of two ends is $10RT$,[27] so that the results that[2] $\Delta G_e \approx RT$ deduced from the fractionation is probably not unreasonable.

DISCUSSION

It is confirmed that segregation according to molecular weight can be important in the crystallization of polyethylene from solution. The GPC results are presented in Figures 1–5, although a more accurate representation of the results is given by Table II. (The standard deviations s indicate which fitted equation describes the results most precisely.) A fairly detailed description of the MWD in the separated phases is given in this way, although, because of the neglect of instrumental broadening, the sharpness of the separation is slightly underestimated.

From a practical point of view, it is hoped that some estimate can now be made of the effects on other measurements of the segregation by molecular weight which may occur during the preparation of crystals from solution. In addition, a guide is provided for the use of fractional crystallization for the production of low molecular weight fractions of polyethylene.

It has been shown[3–5,33] that segregation by molecular weight occurs during the formation of large extended-chain crystals: molecules of similar length crystallize together from the polydisperse melt. Fractionation during crystallization from the melt may also be important in other ways,[1,6,7] but is rather intractable experimentally because of the difficulty of separating crystalline and noncrystalline regions for molecular weight analysis. The present results may be of some interest in this context, since some features of fractional crystallization are likely to be common to the melt and to the solution.

When considering the best way to explain the fractionation from solution, the particular interest is the usefulness of the equilibrium approach. The remainder of the discussion is therefore devoted to this point.

Application of the Equilibrium Approach

A short discussion has been given above of *a priori* reasons why an equilibrium approach should not be valid. The preceding analysis takes

account of one of these reasons, namely that the crystals are unlikely to readjust after growth. Another significant objection is that polymer crystallization is controlled to some extent, if not largely, by kinetic factors: the lamellar nature of the crystals is usually attributed to the kinetics of the nucleation process. It was on this basis that lack of fractionation in the case of poly(ethylene oxide) in pure solvents was explained.[34] It is, however, possible that the phase separation valid for a crystal–liquid interface, across which there is a significant transport of polymer, may satisfactorily be approximated by the separation calculated for equilibrium. This result has been predicted for paraffin mixtures[28] and it is possible that it may apply also to the more complex chain-folded system.

Comparison with Experiment

It may well therefore be premature to reject completely a basically thermodynamic approach, even if more fundamental modifications than presented here would be necessary in a definitive theory of fractionation. In support of this is the GPC evidence, which may be discussed in three parts.

A significant feature of the experimental results is that the same fractionation is achieved whether the final state is approached from more fully crystalline or more fully dissolved states. This result would be expected if the system was in equilibrium; if lower molecular weights remained in solution as a result of kinetic factors, one may well expect the fractionation to differ according to the direction of approach to the final state.

Secondly, the form of the function $f_P{}^L$ as measured fits very well the predicted eqs. (11) and (13) (Figs. 6 and 7) although eqs. (14) and (15), which result if one assumes that the crystals cannot readjust after growth, fit less exactly (Table II).

Lastly, the parameters which need to be assumed in order to reach agreement are reasonable. The values of surface free energies calculated from the fractionation results by using eq. (11) (Fig. 9) agree well with independently determined values.

Equations (11) and (13) also yield reasonable values for the pre-exponential parameter (K or R_1), when it is considered that this is the quantity most difficult to predict, and that it is the quantity most liable to be in error because of the neglect of instrumental broadening in this analysis.*

* This may be illustrated by the plot in Figure 6 of hypothetical functions $f_P{}^L$. The hypothetical $f_P{}^L$ obey a Gaussian distribution with respect to the GPC elution volume (i.e., to ln P); for this form of MWD the effect of broadening can be readily assessed.[23] The "unbroadened" curve corresponds to what would be the true MWD, and the "broadened" one to what would be the corresponding chromatogram. It can be seen that if straight lines were constructed with the same general slope as these two curves, the effect of the broadening would be to alter considerably their intercepts on the ordinate. In this way the values of the parameters K and R_1, and therefore of ΔG_e [see eqs. (20) and (21)], are made uncertain by the neglect of instrumental broadening. This may explain the anomalous negative values for ΔG_e.

It is hoped that the foregoing will enable a judgment to be made of how well the results can fit predictions based on a thermodynamic approach. It is for this reason that the four relations, eqs. (11), (13), (14), and (15), are all considered. Equations (11) and (13) result if the crystal phase can readjust after growth, (14) and (15) if it cannot. It has already been noted that the former two fit the results much better than the latter two, which would imply that the crystals can readjust with respect to the phase separation. This is an unexpected result, and if it is not fortuitous will almost certainly require some modification of existing kinetic theories of crystallization. The other pair of alternatives considered result from different entropies of mixing for the crystal phase. Both assume that the solution phase obeys the expression derived for concentrated solutions.[24] If the molecules mix to the same degree even in the crystal phase, one obtains eq. (13) or (15). If, however, the molecules in the crystal can exchange position but cannot intermingle, eqs. (11) or (14) are obtained. The experimental results do not clearly distinguish between eqs. (11) and (13); the form of eq. (11) fits the results rather better, but eq. (13) yields more reasonable values for ΔG_c. A better test would be to obtain more results using different initial MWD, since eq. (10) includes a dependence on $\bar{P}_n$ for the unfractionated material. For the one result of this kind reported here, there is a suggestion that f_P^L is lower for a lower initial average molecular weight; this is what would be expected from eqs. (11) or (20).

There are certainly other possibilities in the treatment which have not been considered here. For example, fold length l for a given T_x depends on molecular weight.[21,35] If the crystal phase cannot readjust after growth, the value for l should be put equal to the thickness of the crystal edge. Since the molecular weight constitution of the edge changes during growth, l will vary, and can no longer be considered a constant. However, l varies significantly with molecular weight only for low molecular weights, so that this consideration should only apply to the lower values of T_x.

In summary, the two tests applied to the experimental results for comparison with predictions, i.e., the analytical form of the separation, and the numerical values of parameters, show that an equilibrium theory can predict very well the experimental results. Also, the assumption that the crystals can always readjust by exchanging molecules with the solution gives much better agreement than assuming that the centres of crystals are sealed off from the solution. The agreement does not however depend critically on the assumptions which are made concerning the entropy of mixing in the crystal phase.

CONCLUDING REMARKS

We have verified and documented fractionation during crystallization to an extent which has not, to our knowledge, been reported before. Further, the results can be described by analytical expressions in quantitative agreement with experiment. The best agreement is obtained on the assumption

that there is continuous readjustment between the whole of the crystal and the solution as regards molecular weight composition. It is true that this assumption may seem unrealistic from the point of view of existing knowledge: crystals once formed are not likely to exchange molecules with the solution from their interior. For this reason, one may judge that the better agreement for eqs. (13) and (15) is coincidental, and that kinetic factors (for example) explain the discrepancies found when eqs. (14) and (15) are used. On the other hand, one may search for a justification for the rather remarkable fit achieved with eqs. (13) and (15). One such justification could be based on the striking similarity of the experimental results with those expected from liquid-liquid systems. A similar result for poly(ethylene oxide) in a two-solvent system has been explained on the basis of liquid–liquid separation prior to crystallization.[34] In the present case, however, one would have expected that a concentrated solution phase would not be stable, neither has any evidence for liquid–liquid separation in the polyethylene–xylene system been reported previously.

In the meantime both the experimental findings themselves and the analytical formulation can be used for the study of crystallization, for predicting the molecular composition of crystals, and for preparing fractions in a predictable way.

I would like to express my gratitude to Professor A. Keller for his supervision and encouragement. I would like to thank Dr. T. Williams and Professor I. M. Ward for passing the samples through a chromatograph, and for making available a calibration. I am grateful to Dr. A. Stejny for guidance during the formulation of the section on liquid–crystal phase equilibria and to Professor F. C. Frank for his comments. I would like to thank the S.R.C. for financial support.

References

1. H. D. Keith, *Kolloid Z. Z. Polym.*, **231**, 429 (1969).
2. F. R. Anderson, *J. Appl. Phys.*, **35**, 64 (1964).
3. T. Kawai *Makromol. Chem.*, **84**, 294 (1965).
4. R. B. Prime and B. Wunderlich, *J. Polym. Sci. A-2*, **7**, 2061 (1969).
5. R. B. Prime and B. Wunderlich, *J. Polym. Sci. A-2*, **7**, 2073 (1969).
6. T. Kawai, *Makromol. Chem.*, **84**, 290 (1965).
7. T. Kawai, *Kolloid Z. Z. Polym.*, **229**, 116 (1969).
8. S. W. Hawkins and H. Smith, *J. Polym. Sci.*, **28**, 341 (1958).
9. A. Keller and A. O'Connor, *Polymer*, **1**, 163 (1960).
10. T. Kawai and A. Keller, *J. Polym. Sci. B*, **2**, 333 (1964).
11. R. Koningsveld and A. J. Pennings, *Rec. Trav. Chim.*, **83**, 552 (1964).
12. Pennings, A. J., *J. Polym. Sci., C*, **16**, 1799 (1967).
13. P. W. O. Wijga, I. van Schooten, and J. Boerma, *Makromol. Chem.*, **36**, 115 (1960).
14. A. J. Pennings, *Proceedings of the International Conference on Crystal Growth, Boston*, Pergamon Press, Oxford, 1966, p. 389.
15. M. L. Huggins, *J. Amer. Chem. Soc.*, **64**, 1712 (1942).
16. M. J. R. Cantow, Ed., *Polymer Fractionation*, Academic Press, New York, 1967.
17. T. Kawai, *J. Polym. Sci. B*, **3**, 83 (1965).
18. T. Kawai, *Makromol. Chem.*, **102**, 125 (1967).
19. D. J. Blundell, A. Keller, and A. J. Kovacs, *J. Polym. Sci. B*, **4**, 481 (1966).
20. D. M. Sadler and A. Keller, *Kolloid Z. Z. Polym.* **239**, 641 (1970).

21. D. M. Sadler and A. Keller, *Kolloid-Z. Z. Polym.*, **242,** 1081 (1970).
22. D. M. Sadler and A. Keller, *J. Polym. Sci. A-2*, **8,** 1457 (1970).
23. T. Williams, Y. Udagawa, A. Keller, and I. M. Ward, *J. Polym. Sci. A-2*, **8,** 35 (1970).
24. P. J. Flory, *Principles of Polymer Chemistry*, Cornell Univ. Press, Ithaca, N. Y., 1953.
25. M. G. Broadhurst, *J. Res. Nat. Bur. Stand.*, **67A,** 233 (1963).
26. M. G. Broadhurst, *J. Res. Nat. Bur. Stand.*, **70A,** 481 (1966).
27. P. J. Flory and A. Vrij, *J. Amer. Chem. Soc.*, **85,** 3548 (1963).
28. J. I. Lauritzen, E. Passaglia, and E. A. Di Marzio, *J. Res. Nat. Bur. Stand.*, **71A,** 245 (1967).
29. J. F. Jackson, L. Mandelkern, and O. C. Long, *Macromolecules*, **1,** 218 (1968).
30. J. D. Hoffman, J. I. Lauritzen, E. Passaglia, G. S. Ross, L. J. Frohlen, and J. J. Weeks, *Kolloid Z. Z. Polym.*, **231,** 564 (1969).
31. T. Kawai, *Kolloid Z. Z. Polym.*, **201,** 15 (1965).
32. G. Ställberg, S. Ställberg-Stenhagen, and E. Stenhagen, *Acta Chem. Scand.*, **6,** 313 (1952).
33. T. Kawai, K. Ehara, H. Sasano, and K. Kamide, *Makromol. Chem.*, **111,** 271 (1968).
34. C. Booth and C. Price, *Polymer*, **7,** 85 (1966).
35. T. Kawai, T. Hama, and K. Ehara, *Makromol. Chem.*, **113,** 282 (1968).

Received July 27, 1970
Revised October 12, 1970

JOURNAL OF POLYMER SCIENCE: PART A-2 VOL. 9, 801–814 (1971)

Relationship between Compressive Yield and Tensile Behavior in Glassy Thermoplastics

R. N. HAWARD,* B. M. MURPHY,† and E. F. T. WHITE,
Department of Polymer and Fibre Science, University of Manchester Institute of Science & Technology, Manchester 1, England

Synopsis

The effect of temperature and strain rate on the compressive yield behavior of polystyrene is compared with the effect of the same variables on crazing in tension. The results support the conclusion of other, more extensive work, which shows that crazing involves the same types of molecular processes as those which occur during deformation under compression and shear. An improved method of measuring compressive stress–strain curves is then described, and the compressive yield stress is also compared with an extrapolated tensile yield stress. The difference between the two is in line with concepts which assume a dependence of yield stress on the state of hydrostatic tension (or compression). It can be adequately described by the Mohr-Coulomb yield criterion. Application of this criterion also enables a theoretical stress strain curve in tension to be derived from other results in compression. Comparison of the tensile stress–strain curve so obtained with those which can be directly measured with other plastics, supports the hypothesis that crazing is favored by a marked decline in engineering stress during tensile elongation (plastic instability).

Introduction

Many aspects of the yield process in glassy thermoplastics are not yet well understood, despite the frequent occurrence of large deformations in which yielding has taken place. These deformations can occur either homogeneously over the whole test sample[1] or inhomogeneously, in which case only localized areas of the sample are plastically deformed. The necking of an extended sample[1–3] or the appearance of shear bands[4–6] as shown in Figure 1 (but which may be very much smaller), are the more obvious external features of an inhomogeneous yielding process. In extension, some materials, of which polystyrene is a notable example, fail by fracture before gross yielding can occur. Usually, in these materials however, there is strong evidence that locally large deformations have occurred within crazed regions.

These craze structures[7,8] consist of assemblages of microvoids embedded in a highly oriented and plastically deformed polymer matrix and are usually to be found on a freshly cleaved fracture surface or ahead of the tip of a prop-

* Present address: Centre for Materials Science, The University of Birmingham, Birmingham 15, England.

† Present address: Uniroyal Inc., Mishawaka, Indiana, U.S.A.

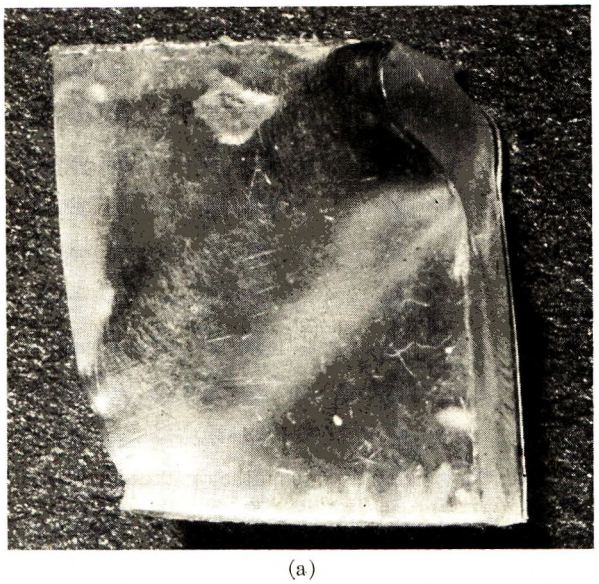

(a)

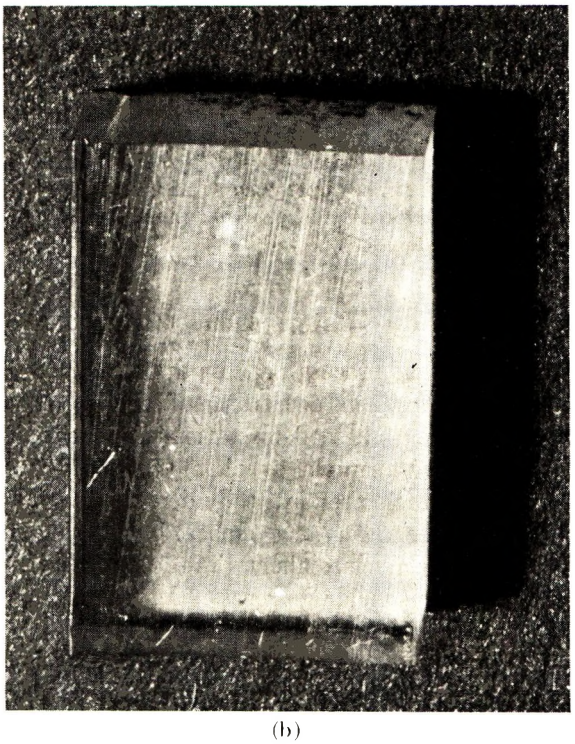

(b)

Fig. 1. Recovery of shear band: (*a*) a broad shear band produced by the compression of a rectangular polystyrene test piece; (*b*) after heating $1^1/_2$ hr at 110°C the original form of the test piece is recovered.

agating crack front. Thus, craze formation can be regarded as essentially an inhomogeneous yielding process. Some further evidence in favor of this view is presented in this paper.

Since the initiation and growth of craze structures are often the significant first steps in the fracture mechanism of organic glasses and are predominant factors in determining the energy associated with the growth of a crack, the concept of the essential similarity of crazing and yielding involves a departure from some of the concepts which have previously been used to interpret fracture processes in glassy thermoplastics. In general, yielding is to be regarded as a form of retarded high elasticity, in which a large non-Newtonian viscosity has been superimposed upon the restrictions due to that of the entangled polymer network, whose distortion leads to "orientation hardening" at high strains. However, even at the highest deformations where there are large molecular orientations, because of the high internal viscosity, these deformations will be only partially recoverable at room temperature. Nevertheless, even large plastic deformations are usually recoverable on annealing at temperatures close to the glass transition temperature of the material, as is shown by the recovery of the large shear band in polystyrene illustrated in Figure 1.

Crazing as a Yield Process

In their early work, Maxwell and Rahm[9] clearly associated the presence of crazes with a plastic deformation similar to creep. It has since become clear that the structure of a craze is that of microvoids surrounded by locally highly oriented material generally centered along a region of stress concentration of the applied stress field within a substantially unstrained glassy matrix. Sobolev[10] has shown how craze structures are generated by the stresses surrounding a circular hole in a polymeric sheet subject to tension. More recently, similar studies have been carried out by Sternstein and coworkers,[11,12] who suggested that the inhomogeneous plastic deformations leading to craze formation arose from a nonuniformity in the stress field owing to local discontinuities in the material. They found that crazing took place when the major principal stress exceeded a threshold value and that craze propagation followed in a direction transverse to the major principal stress vector.

Almost identical conclusions were reached by Murphy et al.[13] from an examination of the internal crazing of injection molded polystyrene test pieces in which crazes were initiated at points at which the variations in the orientation within the sample lead to the most favorable structure. Craze lines initiated at points within the material where the direction of orientation was transverse to the direction of applied stress. With minimal transverse orientation it was possible to measure the crazing stress of essentially unoriented polymer. These results are also in line with the work of Rehage,[14] who used isotropic and oriented poly(methyl methacrylate) specimens. The latter showed either a reduced tendency to craze or no crazing and the difference can be related to differences in the plastic deformation response beyond the yield point.[14]

In our previous work,[13] the effects of temperature and strain rate on the crazing process in glassy polystyrene were investigated, and it was shown by using the compressive yield stress–temperature data of Binder and Muller,[15]

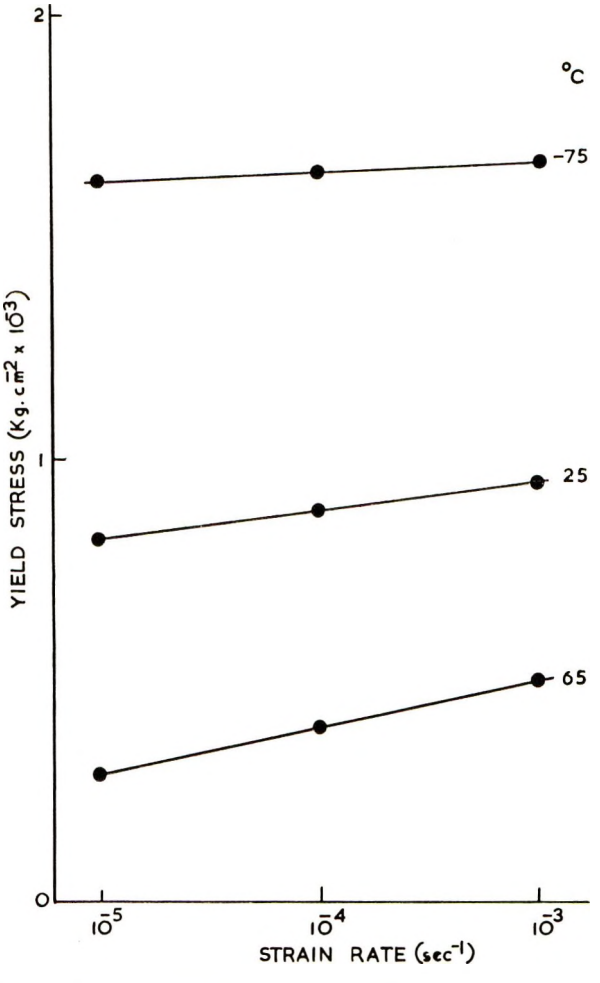

Fig. 2. Effect of strain rate on the yield stress of GP polystyrene in compression.

that the stress required to initiate craze formation (the crazing stress) responded to temperature in the same way as the yield stress. As will be shown later, we have been able to make new measurements of the compressive yield stress of polystyrene to cover a series of shear rates and temperatures and we are now able to investigate more fully the relation between yield and crazing behavior of polystyrene. Some of these results are shown in Figure 2, in which the compressive yield stresses obtained at various temperatures are plotted against the logarithm of strain rate for Carinex GP (molding grade) polystyrene. In each case a linear relation was obtained.

Comparison of these yield stress results with the previously obtained relationships between crazing and the stress-strain rate-temperature variables[13] is made in Figure 3. There is a broad similarity between the two sets of measurements which indicate response to temperature in a similar manner. However, we have not drawn a linear graph through Binder and

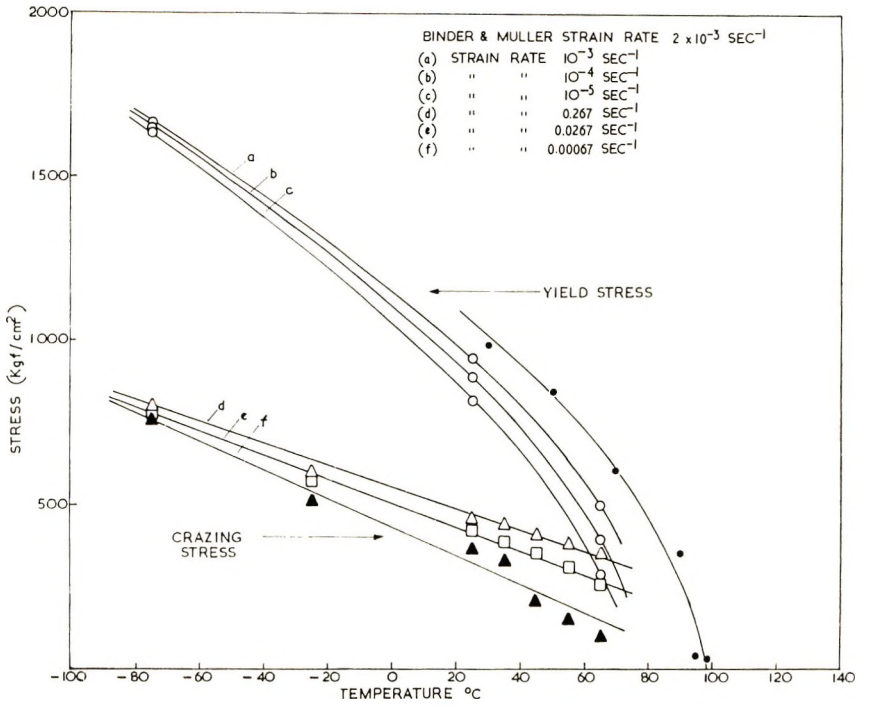

Fig. 3. Relations among yield stress, crazing stress, and temperature.

Muller's[15] data on this occasion, since recent work has clearly demonstrated that the relation between yield stress and temperature (constant strain rate) is not linear,[16,17] as indeed found by Binder and Muller[15] and confirmed in the experiments reported here. The differences involved, however, are not very large. It will also be seen that the crazing stress does not fall so sharply at high temperatures as the yield stress. This would be an expected result if crazing has to provide the nucleation surface energy for voids since this quantity would not be expected to change very quickly with temperature and would therefore be relatively more important at high temperature.

The strain rates indicated for the crazing stress experiments are those for the overall dimensional changes of the specimen and do not allow for the highly inhomogeneous character of the deformation. The true strain rate for these samples should be appreciably higher. Nevertheless, we have also plotted, in Figure 4, the slopes of the curves of yield stress against strain rate obtained from Figure 2 and the slopes of the crazing stress against log strain rate previously reported[13] as a function of temperature. Since these relations are generally linear over a wide range of strain rates (as in the Eyring equation), these results should now be more directly comparable irrespective of the actual strain rates employed and it is clearly seen that the two sets of data for crazing and yield respond to temperature in the same way. Support is thus given to the hypothesis that crazing and yielding are similar processes, in the sense that similar molecular conformation changes and molecular backbone motions are involved.

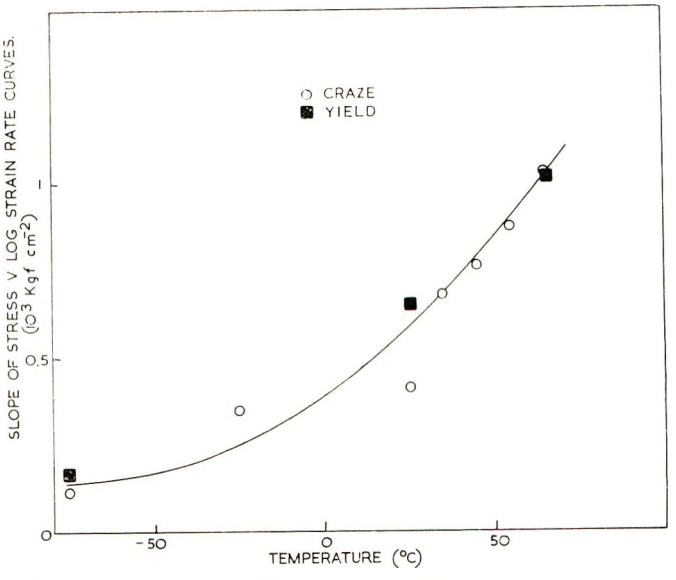

Fig. 4. Slopes of crazing and yield stress against log strain rate plotted as a function of temperature.

The two processes may also be analyzed by the Eyring treatment of viscous flow as employed by Coleman,[18] and in this way, similar values for the energies and volumes of activation may be obtained for each of them.[19] On account of the difficulties in the assignment of strain rates in the inhomogeneous deformations, much of this evidence is generally suggestive rather than quantitative. However, the occurrence of yielding and locally large plastic deformation in a craze is strongly supported by studies of the morphology of crazes such as those carried out by Kambour[7] and Van den Boogart[20] and by the electron micrography of fracture surfaces.[21,22]

Tensile and Compressive Yield of Polystyrene

The results considered above qualitatively compare the crazing behavior of polystyrene under tensile loading with homogeneous compressive yield. The former appears to have some analogies with homogeneous tensile yield, but, as shown by Whitney,[23] the compressive and tensile yield behavior of isotropic polymers are not identical, even though the fundamental molecular processes may be alike. Strictly, therefore, crazing processes should be compared with tensile yield experiments.

It is not usually possible to obtain directly the yield strength of polystyrene in tension since crazing and fracture intervene before sufficient stress can be applied to bring about bulk yielding. Nevertheless, it is possible to overcome this difficulty by the application of a large hydrostatic pressure as has been carried out by Holliday et al.[24] and Biglione.[25] Such methods make it possible for the tensile yield stress at zero applied pressure to be extrapolated from measurements made at different applied hydrostatic

pressures. Similarly, it may prove possible to obtain tensile yield stresses for variously oriented polystyrenes and to extrapolate the results to give the yield stress of an isotropic material. Alternatively, a more complete stress–strain curve may be produced in compression.[15]

Several different techniques have been described for measuring the yield strength of brittle polymers under the action of compressive forces, including the plane-strain procedure used by Ford,[26] Williams,[27] and by Bowden and Jukes.[28] Alternatively, the simple compression of cylinders between plates may be carried out and we describe an improved form of this procedure.

Compression Stress–Strain Curves for Polystyrene

The method adopted by Binder and Muller[15] for determining compressive strength was that of placing a polymeric cylinder between plates, applying a compressive strain, and measuring the resultant stress. Cylinders are usually preferred to rectangular test pieces as they are less prone to develop massive shear bands (Fig. 1). This procedure, although simple and practical, is open to theoretical criticism. It is apparent that the friction between the ends of the cylinder and the test apparatus prevents the former deforming in a uniform way, even at low strains, and results in the well known "barrel" type of distortion. Other test pieces, such as those used by Whitney,[23] in which a constricted neck is incorporated in the sample, are equally open to criticism since the boundaries of the deforming zone are rigidly attached to the remaining relatively undeformed part of the test piece.

In order to overcome these problems, Cooke and Larkes[29] suggested an experimental method for eliminating frictional end effects. Their method involves the compression of test pieces of identical cross section and varying length. The load required to create an identical compressive strain in each test piece is found and these load values are plotted against the diameter/length (d/l) ratio of the appropriate cylinders. The resulting linear plots are extrapolated to $d/l = 0$, thus allowing a value of the load required to cause the given deformation in a "very long" test piece to be estimated. By carrying out this procedure for a number of deformations, a load-strain plot can be produced for an idealized test piece in which frictional end effects have been discounted, and from these data, either a compressive or a true stress–strain curve may be produced. This technique has previously been used with metals, and the range of different strain rates to which the samples of different lengths are subjected is generally not important. However, as plastics are highly strain-rate-sensitive, we have modified the technique for use with polymers by compressing the samples and changing the crosshead speed for each cylinder length so that overall equality of average strain rate is achieved.

Sample Preparation and Testing

Well annealed, compression-molded, cylindrical test pieces of both Carinex GP and Carinex HR polystyrene were machined to produce cylin-

ders of $^{7}/_{16}$ in. diameter, and lengths of $^{5}/_{16}$, $^{5}/_{8}$, and $1^{1}/_{4}$ in. The ends of these samples were carefully polished with progressively finer grades of abrasive so that frictional end effects were minimized as far as possible. An Instron machine was used to compress the cylinders by means of a compression cage within the Instron environmental chamber. The compression platens were lubricated with molybdenum disulfide grease which Ford[26] recommends as the most satisfactory compression lubricant.

A constant strain rate of 10^{-3} sec^{-1} for all the test pieces, whose lengths are in the ratio 1:2:4, could be achieved by arranging the platen closing speeds to be in the same ratio.

Using these methods, we have obtained the lines shown in Figure 5 which shows that the extrapolation technique works well at low strains but begins

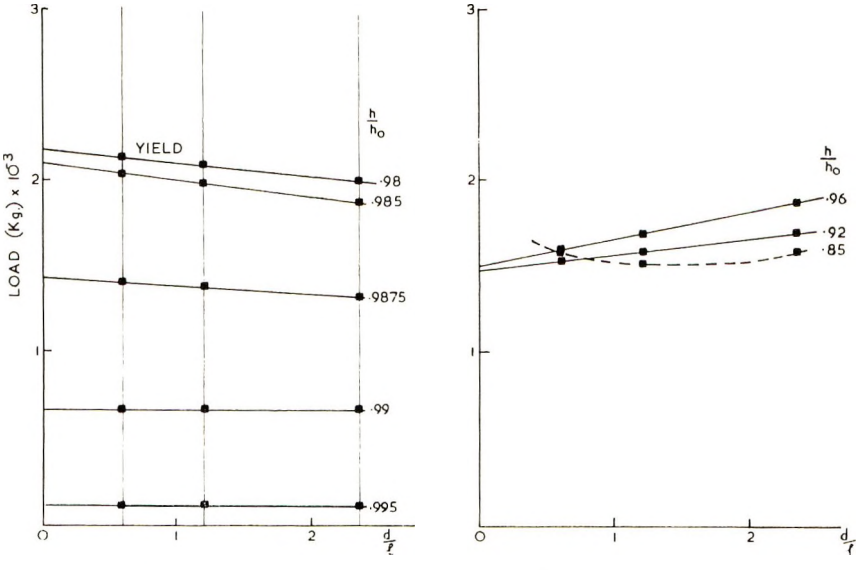

Fig. 5. Stress at a particular strain plotted against the ratio diameter/length for cylindrical polystyrene test peices according to the modified Cooke and Larkes procedure.[29] Strain rate 10^{-3} sec^{-1}, temperature 25°C. Area of test piece, 1.985 cm^2.

to break down at compression ratios of $h/h_0 < 0.85$ where h is the height and h_0 the initial height of the test piece. In this way it has proved possible to obtain the first part of a stress–strain curve comparatively free of the inaccuracies produced by strain rate variation and frictional end effects up to a compression ratio of 0.88, as shown in the upper curve of Figure 6. This curve refers to Carinex HR, a heat-resistant grade of polystyrene, and not to Carinex GP, the softer general-purpose molding grade used in our crazing studies (injection-molded test pieces). The HR material was selected in order to facilitate comparison of the compression results with those of Holliday et al.[24,30] Carinex GP was, however, used for the results quoted in Figures 2 and 4, where direct comparison was made with results from injection-molded specimens.

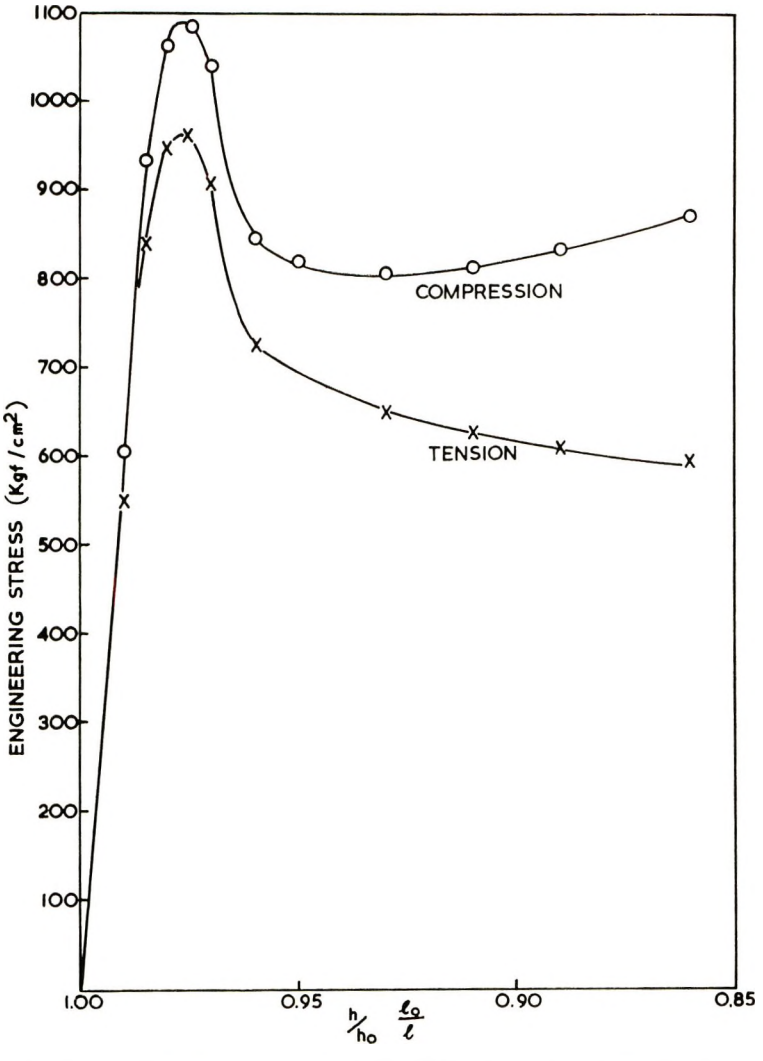

Fig. 6. Engineering stress–strain curve for HR polystyrene in compression as obtained by the modified Cooke and Larkes procedure[29] and the theoretical tensile curve derived from it.

Care was taken to ensure that the heat produced by the deformation process was not significantly influencing the results. Insertion of a thermocouple at the interface of two cylinders and compression of the composite test piece at the maximum strain rate used gave temperature rises of less than 5°C.

Relationship between Compressive and Tensile Yield

As previously stated, Whitney[23,31] has shown that the compressive and tensile stress–strain behavior of polymers are different and has explained this phenomenon in terms of polymeric yield being influenced, not only by

shear stresses but also by normal stresses acting perpendicular to the shear plane, thus producing a dilation or contraction of this plane. Sternstein et al.[11,12] and Bowden and Jukes[28] have both reinforced this conclusion, which may be expressed by means of the Mohr-Coulomb (Navier) yield criterion:

$$|\tau| = S_0 + \mu\sigma \tag{1}$$

Here $|\tau|$ and σ are the observed shear yield stress and normal stress acting across the plane of shear respectively, and S_0 is the shear strength of the material in the yield plane at zero σ; μ is a constant sometimes called the coefficient of internal friction of the material. Sternstein et al.[11,12] have firmly demonstrated the applicability of this relation to poly(methyl methacrylate) and concluded that it probably also applies to polystyrene.

However, in a more recent paper,[32] Sternstein et al. have proposed a relation between octahedral shear stress and mean normal stress. We consider the Mohr-Coulomb treatment is adequate for our results but do not claim that our work discriminates significantly between the two theories.

The relationship between yield in compression and yield in tension following from this criterion is already well known[33] and may be stated as

$$\sigma_Y{}^T/\sigma_Y{}^C = [(\mu^2 + 1)^{1/2} - \mu]/[(\mu^2 + 1)^{1/2} + \mu] \tag{2}$$

where $\sigma_Y{}^T$ and $\sigma_Y{}^C$ are the tensile and compressive yield stresses, respectively. Thus a knowledge of μ allows a theoretical ratio of yield stresses in compression to tension to be evaluated. Now it can be seen[34] that the normal stress σ and shear stress $|\tau|$ acting in the plane parallel to the vertical 3 axis are given by:

$$\sigma = {}^1/_2(\sigma_1 + \sigma_2) + {}^1/_2(\sigma_1 - \sigma_2)\cos 2\theta \tag{3}$$

$$\tau = -{}^1/_2(\sigma_1 - \sigma_2)\sin 2\theta \tag{4}$$

where θ is the angle between the normal to the plane and the line of application of the tensile or compressive stress. Using the Mohr-Coulomb yield criterion,[1] we have from eqs. (3) and (4) that

$$\begin{aligned} S_0 &= \mu\sigma + |\tau| \\ &= {}^1/_2\mu(\sigma_1 + \sigma_2) + {}^1/_2(\sigma_1 - \sigma_2)(\mu\cos 2\theta + \sin 2\theta) \end{aligned} \tag{5}$$

This equation represents the general yield relationship for the material. If now the tensile test is carried out under an applied external hydrostatic pressure P, then we have $\sigma_1 = \sigma_3 = -P$ and $\sigma_2 = \sigma_Y{}^{T(P)} - P$, where $\sigma_Y{}^{T(P)}$ is the tensile yield stress of the material when subjected to an applied pressure P.

Substitution for σ_1 and σ_2 in eq. (5) shows that the maximum value of S_0 will occur when $\tan 2\theta = \mu^{-1}$, at which point

$$2S_0 = \sigma_Y{}^{T(P)}\{\mu + (1 + \mu^2)^{1/2}\} - 2P\mu \tag{6}$$

On differentiating with respect to P, we obtain

$$d\sigma_Y{}^{T(P)}/dP = 2\mu/[\mu + (1 + \mu^2)^{1/2}] \tag{7}$$

Here $d\sigma_Y^{T(P)}/dP$ represents the effect of pressure on the yield stress $\sigma_Y^{T(P)}$ determined at a pressure P. This pressure dependence has recently been measured by Holliday and Pogany[30] and Biglione et al.[25] and found by the former to have the value 0.09 for Carinex HR polystyrene. By using this value in eq. (7), μ is calculated to be 0.047; it then follows that the ratio of the tensile to compressive yield stress from eq. (2) is $\sigma_Y^T/\sigma_Y^C = 0.91$. This compares with a value of 0.89 calculated by Christiansen et al.[35] for their polystyrene. Thus the theoretical relationship between tensile and compressive yield strengths is now in a readily applicable form.

The application of this relationship may be checked by estimating the yield stresses of the same polystyrene (Carinex HR) under tension and compression at similar temperatures and strain rates.* Thus σ_Y^T may be obtained by extrapolating the results of Holliday and Pogany[30] to zero applied hydrostatic pressure and σ_Y^C from our experiments at the lowest d/l ratio. In this way, we find $\sigma_Y^C/\sigma_Y^T = 0.94$, a result which generally supports the proposed Mohr-Coulomb criterion but does not, of course, provide any evidence to distinguish between this treatment and other proposals which give broadly similar results.[32,36]

Prediction of Idealized Stress–Strain Curves in Tension

Any compressive stress–strain curve may be readily converted from the measured engineering stress to a true stress–strain relation,[15] but in the past it has not been possible to convert these curves to equivalent tensile curves because the relation between tensile and compressive yield was not established. However, now that the validity of the Coulomb principle (or its near equivalents) has been demonstrated[11,12,21,25,29,32,36] it is possible to take some further steps in this direction. The principle can be employed to convert the true stress–strain curve for polystyrene in compression into the true stress–strain curve for tension (by using $\sigma_Y^T/\sigma_Y^C = 0.925$). This in turn may be converted back into a conventional engineering stress–strain curve in tension.* This has been carried out for the curves shown in Figure 6. As the modified Cooke and Larkes[29] procedure can only be used a short way beyond the yield point, our results can only be extended to moderate strains. However, by treating the results of Binder and Muller[15] in the same way, we can obtain a more approximate but also more extended stress–strain relation as shown in Figure 7*a*. However, this procedure cannot be reliably extended into the high-strain region, where substantial orientation hardening sets in, because the way in which this effect changes between the different types of strain associated with tension and compression

* 2.5×10^{-3} sec^{-1} and 20°C, i.e., different from those conditions used in Figure 6.

* This treatment provides that the yield strains in tension and compression are the same, an assumption which is not of course justifiable in principle. However, the yield strain will be substantially determined by the linear (Hookean) part of the stress–strain curve, where the linear modulus in compression will be slightly higher than that in tension (effect of pressure). On the other hand the higher yield stress in compression will act in the opposite sense. Thus the quantitative errors arising from this treatment are likely to be fairly small.

is unknown. Nevertheless, it is clear that both of the predicted stress–strain curves show a large drop in the engineering stress at yield. This follows the compression curves which also show a drop and therefore exceed considerably, the purely geometric effects, a result which agrees with the measurements of Holliday et al. under hydrostatic pressure.[24] Similar sharp yield drops have been observed for poly(ethylene terephthalate) by Brown and Ward.[37]

Stress–Strain Characteristics of Different Polymers

The predicted tensile stress–strain curves for polystyrene given in Figure 6 are compared with the measured stress–strain curves for PVC and cellulose nitrate in Figure 7. It will be seen that the magnitude of the fall in stress after yield is much greater in the case of polystyrene than with the other two materials. This means that the energy associated with plastic instability in tension is much greater with polystyrene than it is with the other two plastics. As a consequence, the energy required to impose a large inhomogeneous extension on a small part of the test piece is much less than that necessary to extend the whole test piece by an equivalent total displacement at yield. For example, taking the curve derived from Binder and Muller's results for polystyrene, we find that the energy required to obtain a homogeneous strain of 0.01 at yield for a 1-cm specimen is approximately 9.0 kgf/cm. However, if the same overall extension of the specimen were achieved by an inhomogeneous strain acting on a 0.1 cm length of the 1 cm

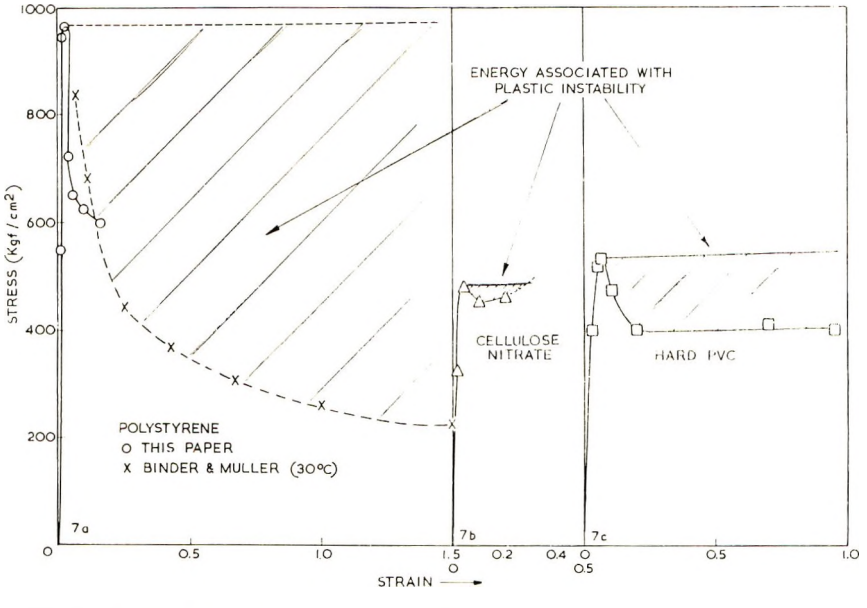

Fig. 7. Tensile stress–strain curves for different thermoplastics plotted on the same scale. The three plastics show quite different behavior: (*a*) the polystyrene exhibits crazing followed by brittle fracture; (*b*) the cellulose nitrate appears to extend quite uniformly; (*c*) the PVC necks, and the observed stress–strain curve is, of course, distorted by this effect.

long specimen, as one gets in a crazing type of deformation, then the energy associated with this would be only some 4 kgf/cm. Thus the situation at yield is clearly unstable. A similar situation, in which there is a large yield drop, has also been shown to lead to localized shear bands in polystyrene,[6] i.e., a large deformation occurs preferably in a small volume of material.

However, the question remains as to why this instability leads, under conditions of tension, to necking with some polymers and to crazing and fracture with others. Evidence relating the occurrence of plastic instability to crack propagation and fracture has previously been given by Vincent,[38] Williams,[39] and Haward.[40] At the present time it is not possible to give a firm answer to this question, but the much larger energy to be associated with plastic instability of polystyrene in comparison with the other two polymers shown in Figure 7 suggests a possible line of investigation. To assist us in this enquiry, Dr. R. P. Kambour kindly supplied us with a series of polymers whose crazing tendency had previously been studied.[41] The results showed that all the polymers which he reported as exhibiting crazing showed substantial yield drops in compression, and therefore by inference, a high level of plastic instability. In addition, the materials which Kambour reported as having the highest crazing tendency, i.e., poly(methyl methacrylate), polystyrene, styrene–acrylonitrile copolymer, and poly-α-methylstyrene, also had high yield stresses.[16] This, in turn, would seem to be a precondition for a high energy difference to be associated with inhomogeneous as compared with a homogeneous deformation.

This requirement for a high energy for the crazing process seems a reasonable one, since such a process must include an additional energy requirement as compared with simple necking to account for the nucleation and growth of the tiny voids which are distributed throughout the craze structure. Any full understanding of the crazing process must take these factors into account.[42,43]

The authors wish to express their thanks to Dr. M. D. Heaton for helpful discussions and to Professor Hull of the Department of Metallurgy, University of Liverpool, for the use of experimental facilities. They are also indebted to Shell Research Limited, Carrington Plastics Laboratory, for help with materials and equipment.

References

1. P. I. Vincent, *Polymer*, **1**, 7 (1960).
2. I. M. Ward and P. R. Pinnock, *Brit. J. Appl. Phys.*, **17**, 3 (1966).
3. R. N. Haward and G. Thackray, *Proc. Roy. Soc. (London)*, **A302**, 453 (1968).
4. J. C. Bauwens, *J. Polym. Sci. A-2*, **5**, 1145 (1967).
5. N. Brown, R. A. Duckett and I. M. Ward, *Phil. Mag.*, **18**, 483 (1968); *Brit. J. Appl. Phys.*, **1**, Sec. 2, 1369 (0000).
6. P. B. Bowden and J. A. Jukes, *Nature*, **221**, 462 (1969).
7. R. P. Kambour, *Polymer*, **5**, 193 (1964); *J. Polym. Sci. A-2*, **7**, 4159 (1969).
8. R. P. Kambour, *J. Polym. Sci., A-2*, **4**, 349 (1966).
9. B. Maxwell and L. F. Rahm, *Ind. Eng. Chem.*, **41**, 1989 (1969).
10. V. Sobolev, *Zh. Tekh. Fiz.*, **27**, 2273 (0000).
11. S. S. Sternstein, L. Ongchin, and A. Silverman, in *Polymer Modification of Rubbers and Plastics* (*Appl. Polym. Symp.*, **7**) H. Keskkula, Ed., Interscience, New York, 1968, p. 175.

12. S. S. Sternstein and L. Ongchin, paper presented at 158th American Chemical Society Meeting, New York, N. Y., September 5, 1969.

13. B. M. Murphy, R. N. Haward, and E. F. T. White, paper presented at the International Fracture Conference, Brighton, England, 1969.

14. G. Rehage and G. Goldbach, *Angew. Makromol. Chem.*, **1**, 125 (1967).

15. G. Binder and F. H. Muller, *Kolloid Z.*, **177**, 129 (1961).

16. R. E. Robertson, *The Yield Deformation and Fracture of Polymers, Conf. Handbook*, 1.5/1, Cambridge, England, March–April 1970.

17. C. Bauwens-Crowet, J. C. Bauwens, and G. Homès, *J. Polym. Sci. A-2*, **7**, 735 (1969).

18. B. D. Coleman, *J. Polym. Sci.*, **20**, 447 (1956).

19. B. M. Murphy, Ph.D. Thesis, University of Manchester Institute of Science and Technology, 1969.

20. A. Van den Boogart, paper presented at Institute of Physics Conference on The Physical Basis of Yield and Fracture, Oxford, 1966.

21. R. J. Bird, J. Mann, G. A. Pogany, and G. Rooney, *Polymer*, **7**, 307 (1966).

22. R. N. Haward and I. Brough, *Polymer*, **10**, 724 (1969).

23. W. Whitney, Sc.D. Thesis, Department of Civil Engineering, MIT, Cambridge, Mass., November 1964.

24. L. Holliday, J. Mann, G. A. Pogany, H. Ll. D. Pugh, and D. A. Gunn, *Nature*, **202**, 381 (1964).

25. G. Biglione, E. Baer, and S. V. Radcliffe, paper presented at the International Fracture Conference, Brighton, England, 1969.

26. H. Ford, *Trans. J. Plast. Inst.*, **30**, 55 (1962).

27. J. G. Williams, *Trans. J. Plast. Inst.*, **37**, 505 (1967).

28. P. B. Bowden and J. A. Jukes, *J. Mat. Sci.*, **3**, 183 (1968).

29. M. Cooke and E. C. Larkes, *J. Inst. Retal.*, **71**, 371 (1945).

30. L. Holliday and G. A. Pogany, private communication.

31. W. Whitney and R. D. Andrews, in *Macromolecular Chemistry, Prague 1965*, (*J. Polym. Sci. C*, **16**), O. Wichterle and B. Sedlaček, Eds., Interscience, New York, 1967, p. 2981.

32. S. S. Sternstein, J. Paterno and L. Ongchin, *The Yield Deformation and Fracture of Polymers Conf. Handbook*, 1.4/1, Cambridge, England, March–April 1970.

33. J. C. Jaeger, *Elasticity, Fracture and Flow*, Wiley, New York, 1962, pp. 74–83.

34. A. E. H. Love, *A Treatise on the Mathematical Theory of Elasticity*, Dover, New York, 1944.

35. A. Christiansen, S. V. Radcliffe, and E. Baer, *The Yield Deformation and Fracture of Polymers Conf. Handbook*, 1.1/1, Cambridge, England, March–April 1970.

36. P. B. Bowden and J. A. Jukes, *The Yield Deformation and Fracture of Polymers Conf. Handbook*, 1.3/1, Cambridge, England, March–April 1970.

37. R. Brown and I. M. Ward, *J. Polym. Sci. A-2*, **6**, 607 (1968).

38. P. I. Vincent, *The Physical Basis of Yield and Fracture Conference*, Oxford, 1966, p. 155.

39. J. G. Williams and C. E. Turner, *Appl. Mat. Res.*, **1964**, 144 (July 1964).

40. R. N. Haward, *Brit. Polym. J.*, **2**, 209 (1970).

41. R. P. Kambour, *J. Polym. Sci. A-2*, **4**, 17 (1966).

42. J. C. Fisher, *J. Appl. Phys.*, **19**, 1062 (1948).

43. R. N. Haward, *Trans. Faraday Soc.*, **38**, 392 (1942).

Received August 3, 1970
Revised October 28, 1970

JOURNAL OF POLYMER SCIENCE: PART A-2 VOL. 9, 815–827 (1971)

Formation of Spherulites in Polyamides. V. "Odd-Odd" Polyamides

J. H. MAGILL,* *Carnegie-Mellon University, Mellon Institute, Pittsburgh, Pennsylvania 15213*

Synopsis

The crystallization of a series of "odd-odd" polyamides has been examined for a variety of fusion conditions and crystallization temperatures. Diverse kinds of spherulites and other crystalline structures have been formed in these nylon polymers by direct crystallization from the melt and by melt-seeding techniques. The structures formed in this way have been characterized primarily with the aid of optical microscopy. In this series of polymers, characteristic textural features yield a fairly unified pattern of crystallization behavior. Crystalline aggregates are formed near the respective melting points of these polymers. In very thin sections (ca. 0.1μ), plateletlike crystals of high crystallinity exhibit optical and diffraction behavior characteristic of single crystals.

INTRODUCTION

A variety of polyamides have been studied in order to ascertain the underlying pattern of spherulitic crystallization and so enhance our knowledge of the broader aspects of spherulitic growth in high polymers.[1–5] This preliminary study indicates that the diverse crystalline structures found in the "odd-odd" class† of polyamides follow a general characteristic pattern. Crystallization experiments were conducted over a wide range of fusion and crystallization temperatures in an attempt to exhaust all possible structures which may form from the supercooled polymer melt. Some spherulites were also given from solution. Characterization of the crystallized structures was made mostly with the polarizing microscope by using the sign of the birefringence of the crystalline species as a characterizing parameter.[1] Highly crystalline structures were grown in thin films of all these polyamides when the samples were crystallized near their respective melting temperatures.

The main purpose of this paper is to outline the broader aspects of crystallization behavior which have not been described in the literature for odd-odd polyamides. At the same time, it is hoped that this preliminary

* Present address: Department of Metallurgical and Materials Engineering, University of Pittsburgh, Pittsburgh, Pennsylvania 15213.

† Defined in the conventional manner, i.e., the first integer refers to the number of carbon atoms in the diamine constituent and the second integer refers to the carboxylic acid part.

investigation will provide, along with Parts I–IV[1,2] a useful catalog of spherulite morphology which will form a basis for further study.

EXPERIMENTAL

Materials

The odd-odd polyamides studied are listed in Table I.

TABLE I

Polymer	Intrinsic viscosity,	Carboxyl endgroups[a]	Amine endgroups[a]
55	0.540	—	20.3
57	0.893	68.4	63.3
77	—	—	—
97	0.900	6.18	39.7
99	0.890	63.8	40.3

[a] Measured in 90% w/w formic acid solution.

Sample Preparation

Sections of polymer chip were melted between cleaned, glass cover slips on a hot stage and isothermally crystallized on a thermostatted Köfler hot stage fitted to a polarizing microscope. Further experiments of longer duration (>3 hr) were made in silicone oil thermostatted baths according to procedures outlined in earlier papers.[1–3] Most experiments were made with polyamide films about 10–20 μ thick. Some experiments were conducted at temperatures close to the melting points of the respective polymers with much thinner films, which contained thin regions down to 0.1 μ or less in thickness. In these experiments, the glass cover slips containing the polymer was held in a specially constructed spring loaded device patterned after a design by Harris.[6] This enabled the polymer sample to be ejected and quenched rapidly in solid CO_2–acetone or liquid nitrogen in order to arrest the crystallization. Further thinning (or etching) of specimens for electron microscopy was carried out according to conventional glow-discharge techniques.[7,8] The sample thickness was estimated from the interference fringes which formed around holes in the thin film, as etching proceeded.

Two main procedures[1,3] were adopted in these crystallization experiments: (a) direct fusion of the samples at temperatures about 10 to 50° above the optical melting point T_m, followed by undercooling to the crystallization temperature; (b) rapid heating of the sample up to temperatures in the interval between T_m and T_m − 10°C for periods ranging from 10 to 30 min, followed by isothermal crystallization in this temperature interval. In this process, the small crystallites melt before they have time to re-equilibrate to larger sizes compatible with the imposed high temperature conditions. An optically isotropic melt is formed. Birefringent

structures readily appear in this "isotropic" matrix. They nucleate and grow on heterogeneities and any crystallites that have survived the rapid melting process. This technique may be regarded as a *melt-seeding* process and is analogous to the solution-seeding method[9] used for producing single crystals. Basically, growth occurs on heterogeneities in both instances. The rapid fusion method predates the solution-seeding techniques and has been described previously in detail.[1,3]

RESULTS AND DISCUSSION

General Pattern of Crystallization

Owing to the wide variety of morphological textures encountered in this investigation, optical micrographs are selected to represent features which are common to this particular group of polyamides. The schematic diagram (Fig. 1) which summarizes the polymer morphology of these polyamides is used to discuss the micrographs and other observations. (Nylon 97 and nylon 99 are not included in this figure because their range of morphologies was not completely investigated owing to lack of materials. Available data showed that they behave similarly to nylon 77.) The ordinate in this figure is an arbitrary birefringence scale which serves to give

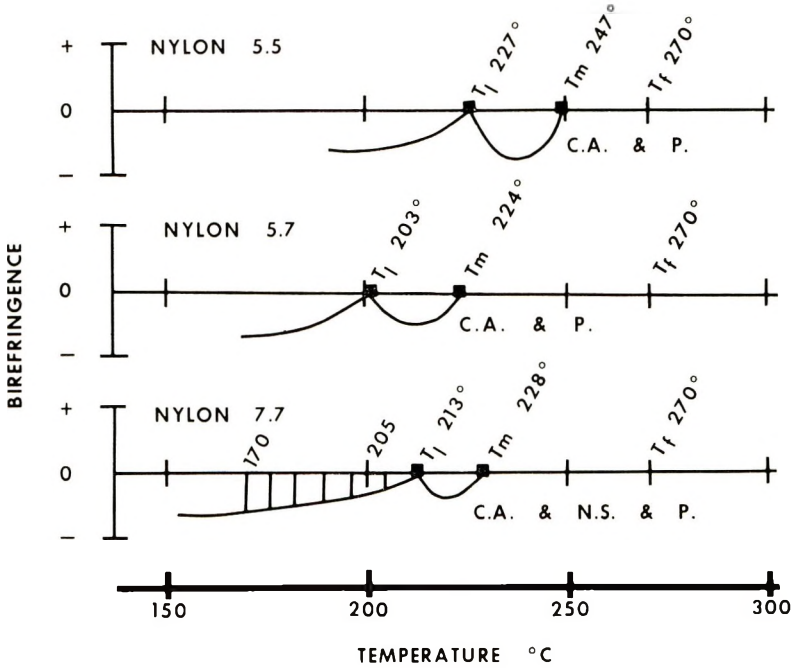

Fig. 1. Schematic plot of birefringence (arbitrary scale) vs. crystallization temperature: T_m denotes the polymer melting point; T_f is the maximum melting temperature used in this work; C.A. denotes crystalline aggregates; N.S. denotes negative spherulites P denotes platelets; T_l denotes low birefringence region.

the temperature range (abscissa) over which structures have been observed to grow. The upper temperature limit of fusion is denoted by T_f, and the observed optical melting temperature of the polymer is designated T_m.

A detailed description of the crystallization behavior is not given, since it can be inferred from this diagram following the manner outlined in other papers.[1] Of course, the thermodynamic melting point of any of these polyamides must be above this T_m value despite the fact that most of the melting points quoted in this work are higher than values cited in the literature.[10,11]

Procedure (b) is especially useful when one needs to crystallize a polymer fairly close to its melting temperature. Induction times for nucleation of hours, days, or even weeks, are avoided by this melt-seeding process. Furthermore, the method is useful in revealing new structures which do not form readily by the direct method (a). This is particularly true for the "even-even" polyamides which have been studied (by this technique) in some detail in earlier papers.[1,3,4]

Spherulitic and Platelet Habits

A few of these spherulitic structures have been mentioned in an early publication,[2] but no details were given in regard to their preparation.

As a general rule, the spherulites exhibit low to zero birefringence when grown at crystallization temperatures T_1 and T_2 (see Fig. 1). A typical low-birefringent nylon 55 spherulite is shown in Figure 2. The higher-birefringent flecks associated with the periphery of these spherulites probably arise because of inadequate quenching of the polymer to arrest the growth process. Spherulites common found in nylon 55 polymer chip are shown in Figure 3. They are fibrillar in appearance and possess a straight Maltese extinction cross and are negatively birefringent. In the early stages of growth (in thin films) a variety of morphologies are seen in nylon 55 at different stages of development (Fig. 4). The thinner regions extinguish uniformly and consistently every 90° on rotation of the sample between crossed polars in the optical microscope. Illustrations and diffraction patterns of thin platelets of these crystals have been given elsewhere.[8,12] In very thin samples (well below 0.1 μ), discrete Bragg reflections (four or more orders) are observed when specimens are examined by electron diffraction. The sample thickness and polymer chain length requires that the molecules fold in order to be incorporated within these platelets.

Platelets of nylon 57 polymers at well advanced stages of their formation are illustrated in Figure 5. Thin platelets display sharp diffraction patterns representative of high crystalline order.[8] Figure 5, like Figure 4, is also illustrative of other stages of morphological development. Optical examination of these platelets in conoscopic illumination shows that they are negatively birefringent and diffraction studies indicate that the spherulitic aggregates encountered at later stages of growth are merely thickness

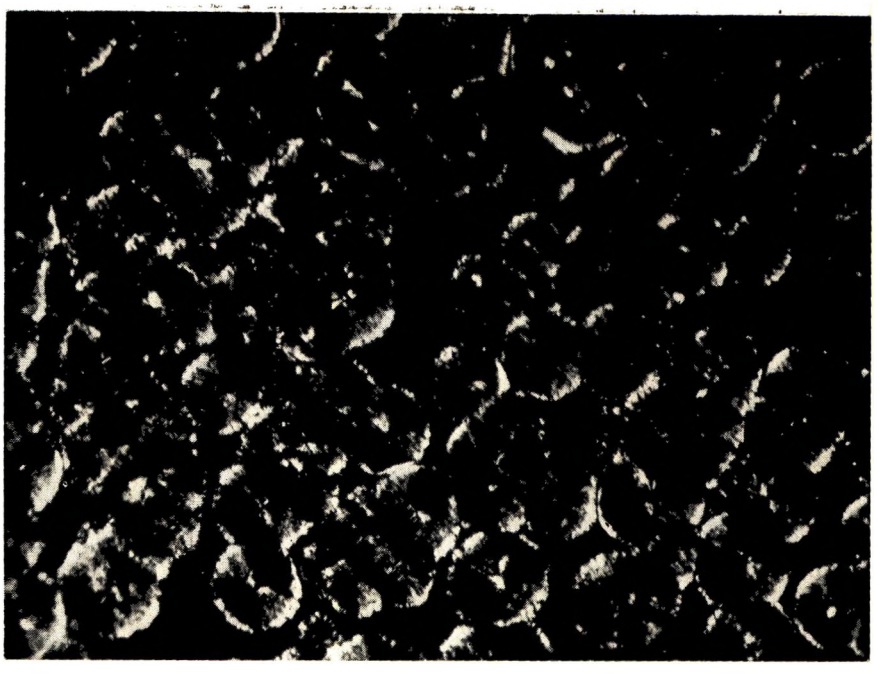

Fig. 2. Nylon 55 low negatively birefringent spherulites formed at 220°C (1/6 hr) after fusion at 270°C (1/2 hr). Low orientation revealed by a Berek compensator; the extinction direction is indicated by the arrow in the micrograph. ×307.

modifications of the basically well-ordered entities which are observed in very thin films.[8]

Banded spherulites are frequently found among many members of the odd-odd polyamides. The temperature range of their formation is given in Figure 1. An example of a nylon 77 ringed spherulite with a zigzag extinction pattern is given in Figure 6. Note that some spherulites with a nonringed overgrowth formed isothermally. A wide range of clearly defined ring spacings is found in nylon 77. A plot of the temperature dependence of this spacing is given in Figure 7. The periodic optical extinction is due to crystallite rotation along the spherulite radius. Extinction is known to occur when the vibration directions of the microscope corresponds to an optic axis in the crystallites. The polymer chains tend to lie transverse to the radius. Such patterns are typical of other classes of odd-odd nylon spherulites but it is best illustrated for nylon 77. The synchronous twist of nylon 77 spherulites has been studied optically by using a Universal (Federov) stage and by microbeam x-ray diffraction[13] in the manner described by Fujawara[14] for polyethylene with wide extinction rings. The diffraction pattern is observed to rotate as one moves the x-ray beam along a radius between extinction bands. This indicates that a consistent behavioral pattern exists for both polyolefin and polyamide spherulites. It should be noted that spherulites with large extinction bands (ca. 50 μ spacing) and not readily obtained in polymers. This value

Fig. 3. Nylon 55 negatively birefringent spherulites formed at 195°C after melting polymer at 270°C for 1/4 hr. ×400.

Fig. 4. Nylong 55 platelets and crystalline aggregates formed in early stages of growth at 232.5°C after sample was melted at 270°C (1/2 hr). ×265.

Fig. 5. Nylon 57 low-birefringent platelets and higher-birefringent aggregates formed at 215°C (3 hr); fusion temperature 230°C (1/2 hr). ×415.

Fig. 6. Nylon 77 ringed negative spherulites (4.3 μ spacing) with zigzag extinction cross formed at 187°C. Fibrillar overgrowths are also apparent. Fusion temperature was 260°C (1/2 hr). ×790.

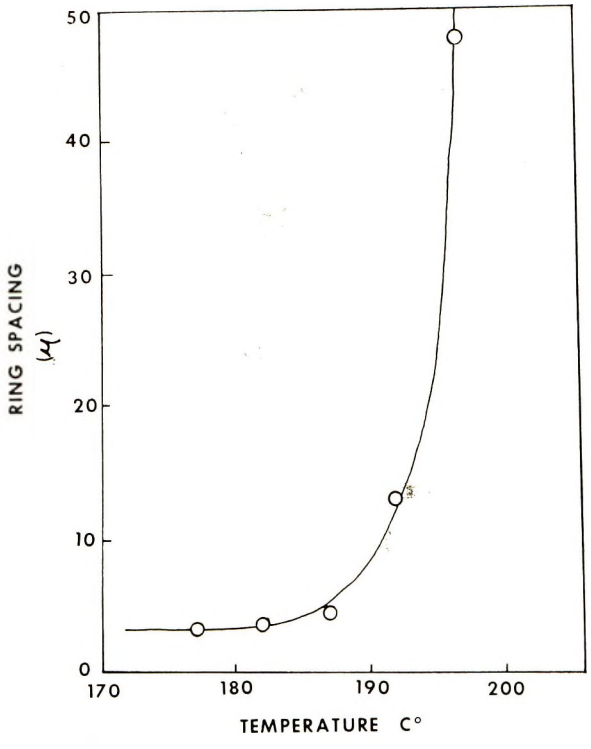

Fig. 7. Ring spacing vs. temperature for nylon 77 spherulites.

represents about the upper limit for which extinction rings are clearly discernible. Smaller rings which occur at lower crystallization temperatures are usually better defined optically. At sufficiently large degrees of undercooling polyamide spherulites do not appear to possess ringed structures. However, it is known that negative spherulites of nylon 66 appear ringed when examined by electron microscopy.[15] Although there are several theories[16–19] which attempt to predict the observed temperature dependence of the ring-spacing in spherulites, no quantitative model or theory exists at the present time.

Again, platelets of nylon 77 can be obtained when the spherulites (or more accurately aggregates) shown in Figure 8 (enlarged view Figure 9) are restricted to grow in two dimensions. The apparent undulations observed in the spherulite (in Fig. 9) are due to orientational changes which get eliminated in very thin samples when the mode of growth is constrained to a given plane, (i.e., that of the confining microscope cover slips). A typical electron diffraction pattern obtained from a thin nylon 77 platelet is depicted in Figure 10. The pattern has the pseudohexagonal symmetry characteristic of the other odd-odd polyamide crystal platelets in this series of nylons. The odd-odd polyamides described here have been shown to crystallize in the structure.[20,21] This conformation is accomplished by favored rotation or orientation around the C—C and C—N groups in the

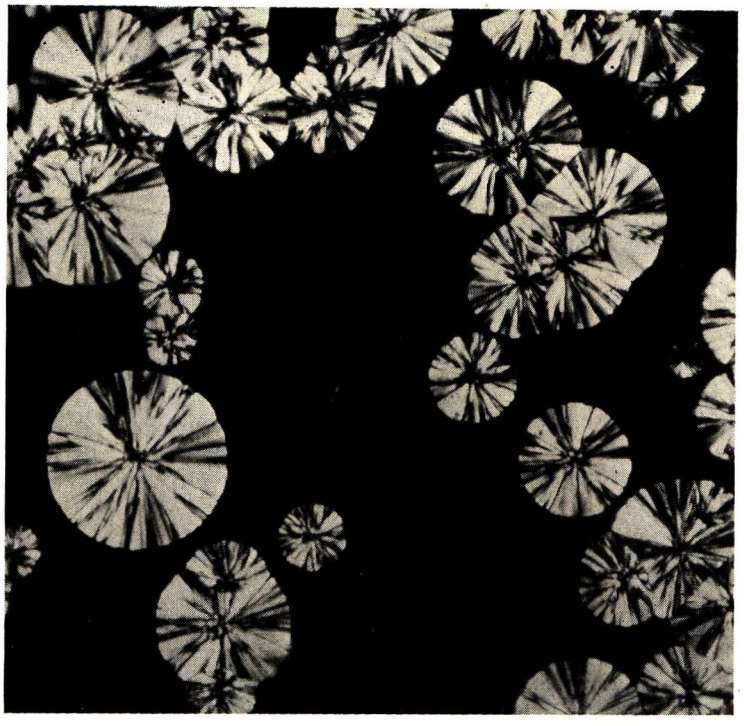

Fig. 8. Sporadic formation of nylon 77 spherulitic aggregates negatively birefringent in thin areas, crystallized at 220°C (120 hr). Fusion temperature 260°C (1/2 hr). ×79.

backbone vicinal to the C=O group. The pseudohexagonal nylon 77 structure has $a = b = 4.8$ Å with $c = 18.95$ Å (i.e., contracted c-axis molecular chain as in the other members of this series). Polyamides are comparatively stable in the electron beam at 100 KV when compared with polysiloxanes.[22,23] Presumably the hydrogen bonding plays a significant role here.

It has been demonstrated that similar thin platelets of the other odd-odd polyamides, examined by electron diffraction, do show well-defined diffraction patterns. The density of nylon 57 and nylon 55 platelets has been measured (density gradient column) as ca. 1.2 g/cc, while that of doubly-oriented nylon 57 yarn is 1.159 drawn fiber is 1.139 g/cc. By way of comparison, nylon 56 doubly-oriented and drawn fibers yield density values of 1.145 and 1.140 g/cc, respectively. Nylon 55 crystalline aggregates (which are a thickness modification of the thinner platelets) exhibited values around 1.167 g/cc which are higher than those found for nylon 56 aggregates (ca. 1.143 g/cc). Theoretical unit-cell x-ray densities are not available for nylon 55 and nylon 57 at present, but it believed that the measured values just quoted, correspond to polymers of comparatively high crystallinity.

The seedlike centers displayed in the nylon 77 spherulites (Figs. 8 and 9) are associated with the onset of a morphological change with temperature

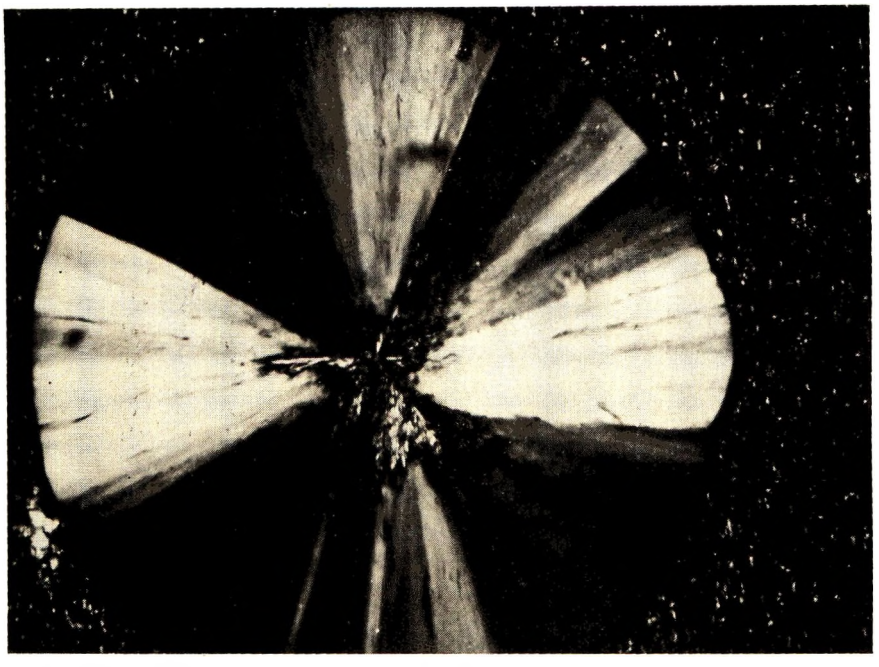

Fig. 9. Nylon 77 crystalline aggregate structure with "seedy" center crystallized at 220°C (19 hr) after fusion at 260°C (1/2 hr). × 520

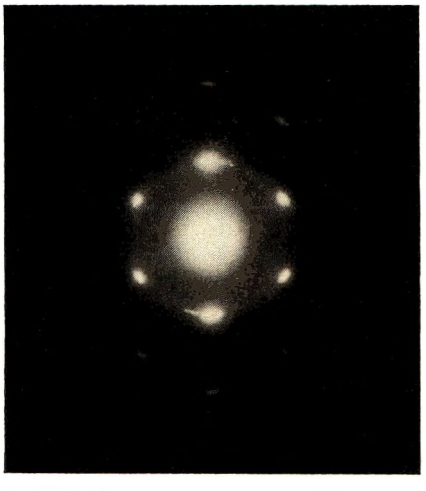

Fig. 10. Typical electron diffraction pattern for nylon 77 thin platelets taken at 100 kV. Sample was crystallized at 220°C after fusion at 285°C (1/4 hr).

of crystallization. In terms of Figure 1, they can be attributed to the transition from a fibrillar habit to extinction ring contours of the type depicted for example in Figure 11 for nylon 97. Again, it is clear that no well-defined extinction directions are present in these negatively birefringent spherulites. It should be pointed out that some other regions of the same sample are completely ringed. This is typical of crystallization occurring near a morphological transition region.

Fig. 11. "Mixed" nylon 97 positively birefringent spherulites with ringed centers (spacing 3.8 μ) which fan into an aggregatelike structure. Fusion temperature 254°C (1/4 hr); crystallized 200°C (16 hr). ×400.

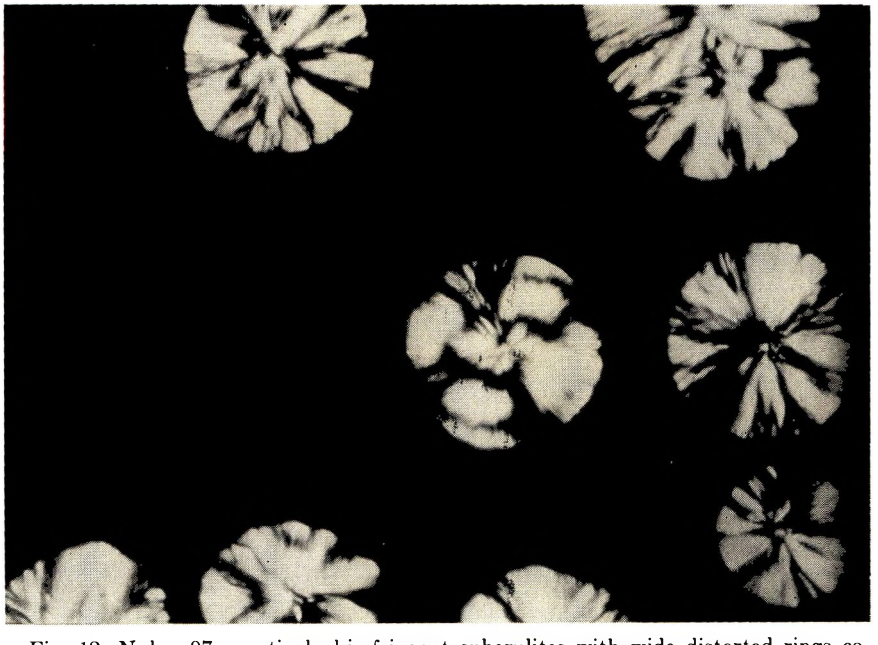

Fig. 12. Nylon 97 negatively birefringent spherulites with wide distorted rings coexisting with spherulitic aggregates; spherulites formed at 191°C (1/4 hr) after polymer was melted at 254°C (1/4 hr). ×475.

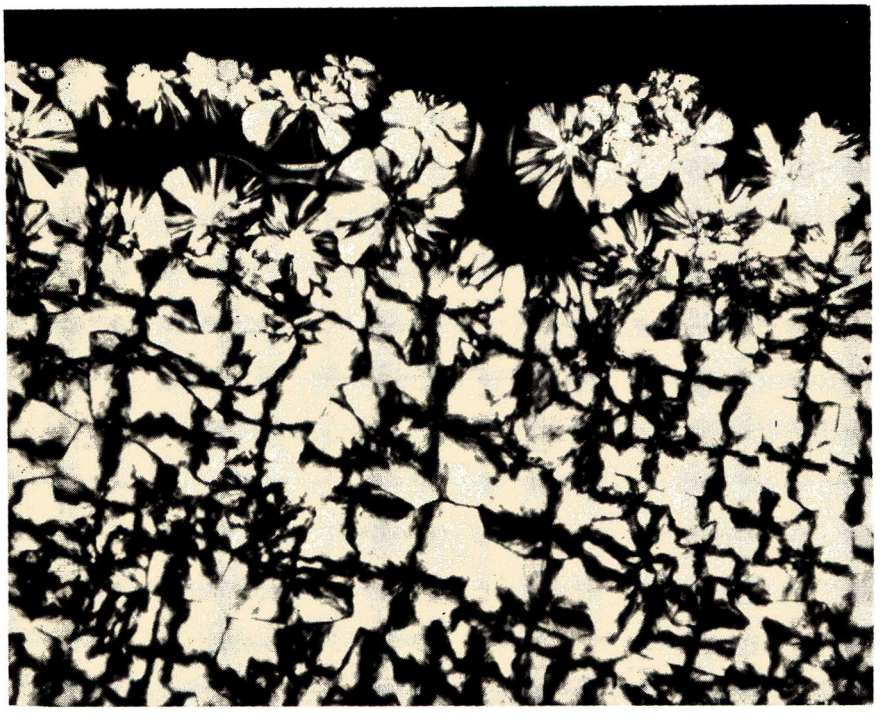

Fig. 13. Two types of nylon 99 spherulites formed at 182°C (2 hr): (*a*) negatively birefringent with ill-defined Maltese extinction cross; (*b*) spherulitic aggregate with no clear extinction cross near edge of sample. Fusion temperature 254°C (1/4 hr). ×400.

Widely banded spherulites can also be obtained in nylon 97. The spherulite near the center of Figure 12 shows an extinction pattern with a broad sweep which is absent in most of the adjacent spherulites.

As in the other polyamides, nylon 99 spherulites (Fig. 13) typically displays a straight extinction cross when crystallized in the lower temperature region below T_1 (see Fig. 1). At the lower edge of the photograph, where the sample is thicker, the spherulite morphology closely resembles that depicted in Figure 6.

CONCLUSION

A unified pattern of spherulite morphology is found for the odd-odd polyamides which all crystallize in the γ conformation. It is clearly shown that the plateletlike sturctures that are formed in thin films (crystallized from the melt) exhibit a high degree of crystalline order, in keeping with earlier work on polyamides. They are also of high density, as assessed by density-gradient column measurements.

The author is indebted to C. Mumford for experimental assistance during the early stages of this work which was initated at British Nylon Spinners Ltd., Pontypool, Monmouthshire, U.K. Thanks are also due to the Office of Naval Research which provided some support for this project at the Mellon Institute.

References

1. J. H. Magill, *J. Polym. Sci.*, *A*, **3**, 1195 (1965); *J. Polym. Sci. A-2*, **4**, 243 (1966); ibid., **7**, 123 (1969).
2. J. H. Magill, *Res. Dev.* (London), **1962**, No. 11, 30.
3. F. Khoury, *J. Polym. Sci.*, **26**, 114 (1957); *ibid.*, **33**, 389 (1958).
4. C. G. Cannon, F. P. Chappel, and J. Tidmarsh, *J. Tex. Inst.*, **54**, T210 (1963).
5. F. P. Price, *Fundamental Phenomena Mat. Sci.*, **3**, 85 (1966).
6. P. H. Harris, private communication.
7. B. J. Spit, *Proceedings of the European Regional Conference on Electron Microscopy, Delft*, Vol. 1, De Nederlendse Verenigenge Voor Electronen Microscope, N. V. Brukkerij Trio, Hague, 1960, p. 564.
8. J. H. Magill and P. H. Harris, *Polymer*, **3**, 252 (1962).
9. D. J. Blundell, A. Keller, and A. J. Kovacs, *J. Polym. Sci. B*, **4**, 481 (1966).
10. C. W. Bunn, in *Synthetic Fibres*, R. Hill, Ed., Elsevier, Amsterdam-New York, 1953, Chap. 12.
11. R. L. Miller, in *Polymer Handbook*, J. Brandrup and E. H. Immergut, Eds., Interscience, New York, 1966, Section III-1.
12. P. H. Geil, *Polymer Single Crystals*, Interscience, New York, 1963, Chap. 4.
13. S. S. Pollack, *Mellon Inst. 51st Ann. Rept.*, **32** (1964).
14. Y. Fujiwara, *J. Appl. Polym. Sci.*, **4**, 10 (1960).
15. C. G. Cannon and P. H. Harris, *J. Macromol. Sci. Phys.*, **B3**, 357 (1969).
16. P. H. Lindenmeyer and V. F. Holland, *J. Appl. Phys.*, **35**, 55 (164).
17. H. D. Keith and F. J. Padden, Jr., *J. Polym. Sci.*, **51**, 54 (1961).
18. J. D. Hoffman and J. I. Lauritzen, Jr., *J. Res. Nat. Bur. Stand.*, **65A**, 297 (1961).
19. J. M. Schultz and D. R. Kinlock, *Polymer*, **10**, 271 (1969).
20. I. Matsubara and J. H. Magill, *Polymer*, **7**, 199 (1966).
21. Y. Kinoshita, *Makromol. Chem.* **33**, 1, 21 (1959).
22. M. N. Haller and J. H. Magill, *J. Appl. Phys.*, **40**, 4261 (1969).
23. J. H. Magill and M. N. Haller, to be published.

Received August 24, 1970
Revised November 23, 1970

JOURNAL OF POLYMER SCIENCE: PART A-2 VOL. 9, 829-839 (1971)

Nuclear Magnetic Resonance Study of Rubber–Carbon Black Interactions

STANLEY KAUFMAN,* *Uniroyal Research Center, Wayne, New Jersey*, and W. P. SLICHTER and D. D. DAVIS, *Bell Telephone Laboratories, Murray Hill, New Jersey 07974*

Synopsis

The mobilities of polymer chain segments in mixtures of rubber and carbon black were investigated by nuclear magnetic resonance. Spin–spin relaxation time (T_2) measurements on *cis*-polybutadiene and ethylene–propylene–diene rubber (EPDM) bound rubbers detected at least two relaxing regions: an immobile region and a relatively free region. The molecular motions in the relatively free region are still constrained compared to those of the pure gum.

Introduction

The interaction of carbon black and rubber is a problem of considerable scientific and technological interest. Knowledge of the structure and interactions in a rubber–carbon black mixture is important for understanding the mechanism of rubber reinforcement by active fillers. One physical model of the interaction between carbon black and rubber is a two-phase model which envisions a shell structure;[1–3] a layer of rubber chains is immobilized on the surface of the carbon black with the remainder of the rubber chains having mobility comparable to that of pure rubber without carbon black present.

While the existence of a layer of rubber chains adsorbed on the surface of the carbon black is generally accepted, the extent of the layer and the degree of the immobilization of the rubber chains remain unresolved. For example, basing his conclusions on dynamic modulus measurements near the glass temperature (T_g), Smit[3] suggested the existence of an adsorbed layer at least 20 Å in thickness and an elevation of T_g by 30°C or so, compared with the value for the bulk rubber. On the other hand, in papers on dynamic-mechanical, free-volume, and thermal-expansion studies of filled rubbers, Kraus and his co-workers[4,5] question the existence of a significant layer of immobilized rubber, arguing that if the physical properties of the adsorbed layer are substantially different from those of the bulk rubber then the adsorbed layer must be extremely thin.

Studies by the NMR technique of reinforcement of rubber have been

* Present address: Bell Telephone Laboratories, Murray Hill, New Jersey 07974.

sparse, even though NMR might be expected to provide direct physical evidence relevant to the two-phase model. Waldrop and Kraus,[6] in a recent NMR spin-lattice relaxation study of rubber–carbon black interactions, found no evidence for an immobilized layer of rubber chains.

They concluded that their data did not confirm the models of rubber–carbon black interactions where the filler is covered with an immobilized layer of rubber which constitutes a significant fraction of the rubber. However, Roe, Davis, and Kwei[7] have recently found, by NMR spin–lattice and spin–spin relaxation measurements, evidence for two regions of molecular mobility in 100 phr mixtures of *cis*-polybutadiene and carbon black. Our results, reported here, also support the two-phase shell model, but indicate that the thickness of the tightly adsorbed layer is a function of temperature.

Materials

The rubbers used in this study were a high-*cis* polybutadiene and an ethylene–propylene-diene (EPDM) terpolymer. Both polymers were produced by solution polymerization and were used without further purification. The polymer compositions were as follows. The EPDM polymer contained approximately 45 wt-% ethylene, 50 wt-% propylene, and 5 wt-% ethylidene norbornene (ENB). Its intrinsic viscosity in tetralin at 135°C was 1.63 dl/g. In the polybutadiene, *cis*, *trans*, and vinyl contents were 88%, 7%, and 5%, respectively. The intrinsic viscosity in toluene at 30°C was 2.37 dl/g. The ethylene and propylene contents of the EPDM and the *cis*, *trans* vinyl contents of the polybutadiene were determined by infrared analysis.[8,9]* The percentage of ENB was determined by the refractive index method and an iodine number analysis.[10] The carbon black used was SAF Statex 160 made by the Columbian Carbon Corporation. The approximate particle diameter is 190 Å and the surface area is 155 m^2/g.

Sample Preparation

The carbon black (50 phr) was incorporated into the rubbers by mixing on a hot two-roll laboratory mill. "Bound rubber" was prepared from the rubber–carbon black mixture by extraction with hot toluene in a Soxhlet extractor under a nitrogen atmosphere. The resulting insoluble material, carbon black and bound rubber, was dried in a vacuum oven and then pressed and inserted into 5-mm NMR sample tubes. The sample tubes were evacuated and sealed.

After extraction of the free rubber, the polybutadiene sample contained 63 wt-% carbon black and the EPDM sample contained 79 wt-%. Since these rubbers do not contain insoluble material or crosslink during milling, all the bound rubber formed is due to rubber–carbon black attachments. The term, bound rubber, is not meant to imply any form of

* The *cis* isomer adsorption occurs at 738 cm^{-1} in a high-*cis* polybutadiene.

molecular interaction between the rubber and the carbon black filler; it merely refers to the insoluble polymer portion of the rubber–carbon black mixture.

Nuclear Magnetic Resonance Measurements

The pulsed NMR apparatus has been described elsewhere.[11] Measurements were made at a frequency of 30 MHz. The pulses were 2–3 μsec in length, and the recovery time of the receiving circuit following a pulse was about 10 μsec. The NMR spin–spin relaxation time T_2 was measured by determination of the time constant of the free induction decay.[12] Free induction decay signals from samples which contain two phases will ordinarily exhibit two components. For example, the free induction decay from semicrystalline polymers[13] is a sum of the signals from the crystalline and amorphous regions.

By visual inspection we were able to determine that many of the free induction decay signals from the bound rubber samples had at least two components. The procedure we used to resolve these two-component curves was to digitize the photographs of the free induction decay curves with an Autotrol digitizer and then fit the data by a nonlinear regression routine which minimized the least squares error between the fitted function and the digitized data. The calculations were carried out on a Scientific Data Systems 940 computer, and the curves were plotted on a Calcomp 565 plotter.

We found that the two-component curves were fitted well by a sum of two exponentials

$$Ae^{-t/T_{2A}} + Be^{-t/T_{2B}}$$

where t is time, A and B are the percentages of rubber in the two regions, and T_{2A} and T_{2B} are the spin–spin relaxation times of the respective regions.

By fitting the free induction decay curves for the pure rubber to the Weibull function[14,15] we were able to show that above the glass transition the free induction decay from the polybutadiene was exponential and that from the EPDM was nearly so. The Weibull function is $e^{-(t/T_2)^E}$, where t is time and E is the Weibull coefficient. The Weibull function can take on either Gaussian ($E = 2$), exponential ($E = 1$) or intermediate character. Fitting to a Weibull function to test for an exponential shape is a better procedure than fitting to an exponential and judging the closeness of the fit because the Weibull function has an additional parameter, the shape parameter E.

Having established the exponential shapes of the free induction decays of the pure rubbers we were confident in the use of an exponential to describe the part of the two-component free induction decay ascribed to amorphous rubber. The use of an exponential to also describe the fast relaxation is justified by the good fits that were obtained with the two-exponential equation.

Below the glass transition, the bound rubber samples yielded only a single component nonexponential free induction decay. These curves were fitted by the Weibull function.

Results

Figure 1 shows the temperature dependence of the spin–spin relaxation time T_2 of the polybutadiene[16] and the EPDM[17] rubber samples without any carbon black added. The familiar glass temperature reflects a macroscopic change measured on a relatively long time scale. The relaxation process seen by NMR reflects the shift in the spectrum of motions to higher frequencies and is characterized by a temperature that occurs well above the familiar T_g. We shall use T_g' to identify the transition in spin–spin relaxation times and consider it to be the center of the transition in T_2; $T_g' - T_g \approx 50°C$.

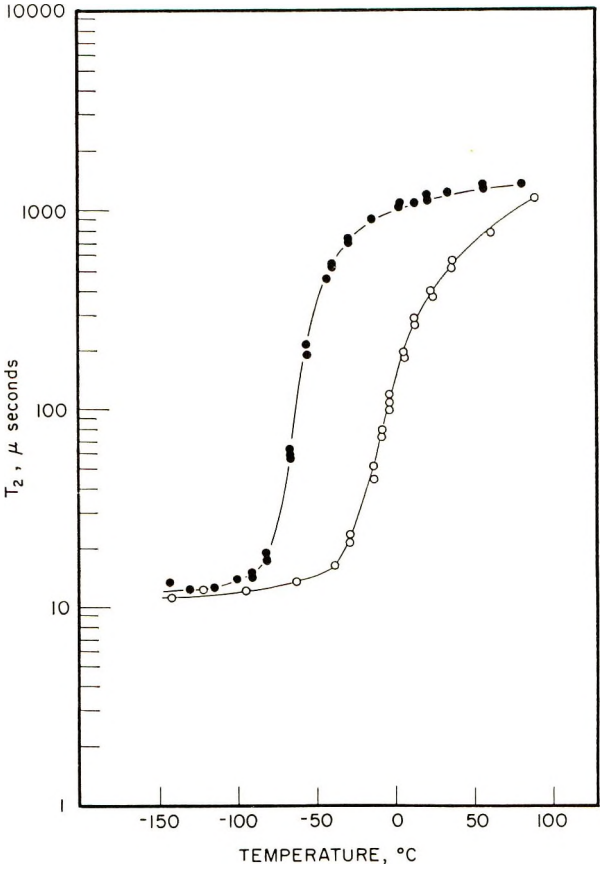

Fig. 1. Temperature dependence of T_2 for the pure rubbers: (●) polybutadiene and (○) EPDM. Note that the flattening of the curves at long T_2 is caused by magnetic field inhomogeneity.

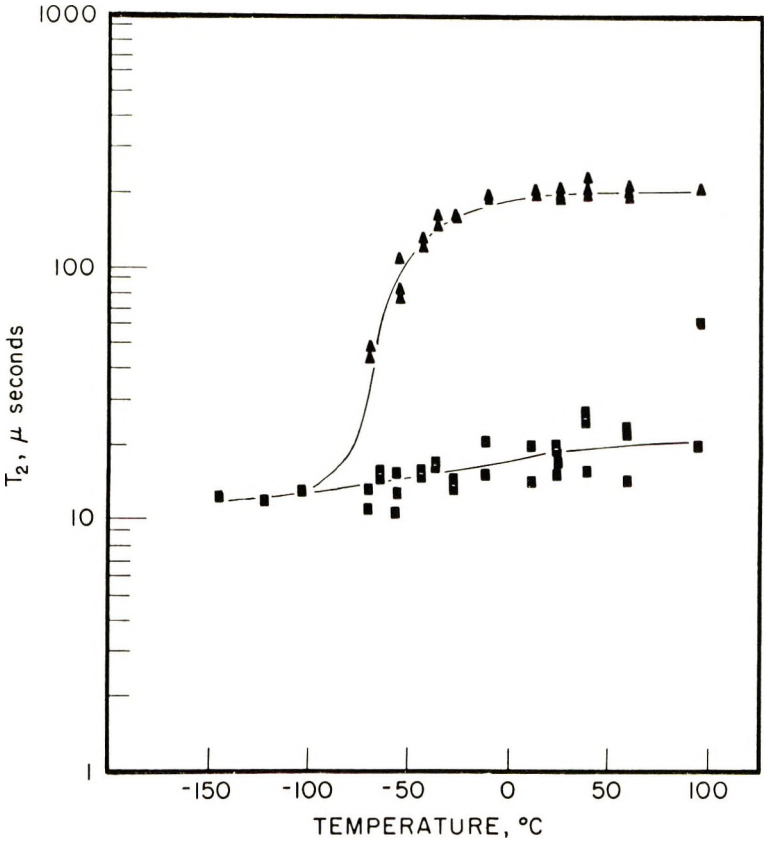

Fig. 2. Temperature dependence of T_2 for the components of the polybutadiene bound rubber: (▲) relatively mobile component and (■) immobilized component.

The transition from the glassy to the rubbery state is detected by an abrupt increase in the NMR spin–spin relaxation time when the polymer segmental and torsional rotation rates are greater than 10^5 Hz and the translational motions of the chain segments occur over distances at least comparable to intermolecular dimensions. Values of T_2 at the higher temperature regions of the curves are limited by the inhomogeneity of the applied magnetic field.

The plot of T_2 versus temperature for the polybutadiene bound rubber sample is shown in Figure 2. The free induction decays were composed of two components, a fast relaxation which is ascribed to rubber chains that are rigid (on the NMR time scale), and a slow relaxation ascribed to the nuclei in the chains whose segmental motions are relatively free. The fast relaxation presumably arises from rubber chains immobilized on the black. If we plot the coefficient A, which is the percentage of rubber in the immobilized layer, versus temperature (Fig. 3), we see that the percentage immobilized undergoes a transition at the glass temperature.

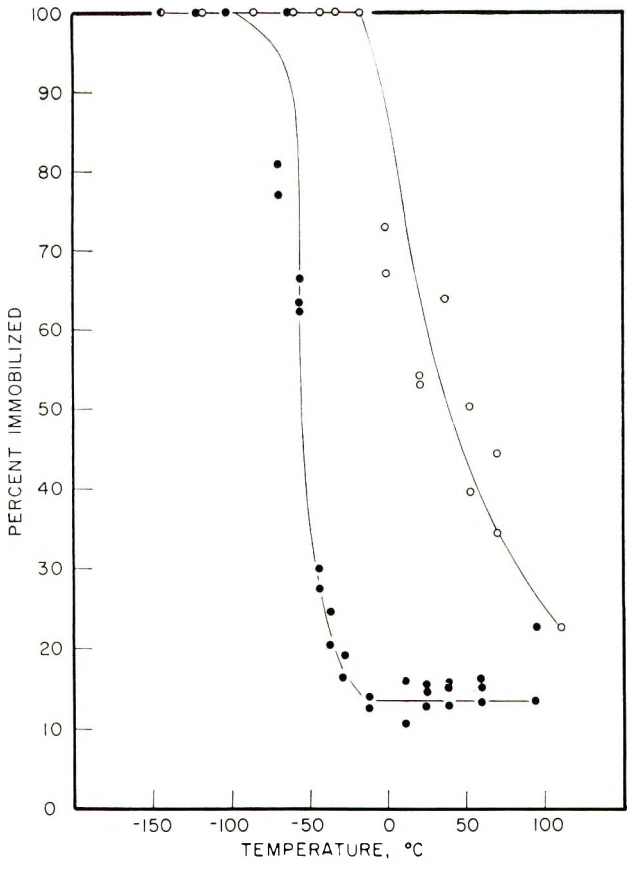

Fig. 3. Temperature dependence of the percentage of the bound rubber immobilized on the carbon black: (●) polybutadiene and (○) EPDM.

Below T_g' the segmental motions are frozen out and all the rubber chains are effectively in the immobilized region. Above T_g' the percentage of immobilized rubber chains decreases, but it levels off at around 14% indicating that a portion of the nuclei remains immobilized on the black at temperatures far above the glass temperature.

Although the remainder of the rubber chains in the bound rubber sample are relatively free compared to the immobilized layer, they are constrained in comparison to the rubber chains in the pure rubber sample. This is shown in Figure 4, where we compare the spin–spin relaxation times of the pure rubber and the bound rubber components.

We find a similar behavior in the EPDM bound rubber. In Figure 5 we show the temperature dependence of the spin–spin relaxation times of the two regions in the EPDM bound rubber and we compare them with the relaxation of the pure EPDM. Aside from a shift toward higher temperatures because of its higher glass temperature, the relaxations of the EPDM samples are very similar to those of the polybutadiene samples.

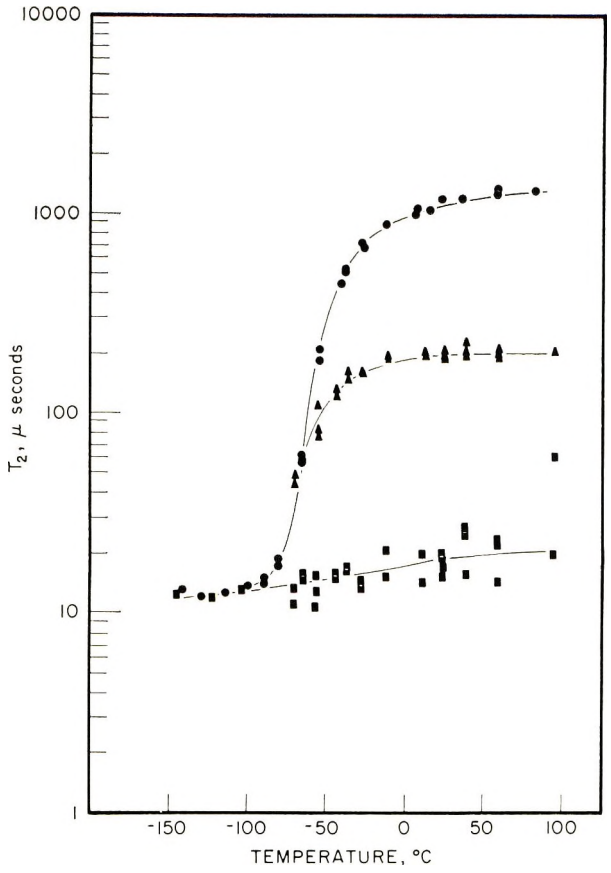

Fig. 4. Temperature dependence of T_2 for (●) pure polybutadiene rubber, (▲) relatively mobile component of the polybutadiene bound rubber, and (■) immobilized component of the polybutadiene bound rubber.

The percentage of EPDM in the immobilized layer versus temperature is also shown in Figure 3.

In Figure 6 we correct for the difference in glass temperatures of the polybutadiene and EPDM rubbers and plot the spin–spin relaxation time versus temperature curves for the two rubbers and the components of the bound rubber samples on a temperature scale relative to the glass temperature T_g'. We see the similarity in relaxation and hence in molecular motion of the two rubbers.

Discussion

The interpretation of the spin–spin relaxation results can be more readily understood if we discuss them in terms of the familiar NMR line width, δH. The spin–spin relaxation time is inversely related to the line width, $2/T_2 = \gamma\delta$H, where γ is the proton gyromagnetic ratio. The discussion below follows closely the treatment of McCall and Anderson.[18]

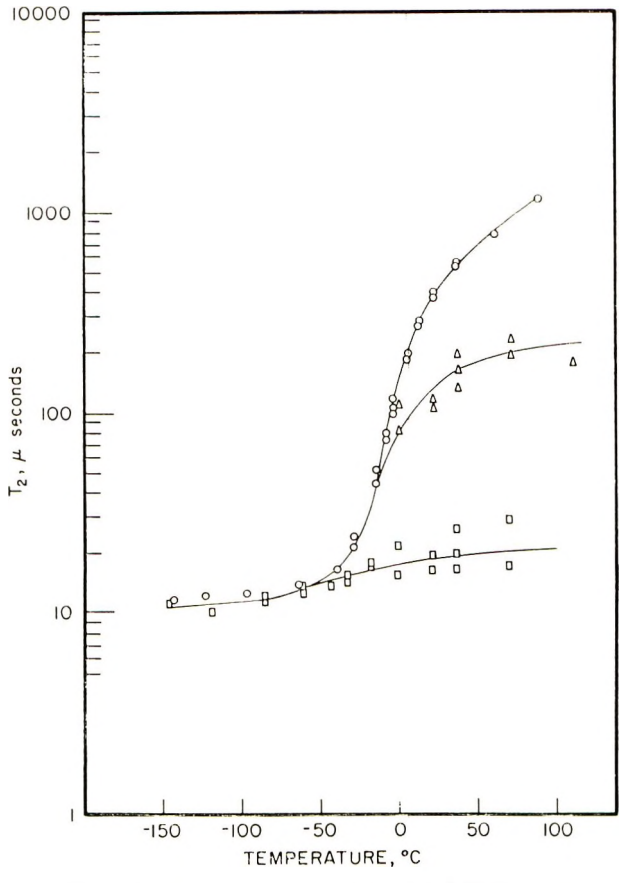

Fig. 5. Temperature dependence of T_2 for (○) pure EPDM rubber, (△) relatively mobile component of the EPDM bound rubber, and (□) immobilized component of the EPDM bound rubber.

The local field at each nucleus is the sum of the fields contributed by the neighbors. Each nucleus contributes a field of

$$\pm (\mu/r^3)[3\cos^2\theta - 1]$$

where r is the internuclear distance, μ is the nuclear magnetic moment, and θ is the angle between the internuclear vector and the applied magnetic field.

When molecular motion takes place the local field becomes time-dependent,

$$\pm \{\mu/[r(t)]^3\}[3\cos^2\theta(t) - 1]$$

If we assume that r is constant and only $\theta(t)$ varies with time, the time-averaged local field is

$$(\mu/r^3)\frac{1}{T_2}\int_0^{T_2}[3\cos^2\theta(\tau) - 1]d\tau$$

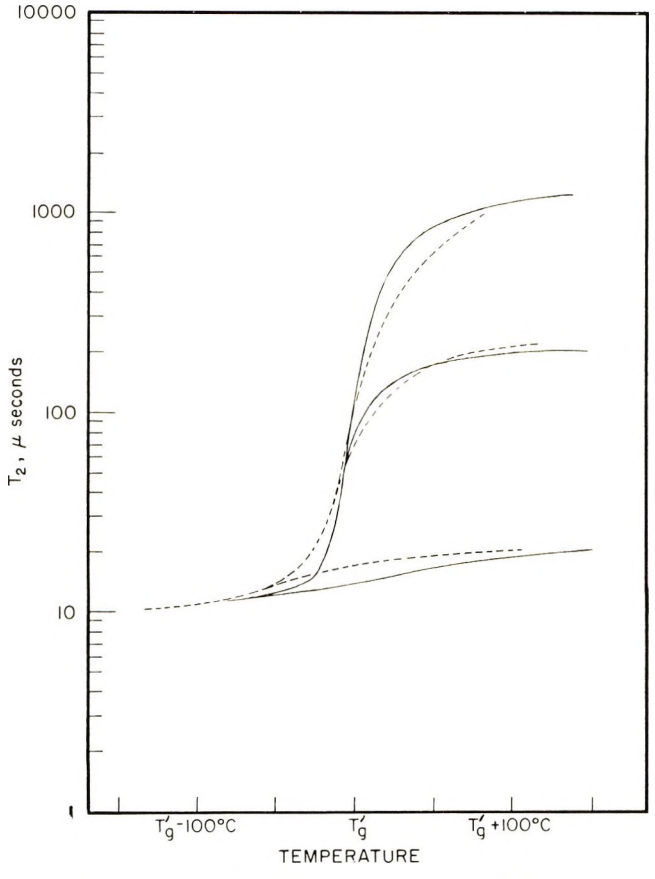

Fig. 6. Temperature dependence of T_2 on a temperature scale relative to the glass temperature T'_g for the pure rubbers and their bound rubber components: (——) polybutadiene and (- -) EPDM.

where T_2 is a time of the order of the time the nucleus resides in a given spin state.

If $\theta(\tau)$ varies rapidly with no restrictions on the directions of the internuclear vector, the time average can be replaced by a space average

$$(\mu/r^3) \int_0^{\pi} (3\cos^2\theta - 1) \sin\theta d\theta = 0$$

This is the reason why liquids exhibit narrow resonance (long spin–spin relaxation times).

There are two interpretations applicable to a partially narrowed resonance such as one observes in molten or amorphous polymers. First, it may be that there are no restrictions on the orientation angle but that the motion is not fast enough to average θ equally over 0 to π in the interval T_2. Second, it may be that the motion is arbitrarily rapid but θ is restricted in some way. In the first case the resonance width should decrease further with increasing temperature, whereas in the second case the resonance

width could be independent of temperature. If the restrictions on θ are temperature-dependent there is no way to choose between the two interpretations.

To get some appreciation for the motion implied by the nuclear resonance widths, McCall and Anderson calculated the width assuming arbitrarily rapid motions subject to the restriction that $\theta > \theta_0$, where θ_0 is to be evaluated from the observed widths. Their result is

$$\delta H \approx (\mu/r^3) \cos\theta_0 \sin^2\theta_0$$

Thus they found that the ratio of the narrowed resonance width to the rigid lattice width is of the order of $\cos\theta_0 \sin^2\theta_0$. In the bound rubbers the rigid lattice T_2 is approximately 10 μsec and the temperature-independent value of T_2 above $T_g' + 50°$C is approximately 200 μsec. Thus $\sin^2\theta_0 \cos\theta_0$ is roughly 0.05, and $\theta_0 \approx 13°$. Thus most, but not all, orientations are accessible to the internuclear vector.

Thus the carbon black, in addition to immobilizing the rubber chains in the immediately surrounding shell, also imposes temperature independent restrictions on the segmental motions of the polymer chains in the outer shell.

Conclusions

The NMR results show that the segmental motions of the rubber molecules in the bound rubber, which is the insoluble part of a rubber–carbon black mixture, are constrained in comparison to the molecular motions in the pure rubber. Within the bound rubber there are at least two regions of molecular mobility, an immobilized region which is presumably the area immediately surrounding the carbon black, and a region of intermediate mobility where the polymer segmental motions are free in comparison to the immobilized region but constrained in comparison to the motions in the pure rubber.

The amount of rubber in the immobilized layer of the bound rubber sample is a function of temperature, increasing sharply as the temperature is lowered toward the glassy region. Far above the glassy region the amount of rubber in the polybutadiene sample reached a plateau. At these temperatures the amount of rubber in the immobilized layer is a very small percentage of the rubber in the original 50 phr mixture. After extraction, 29 wt-% of the polybutadiene rubber remained as bound rubber. However, 14% of this bound rubber is in the immobilized layer, which is only 4% of the rubber in the original mixture, corresponding to a layer thickness of approximately 5 Å.

We are grateful to Drs. W. V. Smith, N. Tokita, and E. G. Kontos for valuable discussions of this research and to Mr. D. J. Bunger and Mr. R. W. Rauscher for writing the computer programs. We are also grateful to Dr. G. Kraus for discussions of the problem of bound rubber and for the communication of some manuscripts before publication. We wish to thank Dr. D. W. McCall for a critical reading of the manuscript and for suggesting the discussion of NMR line widths.

References

1. J. R. Rehner, Jr., in *Reinforcement of Elastomers*, G. Kraus, Ed., Interscience, New York, 1965, pp. 153–155.

2. A. M. Gessler, *Rubber Age*, **101**, No. 12, 54 (1969).

3. P. P. A. Smit, *Rheol. Acta*, **5**, 277 (1966).

4. G. Kraus, K. W. Rollmann, and J. T. Gruver, *Macromolecules*, **3**, 92 (1970).

5. G. Kraus and J. T. Gruver, *J. Polym. Sci. A-2*, **8**, 571 (1970).

6. M. A. Waldrop and G. Kraus, *Rubber Chem. Technol.*, **42**, 1155 (1969).

7. R. J. Roe, D. D. Davis, and T. K. Kwei, *Bull. Am. Phys. Soc.*, [II], **15**, 308 (1970).

8. P. J. Corish and M. E. Tunnicliffe, in *Vibrational Spectra of High Polymers* (*J. Polym. Sci. C*, **7**), G. Natta and G. Zerbi, Eds., Interscience, New York, 1964, p. 187; *Rubber Chem. Technol.*, **39**, 226 (1966).

9. R. R. Hampton, *Anal. Chem.*, **21**, 923 (1949).

10. S. G. Gallo, H. K. Wiese, and J. F. Nelson, *Ind. Eng. Chem.*, **40**, 1277 (1948).

11. W. P. Slichter and D. D. Davis, *J. Appl. Phys.*, **35**, 10 (1964).

12. J. A. Pople, W. G. Schneider, and H. J. Bernstein, *High Resolution Nuclear Magnetic Resonance*, McGraw-Hill, New York, 1959, pp. 44–46.

13. D. W. McCall, D. C. Douglass, and D. R. Falcone, *J. Phys. Chem.*, **71**, 998 (1967).

14. W. Weibull, *J. Appl. Mech.*, **73**, 293 (1951).

15. S. Kaufman and D. J. Bunger, *J. Magn. Resonance*, **3**, 218 (1970).

16. M. Takeda, K. Tanaka, and R. Nagao, *J. Polym. Sci.*, **57**, 517 (1962).

17. E. G. Kontos and W. P. Slichter, *J. Polym. Sci.*, **61**, 61 (1962).

18. D. W. McCall and E. W. Anderson, *J. Polym. Sci., A*, **1**, 1175 (1963).

Received July 6, 1970
Revised October 27, 1970

JOURNAL OF POLYMER SCIENCE: PART A-2 VOL. 9, 841-852 (1971)

Adsorption of Polymers at the Solution–Solid Interface. V. Styrene–Methyl Methacrylate Copolymers on Carbon

A. HOPKINS* and G. J. HOWARD, *Department of Polymer and Fibre Science, University of Manchester Institute of Science and Technology, Manchester 1, England*

Synopsis

The adsorption of a series of block and random styrene–methyl methacrylate copolymers on an animal charcoal and on Graphon has been studied. On charcoal, adsorption decreases with increase of molecular weight because of the inability of larger coils to penetrate into the adsorbent. An analysis is presented which requires that coils undergo considerable distortion on adsorption in pores. The adsorption of random copolymers on Graphon is also in reverse order of molecular weight; this effect may be due to particle bridging leading to the formation of interparticle "pores." The relative affinity of the styrene and methyl methacrylate residues is different on charcoal and Graphon, respectively; on both surfaces, however, relatively few of the more active residues are required for adsorption. Block and random copolymers are adsorbed to different extents which depend on the nature of the adsorbent surface.

INTRODUCTION

The work reported in the present paper is part of an extended investigation of the solution adsorption of linear copolymers. In the present case the adsorption behavior of random and block copolymers of styrene and methyl methacrylate on to charcoal and Graphon has been studied.

EXPERIMENTAL

The preparation and characterization of the polymers has been described previously.[1] Solvents were rigorously purified and dried by standard procedures; freshly distilled, middle-cut, fractions were used throughout.

The charcoal (B.D.H.) was of animal origin and contained 4.3% ash; it was dried by heating at 110°C at 0.10 torr for 24 hr and subsequently stored *in vacuo*. The B.E.T. surface area found from nitrogen adsorption at 77°K is 110 m^2/g and from methanol adsorption at 303°K is 94 m^2/g. In the case of the latter vapor, the adsorption experiment was continued up to high partial pressure ($p/p_0 = 0.95$) and then the desorption branch measured. The pore size distribution of the charcoal was determined by the

* Present address: Phillips Fibers Corp., Greenville, South Carolina, U.S.A.

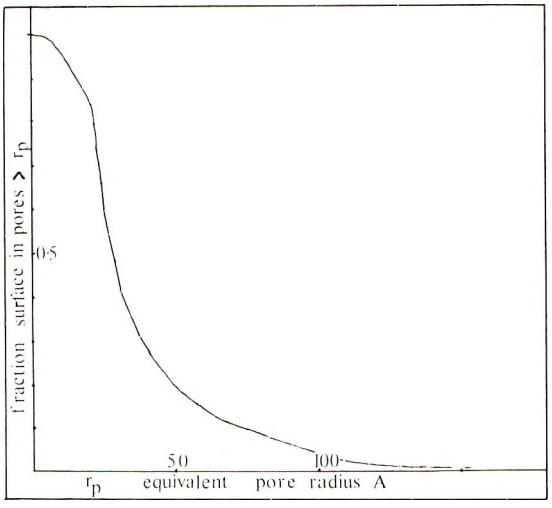

Fig. 1. Pore size distribution (radii of equivalent cylinders) of charcoal sample.

method described in detail by Gregg and Sing[2] and is shown as Figure 1. The average radius of the equivalent cylindrical pore is 42 Å, when calculated from the B.E.T. surface area and the limiting vapor sorption at $p/p_0 \rightarrow 1$.

The Graphon, a graphitized carbon black, was kindly supplied by Cabot Carbon Limited. It was dried and stored in a manner similar to that used for the charcoal and had a B.E.T. surface area of 84 m^2/g (N_2, 77°K); solution adsorption of methylene blue led to an apparent surface area of 96 m^2/g. A gravimetric technique[1] was employed to estimate specific adsorptions which are recorded in units of mg/g: all solution adsorption measurements have been made at 298°K.

RESULTS AND DISCUSSION

Adsorption on Charcoal

The rate of adsorption was found for three poly(methyl methacrylates), one random copolymer and one block copolymer; solutions in benzene (concentration ca. 10 mg/ml) were used. Gentle agitation, in a horizontal plane, was used and a practically constant specific adsorption was reached in 16–24 hr, the samples of higher molecular weight requiring longer periods to attain equilibrium. Equilibrium is noticeably slower than on to silica,[1] and this is attributed to the porous nature of the adsorbent. The standard procedure adopted was to agitate for periods of ca. 48 hr.

Typical adsorption isotherms are shown as Figure 2; no consistent agreement with the Langmuir, the Simha-Frisch-Eirich,[3] or the Frisch-Hellman-Lundberg[4] equations is observed on analysis of 30 isotherms. A strong solvent dependence of adsorption is shown, as is commonly observed in polymer adsorption,[5] and is exemplified by the data of Table I.

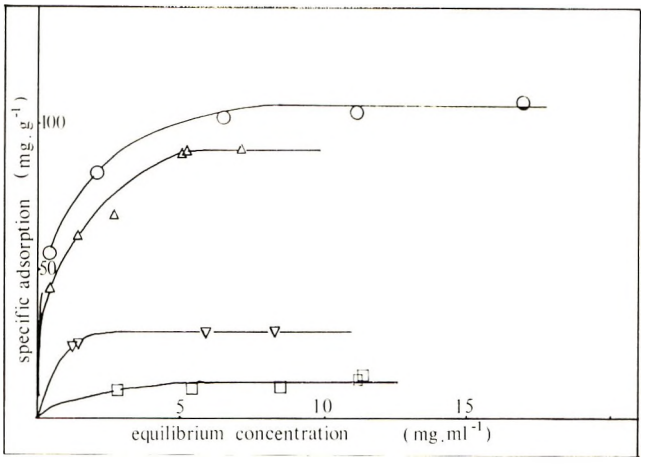

Fig. 2. Adsorption isotherms on charcoal (25°C): (⊙) Cop 4; (△) Cop 0; (⊡) Cop 2, in benzene; (▽) PS 2 in carbon tetrachloride.

With one exception, the adsorption is increased on moving from good to poorer solvents (as judged by the value of $[\eta]$). However, allowance has to be made for the relative affinities of polymer and solvent for the charcoal surface; even so, the low adsorption of Cop 1 from carbon tetrachloride seems anomalous. Addition of benzene to systems in which either PMM 2 or PS 2 had come to equilibrium adsorption from carbon tetrachloride brings about partial desorption; with Cop 1 adsorbed from carbon tetrachloride, however, addition of benzene causes enhanced adsorption.

A systematic study of adsorption behaviour was made from benzene solution. Table II lists the measured specific adsorptions at the isotherm plateau, together with pertinent characterisation of the polymers. The polymers are grouped in sets of similar composition in order of increasing molecular weight. The root-mean-square radii of gyration in Table II are calculated from the measured molecular weights and intrinsic viscosities via the Flory-Fox equation; many of the block copolymer viscosities were determined in toluene solution and it is assumed that there is no sig-

TABLE I
Solvent Dependence of Adsorption on Charcoal

Polymer[a]	Benzene		Carbon tetrachloride		Butanone	
	a_{∞}, mg/g[b]	$[\eta]$, dl/g	a_{∞}, mg/g	$[\eta]$, dl/g	$[\eta]$, dl/g	$[\eta]$, dl/g
PMM 2	16	1.250	28	0.230	—	—
PS 2	0	0.886	29	0.078	—	—
Cop 0	95	0.360	—	—	125	0.222
Cop 1	25	1.545	17	0.330	—	—

[a] See Table II for polymer code.
[b] Isotherm plateau specific adsorption.

TABLE II
Specific Adsorption from Benzene Solution

Polymer code[a]	Mole fraction styrene	$\bar{M}_n$[b]	$[\eta]$, dl/g (benzene, 25°C)	$\langle s^2 \rangle^{1/2}$, Å	a_∞, mg/g	
					Charcoal	Graphon
PMM 1	0.00	33,000	0.160	52	150	8
PMM 4	0.00	110,000	0.519	116	20	0
PMM 3	0.00	149,000	0.651	138	20	0
PMM 2	0.00	290,000	1.250	214	16	0
PS 1	1.00	10,000	0.091	29	0	44
PS 2	1.00	86,000	0.886	128	0	55
Cop 16	0.06	127,000	—	—	5	0
Cop 15	0.11	148,000	0.612	135	30	0
Cop 10	0.18	425,000	1.212	241	12	6
Cop 17	0.12	832,000	1.960	354	8	0
Cop 5	0.49	7,400	0.102	27	130	38
Cop 4	0.47	26,000	0.249	56	110	55
Cop 0	0.60	31,000	0.369	67	95	51
Cop 1	0.58	273,000	1.545	225	25	25
Cop 2	0.56	316,000	3.420	309	14	10
Cop 3	0.49	430,000	4.390	372	9	2
Cop 7	0.69	62,000	—	—	31	65

Cop	6	0.85	43,000	0.431	80	28	58
Cop	8	0.80	280,000	0.891	189	17	46
Cop	12	0.92	50,000	0.397	81	36	55
Cop	14	0.93	203,000	—	—	17	48
Cop	13	0.94	220,000	0.852	172	16	43
BC	10	0.15	28,000	—	—	39	—
BC	17	0.14	88,000	0.403 (0.410[c])	99 (100)[c]	30	50
BC	16	0.14	118,000	0.860[c]	140[c]	19	40
BC	15	0.42	190,000	1.000[c]	173[c]	26	54
BC	7	0.51	16,000	—	—	180	52
BC	20	0.50	133,000	0.560[c]	127[c]	29	62
BC	18	0.48	366,000	1.500[c]	246[c]	10	64
BC	4	0.83	11,000	—	—	55	24
BC	8	0.86	8,000	0.086[c]	27[c]	44	—
BC	14	0.90	56,000	—	—	24	59
BC	9	0.90	66,000	0.294[c]	81[c]	14	—
BC	11	0.97	46,000	0.430 (0.302[c])	81(72[c])	14	58
BC	19	0.99	140,000	0.980[c]	155[c]	3	58

[a] Cop signifies a statistical copolymer, BC an ABA-type block.
[b] Osmometry, toluene, 35°C.
[c] Toluene, 25°C.

nificant difference between the dimensions of the molecular coils in benzene and in toluene solution.

The relationship between $\langle s^2 \rangle^{1/2}$ and $\bar{M}_n$ is represented approximately by the equation

$$\log \langle s^2 \rangle^{1/2} = 0.585 \log \bar{M}_n - 0.855 \quad (1)$$

and, irrespective of composition, the radii of gyration fall within ca. $\pm 10\%$ of the mean given by the above expression. There is a distinct tendency for random copolymers of ca. 50% styrene to exhibit larger coil dimensions than the parent homopolymers. The above relationship is very close to that which may be deduced from the more accurate data on well fractionated styrene–methyl methacrylate random copolymers in toluene at 303°K reported by Kotaka et al.[6]

The necessity of regarding the molecular size of the adsorbate as a prime factor determining the adsorption into the porous adsorbent is clearly seen from inspection of Table II. On disregarding for the present the data from styrene homopolymers and from copolymers, particularly blocks, of very high styrene content, it is seen that increasingly high specific adsorptions are exhibited by polymers with radii of gyration less than ca. 80 Å but that the dependence of adsorption on molecular size is much less severe at high coil radii. Furthermore, with the above proviso, the overall adsorption pattern is determined by molecular size rather than by molecular composition.

The general similarity between the shape of the specific adsorption-radius of gyration curve and the adsorbent pore size distribution curve (in cumulative form) tempts us to make a closer analysis. The molecular weight dependence of adsorption on to a plane surface of the same composition as the charcoal is not known, but as an approximation is it assumed that on such a hypothetical surface, adsorption would be molecular weight independent. This is the case when representatives of the present set of polymers are adsorbed from benzene to nonporous Aerosil silica.[1] Having made the assumption that

$$a_\infty = K_1 S \quad (2)$$

where S is the available surface area, the second relation required is that between the equivalent pore radius r_p which will accept molecules of radi of $\langle s^2 \rangle^{1/2}$ and below. Again, the simplest assumption is that

$$\langle s^2 \rangle^{1/2} = K_2 r_p \quad (3)$$

On log–log plots of the requisite data it is found that the limiting cases are (1) the block copolymers of high styrene content and (2) the random copolymers with approximately 50% styrene (azeotropic copolymers) with the other polymers approaching the latter limit.

For high styrene blocks, $K_1 = 0.51$ and $K_2 = 2.32$: that is, 0.51 mg of polymer would be adsorbed on 1 m² of accessible surface, while a molecule of radius of gyration 100 Å would be able to enter pores of an equivalent

radius of 43 Å or greater. For the azeotropic copolymers $K_1 = 1.36$ and $K_2 = 3.98$. Among other limitations of this analysis, eq. (3) presupposes that molecular coils will, in order to enter a pore, deform by a constant factor whereas the larger coils are likely to be more deformable. An alternative analysis on the basis of the relation

$$\langle s^2 \rangle^{1/2} = r_p^{K_3} \tag{4}$$

leads to the following result. For high styrene blocks, $K_1 = 0.51$ and $K_3 = 1.15$; that is, pores of radius 50 Å will not accept coils of radius greater than 90 Å, while for pores of 100 Å the limiting coil size is 200 Å. At the other extreme, for the azeotropic copolymers, $K_1 = 1.36$ and $K_3 = 1.35$; this means that pores of 50 Å will be inaccessible only to coils in excess of 197 Å.

The values of adsorption per unit area of available surface appear to be of reasonable magnitude and are equivalent to specific adsorptions of the order 50–140 mg/g on a nonporous material with a specific surface area 100 m^2/g if that surface possessed the same composition as charcoal. However the amount of deformation apparently required of the chains on moving from the solution phase to the most constricted regions of the absorbent available to them appears quite excessive. A copolymer of molecular weight 10^5 whose size could be represented by eq. (1) would contract by only some 20% in radius of gyration on passing to θ conditions. The close relationship between the surface thickness of adsorbed polymer and its hydrodynamic radius in solution which has been established on plane surfaces by ellipsometry[7] and in sintered-glass disks by viscometry[8] is unlikely to be obeyed by chains adsorbed in narrow constrictions. Nonetheless, it is more likely that the large discrepancy between the critical r_p and $\langle s^2 \rangle^{1/2}$ values [eqs. (3) and (4)] is partially caused by the limitations of the pore size distribution analysis. It is perhaps necessary to recall the assumptions involved in the distribution analysis: these are that the pores are open-ended cylinders, that the surface tension and density of the capillary condensate have the same values as in the bulk liquid, that there is complete wetting between the capillary condensate and the adsorbed film, and that the Kelvin equation represents the equilibrium properties of the condensate interface. de Boer[9] has considered the relationship between pore geometry and the nature of the hysteresis loop in vapor sorption; the methanol adsorption–desorption isotherm observed in the present investigation, which shows a steep adsorption branch at high partial pressure, but a sloping desorption branch, could indicate several pore geometries. The indicated structures are (1) a set of wide-bore capillaries with a range of short narrow necks, (2) open wedge-shaped capillaries, or (3) a set of platelike capillaries of a range of separations.

In order to assess the effect of copolymer composition on adsorption it is necessary to concentrate on samples of similar coil size in solution. Figure 3 shows the adsorption as a function of composition for polymers with radii of gyration within the range 126–175 Å. The results are not

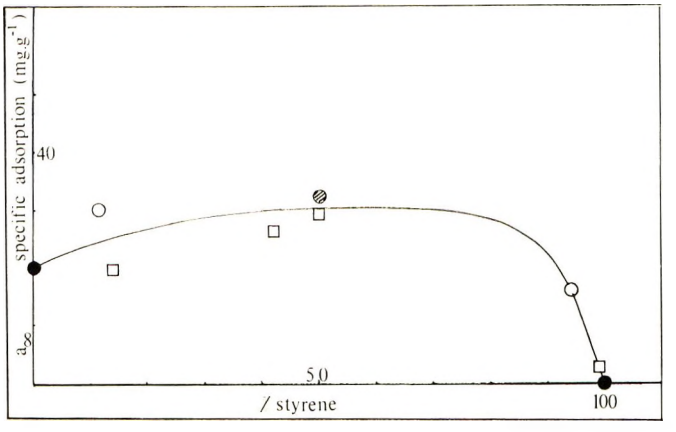

Fig. 3. Dependence of plateau specific adsorption on copolymer composition (charcoal, 25°C): (○), random copolymers; (□) block copolymers. Radii of gyration within range 126–175 Å (cross-hatched point interpolated).

unlike those previously reported[1] on the silica surface. Polystyrene is not adsorbed, but only a few methyl methacrylate units are required to bring about adsorption; the isolated methacrylate units in the high-styrene random copolymers are more efficient than the short end sequences in the block polymers. Except at the extreme ends of the composition range, copolymers are better adsorbed than is polymethacrylate homopolymer; generally, random copolymers have slightly higher specific adsorptions than block polymers of similar comonomer compositions.

The final feature of polymer adsorption on charcoal reported is that of preferential adsorption; it may be expected that the smaller species of the solute will be preferentially adsorbed and, in addition, at high styrene contents there may be preferential adsorption in terms of composition. We report one experiment, which used a block copolymer, as an example of preferential adsorption (Table III). The increase in supernatant in-

TABLE III
Time Dependence of Adsorption of BC 17 from Benzene Solution onto Charcoal at 25°C

Contact time, hr	Specific adsorption, mg/g	Intrinsic viscosity, dl/g
0	0	0.40
22	15	0.43
41	17	0.43
64	21	0.44
88	22	0.45
162	23	0.46

trinsic viscosity results from the loss of smaller species into the porous adsorbent. It is likely that the random copolymers, because of their broader molecular weight distribution, would show a more extensive fractionation effect. It should also be appreciated that the coil size–pore

radius analysis presented above is based on the coil dimension of the whole polymer rather than on that of the adsorbed fraction.

Adsorption on Graphon

Rate experiments with polystyrenes and representative copolymers from both benzene and chloroform solutions were performed. Adsorption is practically complete in ca. 24 hr. Thus, adsorption on to the nonporous Graphon is hardly more rapid than onto charcoal and is much slower than on Aerosil silica.[1] The adsorption isotherms had the form usual to polymeric adsorbates in that a rapid increase to a plateau adsorption at low equilibrium supernatant concentrations (2–5 mg/ml) is shown. As with charcoal, no systematic fit to theoretical isotherms was found on analysis of 29 isotherms, the majority of which referred to benzene solutions. The limited number of experiments made in solvents other than benzene preclude a detailed discussion of solvent effects on adsorption. However the results of Table IV show that carbon tetrachloride, although a poor solvent, does not lead to high adsorptions, presumably because of a high specific interaction with the carbon surface. The low amount of poly(methyl methacrylate) adsorbed from carbon tetrachloride is readily desorbed by a subsequent addition of benzene. However when benzene is added to systems in which either polystyrene or Cop 1 had been adsorbed on to Graphon from CCl_4, high specific adsorptions were observed. This effect is not readily explained since, to judge from solubility parameters, a benzene–carbon tetrachloride mixture should be a better solvent for these samples than either solvent alone.

For convenience in presentation, the specific adsorptions found from benzene solution are included as the final column of Table II. The effect of molecular weight on adsorption presents a puzzling feature. The random copolymers of approximately azeotropic composition show, except for the very low molecular weight sample, a specific adsorption which decreases with increase of molecular size. This trend is shown to a reduced extent by random copolymers of higher styrene content but is not clearly evidenced by the block polymers. A relation between adsorption and adsorbate size of this kind is invariably shown by porous adsorbents. Indeed, only one report in the literature[10] is known to us which describes a negative molecular weight dependence of adsorption on to an unambiguously nonporous substrate. Kraus and Gruver[10] showed that the adsorption of polybutadienes on to furnace blacks increased slowly with molecular weight up to a critical, rather high, value, after which the adsorption dropped markedly. These authors attributed the anomalous behavior to the inability of the high molecular weight species to penetrate the interstices between the particles of the carbon black agglomerates. We envisage a rather similar picture in which the larger adsorbed molecules are able to bridge several of the primary Graphon particles to form an aggregate in which some of the surface is inaccessible for further polymer adsorption. The fact that block copolymers of similar size and composi-

TABLE IV
Solvent dependence of adsorption on Graphon

Polymer	Benzene		Carbon tetrachloride		Butanone		Chloroform	
	a_∞, mg/g	$[\eta]$, dl/g	a_∞, mg/g	$a[\eta]$, dl/g	$_\infty$, mg/g	$[\eta]$, dl/g	a_∞, mg/g	$[\eta]$, dl/g
PMM 2	0	1.250	4	0.230	—	—	—	—
PS 2	55	0.886	58	0.078	—	—	31	0.783
Cop 0	51	0.360	—	—	100	0.222	25	0.396
Cop 1	25	1.545	16	0.330	—	—	—	—

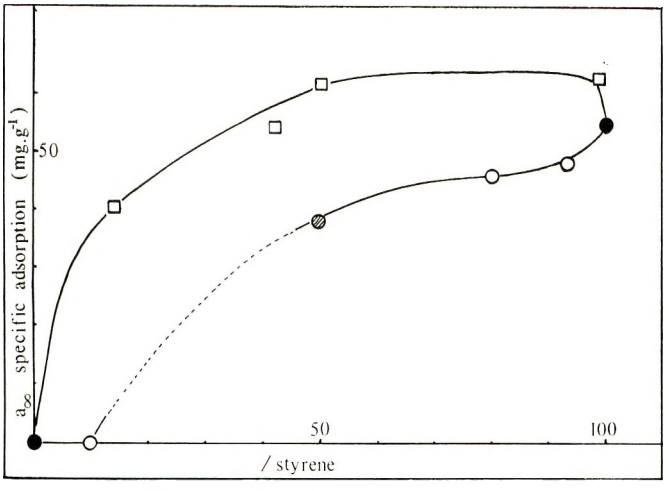

Fig. 4. Dependence of plateau specific adsorption on copolymer composition (Graphon, 25°C): (○) random copolymers; (□) block copolymers. Radii of gyration within range 126–180 Å (cross-hatched point interpolated).

tion do not exhibit this unusual effect is consistent with a bridging process, which, however, stops short of a gross flocculation.

The manner in which the specific adsorption varies with copolymer composition is somewhat complex and is exemplified in Figure 4; here the data points are for samples with radii of gyration within the range 120–180 Å. The first point to notice is that the homopolymer adsorption is reversed from the charcoal results. Now polystyrene is adsorbed whereas polymethacrylate (except at low molecular weights) is not adsorbed. Random copolymers of low styrene content are also rejected by the Graphon surface (in the presence of benzene) but block polymers of similar composition adsorb well. This apparent evidence of a cooperative effect of a block of adsorbable units is curiously opposite to the behavior of low methylmethacrylate polymers on to charcoal. Over the whole composition range, block copolymers adsorb to a greater extent than do the corresponding random copolymers; it is not known to what degree this difference could be attributed to the bridging mechanism postulated above.

A test for preferential adsorption was made as with charcoal, the same block copolymer being used (Table V).

TABLE V
Time Dependence of Adsorption of BC 17 from Benzene Solution onto Graphon at 25°C

Contact time, hr	Specific adsorption, mg/g	Intrinsic viscosity, dl/g
0	0	0.40
22	24	0.39
41	30	0.38
64	24	0.37
88	28	0.37
162	24	0.38

There is, perhaps, a slight evidence for a preferential adsorption of larger molecules but comparison of the data with those of Table III shows the difference in adsorption behavior onto nonporous and porous substrates.

CONCLUSIONS

Polymer adsorption behavior on charcoal is dominated by the porosity of the adsorbent. Our results suggest that considerable distortion is required of a polymer coil on adsorption in a small pore. However, the uncertainties of the pore analysis of a porous adsorbent of unknown internal geometry preclude a close analysis of our data. It should be noted that Burns and Carpenter[11] find that polystyrene on adsorption from a poor solvent (cyclohexane) on porous alumina penetrates pores of an equivalent radius not less than that of the radius of gyration.

Surprisingly, we find apparent evidence of "porosity" in Graphon from the adsorption of azeotropic copolymers of styrene and methyl methacrylate; this may be due to a "bridging" of Graphon spheres by adsorbed polymer to create an interparticulate porosity.

The relation between copolymer structure and adsorbability is complex. Generally speaking, relatively few of the more powerfully interacting residues are necessary to bind polymer to the adsorbent surface. On charcoal, random copolymers adsorb rather more than blocks of the same overall composition but the order is reversed on Graphon. We have earlier found[1] that block and random styrene–methyl methacrylate copolymers behave very similarly on silica when adsorbed from trichloroethylene but, when adsorbed from benzene, block structures are taken up preferentially.

We are indebted to Mr. A. Redfern for experimental assistance in molecular characterisation. One of us (A.J.H.) was in receipt of a Science Research Council Research Studentship during the period of this investigation.

References

1. J. M. Herd, A. J. Hopkins, and G. J. Howard, paper presented at American Chemical Society Meeting, Chicago, September 1970; *Polym. Preprints, J. Polym. Sci. C*, in press.
2. S. J. Gregg and K. S. W. Sing, *Adsorption, Surface Area and Porosity*, Academic Press, New York–London, 1967, p. 160 et seq.
3. R. Simha, H. L. Frisch, and F. R. Eirich, *J. Phys. Chem.*, **57**, 584 (1953).
4. H. L. Frisch, M. Y. Hellman, and J. L. Lundberg, *J. Polym. Sci.*, **38**, 441 (1959).
5. J. Koral, R. Ullman, and F. R. Eirich, *J. Phys. Chem.*, **62**, 541 (1958).
6. T. Kotaka, Y. Murakami, and H. Inagaki, *J. Phys. Chem.*, **72**, 829 (1968).
7. R. R. Stromberg, D. J. Tutas, and E. Passaglia, *J. Phys. Chem.*, **69**, 3955 (1965).
8. F. W. Rowland and F. R. Eirich, *J. Polym. Sci. A-1*, **4**, 2401 (1966).
9. J. M. de Boer, *Adv. Catalysis*, **8**, 18 (1956).
10. G. Kraus and J. T. Gruver, *Rubber Chem. Technol.*, **41**, 1256 (1968).
11. H. Burns Jr. and D. K. Carpenter, *Macromolecules*, **1**, 384 (1968).

Received July 6, 1970

JOURNAL OF POLYMER SCIENCE: PART A-2 VOL. 9, 853–865 (1971)

Adsorption Kinetics in the Polyethylenimine–Cellulose Fiber System*

WILLIAM A. KINDLER, JR.,* and JOHN W. SWANSON,
The Institute of Paper Chemistry, Appleton, Wisconsin 54911

Synopsis

The rate of adsorption of fractionated polyethylenimine (PEI) from water onto regenerated cellulose fibers was studied as a function of the polymer diffusion coefficient. Differences in polymer molecular weight, salt concentration, and pH were employed to vary the diffusion coefficient which was measured independently by a free-diffusion technique. The sorption rate was measured at the same conditions and found to increase with decreasing molecular weight, increasing polymer concentration, decreasing salt concentration, and increasing pH. A simplified rate equation based on diffusion control with Langmuirian adsorption in stirred solution was developed by utilizing the concept of a Nernst diffusional film. The equation was successful in predicting the relationship between adsorption rate and diffusion coefficient for most cases studied. It was found, however, that a very large barrier to mass transfer retards the adsorption rate. For the system studied it was concluded that this barrier is a result of diffusion into and subsequent adsorption onto the internal porous structure of the cellulose.

INTRODUCTION

Many previous workers investigating the rate of polymer adsorption at a solid–liquid interface have suggested a mass-transfer process as the rate-controlling step.[1–4] This report describes an examination of the relationship between the adsorption rate and the polymer diffusivity for the polyethylenimine-cellulose fiber system. This system represents the case of a cationic polyelectrolyte adsorbing onto an oppositely charged surface.

Several system parameters were varied in order to provide the desired information concerning the rate process. Five polyethylenimine (PEI) fractions of different molecular weight were employed to determine if the polymer size affected the sorption rate only through the diffusion coefficient. The sorption rate was measured in the presence of sodium chloride and at two different pH levels to ascertain the effect of polymer charge. Finally the dependence on polymer concentration was determined.

* Present address: Crown Zellerbach Corp., Camas, Washington.

EXPERIMENTAL

Materials

The adsorbent consisted of regenerated cellulose fibers (RD-101) supplied by the American Viscose Division of FMC Corporation. The fibers are 1.5 den and 0.25 in. in length. These fibers are characterized by a particularly high surface area and high conformability for synthetic fibers. The adsorbent was subjected to six, four-hour soaks in distilled water to remove any occluded water-soluble impurities which might have been introduced during manufacutre.

The polymer was adsorbed onto the fibers from aqueous solutions of sodium hydroxide and, in some cases, sodium chloride. The distilled water used to prepare these solutions always had a conductivity of less than 1.5×10^{-6} mho/cm.

The PEI used in this study was provided by The Dow Chemical Company (control number SA 1117-633974). To limit effects of polydispersity, several narrow molecular weight fractions were prepared by gel permeation chromatography. The polymer was eluted from a bed of Bio-Gel P-10 with an aqueous solution of 0.64% sodium acetate. The eluting polymer was monitored with a recording differential refractometer. Eighteen polymer-containing fractions were isolated from the eluting stream but only the fourth through the eighth fractions were studied.

The molecular weights of the five fractions studied were determined by means of a sedimentation equilibrium technique[5] on a Beckman Spinco Model E ultracentrifuge. The molecular weights averaged over the whole cell at infinite dilution are given in Table I. All runs were made in an aqueous solvent of 0.10*N* sodium chloride to suppress charge effects.

TABLE I
Diffusion Coefficients at Infinite Dilution

Fraction number	Molecular weight	pH	NaCl concn. $\times 10^3$, *M*	$D_0 \times 10^6$, cm²/sec
63–8	8,000	10.9	0	2.1
63–8	8,000	10.9	2.0	1.69
63–8	8,000	10.9	5.0	1.25
63–7	9,500	10.9	0	2.0
63–7[a]	9,500	9.6	0	2.6
63–6	11,500	10.9	0	1.90
63–5	14,000	10.9	0	1.80
63–4	20,000	10.9	0	1.60

[a] In $8.0 \times 10^{-5}N$ NaOH; all other runs in $8.0 \times 10^{-4}N$ NaOH.

Diffusion Measurements

The diffusion coefficient of the polymer was measured at the various conditions of interest by means of a free-diffusion technique. A solvent-solution boundary was created in a synthetic boundary cell on the Beckman

Spinco Model E ultracentrifuge. The Rayleigh optical system was employed to follow the rate of polymer diffusion. Diffusion coefficients were calculated by means of the Creeth method[6] for each condition. Each polymer solution was dialyzed against the appropriate solvent prior to loading the cells.

Adsorption Experiments

Adsorption rate curves were measured at the same set of conditions under which the diffusion coefficients were determined. In addition, complete equilibrium isotherms were determined experimentally at each condition.

The adsorption experiments were conducted in screw-top centrifuge tubes of approximately 50-ml capacity. The viscose fibers of known moisture content were weighed directly into the tubes. The weight of fibers was chosen to give the equivalent of 0.130 ± 0.002 g of fiber (on an oven-dry basis) in each tube. A given amount of the appropriate solvent was added to the tubes by buret. The solvent was an aqueous solution made up to the conditions of the adsorption test in terms of sodium hydroxide and sodium chloride concentration. The quantity of solvent added at this stage varied depending on the amount of polymer solution to be added but was always at least 25 ml. The fiber-solvent slurry was agitated on a rotator in a water bath at 25.0°C for at least 12 hr prior to the addition of polymer. This was done to assure complete equilibrium of the fibers with respect to temperature, swelling, dispersion, and the ionic distribution of the solvent.

A stock polymer solution was also prepared under the conditions of the sorption experiment in terms of ionic strength and pH. The concentration of this solution was so chosen that when a convenient volume was added to the slurry, the desired initial polymer concentration was approximated. The volume of the solvent initially added to the fibers was chosen to result in a total system volume of 45.0 ml after the addition of the appropriate quantity of polymer.

The appropriate volume of polymer solution was added to the slurry with a pipet which was moved through the slurry during addition to assure a uniform initial distribution. The tubes were then resealed and returned to the agitation assembly. Approximately 30 sec was required to load the polymer solution and begin agitation.

The loaded tubes were fastened to the periphery of two notched 12-in. wheels mounted on a common axis within a constant temperature water bath controlled at 25.0°C. The wheels were mounted in a manner which permitted varying the angle between the tubes and the axis. All experiments were performed at a rotation speed of 4.5 rpm and an angle of 15°. These conditions provide very little agitation within the tube but allow for no settling of the fibers.

After agitation for a predetermined time interval, (29 hr for the equilibrium runs) the tubes were removed for analysis. A 5-ml aliquot of the

solution phase was removed through a 5-in. length of Teflon spaghetti tubing attached to a 5-ml syringe. The end of the tubing was crimped shut and the sides were perforated with a large number of pin holes. When this tubing was immersed in the slurry and agitated slightly, a portion of the solution phase could be slowly removed without picking up any fibers or forming a mat of the fibers. Approximately 15 sec was required to remove the centrifuge tube from the agitator and withdraw the sample solution.

This 5-ml aliquot was analyzed for PEI content, and the difference between the initial and final concentration was attributed to sorption on the fibers. Blank runs indicated that there was no loss of polymer through handling or sorption on the glassware.

The PEI concentration was determined by a colorimetric technique based on a colored complex formed between the polyamine and cupric ion.[7] A 1-ml portion of a solution which was 0.01*M* in cupric acetate and 0.01*M* hydrochloric acid was mixed thoroughly with 5 ml of the polymer solution to be tested. The absorbance of this mixture was measured at a wavelength of 269 mμ. The concentration was determined by comparing the absorbance with a standard curve determined at the same conditions of pH, salt concentration, and molecular weight. Best results were obtained with PEI concentrations between 5 and 100 mg/l. The absorptivity is typically on the order of 54 mg/l per absorbance unit.

RESULTS AND DISCUSSION

Diffusion Coefficients

The concentration dependence of the diffusion coefficients over the range of concentrations involved in the adsorption tests (less than 200 mg/l.) was negligible. The diffusion coefficients at infinite dilution are listed in Table I at the various conditions of interest.

At constant pH and salt concentration, the diffusion coefficient increases with decreasing molecular weight as expected. The very significant effects of pH and salt concentration may be due to the previously described electrophoretic effect.[8,9]

Equilibrium Isotherms

Early work showed that maximum retention was achieved in $8.0 \times 10^{-4}N$ sodium hydroxide (this gave a solution pH of 10.9 ± 0.2). Most data were taken at this pH level to optimize the amount of adsorbed polymer and the reliability of the results.

An example of the equilibrium isotherms is shown in Figure 1. The upper curve is a standard isotherm representation given as grams of polymer adsorbed per 100 g of fiber versus the equilibrium polymer concentration. The lower curve is plotted according to the Langmuir equation given as:

$$C_e/C^*_e = (1/C_mK) + (C_e/C_m) \quad (1)$$

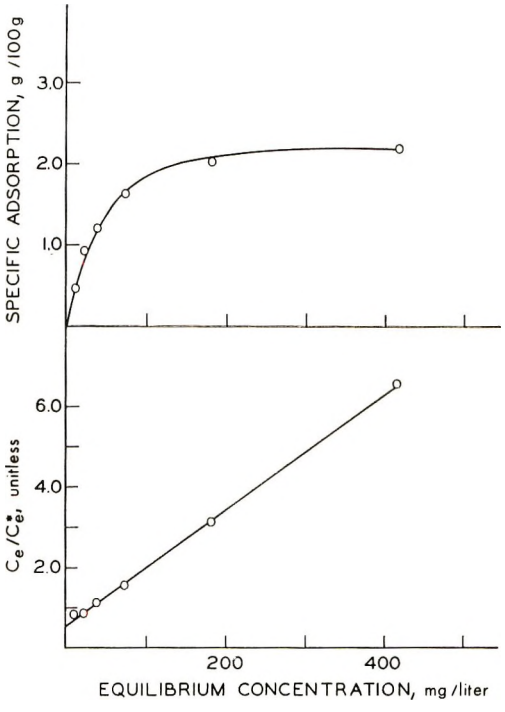

Fig. 1. Equilibrium isotherms for 63-7 (M_w = 9500) in 8.0 × $10^{-4}N$ NaOH.

where C^*_e is the loss in solution concentration due to sorption at C_e, C_m is the loss in solution concentration when the adsorbent is saturated with adsorbate, and K is the Langmuir constant. According to this expression, Langmuir behavior implies a linear relationship between C_e and C_e/C^*_e. Figure 1 shows that the equilibrium behavior can be described by means of the Langmuir equation. All equilibrium isotherms measured exhibited a good fit to the Langmuir equation. Values of C_m and K were determined from the slope and intercept of the Langmuir plots and are tabulated in Table II.

TABLE II
Langmuir Constants and Saturation Adsorption Values For Fractions of PEI in 8.0 × $10^{-4}N$ NaOH

Fraction number	Molecular weight	K, l./mg	C_m, mg/l.
63–4	20,000	0.015	17.0
63–5	14,000	0.0091	34.0
63–6	11,500	0.0081	57.0
63–7	9,500	0.020	65.0
63–8	8,000	0.082	78.0

The amount of polymer adsorbed at saturation is clearly greater for the smaller molecules. This is interpreted as a direct reflection of the dif-

ferences in accessibility due to the porous nature of the adsorbent. The larger molecules are apparently excluded from a significant portion of the fiber which is accessible to the lower molecular weight fractions.

An equilibrium isotherm was also determined for fraction number 7 in $8.0 \times 10^{-5}N$ sodium hydroxide. The pH of this solution was 9.6 ± 0.2 as compared with 10.9 ± 0.2 for the previous runs in $8.0 \times 10^{-4}N$ sodium hydroxide. The constants as determined from the Langmuir equation are 19.6 mg/l for C_m and 0.019 for K. The Langmiur constant was virtually unchanged on going from pH 10.9 to 9.6, but the amount adsorbed at saturation decreased by more than a factor of three.

Adsorption Rate

The adsorption rate was measured for each of fractions 63-4 through 63-8 to cover a range of molecular weights between 8000 and 20,000. Sorption occurred from $8.0 \times 10^{-4}N$ sodium hydroxide to give a pH of

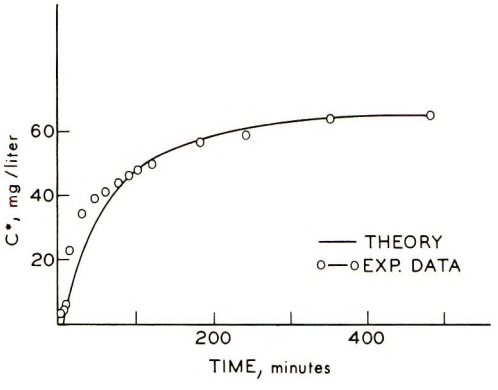

Fig. 2. Rate curve for 63-8 at pH 10.9, C_0 = 133 mg/l.

10.9 ± 0.2. The temperature of adsorption was controlled at 25.0 ± 0.2°C. Examples of the rate curves are shown in Figures 2–6. The drawn curves in these figures are based on the theory described below. The initial rates for each set of curves are listed along with the initial polymer concentrations in Table III.

TABLE III
Effect of Molecular Weight on Initial Rate

Fraction number	Molecular weight	Initial concn, mg/l.	Initial rate × 10^2, mg/l.-sec
63–8	8,000	133	1.87
63–7	9,500	96.0	0.74
63–6	11,500	106	0.50
63–5	14,000	99.0	0.23
63–4	20,000	96.2	0.11

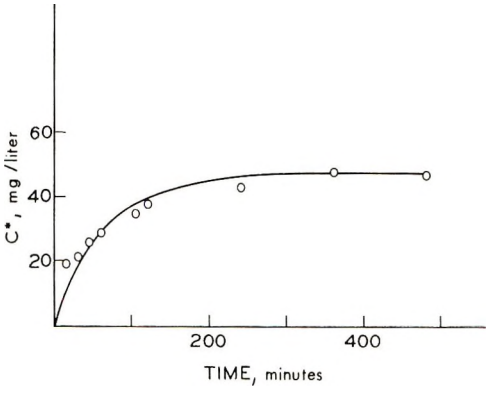

Fig. 3. Rate curve for 63-S at pH 10.9 in 2.0×10^{-3} M NaCl, $C_0 = 133$ mg/l.

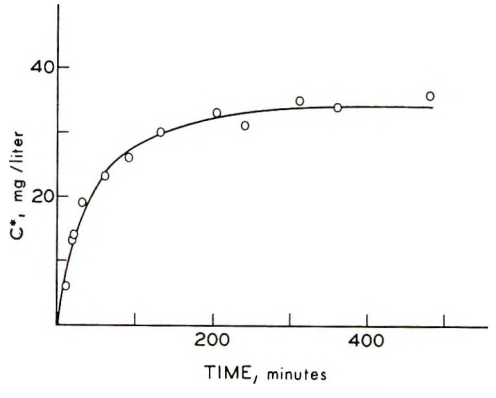

Fig. 4. Rate curve for 63-S at pH 10.9 in 5.0×10^{-3} M NaCl, $C_0 = 133$ mg/l.

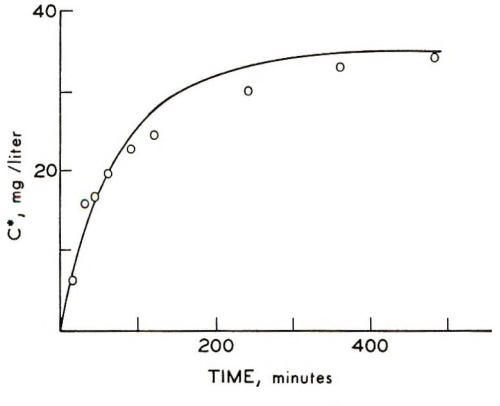

Fig. 5. Rate curve for 63-7 at 10.9, $C_0 = 96$ mg/l.

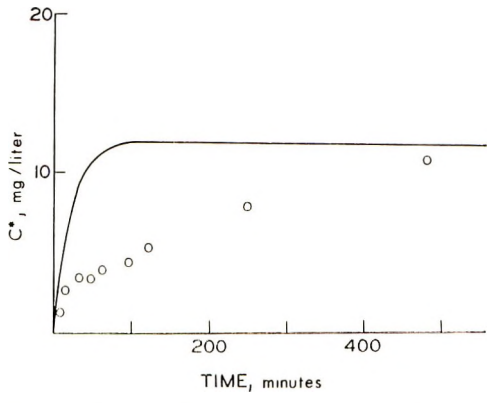

Fig. 6. Rate curve for 63-7 at pH 9.6, C_0 = 96 mg/l.

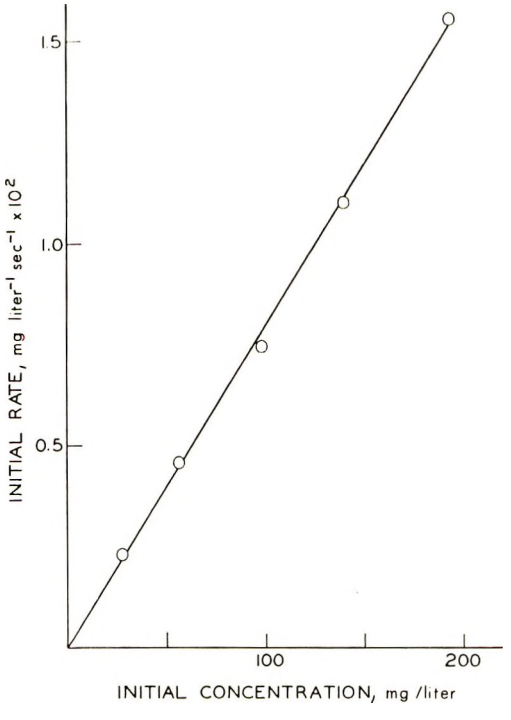

Fig. 7. Effect of polymer concentration on initial rate.

The adsorption rate of fraction 63-7 was measured at a series of initial polymer concentrations ranging from 27.4 to 191 mg/liter. All other conditions were the same as those described for the molecular weight experiments. The apparent first-order behavior is evident in Figure 7.

Adsorption rate measurements were performed by using fraction 63-8 in aqueous solvent consisting of $8.0 \times 10^{-4}N$ sodium hydroxide plus various amounts of sodium chloride. The initial polymer concentration was 133 mg/l. The results of these tests are given in Figures 2–4.

The effect of pH on the adsorption rate was investigated briefly. The adsorption rate of fraction 63-7 was measured at pH 9.6 and compared with the rate at pH 10.9. The initial polymer concentration was the same in each experiment at 96.0 mg/l. The results can be seen in Figures 5 and 6.

Adsorption Rate as a Mass-Transfer Process

In order to relate the polymer diffusion coefficient to the sorption rate, it is necessary to describe the adsorption as a mass-transfer process. For a stirred system involving Langmuirian adsorption, this is no easy task. As a first approximation, however, this problem can be approached by invoking the concept of a Nernst diffusional film.[10] In essence, this concept says that the polymer must diffuse across some barrier to reach an active site and present itself for adsorption. It is assumed that the concentration gradient across the barrier is linear which permits us to write:

$$dN/dt = -(DA/\delta)\ (C_s - C_f) \tag{2}$$

where D is the diffusion coefficient of the polymer, A is the fiber surface area available for adsorption, δ is the distance over which the polymer must diffuse if the only barrier to mass-transfer is a stagnant film of solvent, C_f is the concentration at the fiber–liquid interface, C_s is the concentration at a distance δ from the interface, and dN/dt is the flux at the interface.

If the rate of reaction between polymer segments and the surface is very fast compared to the rate of mass transfer, then the rate of polymer crossing the solid–liquid interface will be equal to the rate of adsorption. Thus, if N^* is the weight of adsorbed polymer, the rate of adsorption can be expressed as,

$$dN^*/dt = (DA/\delta)\ (C_s - C_f) \tag{3}$$

The concentration of polymer in solution at the interface may be assumed to be in equilibrium with adsorbed polymer at any instant in time. It has been shown experimentally that this equilibrium condition is given by the Langmuir equation. Thus, C_f can be written as a function of C^*, the amount of polymer adsorbed at time t, and the Langmuir constants C_m and K.

The concentration of polymer in the bulk phase at any time t is given as the difference between the initial polymer concentration C_0 and the concentration C^* adsorbed at time t.

The surface area A is also a time-dependent quantity since, for monolayer adsorption, the surface area available for sorption decreases as adsorption proceeds. If A_0 is the initial surface area, the time-dependent area can be expressed in terms of the amount of polymer sorbed at time t, as follows:

$$A = A_0(1 - C^*/C_m) \tag{4}$$

It has been shown[10] that δ is proportional to $D^{0.34}$; thus,

$$\delta = g_1 D^{0.34} \tag{5}$$

where g_1 is a constant for a given set of shear conditions. Levich[11] has derived a similar expression from the theory of convective diffusion.

Making the appropriate substitutions into eq. (3) for δ, C_s, C_f, and A and expressing polymer content in terms of concentration yields a differential equation for the rate process:

$$\frac{dC^*}{dt} = \frac{D^{0.66} A_0}{V g_1}\left[\left(\frac{1}{C_m}\right) C^{*2} - \left(\frac{C_0}{C_m} + \frac{1}{KC_m} + 1\right) C^* + C_0\right] \tag{6}$$

where V is the total volume of the system.

The solution to the differential equation is given by,

$$C^* = \frac{C_m(b + \sqrt{-q})\,(1 - \exp\{yt\})}{2\,(\exp\{yt\} - B)} \tag{7}$$

where

$$b = -\left(\frac{C_0}{C_m} + \frac{1}{KC_m} + 1\right) \tag{8}$$

$$q = 4\,(C_0/C_m) - b^2 \tag{9}$$

$$B = (b + \sqrt{-q})/(b - \sqrt{-q}) \tag{10}$$

$$y = (\sqrt{-q}\, D^{0.66}/V)\,(A_0/g_1) \tag{11}$$

For small times when $C^* \cong C_0$, eq. (6) reduces to

$$(dC^*/dt)_{t\to 0} = (D^{0.66} A_0/V g_1)\, C_0 \tag{12}$$

All of the variables in eqs. (7) and (12) have been determined experimentally except for the accessible surface area, A_0, and the constant g_1.

The effective surface area of a porous surface such as cellulose should be a function of the molecular weight of the adsorbing polymer. A smaller molecule would see a greater accessible area than would a larger molecule. The importance of this factor to the cellulose fiber–PEI system is verified by the greater equilibrium saturation adsorption for the lower molecular weight fractions.

An effective surface area accessible to adsorption, S_e, can be estimated from the size of the polymer molecule and the amount of polymer adsorbed at saturation. The size of the polymer molecule can be estimated from the diffusion data.[12] The areas, S_e, calculated in this way vary from 1.3×10^4 to 9.5×10^4 cm^2/g. The geometric surface area of the fibers is 0.2×10^4 cm^2/g. The calculated area S_e is related to A_0 through the expression (13):

$$A_0 = g_2 W_f S_e \tag{13}$$

where g_2 is a proportionality constant to account for packing efficiency, the polymer shape, and lateral interactions between sorbed polymer; W_f is the weight of fiber in the adsorption system. The fiber weight factor must be included since S_e is a specific surface area, and A_0 is the total amount of surface area in the system.

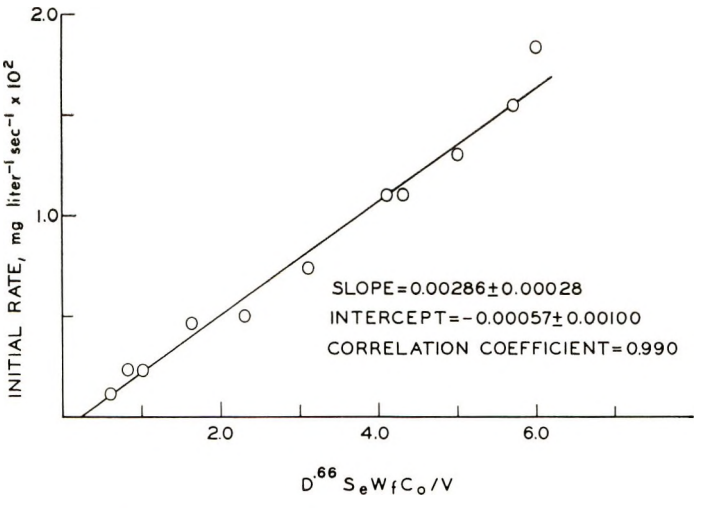

Fig. 8. Plot of initial rate as a function of experimental parameters according to theoretical equation.

Combining eq. (13) and (12) yields the differential equation (14) for the initial adsorption rate:

$$(dC^*/dt)_{t\to 0} = (g_2/g_1)\ (D^{0.66}S_eW_fC_0/V) \tag{14}$$

This expression predicts that the initial rate should be a linear function of the initial polymer concentration as was verified in Figure 2.

With the exception of the two constants g_1 and g_2, all of the quantities in eq. (14) have either been measured experimentally or can be calculated from experimental data. The equation predicts that a plot of the initial rate as a function of $(D^{0.66}S_eW_fC_0/V)$ will yield a straight line passing through the origin and having a slope of (g_2/g_1). Such a plot for all the data taken at pH 10.9 is presented in Figure 8. The data points represent variables of molecular weight, polymer concentration, and salt concentration. The slope and intercept along with the 95% confidence limits for each were determined by least squares analysis. The slope was found to be $2.86 \times 10^{-3} \pm 0.28 \times 10^{-3}$ cm$^{-0.32}$-sec$^{0.66}$. The intercept is $-0.57 \times 10^{-3} \pm 1.00 \times 10^{-3}$ mg/l.-sec which includes the origin as predicted. The correlation coefficient for the linear representation is 0.990, indicating a good straight line fit.

The overall rate curves can be calculated from eq. (7) by utilizing eq. (13) and the value of g_2/g_1 obtained from the slope of Figure 8. Examples of the comparison between the shape of the theoretical and experimental curves are shown in Figures 2–6. The circles represent the experimental data points and the solid lines are the calculated rate curves. With some exceptions, it may be said that the two curves are in good agreement. Seven other runs were treated in the same way but are not shown. The agreement between the calculated and experimental curves for the unreported curves was excellent.

The significant deviations which are apparent in Figures 2 and 6 are thought to be due to electrostatic interactions between the cationic polymer and the anionic fiber.

Figure 2 (at pH 10.9) represents the case of a relatively high degree of fiber ionization and a fairly low degree of polymer ionization (only a few per cent). Thus, in the early stages of adsorption, an electrostatic interaction between fiber and polymer may accelerate the rate of mass transfer. Added salt (Figs. 3 and 4) shields the charges from one another, and the rate is more in accord with that predicted on the basis of mass transfer by Fick's diffusion alone.

In Figure 6 (pH 9.6), the conditions provide for a very low degree of ionization of the fiber but a much higher degree of polymer ionization. In this case the isoelectric point of the fiber is reached after a small amount of polymer has been adsorbed. Past the isoelectric point the fiber has a net positive charge. Thus, the electrostatic interaction becomes one of repulsion and the rate is retarded.

Additional information about the nature of the adsorption process can be derived from a consideration of the magnitude of the effective diffusional film thickness δ. Assuming y_2 is equal to unity, y_1 can be calculated from the slope of Figure 8 and δ can be estimated from:

$$\delta = y_1 D^{0.34} \tag{15}$$

The thickness so calculated is about 4 cm, clearly a physical impossibility. This is about one thousand times greater than the film thickness calculated for many dissolution processes.[10] This impossibly large magnitude for δ indicates that the barrier to mass transfer is not simply a film of stagnant solvent. Several factors could conceivably contribute to this barrier, for example: diffusion and subsequent adsorption within the fibrous structure, entropy barriers, or solvent interactions. For the system under investigation, it is thought that the cellulose gel structure represents the main barrier to diffusion. The inverse relationship between molecular weight and extent of adsorption supports the importance of diffusion and adsorption within the cellulose matrix.

CONCLUSIONS

The rate of adsorption of polyethylenimine onto regenerated cellulose fibers can be described as a mass-transfer process. This process is not, however, adequately described by diffusion across a stagnant layer surrounding the fiber as was previously supposed. It is necessary to acknowledge the presence of additional barriers to mass flow. For the system described in this paper, the diffusion into and subsequent adsorption onto the internal porous structure represents the predominant barrier to rapid adsorption. Evidence is provided which indicates that, under suitable conditions, mass transfer as a result of electrostatic interactions between polymer and fiber may be superimposed on the diffusion process.

This paper is taken in part from the thesis submitted by W. A. K. in partial fulfillment of the requirements of The Institute of Paper Chemistry for the degree of Doctor of Philosophy from Lawrence University, Appleton, Wisconsin, January 1971.

References

1. F. Patat, E. Killman, and C. Schliebener, *Rubber Chem. Technol.* **39,** 36 (1966).
2. E. F. Thode, J. W. Swanson, S. F. Kurath, and G. R. Hoffman, *Tappi,* **42,** 170 (1959).
3. V. A. Russo and E. F. Thode, *Tappi,* **43,** 209 (1960).
4. J. J. Becher, G. R. Hoffman, and J. W. Swanson, *Tappi,* **44,** 296 (1961).
5. D. C. Teller, Ph.D. Dissertation, University of California, Berkeley, Calif., 1965.
6. J. M. Creeth, *J. Amer. Chem. Soc.,* **77,** 6428 (1955).
7. T. D. Perrine and W. R. Landis, *J. Polymer Sci. A-1,* **5,** 1993 (1967).
8. Y. Suzuki, I. Noda and M. Nagasawa, *J. Phys. Chem.,* **73,** 797 (1969).
9. M. Nagasawa and Y. Eguchi, *J. Phys. Chem.,* **71,** 880 (1967).
10. L. L. Bircumshaw and A. C. Riddiford, *Quart. Revs.* (London), **6,** 157 (1952).
11. V. G. Levich, *Physicochemical Hydrodynamics,* Prentice-Hall, Englewood Cliffs, N. J., 1962.
12. C. Tanford, *Physical Chemistry of Macromolecules,* 2nd ed., Wiley, New York, 1963.

Received October 15, 1970

JOURNAL OF POLYMER SCIENCE: PART A-2 VOL. 9, 867–886 (1971)

Mechanical Relaxations in Polyamides

D. C. PREVORSEK, R. H. BUTLER, and H. K. REIMSCHUESSEL,
Allied Chemical Corporation, Corporate Chemical Research Laboratory, Morristown, New Jersey 07960

Synopsis

Dynamic mechanical measurements were carried out as a function of temperature (−100 to +180°C) and frequency (3.5 to 110 cps) for a series of aliphatic terpolyamides, nylon 6 and nylon 12. Effect of crosslinking with toluene diisocyanate, of absorbed water, and of frequency are used to estimate the statistical segment length associated with the α' relaxation. The effects of variations in the aliphatic chain length in the repeating unit on the temperature of the α' relaxation are examined by means of copolymer rules with a view to explaining the reported insensitivity of the glass transition temperature of these polymers to changes in (CH_2)/(amide) group ratio. From the estimated length of the segmental motion associated with the α' relaxation it is inferred that in a series of polyamides of the type nylon X or nylon X,Y (where X or Y = 3, 4, 5, 6, etc.) there should be a relatively small change in the temperature of the α' transition for those polyamides having X or Y less than about 45. Experiments which are intended to establish the position of the crystalline α–γ transition are discussed.

INTRODUCTION

Aliphatic polyamides show three well defined mechanical relaxations in the temperature range between −150 and +120°C. The nature of these relaxations labeled as γ, β, and α' which occur with nylon 6 at −120, −40, and +80°C was studied by several authors.[1] It is now generally accepted that the γ transition involves a cooperative motion of the methylene groups between amide linkages, while β and α' transitions involve motions of non-hydrogen-bonded and hydrogen-bonded amide groups in the amorphous regions respectively.[1,2]

An interesting feature of the α' relaxation (which is considered by many authors to be the glass transition of the polymer) is the low sensitivity of its location in temperature to variations in the length of the aliphatic chain. If one considers a long-chain aliphatic polyamide as a copolymer of polyethylene and a short-chain polyamide, then according to the well known schemes for calculating the T_g of copolymers, one would expect that the glass transition of polyamides would decrease with increasing length of the aliphatic chain. The fact that no such trend has been observed (for example, nylon 6,10 and nylon 18,16 exhibits, according to Komoto,[3] the same temperature of the α relaxation) casts further doubt about the nature of this relaxation.

Another uncertainty which needs clarification concerns the position of the crystalline α–γ transition in nylon 6 which appears to be superimposed on the α' (amorphous) relaxation. According to Takayanagi,[4] this relaxation which involves a crystal structure change from monoclinic to hexagonal, appears as a shoulder on the high-temperature side of the peak at approximately 120°C. In a recent study, Brown and Campbell[5] have used moisture adsorption to separate the α' relaxation from this crystalline relaxation. From their data, these authors conclude that the α–γ crystalline transition occurs at 75°C. This is below the temperature of the α' transition which they observe at 90°C in the dry state.

In this paper we summarize the results of our studies which are intended to clarify some of the questions raised above with regard to the nature of the α' transition and to determine more accurately the temperature of the crystalline transition observed by Takayanagi and Brown. In addition, we include some of our findings which are not pertinent to the above problems, but represent new information regarding the dynamic-mechanical behavior of aliphatic polyamides.

EXPERIMENTAL

Dynamic Mechanical Measurements

Measurements of dynamic tensile moduli (E' and E'') as a function of temperature with specific humidity as a parameter were made by using the Vibron dynamic viscoelastometer. Humidity control was achieved by modifying the Vibron temperature chamber to allow injection of air of known relative humidity (at room temperature, 23°C). The moisture content of the injected stream of air was controlled by mixing known proportions of saturated and dry air at 23°C. The temperature was monitored by a thermocouple placed about 2 mm from the center of the test specimen to provide temperature measurements to ±0.5°C. Experiments to determine the variation in dynamic moduli with temperature were made by increasing the temperature at constant heating rates of 1–2°C/min from the minimum to the maximum temperatures employed. The magnitude of the dynamic tensile modulus and the tangent of the phase angle (tan δ) were measured at various temperatures (usually about every 3–4°C) during this time. The average tensile strain used in the experiments was approximately 0.5%. The tension of the sample was adjusted at each measurement point to allow for thermal expansion and contraction following the operating procedures generally used on the Vibron instrument. The sinusoidal driving frequency used in the experiments was usually 110 cps. The Lissajous figure produced by superimposing the sinusoidal stress and strain was monitored during the experiments on an X–Y oscilloscope.

Preparation of Terpolyamides

The monomers and catalyst were placed in glass polymerization tubes in which a nitrogen atmosphere was maintained. The tubes were immersed in

TABLE I
Composition, Polymerization Condition and Characteristics of Experimental Aliphatic Terpolymers

Terpolymer	Initial composition			Polymerization conditions		Polymer properties		
	Monomers	Wt monomer, g	H_3PO_4, ml	Time, hr	Temp, °C	η_{sp}	Mp, °C	N, %
Nylon 8,11,12	2-Azacyclononanone	10						
	ω-Aminoundecanoic acid	10						
	2-Azacyclotridecanone	10	0.20	64	245	1.18	127	7.86 ± 0.1
Nylon 7,11,12	2-Azacyclooctanone	9.1373						
	ω-Aminoundecanoic acid	9.1629						
	2-Azacyclotridecanone	9.0033	0.20	64	245	1.20	133	8.26 ± 0.1
Nylon 6,11,12	Caprolactam	10						
	ω-Aminoundecanoic acid	10						
	2-Azacyclotridecanoic acid	10	0.20	24	245	1.24	128	9.10 ± 0.1
Nylon 6,8,12	Caprolactam	10.023						
	2-Azacyclononanone	10.006						
	2-Azacyclotridecanone	10.059	0.20	24	245	1.37	128	10.0 ± 0.1
Nylon 6,8,11	6-Aminocaproic acid	10						
	2-Azacyclononanone	10						
	ω-Aminoundecanoic acid	10		64	245	1.68	117	9.95 ± 0.2

an oil bath which was heated to the desired temperature. A stream of nitrogen was passed above the melt throughout polymerization. At the end of the polymerization the reaction mixture was quenched to room temperature, ground, and extracted with water in a Soxhlet apparatus. After extraction the polymers were dissolved in alcohol and precipitated with water. The polymers thus obtained were dried under vacuum over P_2O_5. The reduced viscosities of the polymer solutions were measured at 25°C in an Ubbelohde viscometer employing concentrations of 0.52 g of polymer per 100 ml of *m*-cresol. The melting points were determined by DTA. Initial compositions, conditions of polymerization, and polymer viscosities are given in Table I.

The film samples used in the relaxation studies were prepared by hot pressing of dried polymers (at 210°C) followed by quenching in an acetone–solid CO_2 bath. An x-ray examination of the samples indicated a small amount of α-phase in all cases. The degree of crystallinity varied from 3 to 8% with the exception of the nylon 6,11,12 sample, which was 12% crystalline.

RESULTS AND DISCUSSION

The α' Relaxation and Glass Transition in Aliphatic Polyamides

One of the characteristic features of aliphatic polyamides is the low sensitivity of their α' transition to variations in the length of the aliphatic chain. This behavior is illustrated in Table II, where the data of Takayanagi[4] and

TABLE II
Glass Transition Temperatures of Various Aliphatic Polyamides

Polyamide	T_g, °C
Nylons[a]	
Nylon 6	91
Nylon 7	83
Nylon 8	76.5
Nylon 9	70.5
Nylon 11	68
Nylon 12	70.5
—$NH(CH_2)_x$—$NHCO(CH_2)_y$—CO—[b]	
$x = 6, y = 8$	51
$x = 6, y = 10$	50
$x = 8, y = 10$	50
$x = 8, y = 20$	48
$x = 10, y = 10$	49
$x = 12, y = 16$	50
$x = 14, y = 16$	48
$x = 18, y = 16$	50

[a] Data of Takayanagi.[4]
[b] Data of Komoto.[3]

Komoto[3] for a series of polyamides having different number of CH_2 groups per amide group are presented. Based on the generally accepted assignment of the α' relaxation to the onset of long segmental mobility, many authors consider that the α' transition should be regarded as the glass transition of these polymers. This view appears to be disputable if one examines Table II in terms of the rules established for calculating the T_g of a copolymer.

For example, one can consider a homologous series of aliphatic polyamides such as nylon 6, nylon 7,. . . nylon 12, etc. as a series of copolymers of nylon 6 and polyethylene. According to this scheme, nylon 12 can be regarded as a copolymer consisting of a nylon 6 (N6) unit and a polyethylene (PE) unit of six CH_2 groups in a weight ratio of N6 to PE to 113:84 and nearly equal number of flexible bonds (7 in nylon 6 residue and 6 in PE residue).

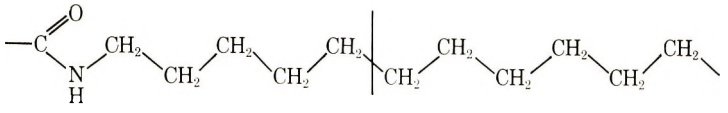

N6 PE

If this scheme and the T_g rule of Fox[6]

$$1/T_g = W_A(1/T_{g_A}) + W_B(1/T_{g_B})$$

(where W_A and W_B and T_{g_A} and T_{g_B} are the respective weight fractions and glass transition temperatures of the polymers A and B) are applied to the data of Table II, one obtains the results shown in Figure 1. These calculations, which are based on the assumption that the T_g of polyethylene is near $-80°C$, reveal a striking discrepancy between the observed and expected behavior. It should be pointed out that there are many cases where experimental data for copolymer systems do not conform to the rule of Fox. Nevertheless, the magnitude of the discrepancy observed in Figure 1 greatly exceeds the deviation encountered in most of the other copolymer systems. Since the data reflect either a peculiarity of the structure of these polymers or an unusual characteristic of the α' relaxation, it would be very desirable to have an adequate interpretation for the observed behavior.

The application of the more elaborate Gordon-Taylor relationship[7,8] between glass transition temperature and copolymer composition also leads to interesting results. This relationship, which has been derived on assuming ideal volume additivity of the different repeating unit, states that

$$T_g = \frac{1}{1 + (W_B/W_A)(1/K)} T_{g_A} + \frac{1}{1 + (W_A/W_B)K} T_{g_B}$$

where

$$K = (\alpha_{L_A} - \alpha_{G_A})/(\alpha_{L_B} - \alpha_{G_B})$$

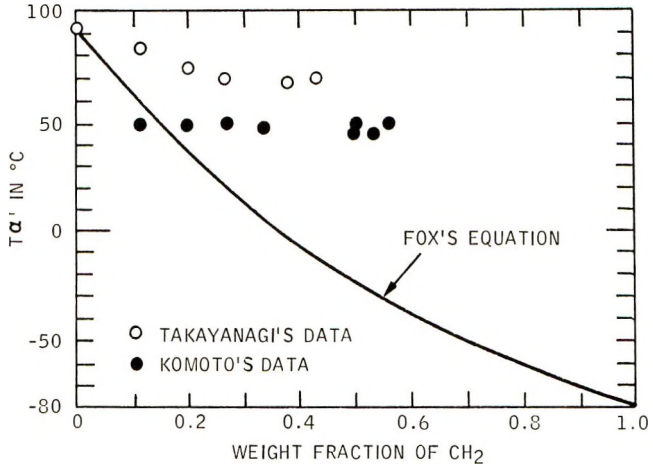

Fig. 1. Effect of CH_2/amide group ratio (expressed as weight fraction of CH_2 in excess of that in nylon 6) on temperature of α' transition in aliphatic polyamides; application of Fox equation.

and α_L is the thermal expansion coefficient above T_g. α_G is the thermal expansion coefficient below T_g.

The results of Figure 2, where we show the plots of the Gordon-Taylor equation fitted to the data of Takayanagi and Komoto, indicate a sharp decline in T_g of polyamides derived from ω-amino acids (nylon X) for polyamides having more than about 30 —CH_2— units per amide group. On the other hand, with the polyamides having less than 20 —CH_2— units per amide group, the sensitivity to changes in X is rather small. With polyamides derived from diacids and diamines the drop in T_g is nearly stepwise at a weight fraction of PE units exceeding 0.75. This corresponds to approximately 50 —CH_2— units per amide group. In terms of the Gordon-Taylor expression, such a stepwise drop indicates an unusually high value of K which implies a large difference between the values of $\alpha_L - \alpha_G$ for N6 and PE. The fact that values of K calculated from volumetric data and those extracted from the plots of Figure 2 differ by factor of 3.2 casts additional doubt on the validity of the assignment of the α' peak to the onset of large scale motion of the polymer chain, which, according to Willbourn,[2] takes place at the glass transition of a polymer. Considering also that aliphatic polyamides tend to crystallize below the temperature of the α' peak, we felt that additional experiments were justified to clarify the ambiguity associated with this relaxation. Specifically, we were concerned that micro order, on a scale not registered by the x-ray technique as crystallinity, may be the cause for the high glass transition of these polymers, since such domains might effectively decrease the free volume and thus increase the glass transition temperature.

In an attempt to clarify this point, we prepared a series of aliphatic terpolyamides. We speculated that if the presence of the microaggregates

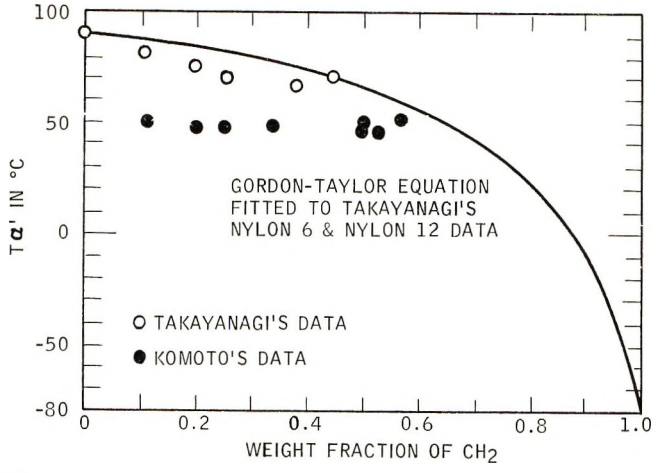

Fig. 2. Effect of CH_2/amide group ratio (expressed as weight fraction of CH_2 in excess of that in nylon 6) on temperature of α' transition in aliphatic polyamides; application of Gordon-Taylor equation.

is indeed the reason for the insensitivity of the α' peak to changes in the length of the aliphatic chains, then this effect should not be operative in terpolymers where the formation of such domains should be greatly diminished, and thus, the glass transition of the terpolyamides might fall closer to that predicted by the Fox relationship.

The data of Table III, where the compositions of the investigated terpolymers are given with their respective glass transition temperatures, show that the T_g values of the terpolymers fall in the same temperature range as those of the corresponding homopolymers. In general, the T_g's of the terpolyamides are somewhat lower than those of the homopolymers having the same average numbers of amide and —CH_2— units. Nevertheless, as it can be seen from the plot of these data in Figure 3, the differences are very small, and when the measured values are compared with those predicted by the Fox relationship (by using the copolymer scheme NX–PE described above), the discrepancy is of the same order of magnitude as found with the homopolymers. These results give strong support for the assignment of Woodward et al.[10] that the α' transition involves the onset of large-scale segmental motion. With the elimination of the possibility that the α' relaxation is associated with morphological factors (i.e., microcrystallinity), the question regarding the insensitivity of the T_g to changes in the CH_2/amide group ratio can be formulated more precisely. Namely, why is the temperature of the onset of the large-scale segmental mobility in aliphatic polyamides so insensitive to the degree of interchain hydrogen bonding? In order to answer this question, it is necessary to obtain an estimate of the length of the moving segment involved in the α' relaxation.

From the value of the activation energy of 100 kcal/mole associated with this transition in N6 (see data below) and assuming a value of approximately 6 kcal/mole for the interchain hydrogen bonding, it appears that

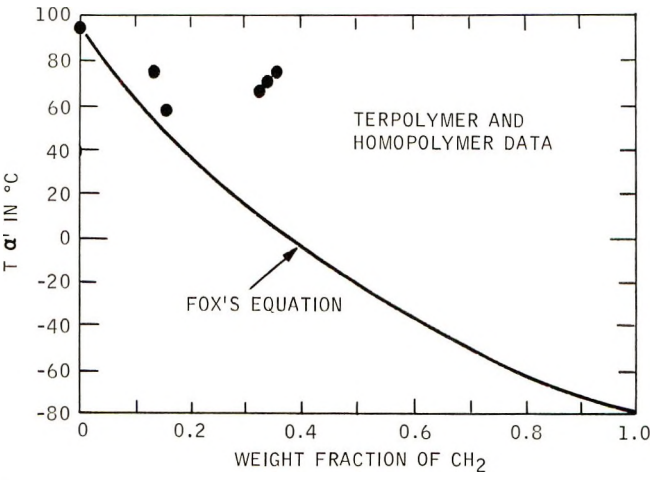

Fig. 3. Effect on CH_2/amide group ratio (expressed as weight fraction of CH_2 in excess of that in nylon 6) on temperature of α' transition in aliphatic terpolyamides; application of Fox equation.

the moving chain segment includes about 15 nylon 6 repeating units. It is important to note that this value agrees with the estimate of Boyd[11] for nylon 6,6 derived from the degree of crosslinking at which this peak disappears.

From the Boyd experiment it also follows that in nylon 6,6 the replacement of only one interchain hydrogen bond in 15 with a stronger bond leads to a large increase in the T_g of the unmodified polymer. Thus, we can imply by analogy that in polyethylene a replacement of one CH_2 group in 90 with an interchain hydrogen-bonded amide group should also raise significantly the T_g of polyethylene. Considering further that because of steric effects and relatively high viscosity there is always a fraction of amide groups which remain unbonded, one would expect that the condition of one interchain hydrogen bond per 90 —CH_2— groups could not be satisfied with nylon 90. At present, the fraction of amide groups which form interchain hydrogen bonds on cooling long-chain polyamides from the melt (e.g., N50 or higher homologs) is not known. It is possible, however, that the condi-

TABLE III
Glass Transition Temperatures of Various Terpolyamides

Terpolyamide[a]	T_g, °C	Degree of crystallinity, %
Nylon 6,8,12	59	3
Nylon 6,11,12	79	12
Nylon 7,11,12	73	5
Nylon 8,11,12	80	8
Nylon 6,8,11	70	3
Nylon 7,8,12	63	7

[a] All compositions based on equal weight fractions.

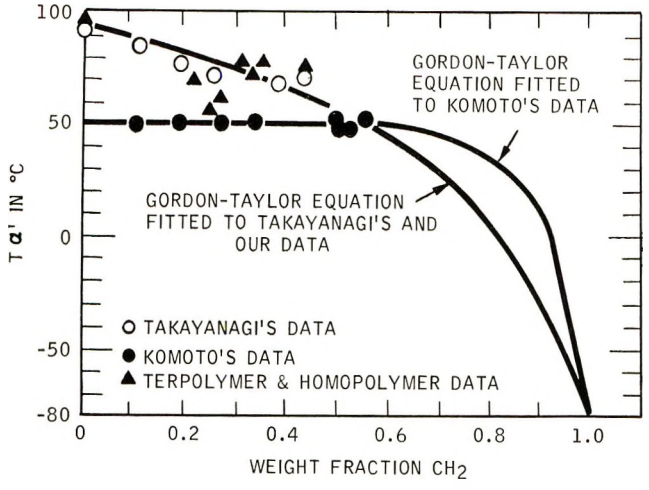

Fig. 4. Effect of CH_2/amide group ratio (expressed as weight fraction of CH_2 in excess of that in nylon 6) on temperature of α' transition in aliphatic polyamides: Gordon-Taylor equation fitted to data of Komoto, Takayanagi, and of this study.

tions of one interchain hydrogen bond per 90 —CH_2— groups may be present in polyamides having two amide groups per 90 —CH_2— groups. Although we do not have the data regarding the mechanical relaxations in N45 or N45,45, one can see from the results of Figure 4, where we show the Gordon-Taylor plots fitted to the available data, that the expected behavior is in good agreement with the above rationale.

In applied polymer science the glass transition is often used to indicate the temperature interval in which polymers meet certain specifications regarding strength, modulus, dimensional stability, etc. It must be pointed out however, that if the data and discussion above are regarded from a practical point of view, the conclusions advanced may prove to be misleading. In cases where a structure–property relationship is sought, then in addition to the effects of structural modification on the temperature of transitions, one must also consider the effects on the magnitude of the relaxation associated with these transitions.

By comparing the intensities of the α' and γ relaxation in the series of polyamides derived from ω-amino acids, we see that with an increase in the length of the aliphatic chain the intensity of the γ relaxation increases while that of the α' relaxation decreases.[12] On the basis of these results, it can then be inferred that in contrast with the temperature of the α' transition which shows a rather abrupt change at an amide/CH_2 group ratio near 45 the change in relaxation strength associated with the α' and γ transitions is gradual. From a practical point this implies that with an increase in the length of the aliphatic chain the α' transition gradually loses its importance. Furthermore, since in the temperature range between the γ and α' relaxation, the properties depend on the relaxation strength of the γ relaxation, one realizes that from the consideration of mechanical proper-

ties, the γ transition gradually assumes the role of the glass transition as the length of the aliphatic chain increases.

This discussion shows quite clearly that the arguments regarding the assignment of a particular transition to the glass transition can be rather futile. In particular, with polymers which exhibit multiple transition, it is not always possible to identify unambiguously one transition as the glass transition, since the selection depends on the choice of the criteria. This is obviously true for the aliphatic polyamides where different parts of the main chain acquire mobility at temperatures which are far apart and where the relaxation strength and the temperature of the relaxation respond so differently to changes in the chemical structure of the polymer.

Effect of Moisture on the α' Relaxation

It has been recognized for some time that the absorbed water in polyamides greatly affects the position of the α' relaxation.[11,13,14] The results of Figure 5 and Table IV summarize the results of our studies regarding the effect of moisture on the position and intensity of the α' and β peaks in tan δ. The measurements were conducted at a frequency of 110 cps with specimens of an unoriented film conditioned at various levels of humidity between 0 and 100% RH at 23°C. With the dry samples, the α' peak is found near 95°C, while with those conditioned at 100% RH containing about 10% moisture the peak shifted to about 0°C. Of considerable interest are the results of Figure 6 showing the position of the α' peak in tan δ as a function of the water content in the films. It can be seen that the position of the peak is very sensitive to changes in water content at levels below 3%, while the increases in water content above 3% produce relatively small effects. The intensity of this peak, however, increases nearly linearly with increasing water content from 0 to 10%. Following the results of x-ray studies indicating that water is absorbed primarily in the amorphous regions, and assuming that one water molecule occupies one site of intermolecular hydrogen bonding, one is able to estimate that one water mole-

TABLE IV
Effect of Moisture on the α' Transition in Nylon 6

Weight fraction H_2O sorbed	Relative humidity (23°C), %[a]	Position of α' transition, °C	tan δ (α' max)
0	0	95	0.116
0.5	11	92	0.114
1	23	82	0.113
2	40	39	0.142
3	50	11	0.155
5	75	10	0.156
10	100	3	0.165

[a] The listed humidities refer to conditions at which the samples were conditioned.

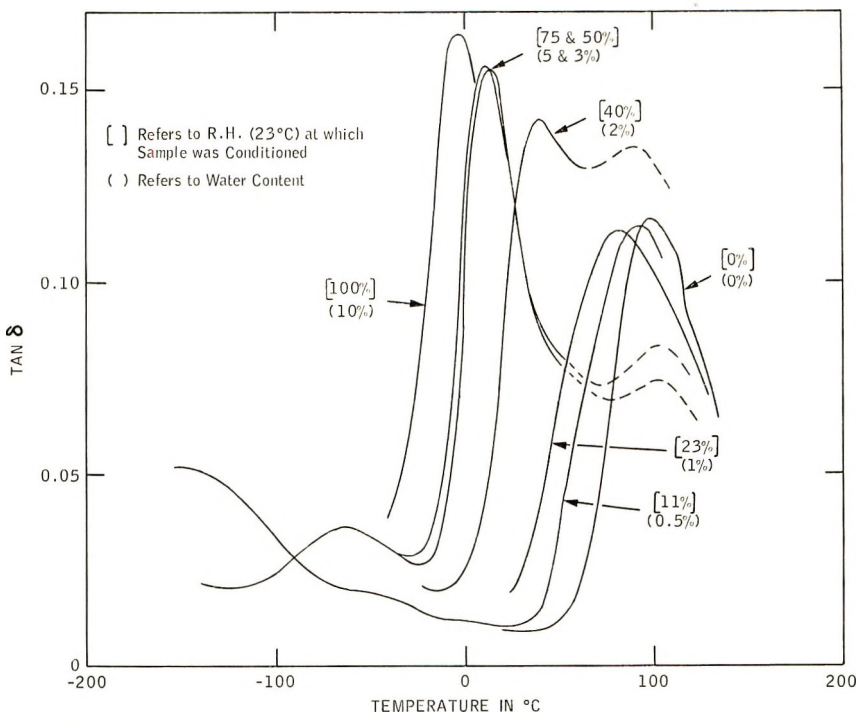

Fig. 5. Temperature dependence of tan δ (measured at 110 cps) for unoriented nylon 6 conditioned at various humidities; broken lines represent data for which loss in moisture is observed.

cule is needed per three nylon 6 repeating units in the amorphous phase to achieve a nearly complete plasticizing effect.

We believe that the high plasticizing effect observed at low levels of water content is associated with the factors which, according to Starkweather,[15] lead to a low partial specific volume of the absorbed water. Following this rationale, the plasticizing effect of water should be attributed to two factors: (a) the weakening of the interchain hydrogen bonding and (b) the reduction of strict steric requirements of the hydrogen bonding which, in the dry state, effectively increases the stiffness of the chains in the vicinity of the bonded amide group. Since the latter effect decreases rapidly with increasing number of plasticized sites, one can infer that at high levels of moisture the plasticization is due only to weakening of the interchain bonding. The reduction in the magnitude of the chain interaction from the dry to the wet state can be estimated from the shifts in tan δ peaks with frequency assuming the Arrhenius relationship. This data shown in Figure 7 and Table IV, indicate an activation energy of about 96 kcal/mole for the α' peak in dry nylon 6 and only 64 kcal/mole for the peak in samples containing 10% water.

The sensitivity to moisture decreases with the increasing length of the aliphatic chain. This can be seen from the data of Figure 8 showing the

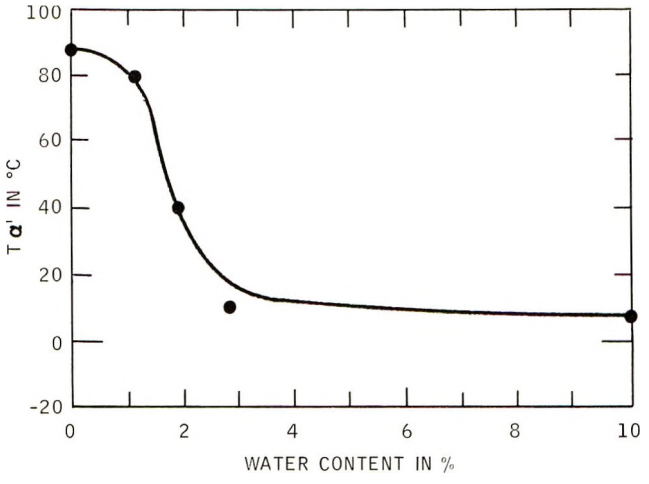

Fig. 6. Effect of sorbed water on temperature of α' relaxation in nylon 6.

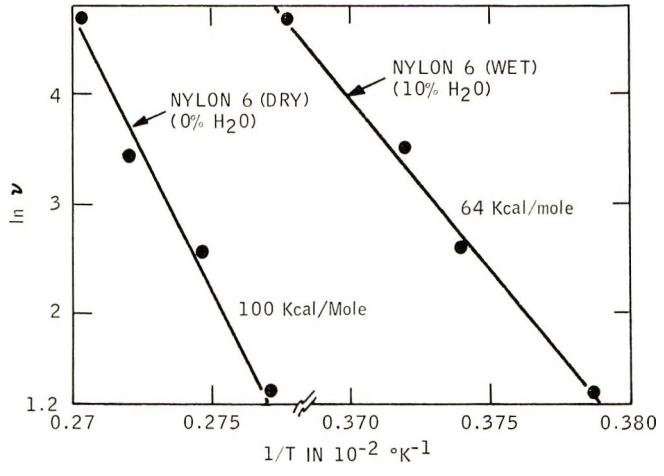

Fig. 7. Plots of log (frequency against $1/T$ for wet and dry unoriented nylon 6.

temperature dependence of the α' peak in tan δ for nylon 6,11,12 terpolymer and from nylon 12 homopolymer as a function of the water content. The characteristic features of the plot are similar to those observed with nylon 6. The effects which are very large at low levels of absorbed water level off rather abruptly when the water content approaches about 3%. The difference in the tan δ peak temperature between dry samples and those conditioned at 100% RH is smaller with the terpolymer (about 45°C) than with nylon 6 (about 95°C). This effect should be attributed to a generally lower water equilibrium content observed with polyamides having longer aliphatic chains. The sensitivity to moisture is further reduced in nylon 12, which in our experiments shows a difference of only 20°C in the position

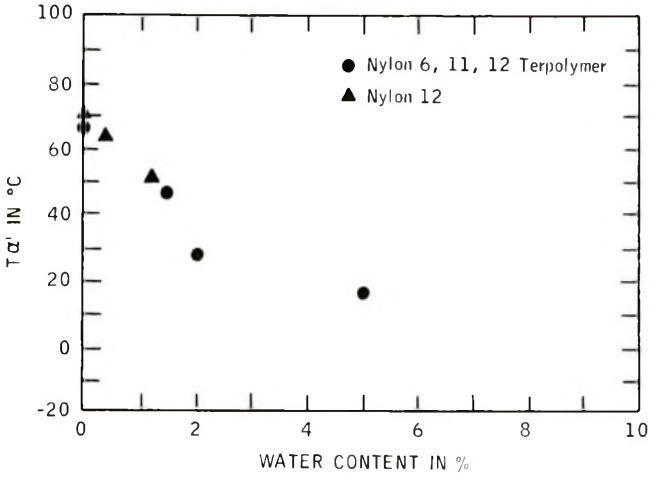

Fig. 8. Effect of sorbed water on the temperature of α' peak in tan δ for N 6, 11, 12 terpolymers and nylon 12.

of the α' peak in tan δ between dry samples (72°C) and those conditioned at 100% RH (52°C).

The increase in the length of the aliphatic chain leads also to a reduction in the activation energy associated with the α' relaxation. From the shifts in the α' peak in tan δ in the frequency range of our apparatus (3–110 cps) shown in Table V one obtains an activation energy of about 69 kcal/mole for nylon 12 and about 95 kcal/mole for nylon 6.

TABLE V
Frequency Dependence of α' Maximum in tan δ for Wet and Dry Nylon 6 and Dry Nylon 12

Polymer	Frequency, cps	T (α' max), °C
Nylon 6 (dry)	110	97
	35	95
	11	91
	3.5	87
Nylon 6 (wet)	110	−1
	35	−4
	11	−6
	3.5	−9
Nylon 12 (dry)	110	74.5
	35	70.5
	11	64.5
	3.5	63.5

The plasticizing effect of water changes into an antiplasticizing one at temperature below the transition. This can be seen from the plots of E' as function of temperature shown in Figure 9. This observation can be explained on the basis of density changes produced by absorption of water,

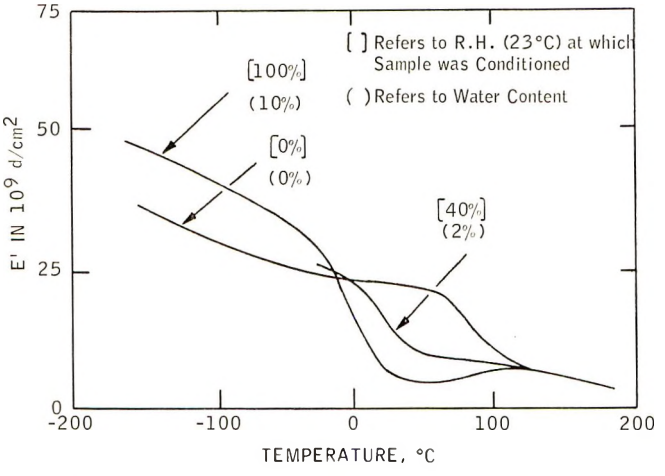

Fig. 9. Temperature dependence of E' for nylon 6 films conditioned at various humidities.

indicating that partial specific volumes of water in aliphatic polyamides are considerably below 1.0. Consequently, the water must reduce the free volume of the system, which in turn leads to the observed increase in the modulus while the system is the glassy state. Thus, this argument also supports the assignment of the α' relaxation to the glass transition of this polymer. The fact that the temperature of the α' transition decreases with increasing water content, however, implies that in this case a decrease in free volume of the system leads to a decrease in the glass transition temperature. Thus, these data show very clearly that in this case the free volume concept of glass transition cannot be applied to explain the observed behavior.

One of the objectives of these experiments was to separate the amorphous α' relaxation from the relaxation attributed by Takayanagi[4] and Brown and Campbell[5] to the α-γ crystal transition. Takayanagi found this relaxation as a shoulder on the high temperature side of the tan δ peak associated with the α' transition near 120°C, while Brown observed this peak very clearly in wet sample near 75°C. The pertinent data are shown as dotted lines in the tan δ–temperature plots shown in Figure 5. These results, which indicate a well defined maximum near 90°C, are in good agreement with the results of a similar experiment reported by Brown and Campbell. There is, however, an essential difference between their results and ours. While Brown and Campbell report no loss in moisture from films which were 20 mils thick, we observed a substantial loss in water during heating as indicated by the thermograms obtained under the same environmental conditions (control of humidity) and the same rate of heating. In order to further verify this result, we next measured the dynamic properties through both a heating and cooling cycle along with a parallel determination of specimen weight. From the results of Figures 10 and 11 where

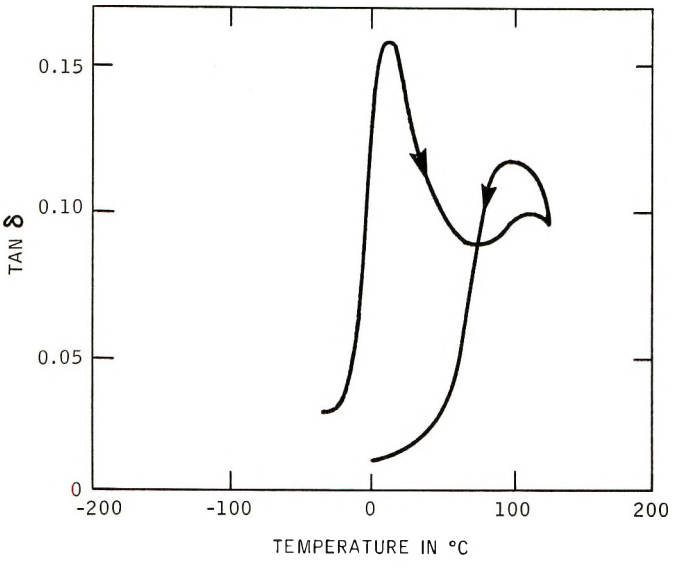

Fig. 10. Temperature dependence of tan δ for wet nylon 6 data obtained during the heating and cooling cycle at constant specific humidity (equivalent to 50% RH at 23°C).

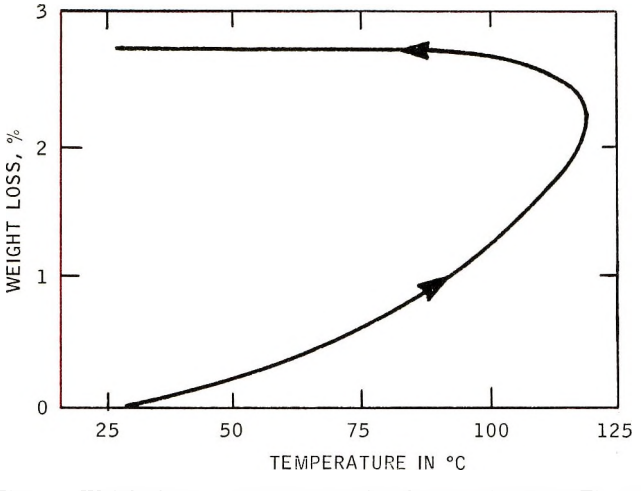

Fig. 11. Weight loss vs. temperature for the experiment of Fig. 10.

the data are presented, we see that the tan δ data agree with the results of moisture content. Consequently, we concluded that the appearance of the 90°C tan δ peak in these experiments is a result of drying the specimens and not of the α–γ crystal transition as suggested by Brown and Campbell.

Effect of Crosslinking with Toluene Diisocyanate

The studies of the effect of crosslinking on the intensity of the α' transition were carried out by Deeley et al.[16] and Boyd.[11] Deeley et al. used cobalt radiation which led to both crosslinking and destruction of crystal-

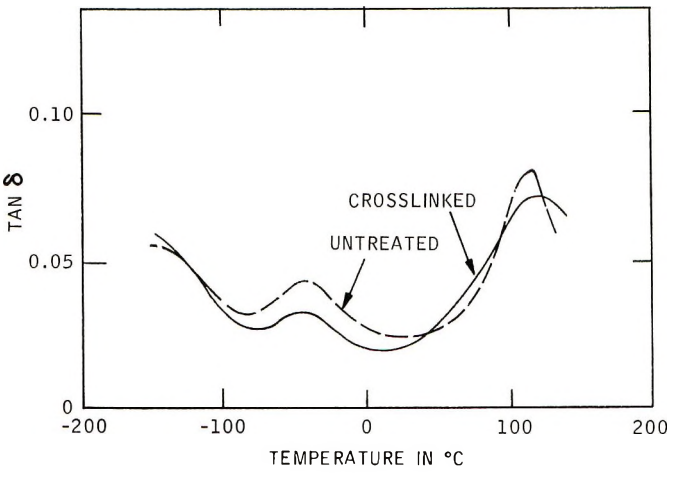

Fig. 12. Temperature dependence of tan δ for untreated and TDI-crosslinked unoriented nylon 6. Estimated degree of crosslinking = 1 crosslink/~110 amide groups.

lites as indicated by the results of x-ray measurements. Boyd, on the other hand, found that the dielectric peak of nylon 6,6 decreases and finally disappears with increasing times of exposure to 2-MeV electron radiation. We were interested in how chemical crosslinking (which takes place primarily in the amorphous phase while the crystalline regions remain essentially intact) affects the position of the peak. For this purpose, we treated samples of annealed oriented nylon films with toluene diisocyanate (TDI). Crosslinking was carried out at 140°C using propylenecarbonate as the carrier for the TDI. The x-ray data obtained from the control and crosslinked samples confirmed that the attack on the crystalline phase was insignificant. The results of Figure 12, where we show the plots of tan δ obtained with a sample containing 6% by weight of TDI and the control, indicate that this type of crosslinking leads to a broadening of the α' peak and a reduction in its magnitude.

It is interesting to note that at this level of crosslinking no significant effect on sensitivity to moisture was observed. The sample conditioned at 100% RH at 23°C had approximately the same position of the α' peak in tan δ–temperature plots as the uncrosslinked control (see Fig. 5). This behavior is not surprising if one considers the low level of crosslinking achieved with these samples. From the measurements of the degree of swelling in formic acid we estimated that the efficiency of crosslinking (defined as the ratio of the weight of the bonded TDI which formed crosslinks to the total TDI uptake) was about 9%, while the total TDI uptake was about 6%. This implies that in the amorphous phase only one amide group in 110 was crosslinked.

If the crosslinking is carried out under more severe conditions and for longer times, it is possible to eliminate the α' peak. We have observed this with nylon 6 fibers which were treated for 6 hr in a boiling solution of

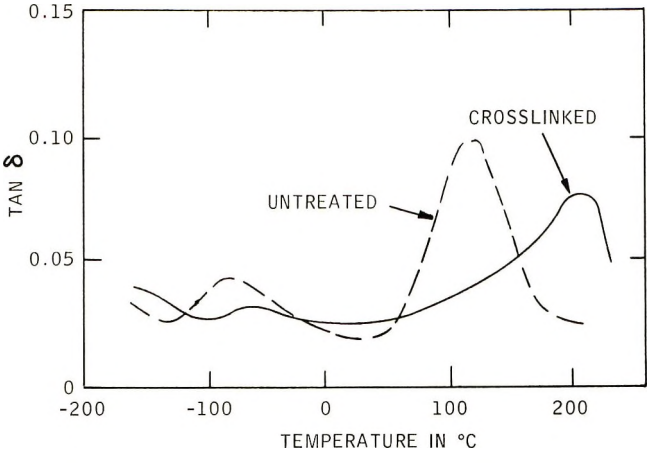

Fig. 13. Temperature dependence of tan δ for untreated and heavily crosslinked nylon 6 fibers. Estimated degree of crosslinking = 1 crosslink/~30 amide groups.

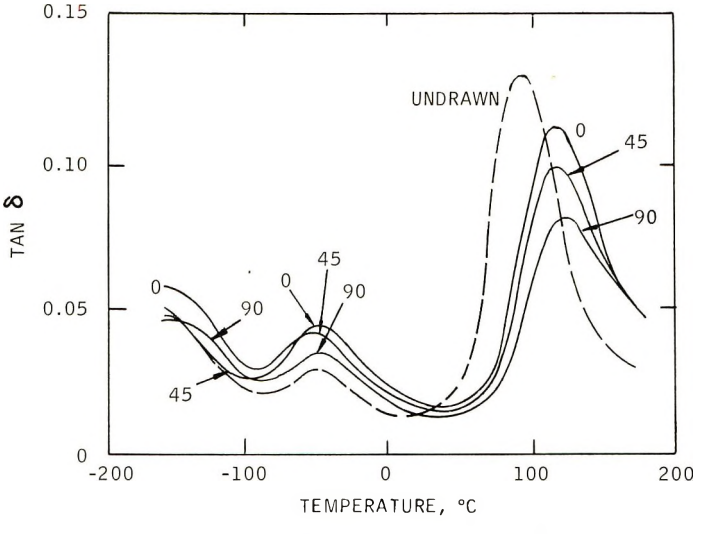

Fig. 14. Temperature dependence of tan δ for unoriented and oriented nylon 6. With oriented samples the measurements are carried out at 0°, 45°, and 90° to the axis of orientation.

TDI in propylene carbonate (173°C). The weight uptake with these samples was 22% and the estimated efficiency of crosslinking was about 9%. From these results in follows that approximately one crosslink per 30 amide groups was required to achieve the effect shown in Figure 13. Thus, it might appear that crosslinking with TDI is somewhat more efficient than crosslinking by electron radiation, where, according to Boyd, one amide group in 15 had to be crosslinked in order to achieve a similar effect. Considering, however, that this discrepancy could also be the result of error in

the estimated degrees of crosslinking, in ours as well as Boyd's experiments, we regard these results as essentially supporting one another.

Effect of Orientation

The results of tan δ measurements obtained from oriented films are shown in Figure 14. The orientation products a shift of about 20°C to higher temperatures for the α' peak and reduces its intensity, regardless of the direction of measurement. The position of the β peak, however, is unaffected by the orientation. Its intensity is increased however. These data indicate that the orientation leads to a general tightening of the structure which is probably accompanied by an increase in the density of the amorphous phase. Thus the α' peak is shifted to a higher temperature on orienting. The increase in the number of unbonded amide groups inferred from the increase in the intensity of the β peak is most likely a result of internal strain produced by the plastic deformation (uniaxial drawing). Plots of tan δ from oriented samples cut at 0, 45 and 90° to the direction of orientation show that the α' and β peak have very similar anisotropic characteristics, namely ($\tan \delta_0 > \tan \delta_{45} > \tan \delta_{90}$). The fact that both relaxations respond similarly to orientation is another argument in favor of the hypothesis that the α' and β relaxations involve similar molecular motions. Since Takayanagi's[4] results indicate a well pronounced shoulder (near 120°C) on the high-temperature side of the α' peak, one would expect that in addition to differences in the intensity of tan δ_0, tan δ_{45} and tan δ_{90} peaks, the orientation might also produce differences in the shapes of these peaks. The fact that all three curves are very similar, both on the low- and high-temperature side, indicates that in this temperature range we did not have another relatively strong transition whose anisotropic characteristics would differ from those of the α' relaxation. Since our samples had a high level of crystallinity, (approximately 60%), we cannot establish the position of the expected α–γ transition on the basis of these results.

SUMMARY AND CONCLUSIONS

The temperature of the α' transition in aliphatic polyamides is very insensitive to changes in the length of the aliphatic chain. The fact that the temperature of this relaxation is generally accepted as the glass transition temperature of the polymer raises doubts about the validity of the original assignment of the α' transition to the onset of large-scale molecular motion.

New data from terpolyamides are presented favoring the original assignment of Woodward. The statistical length of the segmental motion involved in this relaxation is estimated from activation energies and degrees of crosslinking at which the α' relaxation disappears. It is then inferred that the observed insensitivity of the α' transition to changes in the groups in the repeating unit should be attributed to two factors: (1) at temperatures below which the average energy of segmental motion is low compared with the energy of the interchain (hydrogen) bond, a very small

number of interchain bonds per segment length (on the order of 1 per 100 Å) is sufficient to prevent the α' relaxation; (2) the energy of the interchain hydrogen bond in polyamides is not affected significantly by variations in the length of the aliphatic chain between bonds.*

Unlike the temperature of the α' relaxation, which remains rather constant in the series of nylon X or nylon X,Y where X or Y are less than 45, the intensity of the α' relaxation is expected to change gradually, even in this range of X and Y. The fact that the relaxation strength of the γ transition increases at the expense of the relaxation strength of the α' relaxation has important practical consequences. Because the γ and β relaxations in short-chain aliphatic polyamides, e.g., X and $Y \leqq 12$, are very weak, the properties of these polymers in the temperature interval between the γ and α' transitions are affected primarily by the strength of the latter transitions. Thus, from the practical point of view, and for short chain polyamides, the temperature of the α' relaxation represents the glass transition of these polymers.

With the long chain polyamides (e.g., X and Y = 20–40) the situation is reversed. There the α' transition is weak and the γ is strong, the change in relative strength being gradual as a function of X and Y. Consequently, as X and Y increase, the properties of the corresponding polyamides in the temperature range between the γ and α' transitions become more and more affected by the relaxation strength of the γ transition.

Finally, with the polyamides in which X and Y are very large (e.g., X and Y = 50) one would expect the α' transition to be so weak as to have only negligible effects on the practical performance characteristics of these polymers. Consequently in this case, if a temperature interval for a specific application is the consideration, one should regard the temperature of the γ relaxation as the practical T_g of the polymer, despite the fact that the onset of large-scale segmental mobility and therefore its "true" glass transition may lie at the considerably higher temperature of the α' transition.

This discussion shows quite clearly that when a polymer exhibits multiple transitions, it is rather difficult to identify the glass transition. Since there are several criteria which are used in defining this transition, it is apparent that when the onset of mobility of the main chain occurs at not one but several temperatures, a unique assignment of one of these relaxations to the glass transition is not possible. This is obviously the case for the aliphatic polyamides.

References

1. N. G. McCrum, B. E. Read, and G. Williams, *Anelastic and Dielectric Effects in Polymer Solids*, Wiley, New York–London, 1967.

2. A. H. Willbourn, *Trans. Faraday Soc.*, **54**, 717 (1958).

3. H. Komoto, *Rev. Phys. Chem. (Japan)*, **37**, No. 2, 105 (1967).

* This point is not trivial, since the observation refers to the conditions in the solid polymer and not to an isolated amide hydrogen bond.

4. M. Takayanagi, *Rept. Progr. Polymer Phys. Japan*, **6**, 121 (1963).
5. W. B. Brown and G. A. Campbell, paper presented at American Chemical Society Meeting, New York, September, 1969; *Polym. Preprints*, **10**, No. 2, 647 (1969).
6. T. G. Fox, *Bull. Am. Phys. Soc.*, **1**, No. 3, 123 (1956).
7. L. A. Wood, *J. Polym. Sci.*, **28**, 319 (1958).
8. M. Gordon and J. S. Taylor, *J. Appl. Chem.*, **2**, 493 (1952).
9. J. H. Dumbleton and T. Murayama, *Kolloid-Z.*, **220**, 41 (1967).
10. A. E. Woodward, J. A. Sauer, C. W. Deeley, and D. E. Kline, *J. Colloid Sci.*, **12**, 363 (1957).
11. R. H. Boyd, *J. Chem. Phys.*, **30**, 1276 (1959).
12. T. Kawaguchi, *J. Appl. Polym. Sci.*, **2**, 56 (1959).
13. K. H. Illers, *Makromol. Chem.*, **30**, 234 (1960).
14. A. E. Woodward, J. M. Crissman, and J. A. Sauer, *J. Polym. Sci.*, **44**, 23 (1960).
15. H. W. Starkweather, *J. Appl. Polym. Sci.*, **2**, 129 (1959).
16. C. W. Deeley, A. E. Woodward, and J. A. Sauer, *J. Appl. Phys.*, **28**, 1124 (1957).

Received August 25, 1970
Revised November 20, 1970

JOURNAL OF POLYMER SCIENCE: PART A-2 VOL. 9, 887-893 (1971)

Contact Angle of Polyethylene on Copper and Its Effect on Adhesion

J. M. SYKES and T. P. HOAR, *University of Cambridge, Department of Metallurgy, Cambridge, England*

Synopsis

To determine whether the large differences in adhesion for polyethylene coatings applied to different types of copper surface could be attributed to changes in work of adhesion or wettability, the variations of contact angle with time has been measured for molten polyethylene droplets on these surfaces. It is concluded from these measurements that the low peel strengths obtained on certain substrates cannot be accounted for by a low work of adhesion of poor wetting of the surface.

INTRODUCTION

The relevance of contact angle in adhesion has been pointed out by several authors.[1-4] There are two reasons why a liquid having a low contact angle on a substrate should bond well to that material after solidification. Firstly, the work of adhesion W_a, as defined by Dupré,[5] is directly related to the contact angle θ by

$$W_a = \gamma_{LV} (1 + \cos \theta)$$

where γ_{LV} is the surface tension of the liquid; θ is therefore a measure of the attractive forces between the phases. Secondly, the contact angle will determine how well the adhesive penetrates into crevices in the substrate[4]; unless complete wetting occurs, the area of the interface, and therefore the strength of the bond, will be reduced. The stress at the interface will also be higher at the edges of unfilled crevices.

We have reported previously[6] that coatings of polyethylene applied to copper sheet by melting adhere weakly unless the copper is treated to form a thick layer of cupric oxide on its surface, or the polyethylene is oxidized to give C=O groups. Both processes lead to an increase in the forces between the molecules of the polymer and the metal, or oxide, surface and the adhesion is increased. We have now measured contact angles for molten polyethylene on copper to see whether there is a significant correlation between adhesion as measured in a dead-load peel test[6] and values predicted from the contact angle.

EXPERIMENTAL

Apparatus

The contact angle was measured by a sessile drop method using small pellets of polyethylene melted on flat horizontal copper specimens maintained at 200°C in a tube furnace controlled manually with a Variac autotransformer. To prevent atmospheric oxidation of both metal and polymer, the specimens were enclosed in a Pyrex glass tube filled with high-purity nitrogen (B.O.C. White spot). The ends of the tube were optical flats so that a parallel beam of light from a lamp and condenser lens could be

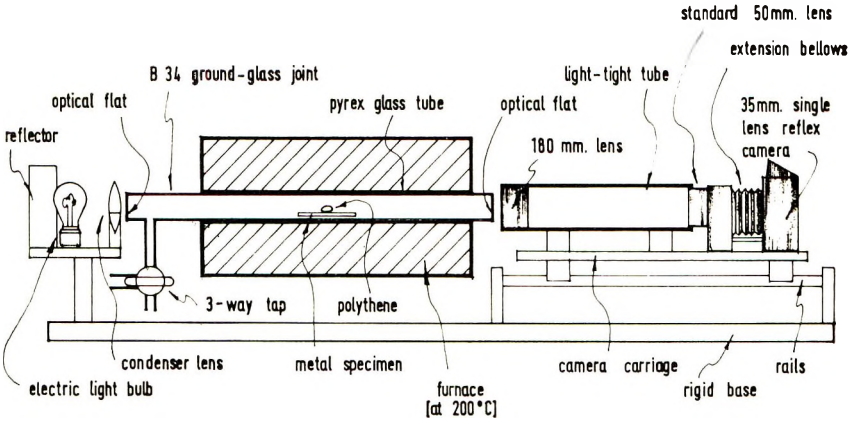

Fig. 1. Apparatus for measuring contact angles of molten polyethylene on metals.

shone along the tube from one end, and photographs of the silhouetted drop taken from the other. A long-focus enlarger lens was used to produce an image of the drop outside the furnace and this was photographed at ca. 10× magnification with a 35-mm single-lens reflex camera having the standard 50-mm lens on an extension bellows. The camera and lens assembly was mounted on a carriage running on rails which were fixed to the same rigid base as the furnace (Fig. 1). Screw adjustments were provided to allow the components to be leveled and aligned.

Method

In order to produce unoxidized polyethylene sheet, polyethylene powder (Alkathene WRM-19, I.C.I. Plastics, Welwyn Garden City, England) was melted on a PTFE sheet in a nitrogen atmosphere to form sheet ca. 3 mm thick. This showed no infrared absorption by C=O groups. Oxidized polyethylene sheet was prepared by treating the powder for 30 min in an acid solution of sodium dichromate (220 g $Na_2Cr_2O_7$, 140 ml concentrated H_2SO_4 and 200 ml distilled water) at 60°C, washing and drying it, then melting it into sheet as above. This procedure gave a fairly homogeneous composition. Pellets ca. 2 mm in diameter were cut from the sheet with a clean cork borer.

The copper specimens, 2.54 cm squares of 0.146 cm sheet were degreased by swabbing and then rinsing with acetone and etched in 25% nitric acid. Some were washed with distilled water and dried with acetone, the others were anodized in 15% aqueous sodium hydroxide solution at 90°C at a current density of 50 mA/cm^2, and then washed and dried.

A pellet of polyethylene was placed at the center of a copper specimen, which was then put into the tube and pushed along to the middle. The tube was closed, then evacuated and refilled with nitrogen at least five times. Afterwards the pump was replaced by a wash-bottle through which the expanding gas could escape without allowing air to enter. (Oxygen was removed from the wash-bottle before it was connected to the tube by passing the nitrogen stream out through it.) The tube was slipped into the furnace, already heated to 200°C, and the time was noted. The autotransformer was readjusted until the tube had reached the temperature of the furnace. The optical system was immediately set up, aligned and focussed, and, after a check that the specimen was properly in position and level, a photograph was taken. Further photographs were taken at intervals, initially of 5 min but later of several hours.

Experiments were continued for times of up to 3 days, by which time some charring of the polyethylene had begun. This degradation could not have been caused by oxidation, as there was no appreciable oxidation of the copper specimens.

When the photographs had been printed, a base line and tangents at the points of contact were constructed on them and the contact angle measured with a protractor. This gives an accuracy of $\pm 1°$ which is well within the variation between similar specimens.

RESULTS AND DISCUSSION

The variation in cos θ with time is shown in Figures 2–4. With all three types of specimen the contact angle decreased throughout the experiment. This could mean either that a true equilibrium contact angle is never achieved because of high viscosity, or that the contact angle gradually decreases due to polymer degradation. We have no means of telling which is the true situation although the former seems the more likely. After 2000 min the contact angle of unoxidized polyethylene on etched copper was ca. 48° and for oxidized polyethylene on etched copper it was 28°. On anodized copper it was ca. 32°.

If unoxidized polyethylene is applied to etched copper the adhesion is very poor (less than 50 g/cm in a dead-load peel-test), but if the polyethylene is oxidized with chromic acid, bond strengths of up to 3000 g/cm can be obtained. Coatings applied to anodized copper adhere very well (up to 4800 g/cm).

Clearly there is slightly better wetting in the cases where good bonds are produced, but the differences of contact angle are not nearly enough to account for the large differences in adhesion, as will be seen.

There is another point to be considered; in the preparation of specimens with surfaces similar to those used in the adhesion tests the surfaces become roughened. The roughness of the surface r (defined as the ratio: real surface area/apparent surface area) may be at least two,[7] or even three or more.[8]

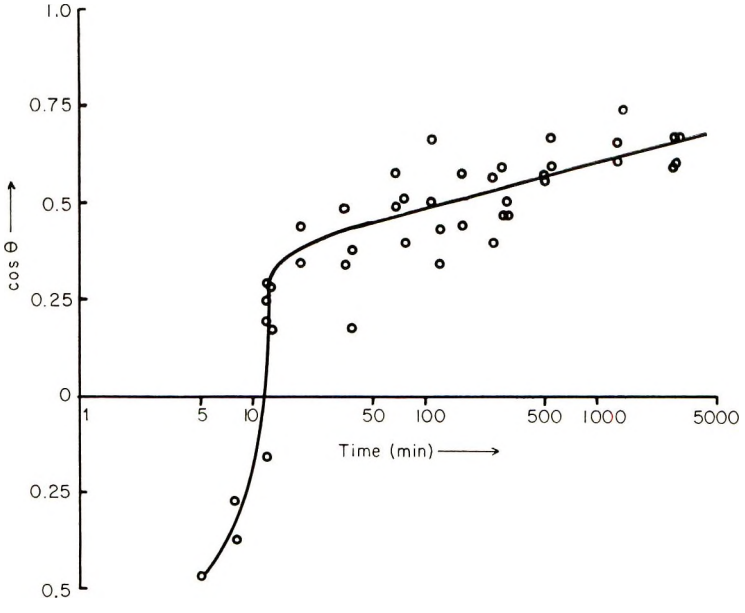

Fig. 2. Variation of contact angle with time for polyethylene on etched copper.

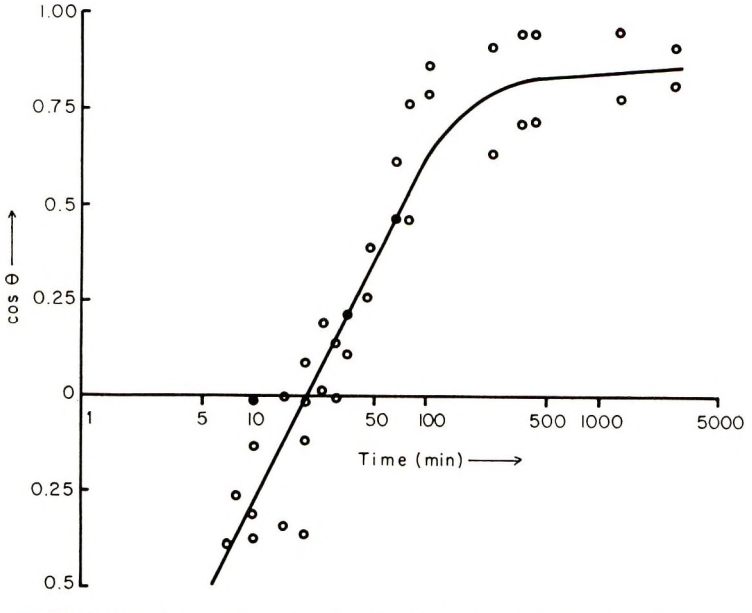

Fig. 3. Variation of contact angle with time for polyethylene on anodized copper.

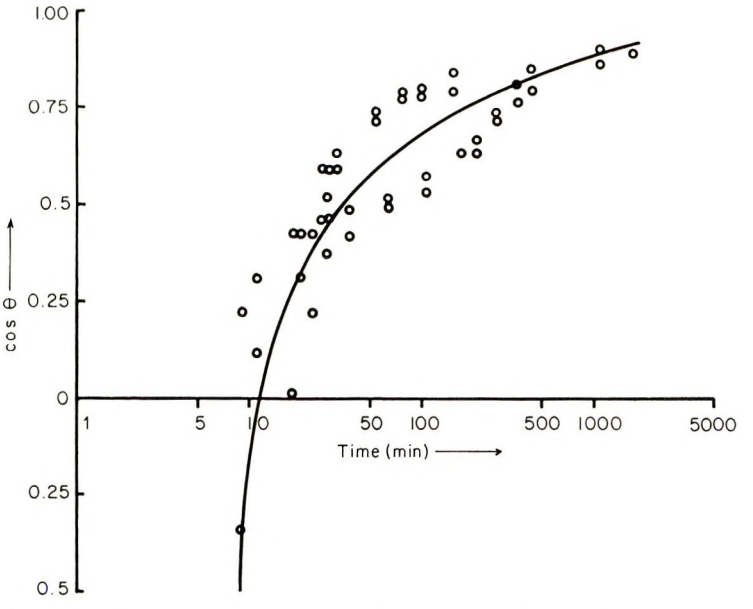

Fig. 4. Variation of contact angle with time for oxidized polyethylene on etched copper.

This means that the contact angles observed on these specimens are not the same as if the drops were on a smooth surface. This problem has been reviewed by Johnson and Dettre.[9] A first correction is needed because the energy of the interface is increased, since its real area is larger than its apparent area.[10] The real contact angle θ and the apparent angle θ' are related by Wenzel's equation,

$$\cos \theta' = r \cos \theta.$$

Thus the apparent contact angle is smaller than the true value for $\theta < 90°$, but larger for $\theta > 90°$. Secondly, if wetting is not complete there may be air trapped beneath the polymer, and the interface will be a composite one. This will increase the contact angle according to[11]

$$\cos \theta' = \sigma_1 \cos \theta - \sigma_2$$

where σ_1 is the area of metal/polymer interface and σ_2 the area of air/polymer interface. Johnson and Dettre present data from experiments by Shepard and Bartell[12] to measure the contact angles of organic liquids on paraffin wax surfaces of different roughnesses. They found that for $\theta = 60°$ when $r = 1$, the value of θ' rises to 90° as r increases to 2, but for $\theta = 40°$ when $r = 1$, θ' falls to 0 as r increases to 2. There are no results for $60° > \theta > 40°$, but if the apparent contact angle is 48° for $r = 2$, then the true contact angle must lie between 40° and 60° because the apparent contact angles diverge outside these limits as roughness increases.

For a real contact angle of 60°, the work of adhesion W_a is

$$W_a = \gamma_{LV}(1 + \cos 60) = 1.5\ \gamma_{LV}$$

For complete wetting ($\theta = 0$),

$$W_a = 2\gamma_{LV}.$$

This means that the increase in interfacial forces is not enough to bring about the increased adhesion.

In the cases of good adhesion the measured contact angles were 28° and 32°, and as these are both less than 40°, then the contact angles on a smooth surface would be increased but will still be less than in our case of poor adhesion with contact angle 48°.

For any crevice from which air can escape, complete wetting will occur, provided that the sum of the real contact angle and the angle the crevice side makes with the surface (measured inside the crevice) is less than 180°. Even a parallel-sided groove will of course be completely filled if the contact angle is less than 90°. This means that if air can escape, complete wetting should occur in all three types of specimen. De Bruyne[4] has calculated the effect of contact angle on the penetration of adhesives into pits of various shapes with trapping of air. For cylindrical pits, the penetration for θ = 60° is ca. 75% of that for θ = 30°. Likewise, for conical pits with a semi-angle of 45°, the dependence on contact angle is very limited. The only case where adhesion varies appreciably with contact angle is at low contact angles when the pits in the surface are very shallow, so that the unfilled pits act as incipient cracks at the interface. These cause stress concentrations so that when stress is applied they initiate cracking in the polymer at comparatively low loads. For this to occur, the polymer must be brittle; this does not apply to polyethylene which can extend up to 500% before fracture.

CONCLUSIONS

The discussion above shows that even the most favorable interpretation of the experimental data shows little correlation between the adhesion of polyethylene to these substrates and the bond strengths predicted from the contact angles on them. It appears that the poor adhesion of polyethylene to copper is caused neither by lack of strong interfacial forces between the polymer and the metal nor the inability of the polymer to achieve adequate wetting of the metal or oxide surface.

Bikerman[13] has demonstrated that when polyethylene is applied to metals by melting, a weak layer separates to the interface from the polymer as it cools, and that only if this is eliminated can good bonds be produced. We have shown[6] that polyethylene will bond to metals if it is oxidized either before or during application, but with coatings applied on copper in air the polyethylene must be oxidized beforehand. Bright[14] has demonstrated that copper suppresses the oxidation of polyethylene by air so it appears that it is only lack of oxidation which prevents good adhesion to copper. It is our belief[6] that the surface-active oxidized polymer molecules are preferentially adsorbed on to the metal or oxide surface, and during cooling remain attached, acting as links between the substrate and the polymer

matrix. As we have demonstrated here that even in the absence of oxidation, when only poor adhesion can be obtained, good wetting is produced, surface energy criteria are not applicable in this case. We suggest that the formation of weak layers at the interface can account for these reduced bond strengths.

We acknowledge with thanks financial assistance from the International Copper Research Association, who sponsored this research and provided a grant for one of us (J.M.S.) during the period of his research studentship. We also thank them for permission to publish these results.

References

1. W. A. Zisman, *Ind. Eng. Chem.*, **55,** No. 10, 19 (1963).
2. F. M. Fowkes, *Ind. Eng. Chem.*, **56,** No. 12, 40 (1964).
3. L. H. Sharpe, *Adv. Chem. Ser.*, **43,** 189 (1964).
4. N. A. DeBruyne, *Aero Research Tech. Notes, Bull.*, 168, (Dec. 1956).
5. A. Dupré, *Theorie Mechanique de la Chaleur*, Paris 1869.
6. J. M. Sykes and T. P. Hoar, *J. Polym. Sci. A-1*, **7,** 1385 (1969).
7. E. C. Potter, *Electrochemistry*, MacMillan and Cleaver, London 1956, p. 129.
8. L. Young, *Anodic Oxide Films*, Academic Press, New York, 1961.
9. R. H. Johnson and R. H. Dettre, *Adv. Chem. Ser.* **43,** 112, 136 (1964).
10. R. N. Wenzel, *Ind. Eng. Chem.*, **28,** 988 (1936).
11. A. B. D. Cassie, *Discussions Faraday Soc.*, **3,** 11 (1948).
12. J. W. Shepard and F. E. Bartell, *J. Phys. Chem.*, **57,** 458 (1953).
13. J. J. Bikerman, *Adhesives Age*, **2,** No. 2, 23 (1959).
14. K. Bright, Passfield Research Laboratories, private communication.

Received August 5, 1969
Revised September 25, 1970

JOURNAL OF POLYMER SCIENCE: PART A-2 VOL. 9, 895–915 (1971)

Electron Microscopy of Drawn Polypropylene

K. SAKAOKU and A. PETERLIN,
Camille Dreyfus Laboratory,
Research Triangle Institute,
Research Triangle Park, North Carolina 27709

Synopsis

Extremely thin polypropylene films formed by evaporation of dilute solutions floating on water, thin films deposited on Mylar or on carbon-coated Mylar, and bulk samples were deformed; after etching with aqua regia or chromic acid, the surfaces were studied by electron microscopy of surface replicas. At small draw ratio, microfibrils with lateral dimensions of about 200 Å, originating in micronecks at crack boundaries of the original crystal lamellae, were obtained in isolated areas exhibiting maximum local strain separated by large regions of much less deformed material. With increasing draw ratio the necked regions grow, the old structure gradually being reduced to smaller and smaller islands until it disappears completely. The inhomogeneity of strain in adjacent bundles of microfibrils creates a great many longitudinal voids with more or less disoriented microfibrils bridging the gaps. The regular arrangement of crystalline blocks of rather uniform length and width can be occasionally seen on surface replicas of drawn samples, and much better on dark-field electron micrographs of drawn and annealed thin membranes. In the latter case the blocks are very uniform and have similar dimensions along and perpendicular to the axis of the microfibril. The evidence from the electron micrographs, together with previous small-angle x-ray scattering data, supports Peterlin's molecular model for plastic deformation of crystalline polymers.

Introduction

The industrial production of fibers and films of crystalline polymers proceeds to a large extent by plastic deformation below the melting point of the polymer. Extensive experimental investigations[1] have clarified many aspects of the process but there is still no generally accepted model of the deformation mechanism at the microscopic level.

A detailed electron microscopy study of plastic deformation of isotactic polypropylene (PP) and a comparison of the results with those obtained on polyethylene (PE),[2–13] the most thoroughly studied polymer, seem to be important from the following points of view: how general is Peterlin's model of plastic deformation of a crystalline polymer solid[14–17] developed on the basis of PE data,[2–4] and what modifications are introduced for PP by the chain conformation and packing in the crystalline state. Both polymers are pure hydrocarbons with the same type of intermolecular forces; but the PE chain is a planar zigzag and PP is a helix with three monomers

per turn. Hence the root-mean-square length per monomer of the amorphous conformation is always smaller in the former but may be larger in the latter case than that of the crystalline conformation. Further, since the minimum distance between the fixed ends of a chain loop with adjacent reentry is larger with PP than with PE, longer loops, and hence a thicker "amorphous" surface layer in single crystals, are favored.

On the basis of experiments with drawing of single crystals,[6-10] of thin layers[11-13] and of bulk samples[2-4] of PE it has been concluded that the decisive step in the plastic deformation which transforms a microspherulitic sample into a highly oriented fiber structure is the complete destruction of every lamella of the original structure by "micronecking." The micronecks occur at those cracks which cut through a sufficient number of chain folds. The chains do not rupture but bridge the gap, partially unfolding and tearing off folded-chain blocks which are incorporated into microfibrils of the new fiber structure. The unfolded-chain sections form intrafibrillar tie molecules which are mainly responsible for the high longitudinal strength of the microfibril and hence of the fiber. The blocks, with lateral dimensions between 100 and 400 Å, already exist in the original lamellae, which like any organic or inorganic crystal exhibit a mosaic structure. The thickness of the lamella determines the thickness of the blocks in the microfibrils obtained by the destruction of isolated single crystals.[10] In the destruction of stacks of parallel lamellae as they occur in bulk samples down to extremely thin layers (ca. 1000 Å), however, a change of long period occurs to a value dependent mainly on the temperature of drawing and completely independent of the thickness of the lamellae in the original sample.[18-21]

The suggested explanation for this effect[2-4] is based on the differences in dissipation of heat generated by deformation. With isolated micronecks or micronecks linearly arranged at the crack in the case of single crystals the heat dissipation is so fast that the temperature rise is too small for any appreciable modification of the crystal blocks. However, in the case of a two-dimensional concentration of micronecks in an extremely thin destruction zone in stacked lamellae, the temperature rise behind the zone persists over a length comparable with the lateral dimensions of the zone. Therefore, under the special conditions of high negative pressure, axial tension, and negative lateral pressure, as a consequence of cross-section reduction by necking, sufficient chain mobilization occurs for the long period to adjust to the temperature of drawing. During cooling of crystal blocks with mobilized chains to the temperature of the unperturbed environment a new long period or thickness of the blocks depending on this temperature becomes established. For low draw rates the temperature of the unperturbed environment is practically identical with the temperature of drawing.

The microfibrils have a pronounced tendency for lateral coalescence, as has been observed in fractured single crystals and thin layers. The lateral cohesion is relatively poor, so that in deformed thin layers one notices a great many longitudinal voids created either by incomplete lateral coales-

cence of adjacent microfibrils or by separation caused by nonuniform strain of the microfibrils. As a consequence of nonuniform strain some microfibrils bridging a void may have an orientation completely different from the rest. They may cross the gap eventually at 90° to the draw direction or even run back.[11] On the other hand, on the boundary between adjacent microfibrils, the van der Waals forces are stronger with a crystal–crystal contact than with a crystal–amorphous layer contact. This favors a more or less perfect longitudinal fit of crystal blocks of adjacent microfibrils to produce fairly well defined crystal lamellae more or less perpendicular to the draw direction.[2–4] Such lamellae exhibit a pronounced mosaic structure with the folded-chain blocks of the microfibrils as the coherent lattice unit. As the irregularity of the lateral fit of these units may be quite appreciable, however, it is only occasionally possible to detect the existence and packing of lamellae by electron microscopy of etched surfaces of samples as drawn. This is particularly so if the drawing was performed at low temperature and to a high draw ratio leading to high paracrystalline disorder and a small density difference between crystalline and amorphous regions. Such a system is characterized by very faint meridional maxima in the small-angle x-ray scattering. However, the simultaneous presence of microfibrils and lamellae in the fully developed fiber structure is a straightforward conclusion derived from the whole body of data from electron microscopy and small-angle x-ray scattering even if surface replicas do not permit the observation of both elements in the same sample.

The lateral extension of the lamellae is most often limited by the boundary between adjacent fibrils, each fibril containing the microfibrils formed by the necking of the same stack of parallel lamellae and hence having practically the same draw ratio. Adjacent fibrils may differ quite appreciably in draw ratio, as is demonstrated by annealing effects.[2–4] This difference leads to poor cohesion on the boundaries and eventually to formation of longitudinal voids, which cause the fibrillation tendency of highly drawn crystalline polymer.

The drawing of single crystals of PP was studied by Cerra et al.,[22] and Kojima[23] has observed cracks on PP single crystals exposed to ultrasonic radiation. Cerra et al. found that a crack parallel to the growth face (100) is bridged by a great many microfibrils, whereas a crack perpendicular to it and parallel to the (010) plane is smooth without fibril formation. These data pose some serious problems about the orientation of folds and the deposition of polymer chains during crystallization, but they also show that, as in PE, at proper orientation of the crack the crystal lamella is transformed by micronecking into the highly oriented fibrillar structure. No investigation was made to check whether the microfibrils from PP single crystals also contain folded-chain blocks connected (as in PE) by tie molecules partially unfolded at the separation of the blocks from the lamella.

Small-angle x-ray scattering of PP drawn between 20 and 155°C over a wide range of draw ratios clearly demonstrates the dependence of the fiber

long period L_T on the temperature of drawing and the complete independence of the lamella thickness of the starting material. This is in complete agreement with the data on PE. The diffraction pattern as a function of draw ratio is very similar to that of PE so that one is tempted to conclude that the basic mechanism of lamella destruction, microfibril formation, and lateral coalescence of folded-chain blocks into lamellae roughly perpendicular to the draw direction is the same for PE and PP.

Here, a detailed electron microscopy study of plastic deformation of ultrathin layers, thin films, and bulk samples of PP will be presented together with observation of annealing effects. The data will be compared with those obtained with linear PE.[2–4,11] The close similarity of the observed effects provides excellent support for the deformation model proposed earlier and its general applicability to crystalline polymers.

Experimental

Isotactic polypropylene (Escon 502, Trademark of Enjay Chemical Co.) with a weight-average molecular weight of 426,000 was investigated in three different types of film: (1) ultrathin membranes case from dilute xylene solution on nearly boiling water; (2) thin layers (ca. 0.01 mm) solution-cast on Mylar and subsequently melted by raising the temperature to 220°C *in vacuo* and then slowly cooled to room temperature; (3) PP pellets as supplied from the manufacturer, pressure-cast in a laboratory press at 180°C to form a 0.5 mm thick film, taken out of the press before solidification, and quenched in ice water. In order to change the cooling velocity, films 4 mm thick were pressure-cast in contact with aluminum foil or Mylar at 180°C and cooled by tap water flowing through the heating plates of the casting stage.

The thin membranes (1) were deformed while still floating on nearly boiling water. The layers on Mylar (2), with or without a carbon coating, were deformed by stretching the Mylar substrate at 65°C. The PP layers deposited directly on Mylar deformed rather uniformly. The deformation, however, was extremely inhomogeneous if a carbon coating was applied to Mylar before casting the PP film from solution; the rigid carbon coating broke with a great many cracks perpendicular to the strain direction. The PP film on the unbroken carbon coating was virtually undeformed. On the cracks, however, the deformation was extreme, several hundred and even a thousand percent, although the total deformation of the Mylar film was only 50%. The drawing of bulk samples was performed with an Instron TM-M Tester in this manner described earlier.[24] Drawn samples with a high tendency to fibrillation were used for electron microscopy because we wanted to see the microfibrillar elements of the fiber structure.

In order to reveal the crystalline morphology we must etch the polymer sample selectively before the surface replication. The etching is supposed to take away the amorphous sections without modifying the crystals significantly. Ion bombardment and inorganic acid treatment are used. The mechanism of attack and the specific reaction of the polymer are not

sufficiently understood. In the case of PP the ion bombardment, even at the lowest energy density of the plasma discharge, produced surface melting which completely obscured the morphology we wanted to study. Etching with fuming nitric acid, which is such a useful method for PE, turned out to be not sufficiently selective with PP.[25] The acid occasionally removes the whole surface layer rather indiscriminately without exposing the crystalline morphology. Therefore etching with other acids was tried. Aqua regia and chromic acid[26] turned out to be satisfactory.

All samples except thin membranes were treated in aqua regia at 0°C (5 hr) or in chromic acid at room temperature (20 min). The surface replicas were made by the one-step replica method with platinum–carbon shadowing and carbon coating. The replicas were stripped off the PP surface with poly(acrylic acid).

Results and Discussion

The very thin membranes (1) obtained on the surface of nearly boiling water from a single drop of boiling dilute PP–xylene solution spreading thinly over the hot water surface were stretched by a pair of tweezers after the xylene evaporated. The deformed membrane floating on the water was lifted by the grid of the electron microscope sample holder and annealed at 158°C in vacuum. The electron diffraction pattern (Fig. 1) showing 12 layer lines in the original negative demonstrates the extremely good orientation of the chains in the direction of deformation, the high perfection of the crystal lattice, and the large size of coherent crystal blocks. The dark-field electron micrograph (Fig. 2) obtained from the (110), (040), and (130) reflections shows isolated crystal blocks throughout the sample without showing sufficiently well their arrangement in single microfibrils or in lamellae perpendicular to the fibrils. The blocks are all nearly the same size. A slight astigmatism forbids a binding statement about the shape of the blocks; but they seem not to be very anisometric. One can conclude that neither in the longitudinal nor in the lateral direction does the coherence of the crystal lattice extend beyond a few hundred angstroms. In both directions the folded-chain blocks adjacent to those showing up in the dark-field micrograph must be so mismatched as far as the orientation of the a and b axes is concerned that they do not scatter electrons in the diffraction spots used for the dark-field picture. The situation is identical with that observed in drawn PE samples after annealing, i.e., isolated folded-chain blocks varying little in dimensions. One feels reasonably sure that exactly the same argument based in the case of PE on dark-field electron micrographs of thin membranes as drawn and on bright-field micrographs of iodine-stained membranes can be applied to PP. Hence the folded-chain blocks are the basic unit of the microfibrils. They are incorporated in the microfibrils during micronecking at cracks in the original lamellae and are connected in the axial direction by intrafibrillar tie molecules unfolded where the blocks break off from the lamellae.

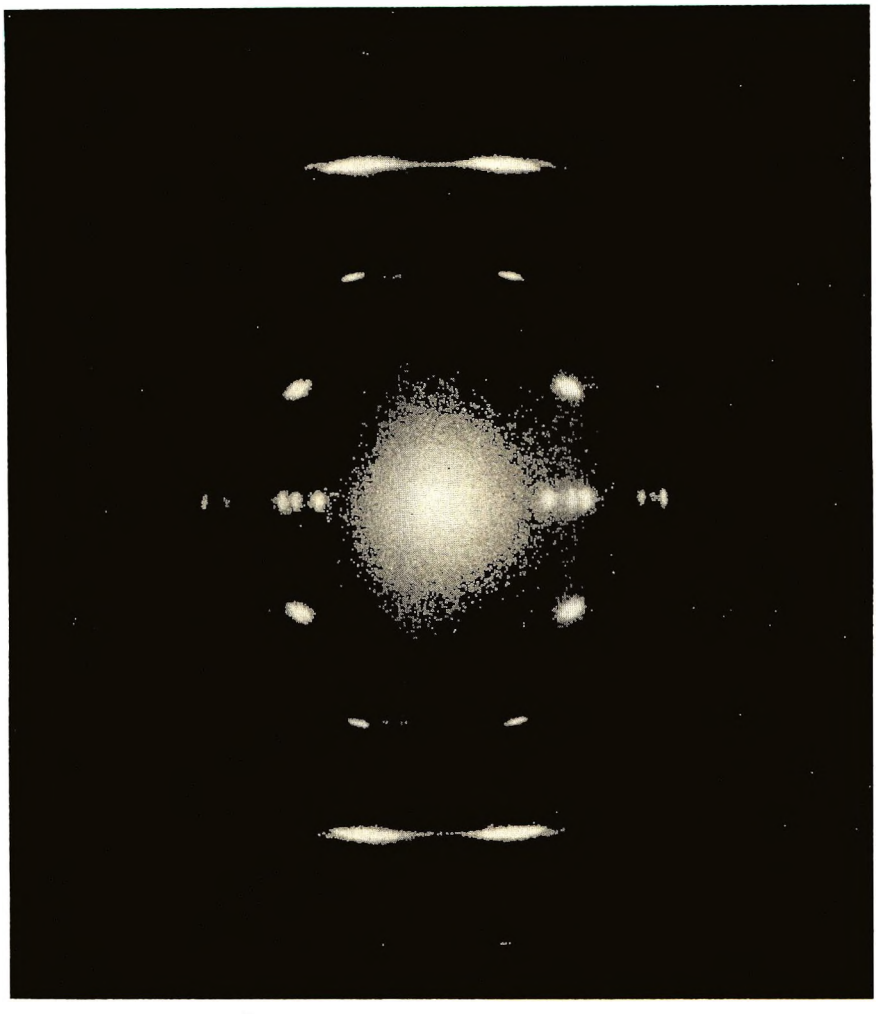

Fig. 1. Electron diffraction pattern of a drawn and annealed (158°C *in vacuo*) PP membrane.

Thin membranes, solution-cast on carbon coated Mylar, subsequently melted by heating to 220°C *in vacuo* and then slowly cooled (2), were deformed at 65°C by stretching the Mylar substrate. As the carbon film cracked, the deposited ultra-thin PP film produced a great many microfibrils bridging the cracks. As Figure 3 shows, the number of microfibrils is so large that very nearly the whole area of the crack is covered by a thin fibrillar layer interrupted laterally by a great many longitudinal gaps. Most of the gaps are bridged by individual or partially coalesced microfibrils. Some of them are oriented at a substantial angle to the draw direction, indicating a large and irregular variation of the local draw ratio (Λ). One concludes from the micrograph that in spite of a pronounced tendency

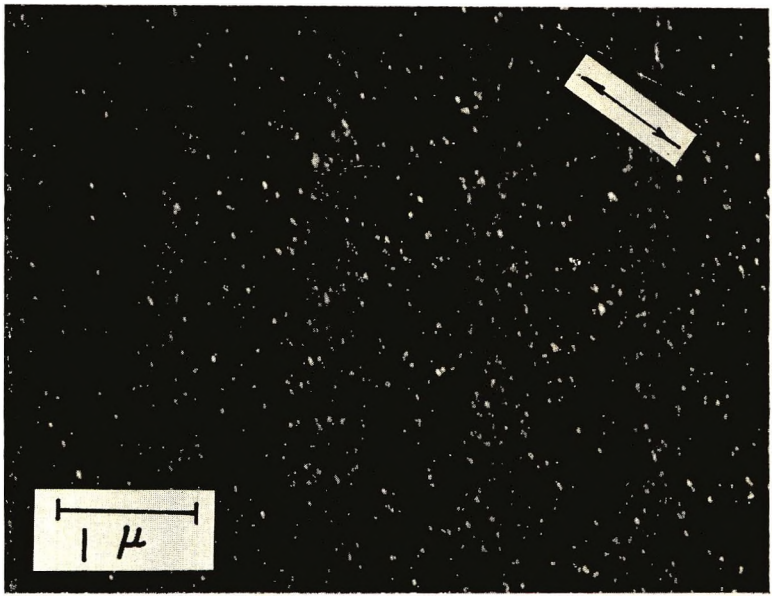

Fig. 2. Dark-field electron micrograph of the PP membrane in Fig. 1: (110), (040) and (130) reflections.

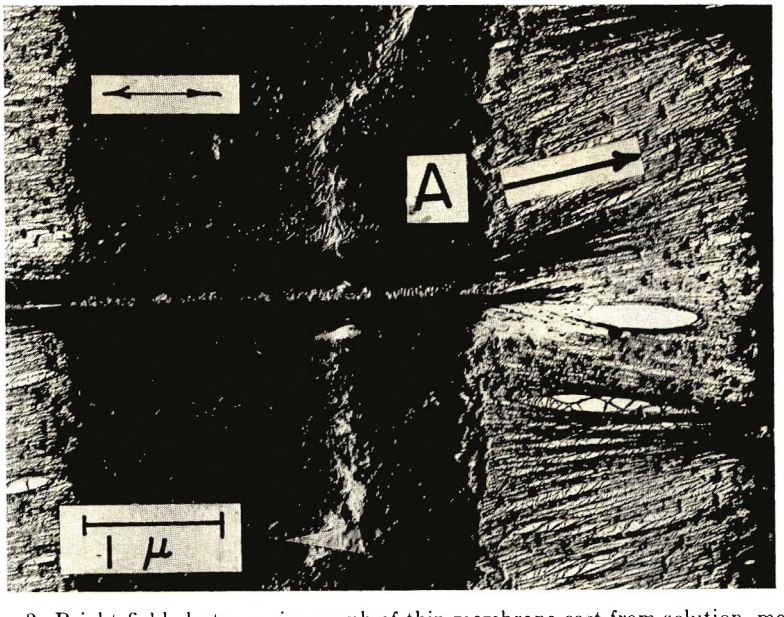

Fig. 3. Bright-field electron micrograph of thin membrane cast from solution, melted on carbon-coated Mylar at 220°C *in vacuo* and slowly cooled. The Mylar substrate was stretched 50% at 65°C.

for lateral coalescence of the microfibrils their lateral cohesion is significantly smaller than the longitudinal strength of the microfibrils.

Most microfibrils are smooth with lateral dimensions ranging from 100 to a few hundred angstroms, with an average about 200 Å. On the fibrillar layer one sees more-or-less randomly distributed remains of the original stacks of lamellae. Their frequency and also their size are larger in the vicinity of the cracked carbon layer. One gets the impression that larger sections of stacked lamellae are broken off first when the gap at the crack begins to grow and that these fractions are gradually transformed into microfibrils by the micronecks on their boundaries. They are smaller and less frequent in the center line of the large crack where the transformation first started and hence proceeded further than at the outer boundary of the crack. The spatial distribution of microfibrils and remains of lamellae seems to be a reflection of the time sequence of the deformation process with zero time at the final crack boundary and maximum time in the center. The incomplete drawing and transformation into the fiber structure with a great many islands of spherulitic structure are of exactly the same type previously observed with thin PE membranes (Fig. 2 in ref. 11).

Annealing at 160°C drastically increases lateral coalescence and leads to very thick (up to 1000 Å) microfibrils separated by large voids occupying most of the gap (Fig. 4). But one still sees the original thin microfibrils particularly in the vicinity of micronecks. Except in a very few places all the isolated remains of original lamellae in the fibrillar layer have disappeared. The formation of thicker microfibrils as a consequence of annealing corresponds very well to the lateral growth of coherent crystal blocks in drawn PE as derived from the radial width of equatorial wide-angle X-ray reflections.[27] However, the shadowing of the sample without previous etching does not produce enough contrast for the detection of an axial periodicity in the microfibrils. The many well ordered but randomly oriented stacks of lamellae in the undeformed areas indicate extensive recrystallization with occasional row nucleation yielding a well developed "shish-kebab" structure. The nearly perpendicular orientation of lamellae in some places reminds one of the basketweave structure obtained by crystallization from dilute solution.[28]

The partial spherulitic structure of the membranes nearly 0.01 mm thick (2) obtained by slow cooling of melted (220°C) solution-cast films on the Mylar substrate without a carbon coating is shown in Figure 5. The stacks of parallel lamellae oriented at right angles to the radius extend over wide areas. In a great many places these stacks are partially covered or contain interwoven lamellae at nearly 90°, i.e., in the radial direction. The structure in such places is similar to that in the basketweave crystal agglomerates obtained from dilute solution. Stretching the Mylar substrate by 50% at room temperature not only partially rotates the lamellae towards the direction of drawing, thus locally creating kink bands, but also produces isolated cracks bridged by a great many microfibrils pulled out of the broken lamellae (Fig. 6). A conspicuous feature is the extreme

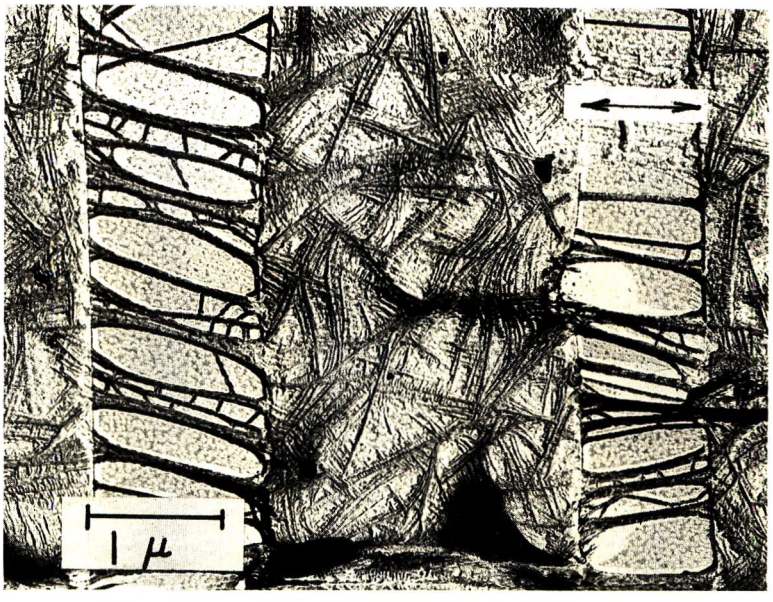

Fig. 4. Same as Fig. 3 after annealing at 150°C *in vacuo*.

heterogeneity of the strain field as a consequence of the inhomogeneity of crystal packing and orientation. Large sections remain nearly undeformed; hence a large strain on the boundaries is created. This leads to crystal fracture and micronecking at a macroscopic strain which in a homogeneous strain field would not produce discontinuous deformation. This observation corroborates the conclusions from small-angle x-ray scattering[24] that the appearance of the new meridional long period is caused by the incipient formation of the new fiber structure, that the transformation occurs already at an elongation $\lambda = 1.3$ for drawing at $T_d = 60°C$, and that the micronecking zones are localized at areas of maximum strain concentration but do not extend as a continuous layer through the whole cross-section of the necking sample. Therefore, extremely early in the drawing experiment, a few areas in the neck are already sufficiently strained for transformation into the new fiber structure whereas the rest still remains microspherulitic. With increasing draw ratio, the strain conditions for micronecking are reached in so many more places that finally very nearly every volume element in the neck is affected and transformed into the new fiber structure. After the neck has passed through a cross section of the sample the effect of the great many isolated micronecking zones is very nearly complete, with only occasional remains of the heavily deformed but not yet destroyed original microspherulites.[2–4]

The 0.5 mm thick film (3) quenched by dipping the pressure-cast molten sheet into ice water has a very poorly developed lamellar structure (Fig. 7). The parallelism of stacked lamellae extends over very large areas. Occasionally one also finds the nearly perpendicular arrangement of lamellae characteristic of PP crystallized from solution. Figure 8 shows the surface

Fig. 5. Surface replica of PP film about 10 μ thick, cast from solution on Mylar substrate and melted at 220°C *in vacuo*.

of a 4 mm-thick sheet cooled in contact with aluminum foil on the casting stage by running water. The spherulitic structure is extremely well developed with most of the lamellae seen edge on. At the boundary between adjacent spherulites the lamellae of one spherulite penetrate the gaps between the stacks of lamellae of the other spherulite in very much the same manner as in polyethylene. In contact with Mylar (Fig. 9) the surface morphology is dominated by the nearly perpendicular arrangement of lamellae. This basketweave structure occurs in large patches of random orientation with local overlapping. The thickness of the lamellae is about 170 Å.

Surface replicas of drawn PP in the necking region were obtained from slowly cooled films. At draw ratios between 1.2 and 1.5 the structure does not yet show very conspicuous orientation effects or micronecking (Fig. 10). At $\lambda = 2$, however, (Fig. 11) one sees a great many micronecks at large isolated cracks (manimum length about 1 μ) bridged by long, partially aligned and coalesced microfibrils separated by longitudinal gaps. A great many bundles of microfibrils are at an angle to the draw direction as a consequence of displacement of micronecks or lamellae. The gaps between the bundles contain some poorly oriented or completely disoriented microfibrils passing from one side to the other in exactly the same manner as shown in Figure 3, indicating the nonuniform strain of the gap boundaries. The thinnest microfibrils are about 200 Å thick, the major fraction of them being

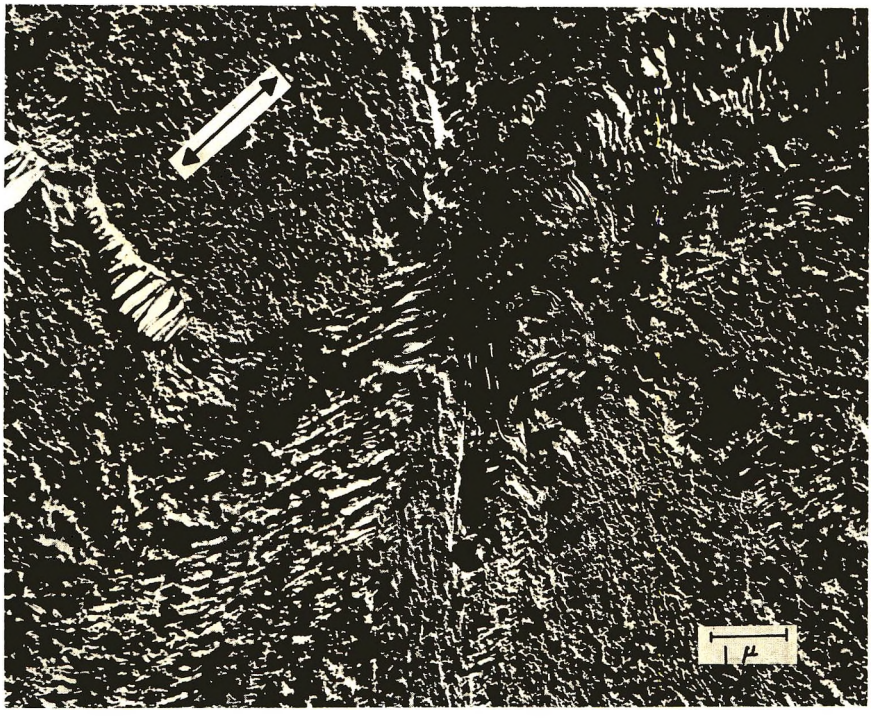

Fig. 6. Surface replica of the film from Fig. 5 after 50% stretching of Mylar substrate.

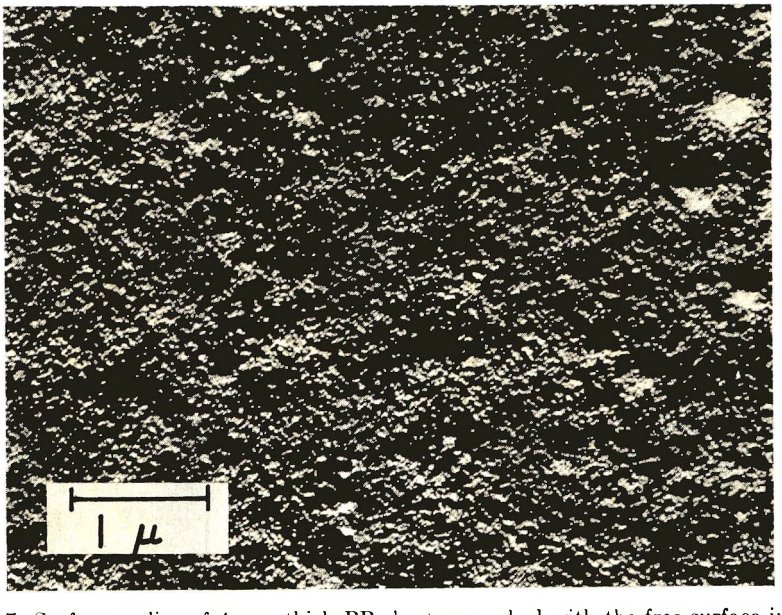

Fig. 7. Surface replica of 4 mm-thick PP sheet, quenched with the free surface in ice water and etched with chromic acid for 20 minutes at room temperature.

between 300 and 400 Å thick. In area *A* one readily observes a stack of lamellae with a long period of 130 Å (identical with that obtained from small-angle x-ray scattering of the original sample). The larger long period (ca. 200 Å) of area *B* may be an indication of longitudinal slip of lamellae,

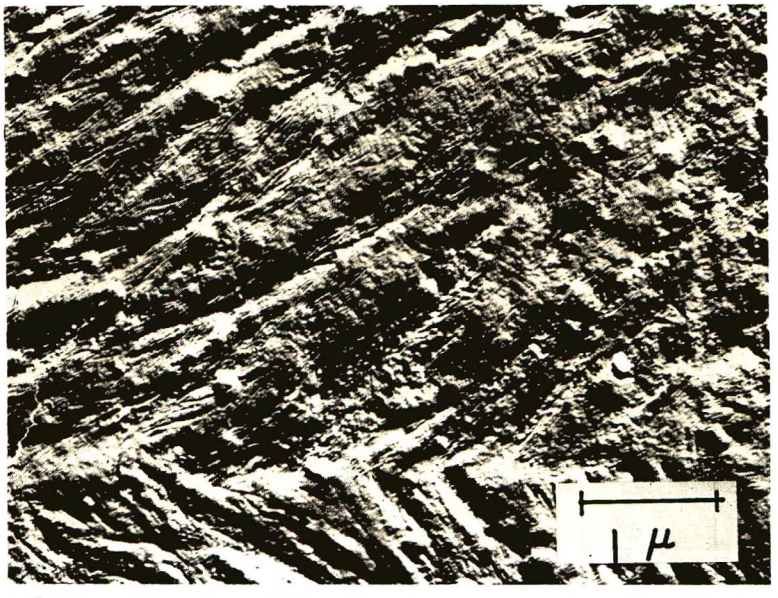

Fig. 8. Surface replica of 4 mm-thick PP sheet, rapidly cooled in contact with aluminum foil in the casting machine and etched as in Fig. 7.

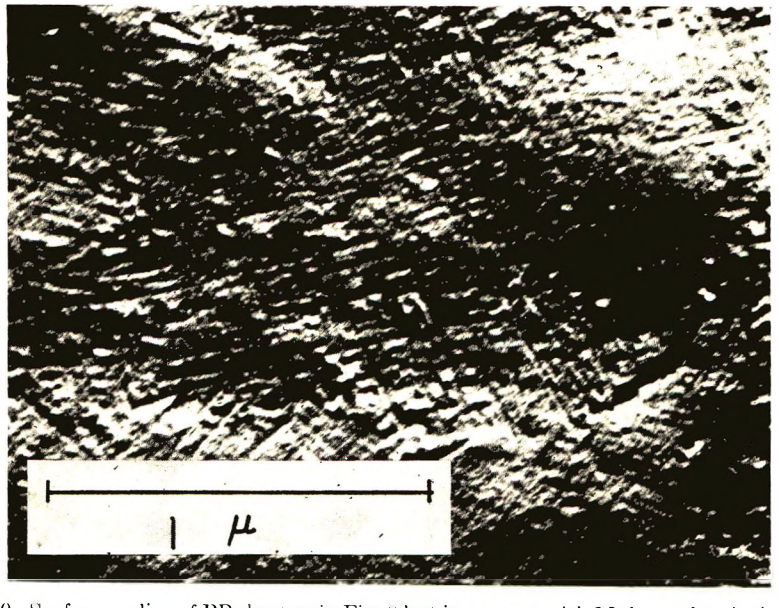

Fig. 9. Surface replica of PP sheet as in Fig. 8 but in contact with Mylar and etched as in Fig. 7.

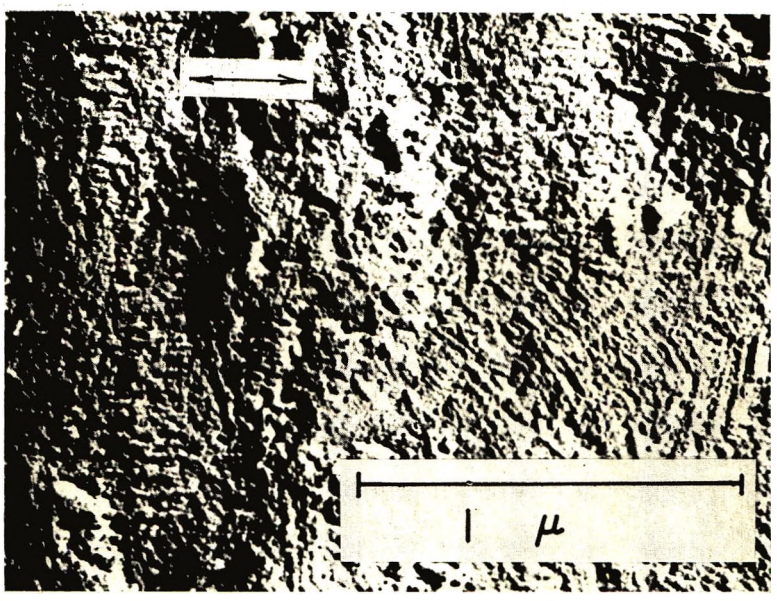

Fig. 10. Surface replica of slowly cooled, 0.5 mm-thick PP film drawn at 65°C at a draw rate of 0.5 cm./min to a draw ratio λ between 1.2 and 1.5. Sample etched with aqua regia at 0°C (5 hr).

which is one of the earliest modes of plastic deformation of crystalline polymers—preceding the plastic deformation of lamellae by chain tilting and slipping and the subsequent destruction of lamellae by micronecking. Section *C* shows a large kink band with the lamellae nearly at 45° to the draw direction. At the lower end, these lamellae are already partially transformed into microfibrils oriented at a small but measurable angle to the draw direction. Figure 12 shows another section of the same sample ($\lambda = 2$) which shows hardly any microfibrils. The whole area is full of basketweave lamellar arrangements which seem to deform more uniformly or resist destruction better than stacks of parallel lamellae without cross-connecting lamellae.

With a draw ratio of 5 (Fig. 13), the transformation into the fiber structure seems to be nearly completed. The whole surface of the sample consists of very nearly perfectly aligned microfibrils with a great many longitudinal voids bridged by poorly oriented isolated microfibrils. The voids definitely give the impression of a finite strain difference between separated boundaries leading to the eventual perpendicular orientation of the bridging microfibrils. Isolated irregularities in the fibrous structure may be the remains of the original lamellae, which will be destroyed at a still higher draw ratio. A similar situation has been already observed in Figure 3. If this interpretation is correct, a substantial part of the inhomogeneous strain in the macroscopic neck and on microfibrils is caused by such incomplete transformation of spherulitic structure into fiber structure, i.e., by local yielding of the weakest elements which suffer the major part of the

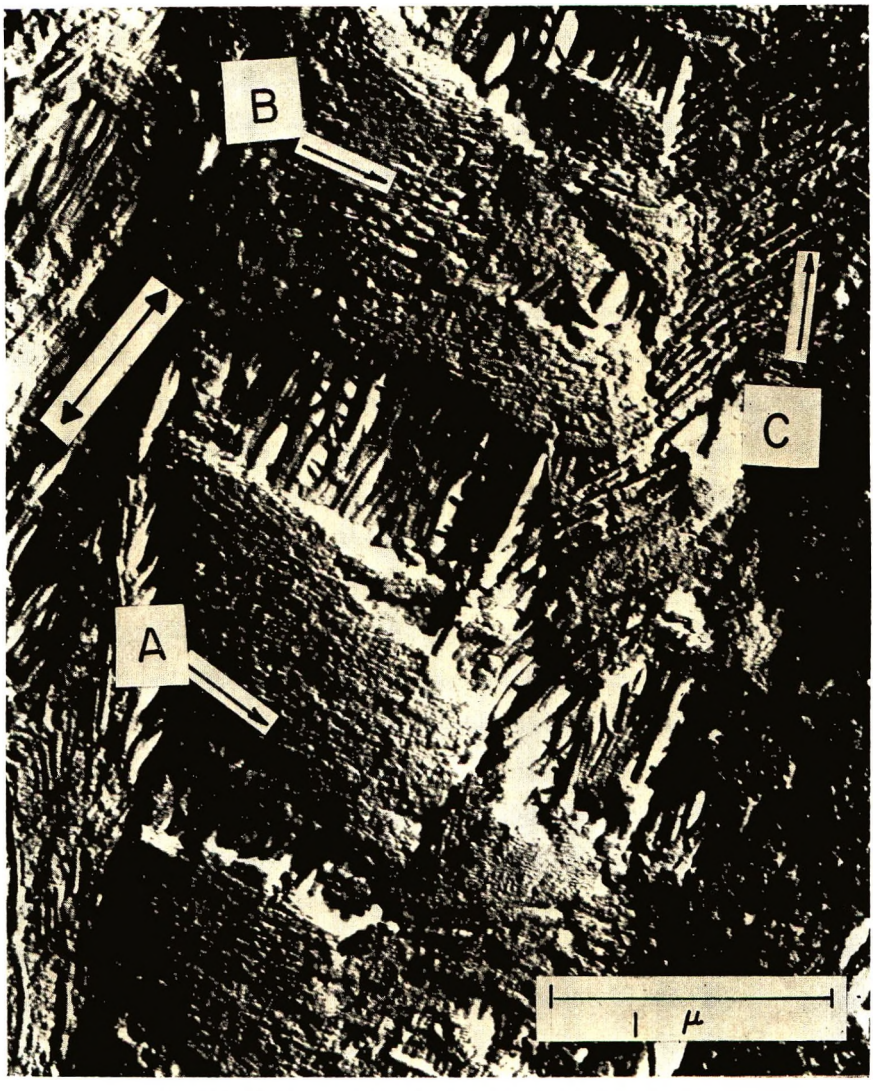

Fig. 11. Surface replica of the sample in Fig. 10, $\lambda = 2$.

strain, leaving more rigid elements nearly unaffected. Another source is the variation of lamellar orientation in the destruction zones as indicated in Figure 11.

A higher draw ratio ($\lambda = 15$ in Fig. 14, $\lambda = 20$ in Fig. 15) of quenched samples improves the alignment of microfibrils and makes the remains of the original lamellae completely disappear. The sample with $\lambda = 15$ is still transparent, but that with $\lambda = 20$ is very opaque indicating the presence of a great many voids with magnitude on the order of optical wave length. Indeed a tendency to bundle formation (between 400 and 1000 Å diameter) and to large voids with a great many bridging microfibrils seems

to show up at $\lambda = 20$. The individual microfibrils are prominent in Figure 15. Their lateral dimension is about 160 Å with very little fluctuation. There is less certainty about the appearance of the crystal blocks in the microfibrils, and their lateral arrangement in lamellae is roughly perpendicular to the draw direction. One sees at *A* some bright spots uniformly

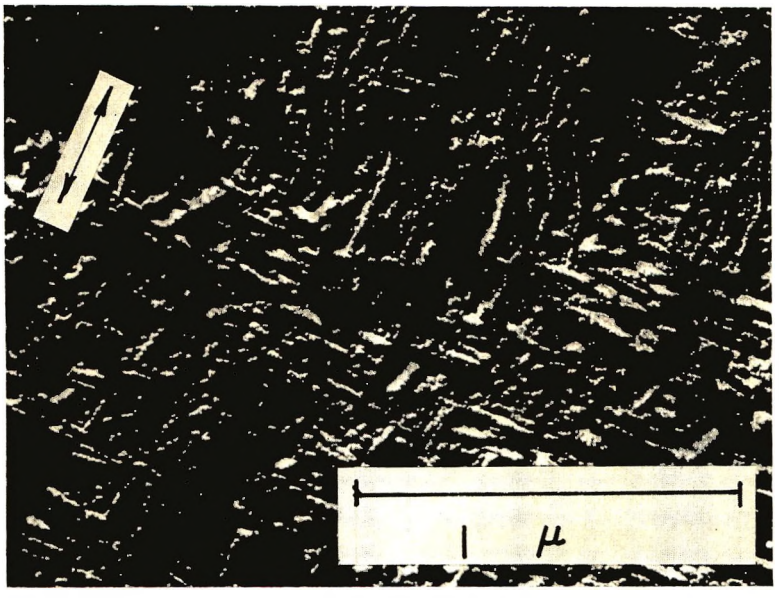

Fig. 12. Surface replica of the sample in Fig. 10, $\lambda = 2$, showing no microneck and microfibrils.

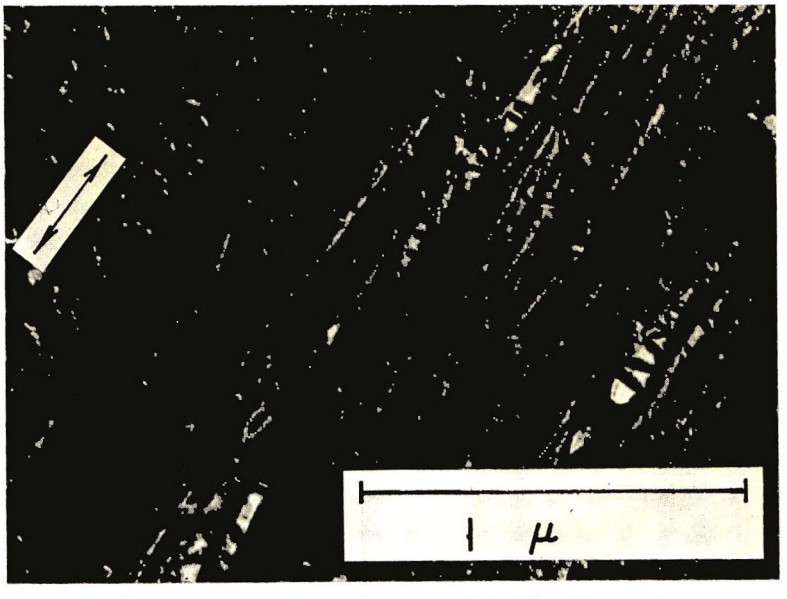

Fig. 13. Surface replica of the sample in Fig. 10, $\gamma = 5$.

spaced along the microfibrils and laterally arranged in as orderly fashion as if they belonged to a stack of lamellae. The long period derived from these spots is 200 Å, which is in rather good agreement with the x-ray value, 220 Å.

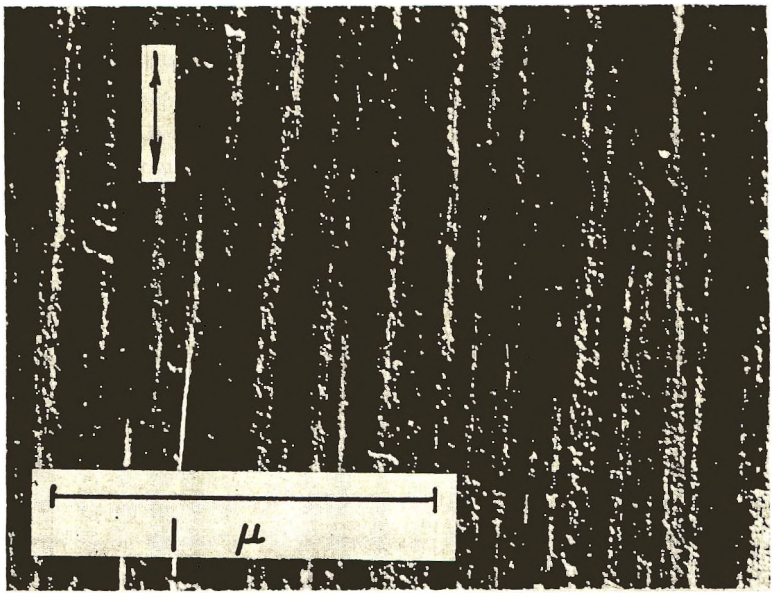

Fig. 14. Surface replica of quenched PP drawn at 140°C to λ —15 (a transparent sample) and then etched with aqua regia at 0°C (5 hr).

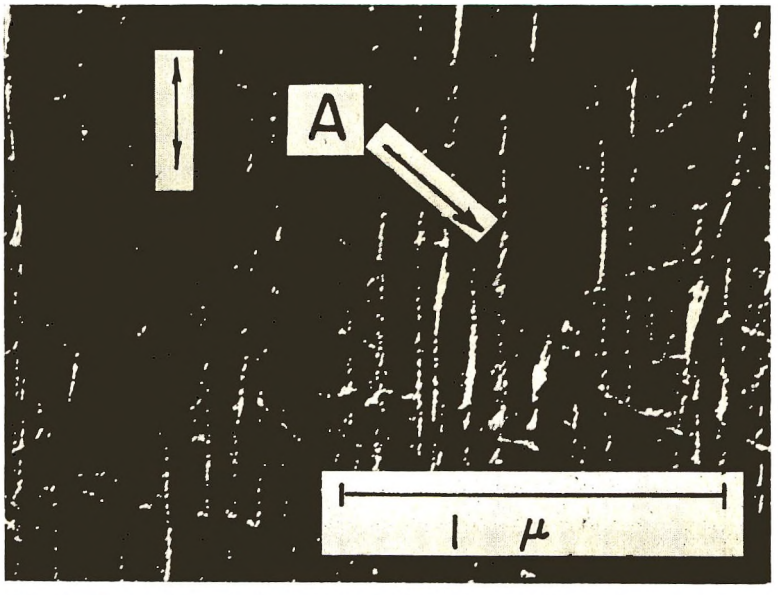

Fig. 15. Surface replica of the sample in Fig. 14, λ = 20–25 (an opaque sample).

Annealing at 150°C of a sample drawn at 140°C to $\lambda = 20$ modifies the free surface in a manner very similar to that observed previously with PE (Fig. 16).[2-4] The lamellae more or less perpendicular to the draw direction become easier to observe. The deviation from perpendicularity is small, in complete agreement with the narrowing of the meridional maximum of

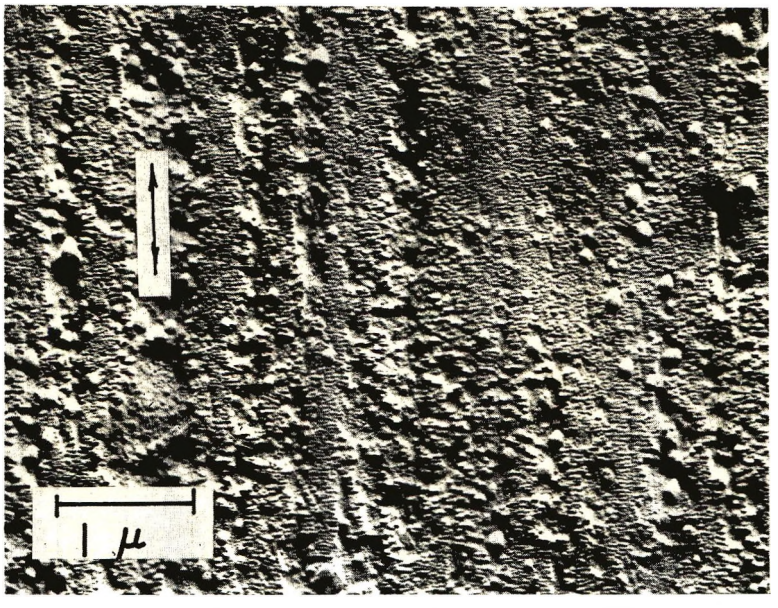

Fig. 16. Surface replica of the sample in Fig. 15 annealed at 150°C for 1 hr *in vacuo*.

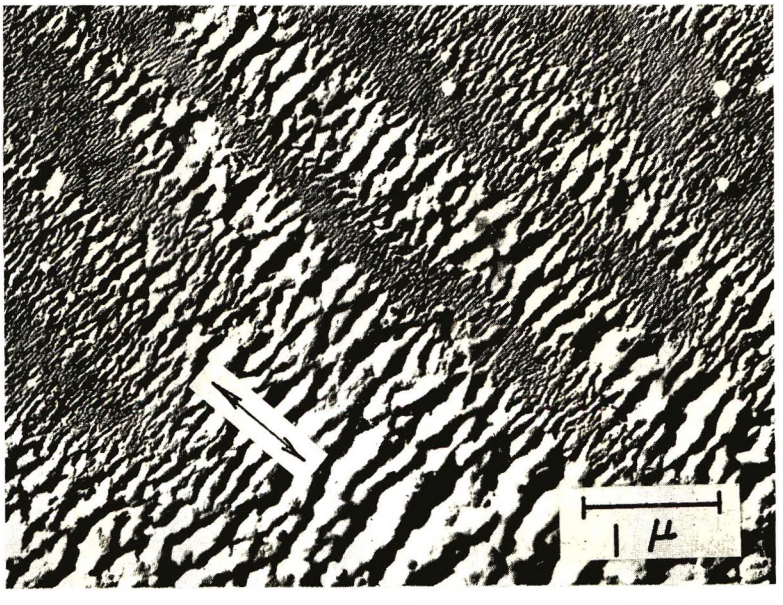

Fig. 17. Surface replica of the sample in Fig. 15 annealed at 160°C 1 hr *in vacuo*.

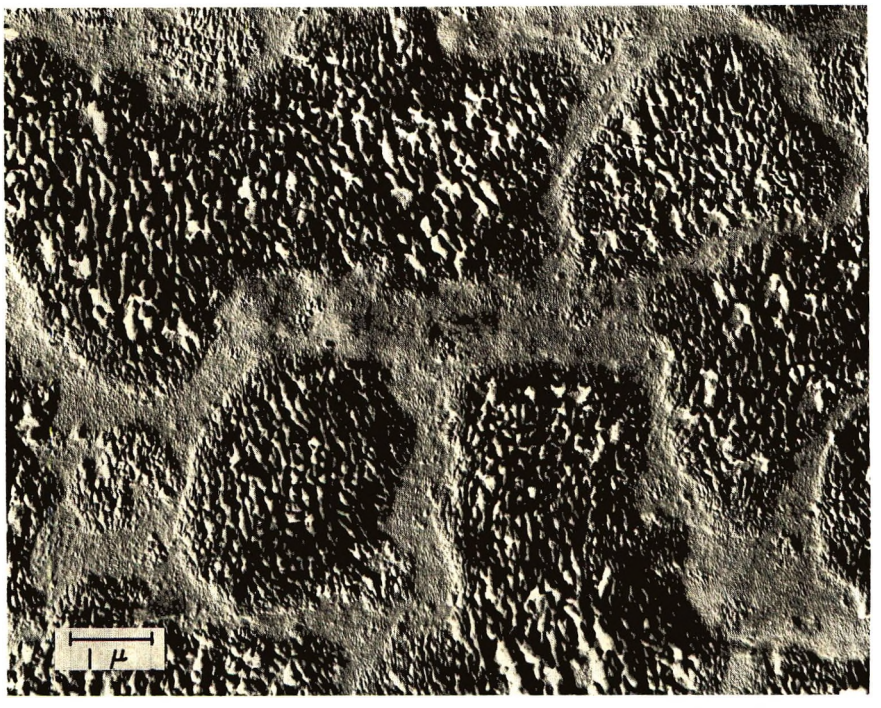

Fig. 18. Surface replica of biaxially drawn Olethane film annealed at 150°C one hr *in vacuo*.

small-angle x-ray scattering.[29] The long period from Figure 16 is 290 Å, as compared with L = 280 Å derived from small-angle x-ray scattering. Moreover, the well-ordered lamellae are arranged in long fibrillar sections of 400–1000 Å lateral width separated from each other by regions of more irregular structure containing protruding multilayer lamellae. These lamellae give the impression of arbitrary rotation about an axis in the surface plane and perpendicular to the draw direction. In many places such lamellae grow laterally beyond the boundary of the fibril so that large areas coalesce into broader ribbons separated by fibrils of well-ordered lamellae. From experiments with linear PE drawn to different draw ratios and annealed at different temperatures one could conclude that the modification of the surface structure is a maximum for the fibril with minimum draw ratio.[2–4]

The situation becomes much more extreme with annealing at higher temperature, e.g., at 160°C (Fig. 17). The protruding multilayer lamellae cover nearly half of the figure so uniformly that one hardly recognizes the original fibril structure. In the rest of the figure the surface transformation has not yet progressed so far, and hence one still recognizes the fibrils of nearly unchanged stacked lamellae separated by fibrils of more or less protruding lamellae. In the case of PE the rotation of surface lamellae during annealing was observed and this was assumed to be caused by unidirectional

torques transmitted through tie molecules in the microfibrils which as a consequence of the constant flow pattern in the neck are all (or nearly all) oriented in the same manner. Annealing sufficiently mobilizes the structure that the rotation can take place. No such rotation was observed in the interior of PE samples except at interior voids and cracks. At such interior surfaces the annealing phenomena are the same as those observed on the outer free surfaces of the sample. The effects are slightly hampered and hence occur at higher temperature if the sample is clamped so that it cannot shrink. An extreme case is drawing at a high temperature (150 or 160°C). It does not produce the irregular rough surface structure. If, however, such a sample after drawing is annealed at the same temperature while kept free or with ends fixed one observes the same annealing effects on the surface with rotation and lateral growth of multilayer lamellae. The effects proceed faster if the sample is unconstrained during annealing.

A commercial PP film biaxially drawn (Olethane) is shown in Figure 18 after annealing at 150°C. The sample was free to shrink. As was expected, the surface shows in every section a single direction of orientation but the direction is not exactly the same on the whole area shown. Such a strain pattern may be derived directly from the geometry of simultaneous stretching in two directions. The nonuniformity of draw ratio is reflected in the local variation of annealing effects: i.e., by islands of lower draw ratio immersed in a sea of higher draw ratio.

Neither as drawn nor after annealing do samples exhibit specific differences in electron micrographs which reflect the different crystal lattice and chain conformation of PP and PE. The basic deformational processes, particularly the chain slipping, tilting and unfolding at the cracks and the incorporation of the broken-off folded-chain blocks into microfibrils, seem to be unaffected as far as the supercrystalline morphology is concerned. Differences, however, may be expected in the conformation of chains in the amorphous regions of the drawn material and in the deviations of heat content, sorption, diffusion, and permeability from thermodynamic equilibrium.[30–33]

Conclusions

The electron micrographs of PP films and thin membranes support the molecular model of plastic deformation of crystalline polymers developed by Peterlin,[14–17] particularly the discontinuous transformation of the original microspherulitic structure into the final fiber structure by micronecks concentrated in more or less randomly distributed destruction zones. In micronecks the lamellae are fractured into small folded-chain blocks and these blocks are incorporated into the microfibrils, the basic element of the fiber structure.

The microfibrillar structure of a highly drawn sample and, to some extent, even the existence of regularly spaced crystal blocks inside the microfibril are well documented in Figures 13–15. The blocks of very uniform size and small anisometry are better visible in the dark field electron micrograph of

the annealed drawn ultrathin membrane (Fig. 2). The chain axis in the crystal lattice of the block is perfectly oriented in the draw direction (Fig. 1) but the orientation of the a and b axes varies from block to block.

The cracks and micronecks appear at small macroscopic strain ($\lambda \simeq 1.2$–1.5) more or less randomly distributed over the sample (Figs. 6 and 10). The local strain at the crack may be several hundred per cent and that of the adjacent undestroyed original structure much less than the macroscopic strain. The large inhomogeneity of the strain field is the consequence of the enormously varying strength and of orientational effects of supercrystalline morphology. An extreme case of such strain heterogeneity can be demonstrated on thin PP film deposited on a carbon coated Mylar film (Figs. 3 and 4). The arrangement of cracks, micronecks, microfibrils and islands of undestroyed microspherulitic structure are a model example of the processes occurring in a drawn bulk sample.

Annealing of drawn bulk samples produces a surface roughness of the type previously observed with PE (Figs. 16–18). Surface areas with similar modification by annealing are arranged on long ribbons containing microfibrils of very nearly the same draw ratio which, one guesses, may have been produced in a single destruction zone from one stack of parallel lamellae.

References

1. K. O'Leary and P. H. Geil, *J. Macromol. Sci. (Phys.), B*, **2**, 261 (1968).
2. A. Peterlin and K. Sakaoku, *Kolloid-Z. Z. Polym.*, **212**, 1, 51 (1966).
3. A. Peterlin and K. Sakaoku, *J. Appl. Phys.*, **38**, 4152 (1967).
4. A. Peterlin and K. Sakaoku, in *Clean Surfaces*, G. Goldfinger, Ed., Dekker, New York, 1970 p. 1.
5. K. Sakaoku and A. Peterlin, *J. Macromol. Sci. B*, **1**, 103 (1967).
6. P. H. Geil, *Polymer Single Crystals*, Interscience, 1963, Chap. VII; *J. Polym. Sci. B*, **3**, 157, 257, 263 (1965).
7. H. Kiho, A. Peterlin, and P. H. Geil, *J. Appl. Phys.*, **35**, 1599 (1964); *J. Polym. Sci. B*, **3**, 157, 257, 263 (1965).
8. A. Peterlin, H. Kiho, and P. H. Geil, *J. Polym. Sci. B*, **3**, 151 (1965).
9. A. Peterlin, P. Ingram, and H. Kiho, *Makromol. Chem.*, **86**, 294 (1965).
10. P. Ingram, *Makromol. Chem.*, **108**, 281 (1967).
11. K. Sakaoku and A. Peterlin, *Makromol. Chem.*, **108**, 234 (1967).
12. L. Hay and A. Keller, *Kolloid-Z. Z. Polym.*, **204**, 43 (1965).
13. R. G. Vadimsky, H. D. Keith, and H. J. Padden, Jr., *J. Polym. Sci. A-2*, **7**, 1367 (1969).
14. A. Peterlin, in *Structure and Properties of Polymers* (*J. Polym. Sci. C*, **9**), A. V. Tobolsky, Ed., Interscience, New York, 1965, p. 61.
15. A. Peterlin, in *U.S.-Japan Seminar in Polymer Physics* (*J. Polym. Sci. C*, **15**), R. S. Stein and S. Onogi, Eds., Interscience, New York, 1966, p. 427.
16. A. Peterlin, in *The Meaning of Crystallinity in Polymers* (*J. Polym. Sci. C*, **18**), F. P. Price, Ed., Interscience, New York, 1967, p. 123.
17. A. Peterlin, *Kolloid-Z. Z. Polym.*, **216**/**217**, 129 (1967).
18. R. Corneliussen and A. Peterlin, *Makromol. Chem.*, **105**, 192 (1967).
19. A. Peterlin and R. Corneliussen, *J. Polym. Sci. A-2*, **6**, 1273 (1968).
20. A. Peterlin and G. Meinel, *Makromol. Chem.*, **142**, 227 (1971).
21. A. Peterlin and F. J. Baltá-Calleja, *Kolloid Z. Z. Polym.*, **242**, 1092 (1971).

22. P. Cerra, D. R. Morrow, and J. A. Sauer, *J. Macromol. Sci. (Phys.), B*, **3**, 33 (1969).
23. M. Kojima, *J. Polym. Sci. A-2*, **5**, 597 (1967).
24. A. Peterlin and F. J. Baltá-Calleja, *J. Appl. Phys.*, **40**, 4238 (1969).
25. R. J. Samuels, *J. Polym. Sci. A-2*, **6**, 1101 (1968).
26. V. J. Armond and J. R. Atkinson, *J. Materials Sci.*, **4**, 509 (1969).
27. H. Čačković, W. Wilke and R. Hosemann, *Kolloid-Z. Z. Polym.*, **234**, 1000 (1969).
28. H. Khoury, *J. Res. Nat. Bur. Stand.*, **70A**, 29 (1966).
29. F. J. Baltá-Calleja and A. Peterlin, *Makromol. Chem.*, **141**, 91 (1971).
30. A. Peterlin and G. Meinel, *J. Polym. Sci. B*, **3**, 783 (1965).
31. A. Peterlin and G. Meinel, *J. Appl. Phys.*, **36**, 3028 (1965).
32. A. Peterlin and H. G. Olf, *J. Polym. Sci. A-2*, **4**, 587 (1966).
33. A. Peterlin, J. L. Williams, and V. Stannett, *J. Polym. Sci. A-2*, **5**, 957 (1967).

Received July 30, 1970
Revised November 12, 1970

JOURNAL OF POLYMER SCIENCE: PART A-2 VOL. 9, 917–926 (1971)

Effect of Water Sorption on the Dielectric Behavior of Calcium Chondroitin-4-Sulfate

LESLIE J. KAUFMAN and F. A. BETTELHEIM, *Department of Chemistry, Adelphi University, Garden City, New York 11530*

Synopsis

The dielectric properties of calcium chondroitin-4-sulfate were studied as a function of frequency, temperature, and water content. The dielectric constant changes very little with water content below "monolayer" coverage, and after that the dielectric constant follows the shape of the adsorption isotherm. The dielectric behavior is discussed as affected by interfacial polarization and by the increase in the rotational freedom of the polymer side chains.

Introduction

The dielectric constant and dielectric loss factor of many materials are greatly influenced by the sorption of water. An abrupt change in these properties sometimes occurs at a coverage associated with primary adsorption sites determined from the Brunauer-Emmett-Teller monolayer.[1] The system aluminum oxide–water, for example, exhibited a discontinuity which was attributed to the completion of a monolyaer.[2] Studies of sorbents, including alumina, porous silica, nonporous rutile, and porous glass,[2–6] have shown that, for the quantity of gas assumed to be adsorbed as a monolayer, there was only a very small dependence of dielectric constant on temperature.

A few studies published on the dielectric properties of swollen polymers such as polyamides[7] and keratin[8] indicated that even small water content modified the behavior of polymers. The dielectric properties of the dry polymer were altered so much by the presence of water molecules that the relaxation process was considered due to a water–polymer complex. On the other hand, in gels of hydrophilic polymers with high water content, the dielectric properties were largely due to the icelike behavior of the sorbed water molecules.[9]

Chondroitin-4-sulfate is one of the most abundant polyelectrolytes found in connective tissues. It is a polymer of (1 → 4)-O-β-D-glucopyranosyluronic acid-(1 → 3)-2-acetamido-2-deoxy-β-D-galactopyranose-4-sulfate.[10] In tissues such as cartilage, cornea, etc., chondroitin-4-sulfate is frequently in a tight matrix with protein. Some proteins are covalently linked to the polysaccharide; others, such as collagen, are in physical entanglement. Its mechanical and dielectric behavior is therefore of physiological importance.

The degree of hydration of chondroitin-4-sulfate varies in different tissues. The water sorptive capacity of chondroitin-4-sulfate has been studied in our laboratory[11] and the nature of water binding in the monolayer has been elucidated by infrared[12] and microwave[13] techniques. Matrices of connective tissues have an important physiological role as structural units as well as intercellular space through which metabolites pass from cell to cell. In order to describe the role of chondroitin-4-sulfate in connective tissue matrices, the knowledge of the degree of the mobility of the different polymer solvents at different degrees of hydration is desirable. Therefore, a study of the dielectric properties of calcium chondroitin-4-sulfate within the temperature range encountered in biological conditions was undertaken as a function of water uptake.

Experimental

Calcium chondroitin-4-sulfate isolated from bovine trachea has been described.[14] The same preparation has been used in previous studies.[11–13]

A pellet of calcium chrondroitin-4-sulfate was prepared by filling a die with finely powdered material, and while the die was connected to a mechanical forepump, compressing the powder by applying a pressure of 12,000 psi for approximately 20 min. The dimensions of the pellet were 1 in. × 0.1950 in.; the thickness was 0.0530 in. The pellet was placed on the lower electrode of a General Radio 1690-A dielectric sample holder enclosed in a modified bell jar that formed part of a vacuum system (Fig. 1). An alternating electric field was supplied by a Hewlett-Packard model 650A signal generator, and the measurements of dielectric constant were made with a General Radio 716 capacitance bridge. In order to maintain a constant temperature, the bell jar, which rests on a neoprene ring supported by a stainless steel plate, was enclosed in a water bath.

Readings of the capacitance and loss factors for the material were made by turning the calibrated upper dial of the dielectric sample holder until it made firm contact with the pellet; the thickness of the sample was thus measured directly, in thousandths of an inch.

After the capacitance and loss factor of the dry material had been determined, the sample was exposed to water vapor, at a pressure measured with a mercury manometer. It was assumed that equilibrium was reached when the pressure remained constant, and two consecutive sets of measurements (separated by at least 10 hr) indicated no change in dielectric behavior. In this manner, the dielectric constant and loss factor of the sample were determined for various water vapor pressures over the frequency range from 20 Hz to 1 MHz.

As part of the determination of the dielectric constant of the sample, the separation of the two plates of the dielectric sample holder that produced the minimum voltage through the voltmeter for a given setting of the capacitance bridge must be determined. Since removal of the sample from the holder and rebalancing the bridge after each measurement was not feasible, the bridge was balanced at a number of water vapor pressures

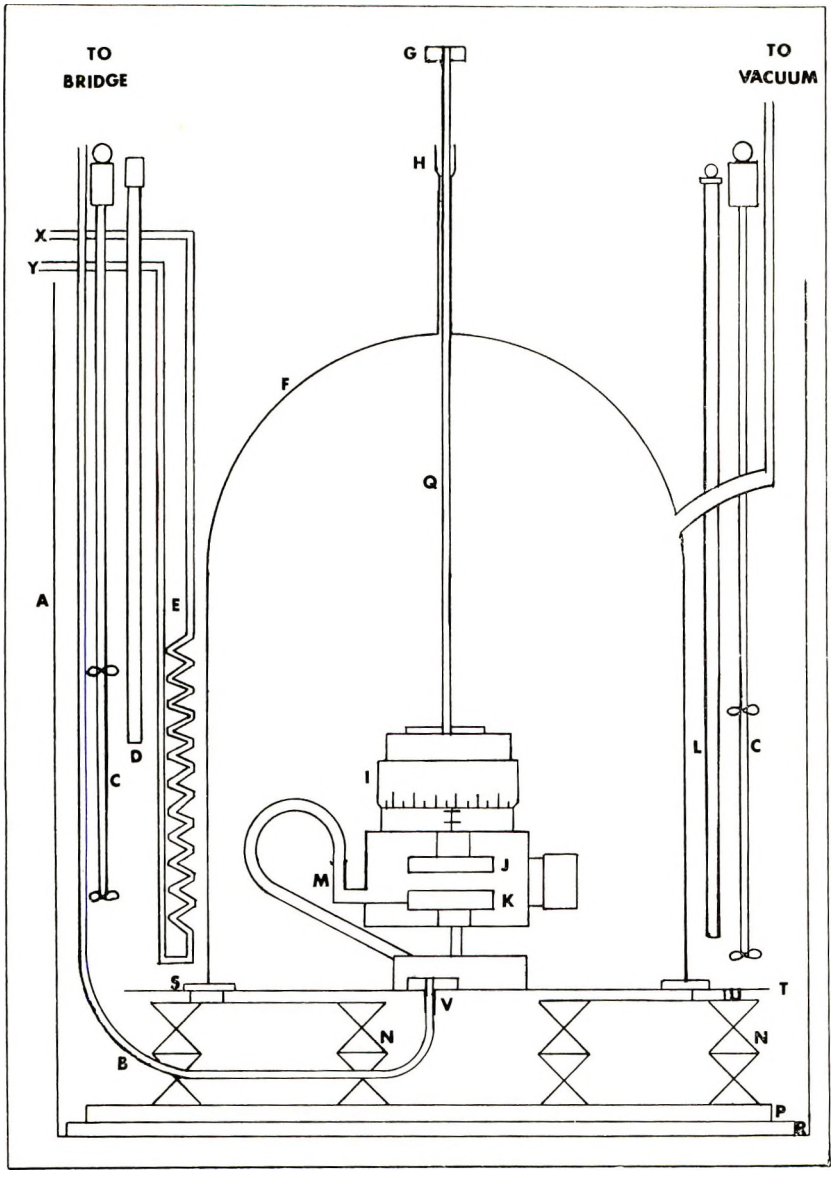

Fig. 1. Dielectric apparatus: (A) constant temperature bath; (B) General Radio CO 874 R20A cable (coaxial); (C) stirrers; (D) heater; (E) cooling coil; (F) bell jar; (G) handle; (H) mercury seal; (I) General Radio dielectric sample holder type 1690A; (J) upper electrode; (K) lower electrode; (L) thermoregulator; (M) General Radio coaxial ell; (N) jacks; (P) 1/4 in. rubber sheet; (Q) Teflon rod; (R) steel plate; (S) 1/8 in. Neoprene sheet; (T) stainless steel plate; (U) feet of stainless steel plate; (V) Amphenol 82-201 hermetic feed-through connector; (X) to tap water; (Y) to drain.

with no solid sample between the plates and for a number of settings of the capacitance dial at several frequencies.

The measured capacitance is found to vary linearly with the reciprocal of the separation of the plates at a given frequency and water vapor pressure. As the water vapor pressure is increased, the slope of this line remains constant but its intercept is shifted to more negative values.

Results

The first observation of importance was that the dielectric constant of the dry chondroitin-4-sulfate remains almost unchanged over the entire frequency range from 20 Hz to 1 MHz, at each of the temperatures studied.

As water is sorbed, the dielectric constant shows almost no increase for equilibrium water vapor pressures of 3 torr or less at each of the temperatures investigated: 20, 27, and 35°C. At these pressures, which are at or below those required to achieve coverage of all primary sorption sites ("monolayer coverage"), the dielectric loss factor showed only a very small rise for any of the frequencies covered.

In general, as the pressure is increased beyond that associated with the monolayer coverage, the dielectric constant at a given frequency is observed to rise. The amount of the increase is largest for the lowest fre-

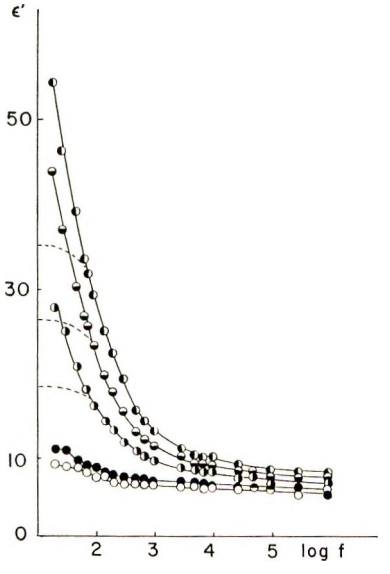

Fig. 2. Dielectric dispersion of calcium chondroitin-4-sulfate-water system: (◑) at 143 mg H_2O/g polymer water uptake (P = 9.1 torr, P/P_0 = 0.52, 20°C); (◒) at 152 mg H_2O/g polymer water uptake (P = 10.5 torr, P/P_0 = 0.60, 20°C), (◐) at 174 mg H_2O/g polymer water uptake (P = 11.8 torr, P/P_0 = 0.67, 20°C); (○) at 143 mg H_2O/g polymer water uptake (P = 11.25 torr, P/P_0 = 0.27, 35°C); (●) at 174 mg H_2O/g polymer water uptake (P = 14.80, P/P_0 = 0.35, 35°C). The broken lines indicate the dielectric dispersions after corrections have been made for electrode polarization.

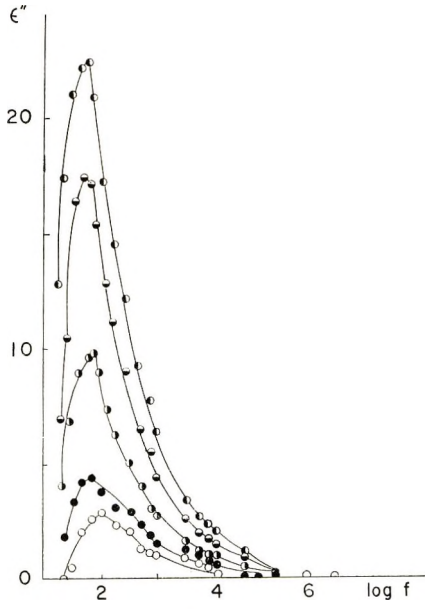

Fig. 3. Dielectric loss factor against frequency for the calcium chondroitin-4-sulfate-water system: (◑) at 143 mg H_2O/g polymer water uptake (P = 9.1 torr, P/P_0 = 0.52, 20°C); (◒) at 152 mg H_2O/g polymer water uptake (P = 10.5 torr, P/P_0 = 0.60, 20°C); (◐) at 174 mg H_2O/g polymer water uptake (P = 11.8 torr, P/P_0 = 0.67, 20°C), (○) at 143 mg H_2O/g polymer water uptake (P = 11.25 torr, P/P_0 = 0.27, 35°C); (●) 174 mg H_2O/g polymer water uptake (P = 14.80 torr, P/P_0 = 0.35, 35°C).

quency and smallest for the highest frequency at each pressure. Thus, dielectric dispersion is observed, with the dielectric constant showing a monotonic decrease as the frequency is increased at a constant pressure (Fig. 2). Part of the increase in dielectric constant with decrease in frequency is due to electrode polarization; especially at low frequencies, almost the total increase is due to this effect. Corrections were made according to the method of Takashima and Schwan,[15] and the values of the dielectric constant after corrections are indicated by the broken lines. In Figure 3 the dielectric loss is given as a function of frequency for several values of water uptake. For the purpose of comparison, in both Figures 2 and 3 the dielectric properties are also given at 20°C and 35°C for identical water uptake.

The shapes of water vapor desportion curves of dielectric constant and dielectric loss factor versus frequency are qualitatively similar to those of the sorption isotherms. In Figure 4 the dielectric constant and dielectric loss factor are plotted against vapor pressure; all measurements were taken at 100 Hz and 35°C. For two reasons, the dielectric constant at 100 Hz is given rather than the static dielectric constant ϵ_0'. (1) The corrections made for electrode polarization at low frequencies[15] are approximate, so the ϵ_0' obtained from the Cole-Cole plot may be in error by as much as 20%. (2) The experimental values at 100 Hz (after correction) may have

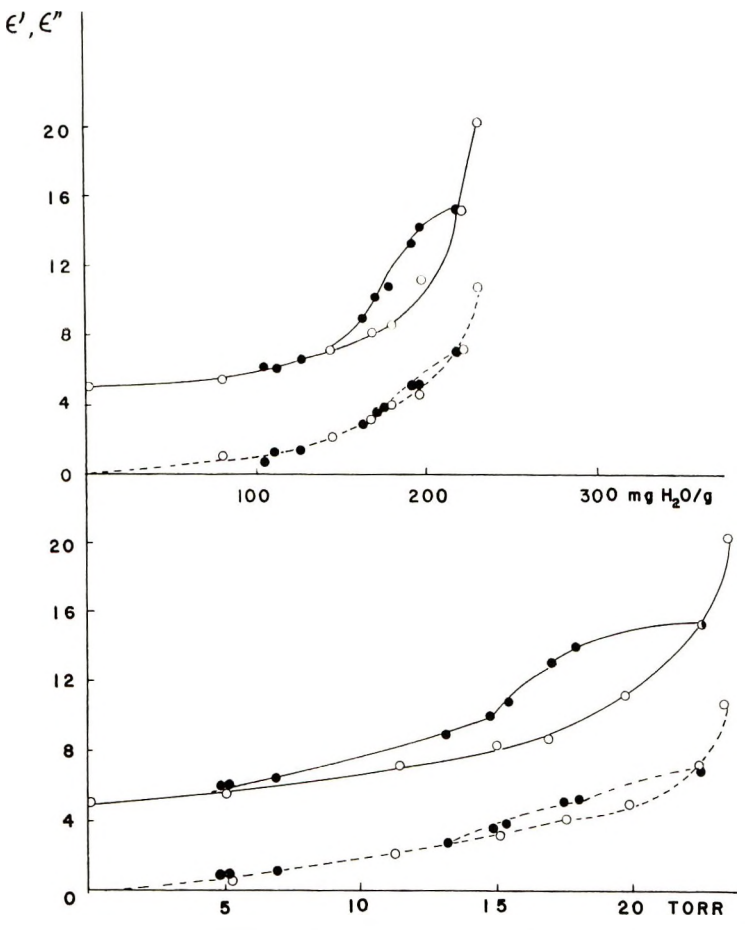

Fig. 4. Plots of (——) dielectric constant and (- -) dielectric loss as a function of equilibrium water vapor pressure and water uptake: (○) sorption branch; (●) desorption branch of the isotherm. The frequency of the measurement was 100 Hz at 35°C.

an estimated error not higher than 5%, and they are relatively close to the calculated ϵ_0' values. Thus the overall shape of the curve is the same for ϵ' at 100 Hz as for ϵ_0'. Both dielectric constant and dielectric loss exhibit a hysteresis regardless of whether they are plotted against vapor pressure or water uptake. The width of the hysteresis loop, however, is considerably narrower for the loss factor than for the dielectric constant.

A comparison of the dielectric behavior at the three temperatures investigated indicates that at constant water content the dielectric constant increased as the temperature was lowered (Fig. 5). For all sorbed water contents up to the highest one attained at 20°C (approximately 172 mg water/g polymer), the dielectric constant and loss factor were higher at 20°C than for the other two temperatures. The same general behavior was observed even at higher water uptakes, where only the 27°C and 35°C isotherms could be compared.

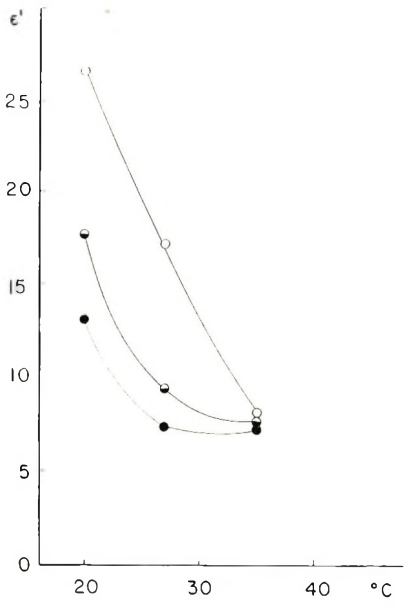

Fig. 5. Dielectric constant at 100 Hz of calcium chondroitin-4-sulfate-water system as a function of temperature at constant water content: (○) 165 mg H_2O/g polymer; (◒) 145 mg H_2O/g polymer; (●) 135 mg H_2O/g polymer.

In Figure 5 the dielectric constant at 100 Hz is given rather than the static dielectric constant for the reason stated above. The data in Figure 5 were obtained by combining graphs such as those presented in Figure 4 with the sorption isotherms.

Discussion

Partially as a result of the restricted rotation around the glycosidic bond between the pyranose rings in calcium chondroitin-4-sulfate, the amount of backbone motion to be expected in the dry state is considerably reduced in comparison to that to be found in other linear polymers. The possible crosslinks between molecules arising from Ca^{++} ions acting as intermolecular and intramolecular bridges between $—COO^-$ and $—OSO_3^-$ groups and from hydrogen bonds would produce a fairly rigid matrix in the dry state of the polymer. The results obtained for the dielectric constant and loss factor after the removal of water are in accord with this model of the dry polymer and substantiate the data obtained in infrared spectroscopy.[12]

The first signs of increase in the dielectric constant and dielectric loss factor occur after a monolayer coverage calculated from the Brunauer-Emmett-Teller[1] treatment of the sorption isotherm has been achieved. Similar results have been observed by Takashima[16] on ovalbumin crystals. The monolayer concept in sorbents with heterogeneous sorption sites simply means a water uptake sufficient to cover the primary polar sites with one molecule of water on each site. Even after this water uptake, the

motion of the side chains and polymer segments is greatly hindered by the frequent crosslinks in the matrix.

The results indicate that the measured dielectric constant is considerably greater than that of water alone for the low frequencies of measurement. The contribution of the dry polymer to the dielectric constant of the water–polymer matrix is small.

As has been observed with other polymers,[7] the dielectric behavior is a complex phenomenon. Two explanations are possible. (1) The dielectric relaxation is simply the sum of individual components—namely, the polymer, the water, and the counterions of the polyelectrolyte. If this is the case, the presence of the polymer should slow down the orientation of the water molecule in the applied electric field. Then the only explanation for a dielectric constant higher than that of water can be in the presence of conducting layers. The conduction may raise from two effects: (a) movement of the counterions of the polyelectrolyte will contribute to the dielectric properties[17] and (b) the water itself may be in an ordered state contributing to the dielectric absorption of the gel.[9] (2) The dielectric relaxation is a property of the polymer–water complex. The fact that the temperature dependence of the dielectric constant at constant water uptake (Fig. 5) shows a negative enthalpy of activation may indicate that the water chondroitin-4-sulfate forms a complex, the structure of which is temperature-dependent. This was also implied in the microwave absorption data,[13] where the relaxation time of the sorbed water was similar to the relaxation time of the liquid water even below monolayer coverage. Thus this second possibility (i.e., water polymer–complex) proposed for the explanation of high dielectric constant may be of equal validity.

The dielectric hysteresis observed, with the desorption points having higher dielectric constants than the corresponding adsorption ones, is somewhat similar to that observed by Nair and Thorp[18] in the sorption of water by silica gels. One conclusion reached by these authors was that dielectric hysteresis did not depend on the porous nature of the adsorbent so that the presence of capillaries in which condensation of water could occur was not the determining factor. Rather, they attributed the phenomenon to the presence of ionic species which led to interfacial polarization so that, in addition to atomic and electronic polarization, ionic polarization could contribute to the observed dielectric constant.

Since calcium chrondroitin-4-sulfate is a polyelectrolyte, the calcium ons could dissolve in the condensed water layers to form an electrolytic olution and hence give rise to hysteresis in a somewhat similar manner.

In addition to effects attributable to interfacial polarization, the dielectric constant and loss factor may reflect molecular motions. Thus, part of the observed dielectric constant and loss factor may result from motions of side-chain units and backbone segments which become possible after the hydrogen bonds are broken and intermolecular and intramolecular forces that restrict the mobility of these groups are overcome as a result of swelling caused by water sorption.

TABLE I
Approximate Relaxation Times at Different Water Contents

T, °C	Coverage, mg H_2O/g polymer	Relaxation time, sec $\times 10^3$
20	122	72
	140	58
	172	48
27	167	60
	220	16
35	199	72
	232	29
	240	26

Since excessive electrode polarization occurs at low frequencies and at high water content, the low frequency limit of the dielectric constant ϵ_0 obtained by extrapolation may be in error as much as 20%.[15] Hence, the values of the relaxation times calculated from Cole-Cole plots and by using such ϵ_0 values are, at best, only approximate (Table I).

Within these limitations, it appears that as the coverage is increased at constant temperature the relaxation time decreases. This result indicates that more freedom of motion is possible at higher coverages, leading to a faster rate of relaxation. If sorption allows groups which were previously unable to orient in response to the applied field to do so, the number of possible relaxation phenomena that could occur simultaneously would be increased. Thus, the dielectric properties of swollen calcium chrondroitin-4-sulfate are the result of the different hindered rotational motions of the side chain groups such as $-SO_3^-$, $-COO^-$ and $HN-\overset{\overset{O}{\parallel}}{C}-CH_3$, as well as of the backbone of the polymer, in addition to the conductance due to ordered water structures around the surface polar sites and effects due to interfacial polarization. These multiple effects cannot be separated easily, although a qualitative attempt can be made. The first observation, that the dielectric constant does not change with increasing water content until a monolyaer coverage is reached, seems to be common to hydrophilic polymers.[9,16,19] Beyond the monolayer, ordered water structures may give rise to an increase in dielectric constant, since the water in the hydration shell around the polar sites may be sufficiently close to cause dielectric polarizability due to proton jumps in the hydrogen-bonded structure. In contrast to ovalbumin,[16] where the dielectric constant leveled off at high water content, in the case of calcium chondroitin-4-sulfate the dielectric behavior follows the shape of the isotherm above the monolyaer uptake. This difference may be explained by the fact that, being a globular protein, the ovalbumin probably experiences little intramolecular swelling with no appreciable gain in the freedom of side chains or polypeptide backbone, while in the case of a linear amorphous polymer matrix the swelling may introduce an increase in the freedom of side-chain rotation and backbone

segmental undulation. The relaxation times indicate that, even at a relatively high degree of swelling, the polymer–water system is a tight matrix with little freedom of motion.

This research was supported in part by a USPHS grant from the National Institute of Health, EY-00501-01.

References

1. S. Brunauer, P. H. Emmett, and E. Teller, *J. Amer. Chem. Soc.*, **60**, 309 (1938).
2. G. Egbert and G. Langhammer, *Kolloid. Z.*, **174**, 5 (1961).
3. M. H. Waldman, J. A. Snelgrove, and R. L. McIntosh, *Can. J. Chem.*, **31**, 998 (1953).
4. J. A. Snelgrove, H. Greenspan, and R. L. McIntosh, *Can. J. Chem.*, **31**, 84 (1953).
5. S. E. Petrie and R. L. McIntosh, *Can. J. Chem.*, **44**, 1153 (1966).
6. G. Ebert, *Kolloid-Z.*, **206**, 44 (1965).
7. A. J. Curtis, *J. Res. Nat. Bur. Stand.*, **65A**, 185 (1961).
8. J. E. Algie, *Kolloid-Z.*, **223**, 13 (1968).
9. M. Masuzawa and C. Sterling, *Biopolymers*, **6**, 1453 (1968).
10. M. L. Wolfram and B. O. Juliano, *J. Amer. Chem. Soc.*, **82**, 1673 (1960); *ibid.*, **82**, 2588 (1960).
11. F. A. Bettelheim and S. H. Ehrlich, *J. Phys. Chem.*, **67**, 1948 (1963).
12. S. H. Ehrlich and F. A. Bettelheim, *J. Phys. Chem.*, **67**, 1954 (1963).
13. I. Lubezky, F. A. Bettelheim, and M. Folman, *Trans. Faraday Soc.*, **63**, 1794 (1967).
14. F. A. Bettelheim and D. E. Philpott, *Nature*, **188**, 654 (1960).
15. S. Takashima and H. P. Schwan, *J. Phys. Chem.*, **69**, 4176 (1965).
16. S. Takashima, *J. Polym. Sci.*, **62**, 233 (1962).
17. C. T. O'Konski, *J. Phys. Chem.*, **64**, 605 (1960).
18. N. K. Nair and J. M. Thorp, *Trans. Faraday Soc.*, **61**, 962 and 975 (1965).
19. D. Rosen, *Trans. Faraday Soc.*, **59**, 489, 2178 (1963).

Received May 7, 1970
Revised December 21, 1970

JOURNAL OF POLYMER SCIENCE: PART A-2 VOL. 9, 927–937 (1971)

Stress-Optical Coefficients of Swollen Polymer Networks

A. N. GENT* and T. H. KUAN, *Institute of Polymer Science, The University of Akron, Akron, Ohio 44304*

Synopsis

Stress-optical coefficients have been determined for crosslinked samples of polyethylen (PE) and polystyrene (PS) at high temperatures, i.e., in the rubberlike state, and when swollen in a variety of liquids. For PE, swelling liquids with long straight molecules gave large values of optical anisotropy whereas liquids with more symmetrical molecules gave minimum values, as found previously for *cis*- polyisoprene and *trans*-polyisoprene. This solvent effect is attributed to short-range orientational order in molecularly asymmetric media. Sizes of the equivalent random link for unperturbed molecules of these three polymers were deduced from the minimum values of optical anisotropy. Measures of shape asymmetry were also obtained by matching the optical anisotropy of samples when unswollen with that observed when swollen with a liquid of known molecular asymmetry. Reasonable agreement was found to hold between the two methods. In contrast, the optical anisotropy of swollen PS was found to be substantially independent of the swelling liquid. The apparent absence of a molecular ordering effect in this case is attributed to the bulky nature of the PS molecule. A marked reduction in optical anisotropy on swelling is ascribed to increased phenyl group motion.

INTRODUCTION

It has recently been shown that the stress-optical coefficients of swollen networks of *cis*-1,4-polyisoprene and *trans*-1,4-polyisoprene depend strongly upon the geometrical asymmetry of the solvent molecule.[1] Solvents with long straight molecules gave large values of the stress-optical coefficient whereas those with compact symmetrical molecules gave minimum values. This effect was attributed to short-range orientational order due to packing requirements in a condensed molecularly asymmetric medium, as proposed by Frisman et al.[2,3] and Nagai.[4] Measurements have now been made on swollen networks of polyethylene and polystyrene in a similar way, at sufficiently high temperatures that they were also rubbery materials. The results are given below.

The stress-optical coefficient C is defined as the ratio of the difference Δn in principal refractive indices to the difference Δt in the corresponding true stresses. For a model network of long flexible molecular chains, each

* Visiting Professor, Queen Mary College (University of London), 1969–70.

one composed of a large number of rigid freely jointed links, C is related to the optical anisotropy α of a single link,

$$C = (2\pi/45\ kT)[(\bar{n}^2 + 2)^2/\bar{n}]\alpha \quad (1)$$

where k is Boltzmann's constant, T is the absolute temperature, and $\bar{n}$ is the mean refractive index.[5] The same relation is obtained for a swollen network, because Δn and Δt are predicted to change by the same factor on swelling (provided that the swelling liquid has the same refractive index as the polymer).[5]

The present measurements of stress-optical coefficient are reported and discussed in terms of α, i.e., the difference in polarizability in the chain direction and at right angles to it for a single hypothetical freely jointed link. Values of α are calculated from the experimentally determined stress-optical coefficients C by means of eq. (1). The value obtained for α, relative to the optical anisotropy β of a chain structural unit, gives a rough indication of the number of structural units equivalent to one freely jointed link and hence of the stiffness of the real chain. This measure of molecular stiffness is not accurate, unfortunately, because the optical and elastic properties of real molecular chains are not fully accounted for by model freely jointed chains.[6] They are better described by the more realistic model of a polymer molecule in which limited numbers of isomeric rotational states about carbon–carbon single bonds are permitted, with specified energy differences between different sequences of bond conformations.[7–17] However, the main purpose of the present work is to draw attention to solvent effects which are not easily included in either model. The equivalent chain of freely jointed links is retained for simplicity, and because experimental results have usually been presented in this way before.

EXPERIMENTAL

Thin sheets of crosslinked polymer were prepared as follows.

Polyethylene

A slurry was made by mixing a solution of dicumyl peroxide in benzene with powdered polyethylene of high molecular weight (ca. 10^6), RCH 1000 lot 469 (supplied by the Goodrich Gulf Chemical Company) so that the slurry contained about 2 g of dicumyl peroxide per 100 g of polymer. It was held at 40°C for about 6 hr to allow the benzene to evaporate and then pressed into a thin sheet about 0.1 cm thick, in a hot-molding operation. Crosslinking was effected by heating the molded sheet for 1 hr at 155°C, i.e., above the melting temperature of polyethylene. It is assumed, therefore, that the molecular chains were in relatively random configurations at the time of crosslinking. An antioxidant (Antioxidant 2246, American Cyanamid Company) was added to the crosslinked sheets by swelling them with a 0.5% solution in hot xylene for 15 min and then allowing the xylene

to evaporate. The same antioxidant was also added to the swelling liquids used in the stress-optical studies.

Polystyrene

Distilled styrene monomer was mixed with 5% divinyl benzene and 0.1% cumene hydroperoxide. The mixture was then floated on mercury under a nitrogen atmosphere and subjected to the following heating schedule to effect polymerization: 3 days at 50°C, 2 days at 60°C, and 2 days at 70°C.

Measurements of the stress-optical coefficients were made in the same way as before.[1,18] Testpieces were cut from the crosslinked sheets in the form of parallel-sided strips about 3 cm long and 0.6 cm wide. They were suspended vertically in a thermostatted cylinder containing air for measurements in the unswollen state and containing a swelling liquid for measurements in the swollen state. They were allowed to swell to equilibrium in the latter case before the measurements were carried out. The swollen width and thickness were calculated from the original dimensions of the testpiece and the measured linear swelling ratio λ_s in the length direction; i.e., isotropic swelling was assumed. As the measurements were carried out quite rapidly, being completed in about 15 min, any increase in swelling with extension was minimized. Measurements at increasing and decreasing tensile loads were found to agree satisfactorily, indicating that such swelling changes were insignificant.

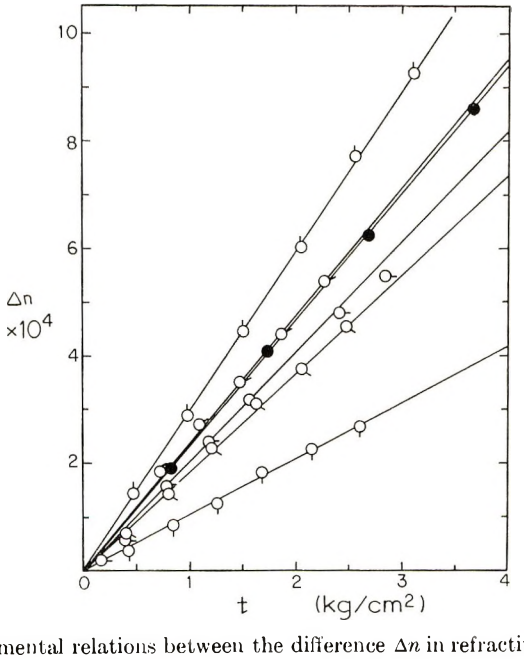

Fig. 1. Experimental relations between the difference Δn in refractive indices parallel and perpendicular to the direction of stress and the tensile stress t for a crosslinked polyethylene sample, (●) unswollen and swollen in various liquids: (♁) biphenyl; (♂) *p*-dichlorobenzene; (○) *p*-xylene; (♌) tetralin; (♀) decalin.

TABLE I
Stress-Optical Coefficients C and Optical Anisotropies α for Swollen Materials

Polymer	Swelling liquid	R	n	Q	$C \times 10^4$, cm²/kg	$\alpha \times 10^{24}$, cm³
Crosslinked polyethylene (150°C)	Decalin	1.55	1.440	2.8	1.08	4.00
	Tetraisobutylene	—	1.415	2.3	1.45	5.40
	Tetralin	1.65	1.500	2.8	1.85	6.65
	p-Xylene	2.65	1.450	2.4	1.95	6.85
	Dibenzyl ether	2.9 ± 0.5	1.520	1.7	2.00	7.20
	p-Dichloro-benzene	3.15	1.500	2.7	2.40	8.65
	None	—	1.440	1	2.35	8.65
	Biphenyl	3.5 ± 1	1.560	2.1	3.00	10.6
Crosslinked polystyrene (125°C)	None	—	1.555	1	−4.00	−12.7
	Di-*p*-tolyl carbonate	2.3	1.495	3.3	−3.00	−9.7
	p-Xylene	2.65	1.465	7.7	−2.80	−9.55
	p-Dichlorobenzene	3.15	1.508	4.8	−2.75	−8.9
	Tetralin	1.65	1.508	5.0	−2.55	−8.35
	Decalin	1.55	1.446	4.0	−2.35	−8.0
	Dibenzyl ether	2.9 ± 0.5	1.520	3.3	−2.35	−7.55
	Biphenyl	3.5 ± 1.0	1.569	3.7	−2.05	−6.5
Crosslinked *cis*-polyisoprene (30°C)	Dibenzyl ether	2.9 ± 0.5	1.562	2.5	1.85	4.45
Crosslinked *trans*-polyisoprene (30°C)	Tetraisobutylene	—	1.447	4.0	2.40	6.15
	Dibenzyl ether	2.9 ± 0.5	1.562	4.5	3.62	8.70

The testpieces were stretched by weights applied by means of a pulley arrangement. The true tensile stress t was computed from the applied weight and the cross-sectional area in the stretched state, calculated from the unstretched value assuming no change in volume. The extension was measured with a cathetometer. Only small extensions, of the order of 10%, were imposed because the swollen materials were extremely weak.

The difference Δn in the refractive indices in the direction of extension and perpendicular to it was determined as described by Treloar,[5] by using a beam of sodium light polarized at 45° to the direction of extension and a Babinet compensator. A direct proportionality between Δn and t was found in all cases. Some typical results for the polyethylene material are shown in Figure 1. Experimental values of the stress-optical coefficient C were obtained from the slope of such relations at a temperature at 150°C for polyethylene and 125°C for polystyrene. The refractive indices of these polymers were taken as 1.438 and 1.555, respectively. Values of refractive index n for the swelling liquids were measured or taken from the literature and adjusted to the test temperature T by using the approximate relation

$$(n - 1)_{T_0} = (n - 1)_T[1 + \gamma(T - T_0)]$$

where T_0 represents the temperature of measurement and γ is the coefficient of volume expansion, taken as 6.7×10^{-4} deg^{-1}. Values obtained in this way are given in Table I.

The mean refractive index $\bar{n}$ of the swollen materials was calculated as a simple volume average of the refractive indices of the swelling liquid and polymer by using the volume swelling ratio Q, i.e., the ratio of the swollen to the unswollen volume of the polymer. Values of Q were calculated from the linear swelling ratios λ_s, obtained from length measurements in the swollen and unswollen state, for each swelling liquid. They are also given in Table I.

RESULTS AND DISCUSSION

Experimentally determined values of the stress-optical coefficient C and values of the link anisotropy α calculated from them by means of eq. (1) are given in Table I for swollen and unswollen samples of polyethylene and polystyrene. Some new results for swollen samples of *cis* and *trans*-polyisoprene are included in Table I. The results are arranged in order of increasing values of α.

Cis-Polyisoprene, *Trans*-Polyisoprene and Polyethylene

A particularly wide range of values of α (2.5:1) was obtained for polyethylene swollen in various liquids. Those swelling liquids with greater asymmetry of molecular shape gave larger values for α whereas those with compact symmetrical molecules gave low values. A similar effect was noted before for crosslinked samples of *cis*- and *trans*-polyisoprene[1] and

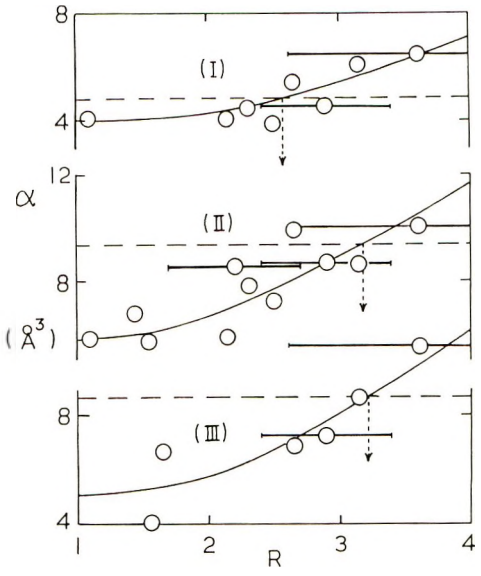

Fig. 2. Optical anisotropy α of swollen polymers vs. molecular asymmetry ratio R of the swelling liquid: (I) *cis*-polyisoprene (30°C); (II) *trans*-polyisoprene (30°C); (III) polyethylene (150°C). The horizontal broken lines denote the values of α for the unswollen polymers.

attributed to packing effects in a molecularly asymmetric medium as proposed by Frisman et al.[2,3] and Nagai.[4]

In order to make a quantitative comparison, estimates of molecular asymmetry for the various swelling liquids were obtained from space-filling molecular models (Catalin Ltd., London, scale 1 cm = 1 Å). The ratio R of the overall length of the molecule to its minimum lateral dimension was chosen as a convenient measure of asymmetry; values obtained from the molecular models are given in Table I. In some cases the result depended strongly upon the conformation chosen for the liquid molecule. Corresponding ranges for R were estimated in these cases and are indicated in Table I.

The experimental values obtained for the optical anisotropy α of a freely jointed link are plotted in Figure 2 against the molecular asymmetry ratio R for the swelling liquid. Horizontal bars represent the approximate range of possible values for R when the swelling liquid has different possible conformations. Previous results for *cis*-polyisoprene (I) and *trans*-polyisoprene (II) and the new results given in Table I are included in Figure 2 for comparison with the present results for polyethylene (III). Horizontal broken lines represent the values of α obtained for the unswollen materials.

For all three materials the value of α increased with increasing molecular asymmetry of the swelling liquid (Fig. 2). By extrapolation to the isotropic case, $R = 1$, values of α may be obtained which are assumed to reflect the properties of isolated molecules, i.e., in an optically and geometrically neutral environment. By comparing this extrapolated value

with the calculated optical anisotropy β of a chain structural unit, we may deduce the number of structural units per equivalent random link and hence the number of carbon–carbon single bonds in the chain backbone corresponding to one random link. Values obtained in this way are 1.25 isoprene units (3.8 carbon–carbon single bonds) for *cis*-polyisoprene, 1.8 isoprene units (5.4 carbon–carbon single bonds) for *trans*-polyisoprene, and 6.2 CH_2 units (6.2 carbon–carbon single bonds) for polyethylene, with Denbigh's values of bond polarizabilities[19] to compute the optical anisotropies β of the structural units. Thus, all three polymers are relatively flexible, but *cis*-polyisoprene appears to be significantly more so than the others.

Ishikawa and Nagai[12,13] consider that the values of bond polarizability obtained by Clément and Bothorel[20,21] are superior to those of Denbigh for the following reasons: (1) they were obtained by using hydrocarbon liquids and are therefore more appropriate for rubbery polymers; (2) they are probably more accurate; (3) better agreement is obtained between theoretical and experimental values of the stress-optical coefficients for *cis*- and *trans*-1,4 polybutadiene and *cis*- and *trans*-1,4 polyisoprene if these values of bond polarizability are used.

When Clément and Bothorel's bond polarizabilities are used to compute the optical anisotropies β of the present polymer structural units, the number of carbon–carbon single bonds in the chain backbone corresponding to one random link becomes 3.0 for *cis*-polyisoprene, 4.9 for *trans*-polyisoprene, and 9.1 for polyethylene for the same extrapolated values of α as before. Thus, although the numerical results are somewhat altered, the although the numerical results are somewhat altered, the same general conclusions are reached with these alternative values of bond polarizability.

There are two other indications of relative flexibility which can be deduced from the results shown in Figure 2. First, relatively flexible chains would be expected to constitute a relatively isotropic environment for each other in the condensed unswollen state. The optical anisotropy α for the unswollen material would therefore be expected to be close to that for unperturbed chains. In contrast, less flexible chains with longer equivalent freely jointed links would be expected to suffer greater packing difficulties and hence be self-constrained to a greater degree in the unswollen state in the same way that an asymmetric swelling liquid has been inferred to constrain polymer molecules and increase their effective rigidity. In accord with these expectations the optical anisotropy of unswollen *cis*-polyisoprene is increased over the value in the presence of a symmetrical swelling agent to a much smaller degree than for *trans*-polyisoprene and polyethylene (Fig. 2), indicating that it does not constitute such a strongly asymmetric medium as the latter two polymers.

Similar conclusions have been reached by Ishikawa and Nagai[13] from a study of the effect of solvents on the stress-optical coefficients of *cis*- and *trans*-polybutadiene and *cis*- and *trans*-polyisoprene. This work was drawn to our attention after our measurements were completed; there is close agreement both in the quantitative results and in the interpretation

placed upon them. (Ishikawa and Nagai have also made absolute calculations of the stress-optical coefficients and their dependence on temperature using rotational-isomeric model chains, and have drawn quantitative comparisons between theory and experiment for unperturbed chains, i.e., when swollen by isotropic liquids.)

The effect of asymmetry of the polymer molecules themselves may be treated in a semiquantitative way, as follows. The degree of geometrical asymmetry R of a solvent molecule which raises the optical anisotropy of the swollen polymer to the same level as in the unswollen state can be regarded as roughly equivalent to the asymmetry of the freely-jointed link in the unswollen state. Those values of R at which the swollen polymer has the same optical anisotropy as the unswollen polymer are represented by vertical arrows in Figure 2; they are about 2.6 for *cis*-polyisoprene and 3.2 for *trans*-polyisoprene and polyethylene. These ratios correspond to segments of the extended polymer chain containing 1.8 isoprene units, 2.2 isoprene units, and 9 CH_2 units, respectively, and are in reasonably satisfactory agreement with lengths of the freely jointed link deduced above from values of the optical anisotropy in the unperturbed state.

A second indication of relative flexibility is provided by the constraining influence of swelling liquids with highly asymmetric molecules. Such liquids would be expected to have less effect on highly flexible polymer molecules because packing difficulties are small in these cases anyway. In accordance with this expectation, the optical anisotropy for *cis*-polyisoprene rises less rapidly with the solvent asymmetry ratio R than the optical anisotropy of the other two polymers (Fig. 2).

There are thus a number of independent observations which suggest that the *cis*-polyisoprene molecule is more flexible than the *trans*-polyisoprene molecule, and that the latter is more flexible than the polyethylene molecule. This conclusion differs slightly from that reached earlier when the general effect of swelling liquids was not appreciated.[9] It should also be noted that allowance has not been made in these comparisons for the different temperatures of observation.

Polystyrene

Quite different results were obtained for the optical anisotropy α of crosslinked polystyrene swollen with different liquids (Fig. 3). First, no clear dependence of α upon the asymmetry of shape of the solvent molecule could be discerned. The results have been treated as independent of the asymmetry ratio R in Figure 3, an average value of about -8.5×10^{-24} cm^3 being assumed to apply irrespective of the swelling liquid, as represented by the horizontal line. There is some slight indication of a reduction in α (towards zero) at high degrees of asymmetry, but this is not regarded as significant. There is certainly no indication that the optical anisotropy becomes increasingly negative at high degrees of asymmetry, as would be expected if the swelling liquid enhanced the intrinsic anisotropy of the polymer in the same way as for *cis* and *trans*-polyisoprene and polyethylene.

The reason for this absence of an effect is probably the bulky nature of the polystyrene chain. The phenyl sidegroups increase the effective cross-sectional area of the polymer molecule and probably prevent relatively small molecules, even if highly asymmetric in shape, from having a significant influence on the chain conformation.

Secondly, all the swelling liquids make the optical anisotropy considerably smaller, i.e., less negative, compared to the value obtained for the unswollen material. At first sight, this can be attributed to the same cause as the equivalent observation for the previous polymers swollen by isotropic liquids; namely, an increase in effective flexibility of the polymer chain brought about by removing packing restraints which are present in the condensed unswollen state. Although the result is substantially the

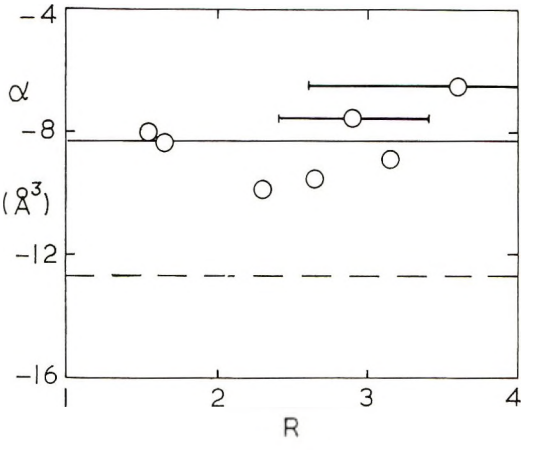

Fig. 3. Optical anisotropy α of a swollen polystyrene sample at 125°C vs. molecular asymmetry ratio R of the swelling liquid. The horizontal broken line denotes the value of α for the unswollen material.

same, a somewhat more complex and more specific mechanism of increasing chain flexibility is considered to be operative in the present case.

The optical anisotropy of polystyrene largely resides in the phenyl sidegroup, which can in principle be oriented independently of the main chain, although in practice a high degree of steric hindrance probably makes the plane of the phenyl ring lie mainly at right angles to the chain axis. The optical anisotropy is therefore not a good measure of main-chain conformation for polystyrene, or other polymers with independent sidegroup activity. The present observation can in fact be interpreted solely in terms of a sidegroup effect. It has previously been proposed that the phenyl rings in neighboring chains associate in a loose parallel arrangement in the bulk state.[22] This cooperative association apparently disappears at a temperature of about 160°C. Such an association would also be lost in the highly swollen state, and the observed reduction in optical anistropy on swelling may well reflect this loss in local order.

CONCLUSIONS

The following conclusions are obtained.

(1) The stress-optical coefficients of *cis*- and *trans*-polyisoprene and polyethylene networks are reduced by swelling them with liquids having roughly spherical molecules but are increased by swelling them with liquids having rod-like molecules. This effect is attributed to variations in conformational freedom of the polymer molecules. Packing effects with rodlike solvent molecules constrain the polymer molecules and make them appear stiffer. Similarly, segments of neighboring polymer molecules constrain each other in the unswollen state. The unperturbed conformation is approached only when the polymer is swollen by a liquid with roughly spherical molecules.

(2) Estimates of molecular flexibility in the isolated state have been obtained from the minimum values of optical anisotropy, i.e., with networks swollen with isotropic swelling liquids. The values obtained for the size of the equivalent freely-jointed link in this way are: 1–1.25 and 1.6–1.8 isoprene units for *cis*- and *trans*-polyisoprene respectively, and 6–9 CH_2 units for polyethylene.

(3) These estimates of molecular flexibility are corroborated by a second method. The optical anisotropy of an unswollen polymer can be matched by that of a swollen version, provided that a swelling liquid of suitable molecular asymmetry is employed. It is assumed that this degree of asymmetry is also characteristic of the polymer molecule, and reflects the size of its equivalent freely jointed link in the unswollen state.

(4) The (negative) stress-optical coefficient of a swollen polystyrene network is reduced by about one-third in comparison with the unswollen state, but the effect is largely independent of the degree of asymmetry of the solvent molecules. This reduction is tentatively ascribed to an enhanced freedom of motion of the phenyl sidegroups in the diluted state. The absence of a packing effect with rodlike solvent molecules in this case is attributed to the much larger cross-section of the polystyrene molecule and the difficulty of significantly constraining it with relatively small molecules.

This work formed part of a program of research on the mechanics of polymeric materials supported by the Air Force Materials Laboratory, Wright-Patterson Air Force Base, Ohio, under Contract F 33615-67-C-1393.

References

1. A. N. Gent, *Macromolecules*, **2**, 262 (1969).
2. E. V. Frisman, A. K. Dadivanyan, and G. A. Dyuzhev, *Dokl. Akad. Nauk SSSR*, **153**, 1062 (1963).
3. E. V. Frisman and A. K. Dadivanyan, *Vysokomol. Soedin.*, **8**, 1359 (1966).
4. K. Nagai, *J. Chem. Phys.*, **47**, 4690 (1967).
5. L. R. G. Treloar, *The Physics of Rubber Elasticity*, 2nd Ed., Clarendon Press, Oxford, 1958, Chap. 10.
6. D. W. Saunders, *Trans. Faraday Soc.*, **53**, 860 (1957).

7. M. V. Volkenstein, *Configurational Statistics of Polymeric Chains*, (Engl. transl.), Wiley, New York, 1963, Chap. 7.
8. K. Nagai, *J. Chem. Phys.*, **40**, 2818 (1964).
9. K. Nagai, *J. Chem. Phys.*, **47**, 2052 (1967).
10. K. Nagai, *J. Chem. Phys.*, **49**, 4212 (1968).
11. K. Nagai, *J. Chem. Phys.*, **51**, 1265 (1969).
12. T. Ishikawa and K. Nagai, *J. Polym. Sci. A-2*, **7**, 1123 (1969).
13. T. Ishikawa and K. Nagai, *Polymer J.*, **1**, 116 (1970).
14. P. J. Flory, R. L. Jernigan, and A. E. Tonelli, *J. Chem. Phys.*, **48**, 3822 (1968).
15. P. J. Flory, *Statistical Mechanics of Chain Molecules*, Wiley, New York, 1969, Chap. IX.
16. Y. Abe, A. E. Tonelli and P. J. Flory, *Macromolecules*, **3**, 294 (1970).
17. D. W. Saunders, D. R. Lightfoot, and D. A. Parsons, *J. Polym. Sci. A-2*, **6**, 1183 (1968).
18. A. N. Gent and V. V. Vickroy, Jr., *J. Polym. Sci. A-2*, **5**, 47 (1967).
19. K. G. Denbigh, *Trans. Faraday Soc.*, **36**, 936 (1940).
20. C. Clement and P. Bothorel, *C.R. Acad. Sci.* (Paris), **258**, 4704 (1964).
21. A. Unanué, C. Clément and P. Bothorel, *C.R. Acad. Sci.* (Paris), **258**, 4754 (1964).
22. H.-G. Kilian and K. Boueke, *J. Polym. Sci.*, **58**, 311 (1962).

Received September 11, 1970
Revised December 28, 1970

JOURNAL OF POLYMER SCIENCE: PART A-2 VOL. 9, 939–957 (1971)

New Approach to the Effects of Pressure Dependence on Sedimentation Velocity Experiments

MENACHEM DISHON, *Department of Applied Mathematics, Weizmann Institute of Science, Rehovot, Israel*, MICHAEL T. STROOT and GEORGE H. WEISS,* *Division of Computer Research and Technology, National Institutes of Health, Department of Health, Education and Welfare, Bethesda, Maryland 20014*, and DAVID A. YPHANTIS,* *Section of Biochemistry and Biophysics of the Department of Biological Sciences and Institute of Materials Science, University of Connecticut, Storrs, Connecticut 06268*

Synopsis

A theory is developed for sedimentation velocity experiments when the sedimentation coefficient s_P depends on pressure P as $s_P/s_0 = (1 + \gamma P)^{-1}$, where γ is a constant. In contrast to the more usually analyzed form $s_P/s_0 = 1 - \gamma P$, this model does not lead, in extreme cases, to a negative sedimentation rate. A theory is presented for homogeneous macromolecules sedimenting with no diffusion. It leads to estimations of s_0 and γ from a knowledge of the point of maximum concentration gradient as a function of time. Results of these calculations are compared with accurate numerical solutions of the Lamm equation with diffusion included.

Introduction

Many authors have discussed the effects of hydrostatic pressure on velocity sedimentation experiments.[1–12] Without exception, their starting point is an empirical relation between pressure and sedimentation coefficient

$$s_P = s_0(1 - \gamma P) \tag{1}$$

where s_P is the sedimentation coefficient, P the pressure, and γ is a constant. In terms of $x = (r/r_a)^2$, where r is the radial position and r_a is the position of the meniscus, eq. (1) imples that for an incompressible solute s_P is given by

$$s_P = s_0(1 + m - mx) \tag{2}$$

in which the parameter m is equal to $(1/2)\gamma\omega^2 r_a^2 \rho_0$, where ω is angular speed and ρ_0 is the solute density at the meniscus. Measurements of m have been interpreted in terms of a theory based on eq. (1), and have led to values of m in the range 0–0.9 for polymer systems of interest.[7–11] However, it is conceivable that values of m greater than the observed maximum

* To whom inquiries should be addressed.

can be attained. This can be done, for example, by increasing the rotor speed, since m is proportional to ω^2. At sufficiently large values of m the theory predicted on eq. (2) leads to the result that the sedimentation coefficient goes to zero at some value of x, and for larger x becomes negative. It is therefore of some interest to analyze a form for s_P/s_0 that is more likely to represent the pressure dependence over a wider range of pressures. In general we can write $s_P = s_0 f(P)$. The particular form of $f(P)$ for which we present detailed results in this paper is

$$f(P) = 1/(1 + \gamma P) \tag{3}$$

which implies that s_P can be written

$$s_P = s_0/[1 + m(x - 1)] \tag{4}$$

At sufficiently low values of $m(x - 1)$ this form of s_P is approximated by the form given in eq. (2). In contrast to eq. (2), there is no value of x for which s_P is negative (since $x \geq 1$). In what follows we make the assumption that the effects of pressure on the diffusion constant are negligible.

Analysis for Linear Sedimentation

We begin by developing results for linear sedimentation (i.e., with s_0 independent of concentration) of a homogeneous species in the absence of diffusion. For this case let $\theta(x,\tau) = c(x,\tau)/c_0$ be the normalized concentration, where c_0 is the initial uniform concentration, and let $\tau = 2\omega^2 s_0 t$ where t is time. The diffusion-free Lamm equation can be written[4]

$$\frac{\partial \theta}{\partial \tau} = -\frac{\partial}{\partial x}[h(x)\theta] \tag{5}$$

where $h(x)$ is defined to be

$$h(x) = x/[1 + m(x - 1)] \tag{6}$$

Equation (5) is to be solved with the initial condition

$$\theta(x,0) = H(x - 1) \tag{7}$$

where $H(u)$ is a Heaviside step function defined by $H(u) = 0$, $u < 0$, and $H(u) = 1$, $u > 0$. Equation (5) can be solved by the method of characteristics.[13] If we denote the solution to the equation

$$R(x) = \int_1^x du/h(u) = \zeta \tag{8}$$

by*

$$x = J(\zeta) \tag{9}$$

* Notice that the analysis does not depend explicitly on the form assumed for $h(x)$ although the final detailed expressions do depend on this function.

then the solution to eq. (5) is shown in the Appendix to be

$$\theta(x,\tau) = \frac{h\{J[R(x) - \tau]\}}{h(x)} H\{J[R(x) - \tau] - 1\} \tag{10}$$

This solution implies that the initial discontinuity at $x = 1$, $\tau = 0$, is transformed into a discontinuity at the solution to $J[R(x) - \tau] = 1$. By referring to the definition of $J(\zeta)$ in eqs. (8) and (9) we see that x_*, the position of the discontinuity, is the solution to

$$R(x_*) = \tau \tag{11}$$

For $h(x)$ specified by eq. (4), this equation becomes

$$m(x_* - 1) + (1 - m) \ln x_* = \tau \tag{12}$$

This last equation is a transcendental equation and cannot be solved exactly. However, it is not difficult to derive approximations that are very good in practice. In particular, if we use a Newton-Raphson method,[14] that is, if we let $x_*^{(n)}$ be the nth approximation to x_*, and compute $x_*^{(n)}$ from the recurrence relation (13),

$$x_*^{(n+1)} = x_*^{(n)} - \left[\frac{m(x_*^{(n)} - 1) + (1 - m) \ln x_*^{(n)} - \tau}{m + (1 - m)/x_*^{(n)}}\right] \tag{13}$$

$$x_*^{(0)} = 1 + \tau$$

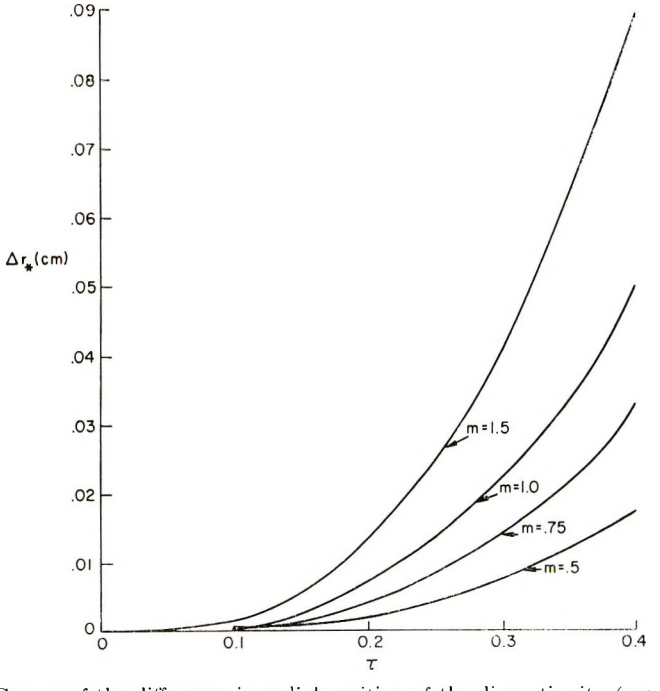

Fig. 1. Curves of the difference in radial position of the discontinuity (approximated by the position of the maximum concentration gradient) predicted by the two theories of pressure dependence.

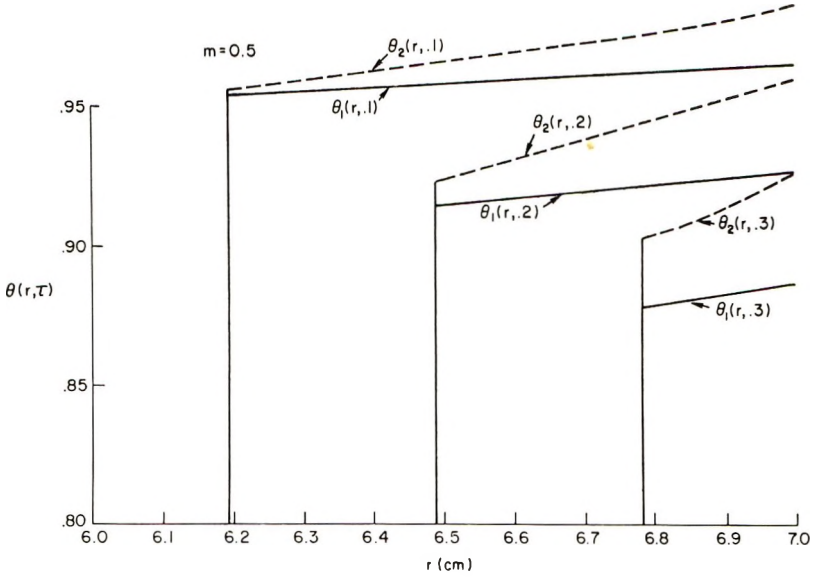

(*a*)

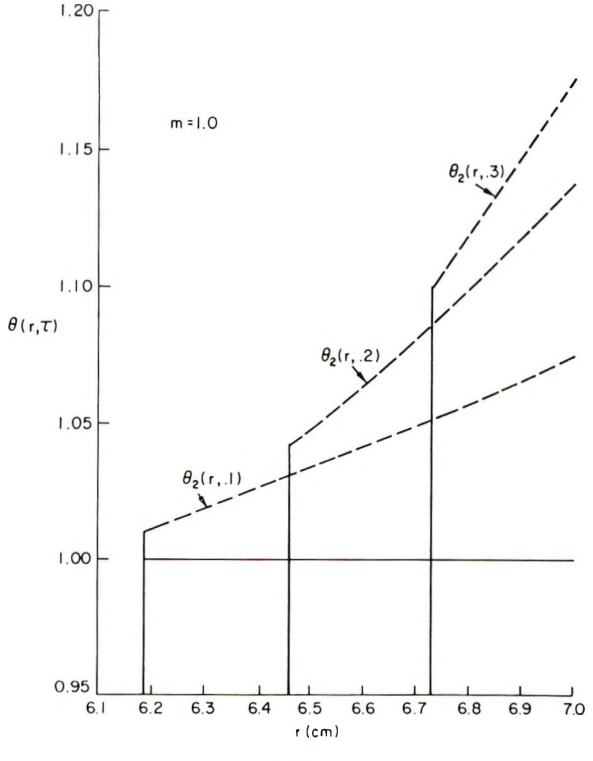

(*b*)

Fig. 2 (*continued*)

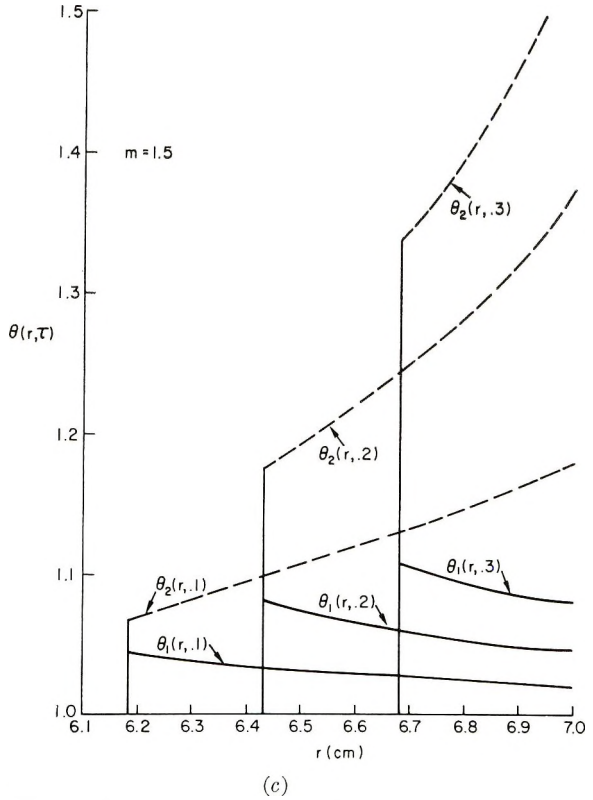

(*c*)

Fig. 2. Theoretical concentration profiles from the two theories for (*a*) $m = 0.5$, (*b*) m = 1.0, (*c*) m = 1. (see text for details).

six-place accuracy is obtained within two or three iterations. The first approximation

$$x_*^{(1)} = 1 + \tau - \{(1 - m)(1 + \tau)[\ln(1 + \tau) - \tau]/(1 + m\tau)\} \quad (14)$$

yields three-place accuracy, or better, for $0 \leqslant m \leqslant 2$ and is sufficient for most purposes. A comparison of the sedimentation coefficient in eq. (4) with that given in eq. (2) shows that for identical values of m the sedimentation coefficient in eq. (4) is the larger

$$1/[1 + m(x - 1)] \geqslant 1 - m(x - 1) \quad (15)$$

Hence the position of the discontinuity in the diffusion-free theory can be expected to move more quickly than that calculated from eq. (2). Figure 1 shows some representative curves of $\Delta r_* = r_{*1} - r_{*2}$, where r_{*1} is calculated from the solution to eq. (12) and r_{*2} is determined from

$$x_{*2} = (r_{*2}/r_a)^2 = (m + 1)/[m + \exp\{-(1 + m)\tau\}] \quad (16)$$

The meniscus position r_a is assumed to be 5.9 cm in the calculations. Figure 1 indicates that the difference in the rate of advance is very small except for fairly large values of m.

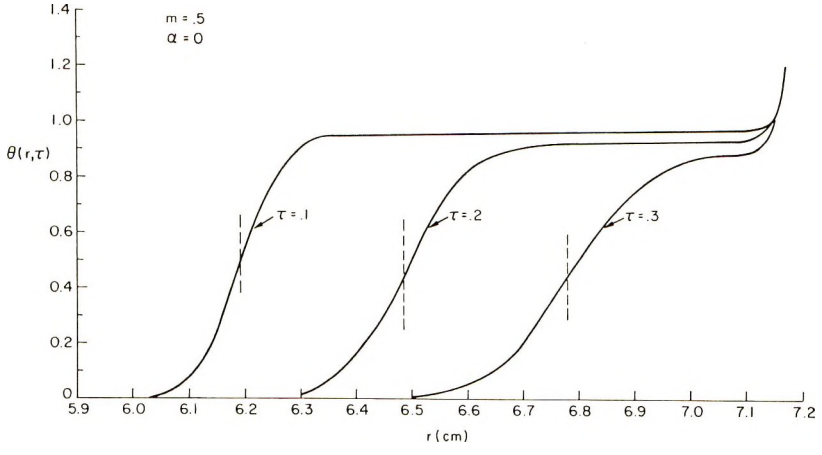

(*a*)

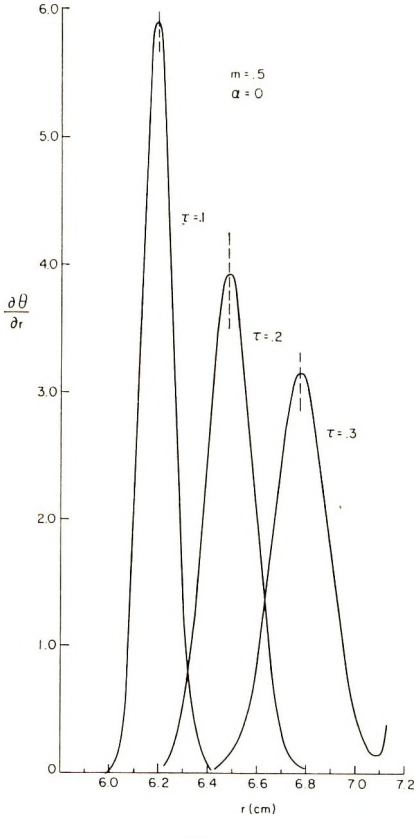

(*b*)

Fig. 3 (*continued*)

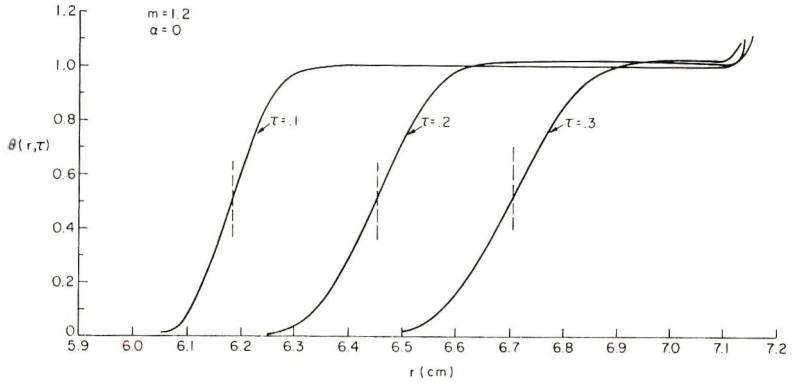

(*c*)

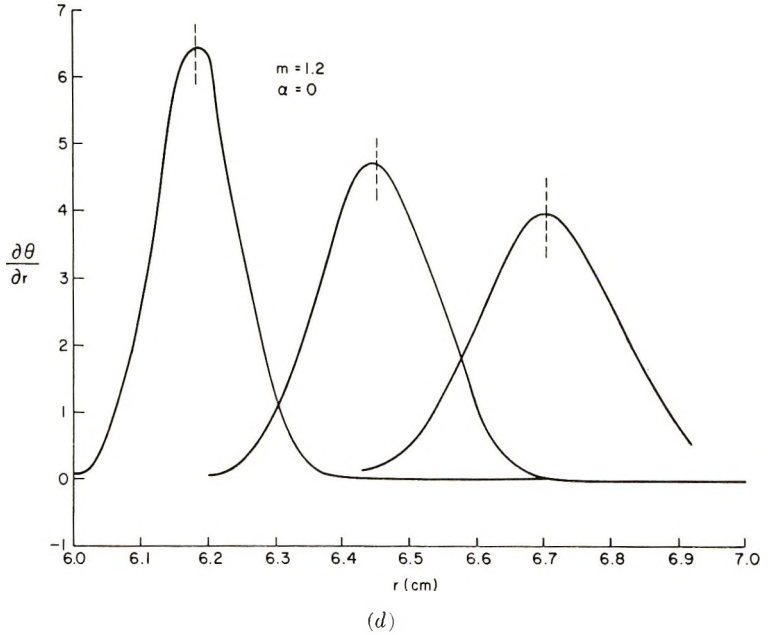

(*d*)

Fig. 3. Plots showing (*a*) concentration profiles for $\sigma_0 = 23.49$ cm^{-2}, $m = 0.5$; (*b*) concentration gradient for $m = 0.5$. (*c*) concentration profile for $m = 1.2$; (*d*) concentration gradient for $m = 1.2$. The dashed lines indicate the theoretical position of the discontinuity in the diffusion-free theory.

A greater contrast to the classical theory is evident if we compare the theoretically predicted concentration profiles for the two theories. Figures 2*a*–2*c* present concentration distributions, $c(r,\tau)/c_0$, calculated for no diffusion, as $\theta_1(r,\tau)$ when the pressure dependence of s is expressed by eq. (4) and as $\theta_2(r,\tau)$ when it is expressed by eq. (2). Figure 2*a* compares the concentration profiles for $m = 0.5$. The concentration distributions for the presently proposed theory are seen to be much flatter than those for the classical theory. At the value $m = 1$ the predicted profile is horizontal

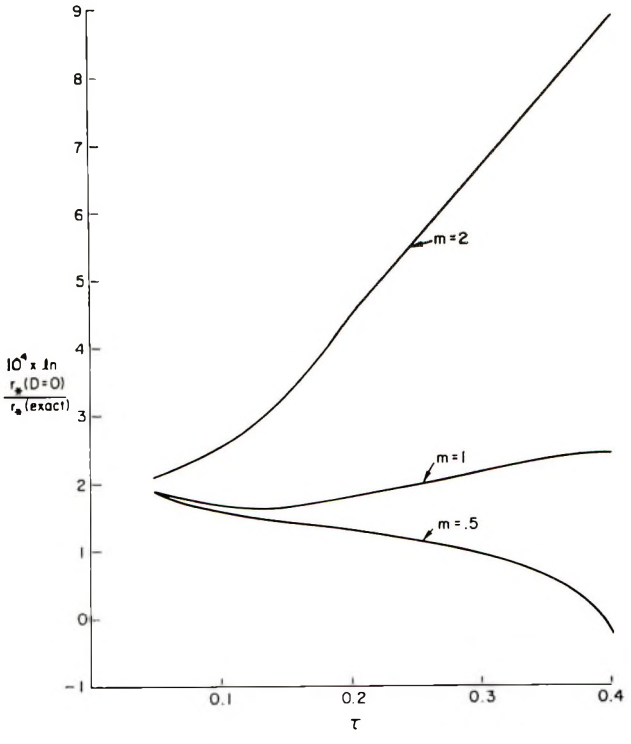

Fig. 4. Curves of $10^4 \times \ln r_*$ $(D = 0)/\ln r$ (exact) as a function of τ for the linear case.

past the discontinuity, while for $m = 1.5$ the theory predicts a slightly negative gradient. Note also that $m = 1$ provides a unique example of a plateau region where concentrations are independent of both time and position: In contrast to these observations, according to the classical theory an increase in m always leads to an increased concentration gradient that is of the same sign as m. The predicted change in qualitative behavior might be used as an experimental means for deciding which theory more closely describes the effects of pressure in velocity centrifugation. Parenthetically we note that Billick's observation[7] that he was unable to observe a positive concentration gradient is more nearly in agreement with the present theory, although other experimental factors, such as convection, might have masked the gradient. Note that the negative concentration gradients predicted here for $m > 1$ will induce convection unless precautions are taken to stabilize the system, as by the presence of an auxiliary positive density gradient sufficient to prevent density inversions.

The most common technique for calculating the parameters s_0 and m from the data consists of plotting $\ln x_*/(\omega^2 t)$ as a function of $\omega^2 t$. Although we do not have an explicit solution for $\ln x_*$ as a function of τ, it is still possible to derive an expansion in powers of τ that can be used for data reduction. We find for small τ, that $\ln x_*$ can be expanded as

$$\ln x_* = \tau - (m\tau^2/2) + m(3m - 1)(\tau^3/6) + \ldots \qquad (17)$$

When s_p is given by the expression in eq. (2), the comparable expansion in powers of τ is

$$\ln x_* = \tau - (m\tau^2/2) + m(m-1)(\tau^3/6) - \ldots \tag{18}$$

Only when cubic terms in $\omega^2 t$ are taken into account can one distinguish in theory between the two pressure models by looking at the position of the maximum concentration gradient.

The theory presented thus far ignores diffusion effects. In order to examine the effects of diffusion we calculated accurate numerical solutions to the Lamm equation by means of the computer program described in a previous paper.[15] The particular parameters for which solutions were obtained were $r_a = 5.9$ cm, $r_b = 7.2$ cm, and $\sigma_0 = \omega^2 s_0/D = 23.49$ cm^{-2}, representing, for example, a protein with a molecular weight of approximately 50,000 daltons at 60,000 rpm. Figures 3*a* and 3*b* show curves of θ and $\partial\theta/\partial r$ for $m = 0.5$, and Figures 3*c* and 3*d* show similar curves for $m = 1.2$. The dotted lines correspond to the position of $r_*(\tau)$ as calculated from the theory for $D = 0$. As can be seen from the curves the peak maximum is quite close to $r_*(\tau)$ and can be identified with it. A more quantitative comparison of the position of the peak and $r_*(\tau)$ is given in Figure 4. Although a negative concentration gradient is predicted for the region usually corresponding to the plateau, i.e. for the region in front of the boundary, when $m = 1.2$, the actual negative gradients are quite small and might be unobservable in practice except for extremely large ($m \geqslant 2$) values of m. Even the predicted convection that should take place (from a negative density gradient, assuming $d\rho/dr \propto d\theta/dr$) may in many cases be prevented by the slight, yet everpresent positive density gradient arising from solution compression occurring on acceleration from standstill to operating speed.

Observations of r_* as a function of time can be used to estimate the parameters s_0 and m. Even though it is possible, for this purpose, to start from the expansion of $\ln x_*(\tau)$ in powers of τ [eq. (17)], it proves to be more accurate to start from the defining relation in eq. (12), since it is linear in both m and s_0. The idea is to measure the position of maximum concentration gradient at times $t_1, t_2, \ldots, t_n$, where the times are so chosen that there are no reflections from the meniscus or from the base. These positions $r_1, r_2, \ldots, r_n$ can then be used to calculate $x_1, x_2, \ldots, x_n$. One can then rewrite eq. (12) as

$$m - s_0\left[\frac{2\omega^2 t_i}{(x_i - 1 - \ln x_i)}\right] = -\ln x_i/(x_i - 1 - \ln x_i) \tag{19}$$

or

$$m = \alpha_i s_0 - \beta_i \tag{20}$$

where

$$\alpha_i = (2\omega^2 t_i)/(x_i - 1 - \ln x_i)$$

TABLE I
Comparison of Estimated and Exact Values of s_0 and m for $\omega^2 s_0/D = 23.49$ cm^{-2}

s_0		m	
Exact	Calculated	Exact	Calculated
1.0	1.000	0.5	0.472
1.0	0.987	1.0	0.971
1.0	0.995	2.0	2.015

and

$$\beta_i = \ln x_i/(x_i - 1 - \ln x_i)$$

The parameters m and s_0 can now be estimated by a least-squares procedure[14] and have the explicit expression

$$\begin{aligned} m &= (\textstyle\sum\beta_i \sum\alpha_i^2 - \sum\alpha_i \sum\alpha_i\beta_i)/\Delta \\ s_0 &= (\textstyle\sum\alpha_i \sum\beta_i - n \sum\alpha_i\beta_i)/\Delta \\ \Delta &= (\textstyle\sum\alpha_i)^2 - n \sum\alpha_i^2 \end{aligned} \tag{21}$$

We have applied this method to the numerical solutions with results given in Table I, the maxima being measured from $\tau = 0.1$ to $\tau = 0.4$. The value s_0 was chosen as 1.0 in dimensionless units. As can be seen, the relative error in s_0 is usually less than 2%, while the relative error in the estimate of m is larger, but of the order of 5% or less. It is important to emphasize that the errors in Table I are due to diffusion effects only and do not include possible experimental errors. That is to say, the errors in the estimates reflect the differences in peak position due to use of a diffusion-free theory in a situation where diffusion is actually present. It is of interest to point out that an analogous treatment of data is more difficult for the pressure model represented by eq. (1), since the expression for x_* [eq. (16)] is nonlinear in m and τ.

An approximation to the effects of diffusion can be made by means of the theory developed by Weiss and Dishon.[16] They have shown that if eq. (5) is replaced by the full Lamm equation expressed in the form

$$\frac{\partial\theta}{\partial\tau} = \frac{\partial}{\partial x}\left(\epsilon x \frac{\partial\theta}{\partial x}\right) - \frac{\partial}{\partial x}[h(x)\theta] \tag{22}$$

in which $\epsilon = 2D/(s_0\omega^2 r_a^2) \ll 1$, then an approximate solution can be written in terms of the function $J(\zeta)$ defined in eqs. (8) and (9). If we define two functions $L(u)$ and $\Delta(\tau)$ by

$$\begin{aligned} L(u) &= h[J(u)] \\ \Delta(\tau) &= \int_0^\tau \frac{J(u)}{L^2(u)}\,du \\ &= \int_0^\tau [mJ(u) + 1 - m]^2 du/J(u) \end{aligned} \tag{23}$$

then the approximate solution to eq. (22) is

$$\theta(x,\tau) = \frac{h\{J[R(x) - \tau]\}}{h(x)} \phi\left[\frac{R(x) - \tau}{\sqrt{2\epsilon\Delta(\tau)}}\right] \tag{24}$$

where

$$\phi(x) = (1/\sqrt{2\pi}) \int_{-\infty}^{x} e^{-u^2/2}\, du \tag{25}$$

is the error function. In order to find a useful expression for $\Delta(\tau)$ we change variables, setting $J(u) = x$, or $u = R(x)$, by eq. (8). Then, since $du = dx/h(x)$, we can write

$$\begin{aligned}\Delta(\tau) &= \int_1^{J(\tau)} \{[1 + m(x - 1)]^3/x^2\}\, dx \\ &= (m^3/2)\,[J^2(\tau) - 1] + 3m^2(1 - m)\,[J(\tau) - 1] \\ &\quad + 3m(1 - m)^2 \ln J(\tau) + [(1 - m)^3/J(\tau)]\,[J(\tau) - 1]\end{aligned} \tag{26}$$

It is possible to get some notion of boundary spreading by examining the character of the function

$$\psi(x,\tau) = \frac{h(x)}{h\{J[R(x) - \tau]\}}\, \theta(x,\tau) = \phi\left[\frac{R(x) - \tau}{\sqrt{2\epsilon\Delta(\tau)}}\right] \tag{27}$$

This function reduces to a step function when $\epsilon = 0$ and therefore contains information about boundary spreading. As in an earlier paper[12] we define the "width" of the curve $\psi(x,\tau)$ to be the distance $W_m(p,\tau) = r_{p+} - r_{p-}$, where $r_{p\pm}$ are the radii at which $\psi(r_{p\pm},\tau) = 0.5 \pm p$. It is possible to calculate $W_m(p,\tau)$ from eq. (27) to be

$$W_m(p,\tau)/r_a = J^{1/3}[\tau + \lambda_{p+}\sqrt{2\epsilon\Delta(\tau)}] - J^{1/3}[\tau - \lambda_{p-}\sqrt{2\epsilon\Delta(\tau)}] \tag{28}$$

where λ_p is the root to $\phi(\lambda_p) = p$. In Figures 5*a* and 5*b* we have plotted curves for $p = 0.4$, and $\epsilon = 4 \times 10^{-3}$ (corresponding to molecular weight of approximately 10^5) and for $p = 0.4$ and $\epsilon = 5 \times 10^{-4}$. To contrast with these curves we present analogous results for the model $s/s_0 = 1 - \gamma P$, and $\epsilon = 4 \times 10^{-3}$. The principal difference between the two sets of curves is that for the model discussed in this paper the curves do not separate as distinctly for different m. Also, the tendency towards steady-state behavior[17] which appears for large values[12] of m when $s/s_0 = 1 - \gamma P$ is not as evident in the present model.

Finally, it is possibly of some interest to point out that an exact solution for $m = 1$ is available for the present model. When $m = 1$ the Lamm equation can be written

$$\frac{\partial\theta}{\partial\tau} = \epsilon \frac{\partial}{\partial x}\left(x \frac{\partial\theta}{\partial x}\right) - \frac{\partial\theta}{\partial x} \tag{29}$$

The calculation can be made by a technique proposed by Weiss[18] and leads to the solution

$$\theta(x,\tau) = (2x^{1/2\epsilon}/(\epsilon\tau)) \int_1^\infty u^{1-1/\epsilon} I_{1/\epsilon}(2u\sqrt{x}/(\epsilon\tau))\, du \tag{30}$$

where $I_p(x)$ is a Bessel function of an imaginary argument.

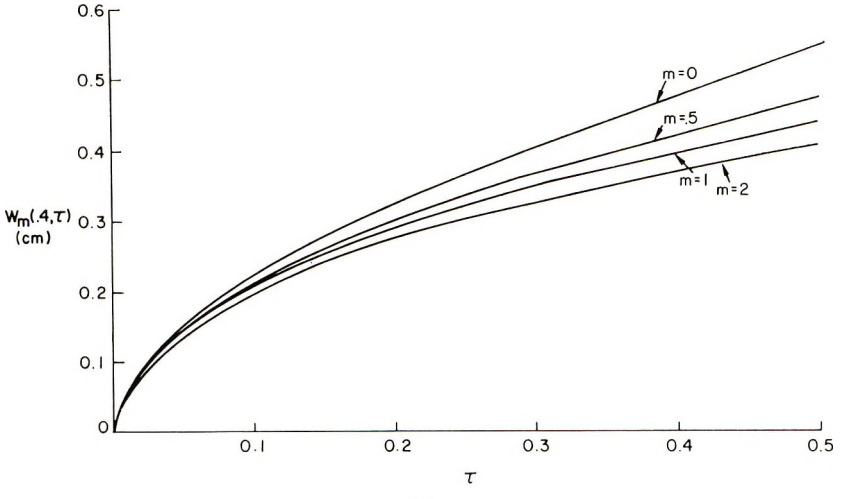

(*a*)

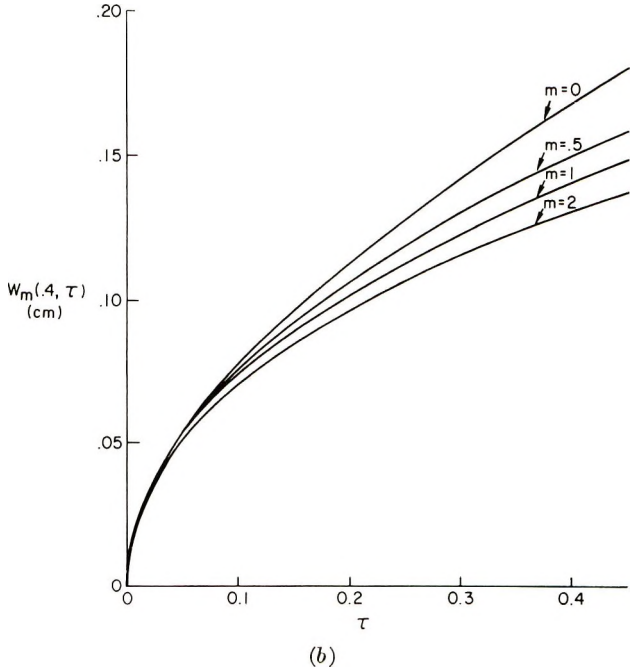

(*b*)

Fig. 5 (*continued*)

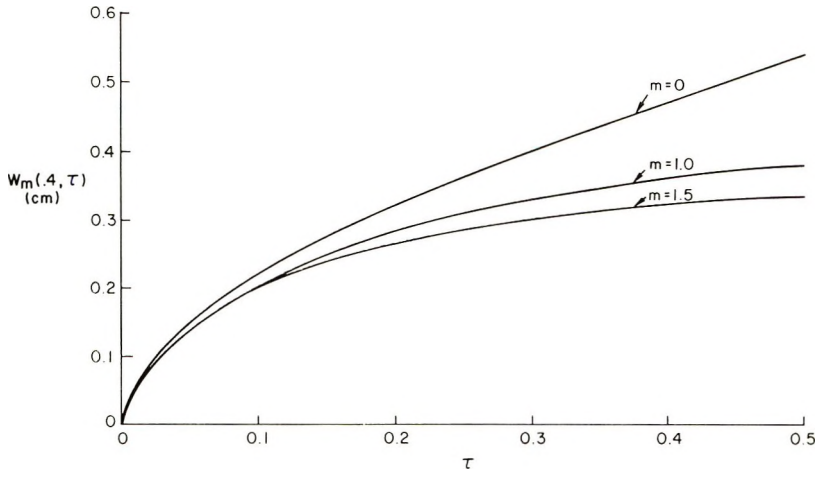

(*c*)

Fig. 5. Curves of the predicted width of concentration gradient: (*a*) for $p = 0.4$ and $\epsilon = 4 \times 10^{-3}$; (*b*) for $p = 0.4$ and $\epsilon = 5 \times 10^{-4}$; (*c*) curves for the model $s_p/s_0 = 1 - \gamma P$, for $p = 0.4$ and $\epsilon = 4 \times 10^{-3}$.

Nonlinear Sedimentation

We now consider the modifications introduced by nonlinear dependence of the sedimentation coefficient on concentration in the form

$$s/s_0 = h(x)/(1 + \alpha\theta) = \{(1 + \alpha\theta)\ [1 + m(x - 1)]\}^{-1} \tag{31}$$

First, we consider the diffusion-free theory, for which the Lamm equation is the first-order equation:

$$\frac{\partial\theta}{\partial\tau} = -\frac{\partial}{\partial x}\left[\frac{h(x)\theta}{(1 + \alpha\theta)}\right] \tag{32}$$

When $\theta(x,0) = H(x - 1)$, where $H(u)$ is a step function, the complete solution of this equation is of the form $\theta(x,\tau) = F(x,\tau)H[x - x_*(\tau)]$ where $x_*(\tau)$ is the position of the moving discontinuity expressed as a dimensionless space variable. It is this quantity that is generally identified with the maximum of the concentration gradient. It has been shown that x_* is the solution to the ordinary differential equation[4,12]

$$dx_*/d\tau = h^2(x_*)/[h(x_*) + \alpha] \tag{33}$$

In the case of present interest this equation can be solved for τ in terms of x, leading to the relation

$$m(1 + \alpha m)\ (x_* - 1) + (1 - m)\ (1 + 2\alpha m)\ \ln x_* + \alpha(1 - m)^2\ [1 - (1/x_*)] = \tau \tag{34}$$

Figures 6*a*–6*d* contain curves of the normalized concentration profile and concentration gradient for the parameters $\alpha = 0.5$, $m = 0.8$ and $m =$

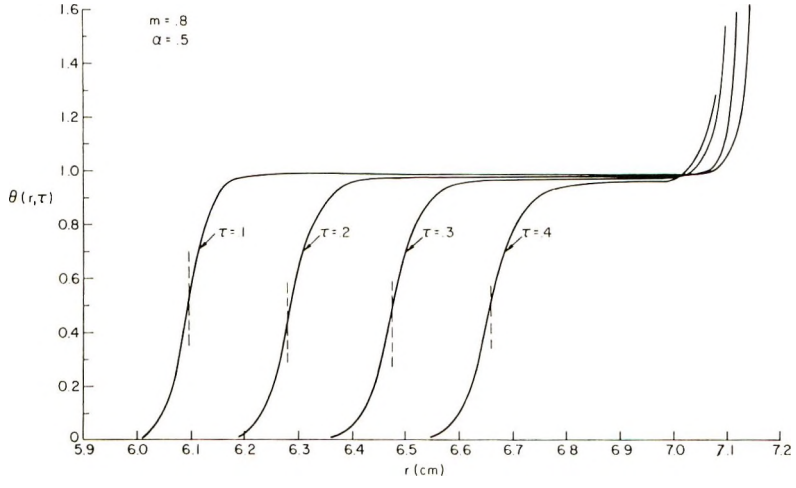

(*a*)

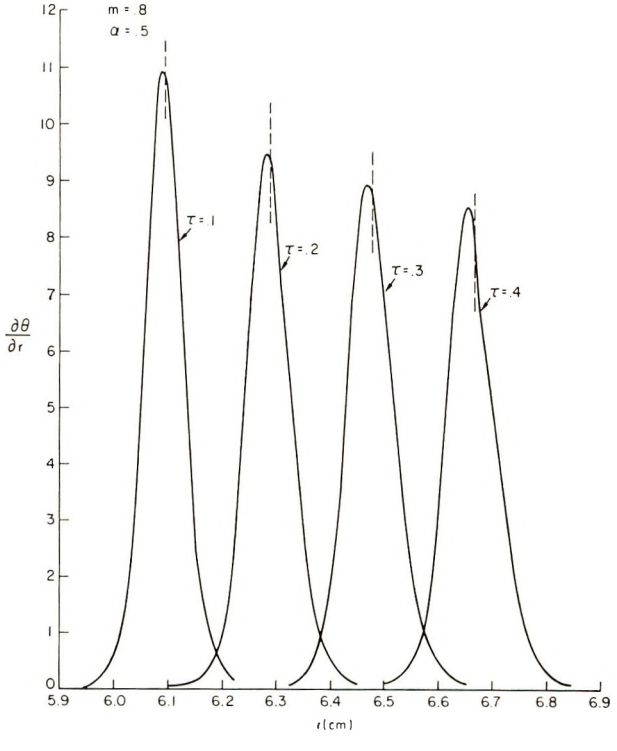

(*b*)

Fig. 6 (*continued*)

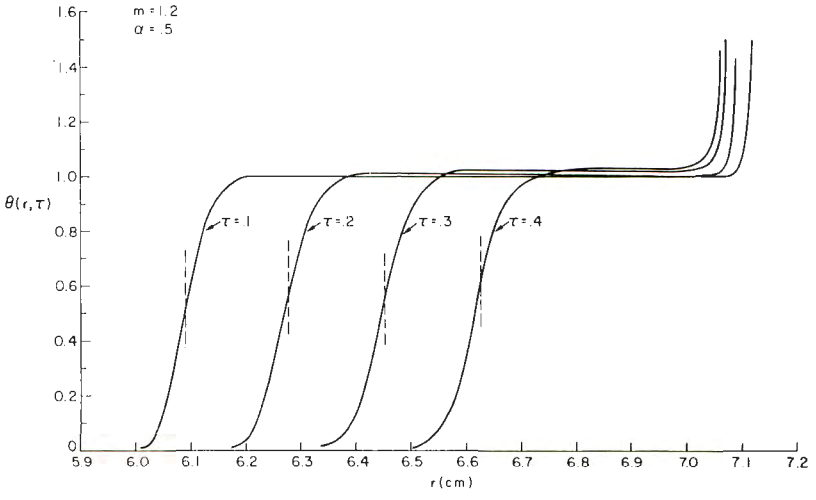

(c)

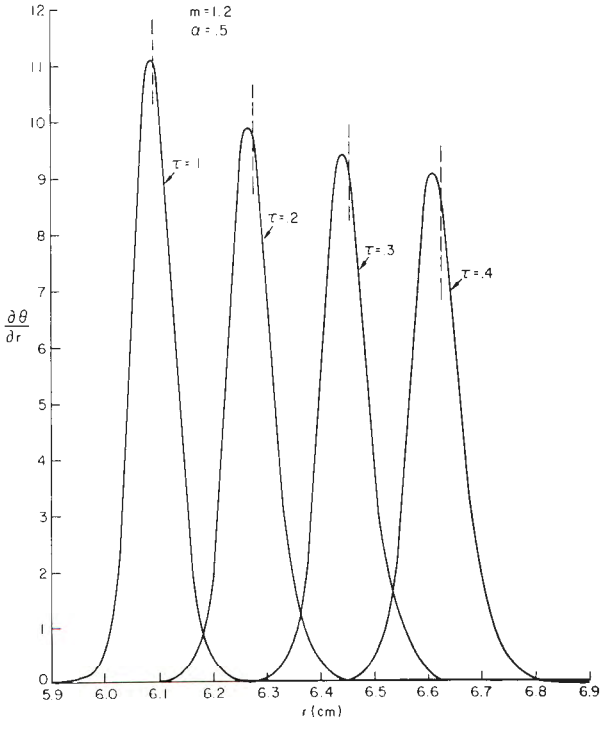

(d)

Fig. 6. Plots showing (*a*) concentration profiles for $\sigma_0 = 23.49$ cm^{-2}, $\alpha = 0.5$, $m = 0.8$; (*b*) concentration gradient for $\alpha = 0.5$, $m = 0.8$; (*c*) concentration profiles for $\alpha = 0.5$, $m = 1.2$; (*d*) concentration gradients for $\alpha = 0.5$, $m = 1.2$.

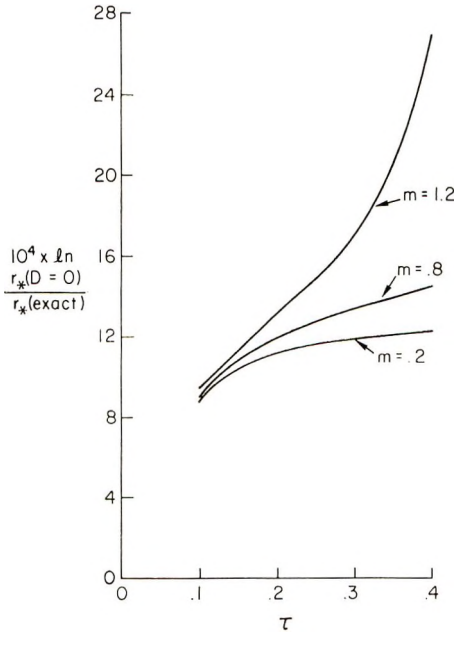

Fig. 7. Curves of $10^4 \times \ln r_* (D = 0)/\ln r_0$ (exact) as a function of τ for the nonlinear case ($\alpha = 0.5$).

1.2. As before, the dashed lines indicate the theoretically predicted discontinuity from the diffusion-free theory. A displacement of this value from the position of maximum concentration gradient increasing in τ can be observed. A further representation of this displacement is shown in Figure 7. The effect of nonlinearity is to increase the deviation over that obtained in the linear case (cf. Fig. 4). The concentration gradient profiles in Fig. 6*d* have negative slope in the region in front of the boundary, as is predicted by the diffusion free theory; but the magnitudes of these negative slopes are too small to be seen on the figure. Typical values of such gradients are, for $m = 1.2$, $\alpha = 0.5$, greater in algebraic value than -0.018 for $\tau \leqslant 0.4$.

It is possible to derive an expansion for $\ln x_*/\tau$ from either eq. (33) or eq. (34). This expansion is

$$\frac{\ln x_*}{\tau} = \frac{1}{1+\alpha} - \frac{(2\alpha+1)m - \alpha}{2(1+\alpha)^3}\tau + \frac{1}{6(1+\alpha)^5}[\alpha(2\alpha-1) - m(10\alpha^2+5\alpha+1) + m^2(10\alpha^2+10\alpha+3)]\tau^2 - \ldots \quad (35)$$

This expansion differs from the one derived for the model of eq. (2) only in the term in τ^2, and the difference might be unobservable in practice. Two techniques suggest themselves for calculating the parameters s_0 and m by using the results of the diffusion-free theory. The first is to express $\ln x_*/(\omega^2 t)$ as a linear function of $\omega^2 t$ from eq. (35) and to fit the parameters

to the linear approximation values. The second technique is to use a least-squares fit to eq. (34), which is linear in s_0 and quadratic in m, by using observed values of x_* and $\omega^2\tau$. In both of these methods it is assumed that the value of α is known independently.

We have compared both methods on data from the computer output, for $\alpha = 0.5$ and $\sigma_0 = 23.49$ cm^{-2}. The two methods appear to be useful in different regions of m. Let us first consider the expansion of $\ln x_*/(\omega^2 t)$ as

$$\ln x_*/(\omega^2 t) = (A/(2\omega^2 t)) + B + C\omega^2 t \tag{36}$$

where A and B are the constants to be found by the least-squares method. The constant A is not necessary for the theory, but its presence leads to substantially increased accuracy in the determination of s_0 and m. It corresponds to assigning a different value to the radial position of the meniscus* and appears to partially compensate for the effect of reflection from the meniscus. If the constants B and C are calculated, then s_0 and m can be expressed as

$$s_0 = (1 + \alpha)B$$

$$m = [1/(2\alpha + 1)]\,[\alpha - (1 + \alpha)(C/B^2)] \tag{37}$$

A comparison between the exact and the estimated values of s_0 and m found in this way is made in Table II. Again the exact value of s_0 is scaled to unity for comparison. We see that except for the lowest value of m, the calculated values of m are less than the exact values. At low values of m the estimated value of s_0 is in very good agreement with the exact

TABLE II

Comparison of Estimated and Exact values of s_0 and m
Calculated from Equation (37) for $\omega^2 s_0/D = 23.49$ cm^{-2}

s_0		m	
Exact	Calculated	Exact	Calculated
1.0	0.999	0.2	0.230
1.0	0.991	0.5	0.488
1.0	0.979	0.8	0.689
1.0	0.967	1.0	0.792
1.0	0.961	1.2	0.905

value. It should be noted that if the parameter A is not retained in eq. (36), the estimated value of s_0 is less accurate. For example, the value of s_0 for $m = 0.5$ is changed from 0.991 to 0.974, and the value for $m = 0.8$ is changed from 0.979 to 0.967. Table III contains the result of curve fitting to eq. (34) to determine s_0 and m.

* The values of A that were calculated correspond to a virtual meniscus displaced from the actual one by not more than 1.2 mm.

TABLE III
Comparison of Estimated and Exact values of s_0 and m
Calculated from Equation (34) for $\omega^2 s_0/D = 23.49$ cm^{-2}

s_0		m	
Exact	Calculated	Exact	Calculated
1.0	0.975	0.2	0.105
1.0	0.973	0.5	0.397
1.0	0.971	0.8	0.686
1.0	0.970	1.0	0.880
1.0	0.968	1.2	1.065

The relative error in s_0 is approximately 3% for all values of m. However, there is a decided improvement in the estimate of m at the upper end of the range, although the errors are still of the order of 12%. So far no theory is available that allows one to take diffusion spreading into account in the nonlinear case. It is possible to calculate the form of the concentration profile past the discontinuity by perturbation theory, but it appears to be very difficult to utilize this information to estimate molecular parameters. Finally, we note that a theory corresponding to the one developed in this paper can be devised for any relation of the form $s_p/s_0 = f(P)$. Extension of the present theory can also be made to deal with pressure effects on noninteracting polydisperse systems.

APPENDIX

Detailed Solution to Equation (5)

Equation (5) can be written

$$(\partial\theta/\partial\tau) + h(x)\,(\partial\theta/\partial x) = -h'(x)\theta \tag{A-1}$$

where $h'(x) = dh(x)/dx$. The corresponding characteristic equations are

$$d\tau/1 = dx/h(x) = -d\theta/\theta h'(x) \tag{A-2}$$

The first and second of these equations can be solved for a constant of integration K_1:

$$K_1 = \int_1^x du/h(u) - \tau = R(x) - \tau \tag{A-3}$$

The second and third equations can likewise be solved to yield a second constant of integration K_2:

$$K_2 = \theta h(x) \tag{A-4}$$

Thus, the general solution to eq. (A-1) can be written

$$\theta h(x) = U[R(x) - \tau] \tag{A-5}$$

where $U(y)$ is an arbitrary differential function set by the initial condition

$$U[R(x)] = h(x)\,H(x - 1) \tag{A-6}$$

where $H(x - 1)$ is a step function with a discontinuity at $x = 1$. The combination of eqs. (A-5) and (A-6) together with eq. (9), then leads to eq. (10).

We are grateful to Richard Shrager of the National Institutes of Health for the use of his MODELAIDE curve-fitting program. Part of this research was supported by NSF Grants GB-8164 and GB-13790 to D. A. Y.

References

1. H. Mosimann, R. Signer, *Helv. Chim. Acta*, **27**, 1123 (1944).
2. J. Oth and V. Desreux, *Bull. Soc. Chim. Belg.*, **63**, 133 (1954).
3. A. F. V. Eriksson, *Acta Chem. Scand.*, **10**, 360 (1956).
4. H. Fujita, *J. Amer. Chem. Soc.*, **78**, 3898 (1956).
5. M. Wales, *J. Amer. Chem. Soc.*, **81**, 4758 (1959).
6. I. H. Billick, *J. Phys. Chem.*, **66**, 565 (1962).
7. I. H. Billick, *J. Phys. Chem.*, **66**, 1941 (1962).
8. I. H. Billick, *J. Polym. Sci.*, **62**, 167 (1962).
9. M. Wales and S. Rehfeld, *J. Polym. Sci.*, **62**, 179 (1962).
10. J. E. Blair and J. W. Williams, *J. Phys. Chem.*, **68**, 161 (1964).
11. T. Kotaka and N. Donkai, *J. Polym. Sci. A-2*, **6**, 1457 (1968).
12. M. Dishon, G. H. Weiss, and D. A. Yphantis, *J. Polym. Sci. A-2*, **8**, 2163 (1970).
13. G. F. D. Duff, *Partial Differential Equations*, Univ. Toronto Press, Toronto, Canada, 1956.
14. A. Ralston, *A First Course in Numerical Analysis*, McGraw-Hill, New York, 1965.
15. M. Dishon, G. H. Weiss, and D. A. Yphantis, *Biopolymers*, **4**, 449 (1966).
16. G. H. Weiss and M. Dishon, *Biopolymers*, **9**, 865 (1970).
17. J. M. Creeth, *Proc. Roy. Soc.* (London), **A282**, 403 (1964).
18. G. H. Weiss, *J. Math. Phys.*, **5**, 675 (1964).

Received November 16, 1970

ERRATUM

Origin of the γ Relaxations in Polyethylene and Polytetrafluoroethylene

R. W. GRAY AND N. G. MCCRUM
(article in *J. Polymer Sci. A-2*, **7**, 1329, 1969)
Department of Engineering Science,
Oxford University, Oxford, England.

In Table I the quoted specimen densities are corrected to 25°C (as stated in the legend) but the quoted values of crystallinity v_2 are those calculated, from the uncorrected specimen densities. The values of v_2 corrected to 25°C are 0.684, 0.723, 0.754, 0.793, 0.804, and 0.817 for specimens Q, Q-An, I, I-An, S, and S-An respectively. It is these values corrected to 25°C which are used in the analysis and shown in the figures, and which should appear in the last column of Table I. The density values in the penultimate column for specimens *Q-An* and *I-An* should read 0.959 and 0.969 g/cc (and not 0.956 and 0.967 g/cc).

The *Journal of Polymer Science* publishes results of fundamental research in all areas of high polymer chemistry and physics. The *Journal* is selective in accepting contributions on the basis of merit and originality. It is not intended as a repository for unevaluated data. Preference is given to contributions that offer new or more comprehensive concepts, interpretations, experimental approaches, and results. Part A-1 *Polymer Chemistry* is devoted to studies in general polymer chemistry and physical organic chemistry. Contributions in physics and physical chemistry appear in Part A-2 *Polymer Physics*. Contributions may be submitted as full-length papers or as "Notes." Notes are ordinarily to be considered as complete publications of limited scope.

Three copies of every manuscript are required. They may be submitted directly to the editor: For Part A-1, to C. G. Overberger, Department of Chemistry, University of Michigan, Ann Arbor, Michigan 48104; and for Part A-2, to T. G Fox, Mellon Institute, Pittsburgh, Pennsylvania 15213. Three copies of a short but comprehensive synopsis are required with every paper; no synopsis is needed for notes. Books for review may also be sent to the appropriate editor. Alternatively, manuscripts may be submitted through the Editorial Office, c/o H. Mark, Polytechnic Institute of Brooklyn, 333 Jay Street, Brooklyn, New York 11201. All other correspondence is to be addressed to Periodicals Division, Interscience Publishers, a Division of John Wiley & Sons, Inc., 605 Third Avenue, New York, New York 10016.

Detailed instructions on preparation of manuscripts are given frequently in Parts A-1 and A-2 and may also be obtained from the publisher.